AD-A255 444

AGE

Form Approved
OMB No 0704-0188

1. AGENCY USE ONLY (Leave blank)	2. REPORT DATE	3. REPORT TYPE AND DATES COVERED
	1992	DISSERTATION

4. TITLE AND SUBTITLE
A Study of Mid-Latitude 5577Å OI Dayglow Emissions

5. FUNDING NUMBERS

6. AUTHOR(S)
Edward E. Hume Jr., Captain

7. PERFORMING ORGANIZATION NAME(S) AND ADDRESS(ES)
AFIT Student Attending: University of Michigan

8. PERFORMING ORGANIZATION REPORT NUMBER
AFIT/CI/CIA-92-012D

9. SPONSORING MONITORING AGENCY NAME(S) AND ADDRESS(ES)
AFIT/CI
Wright-Patterson AFB OH 45433-6583

10. SPONSORING MONITORING AGENCY REPORT NUMBER

11. SUPPLEMENTARY NOTES

12a. DISTRIBUTION AVAILABILITY STATEMENT
Approved for Public Release IAW 190-1
Distributed Unlimited
ERNEST A. HAYGOOD, Captain, USAF
Executive Officer

12b. DISTRIBUTION CODE

13. ABSTRACT (Maximum 200 words)

14. SUBJECT TERMS	15. NUMBER OF PAGES 252
	16. PRICE CODE

17. SECURITY CLASSIFICATION OF REPORT	18. SECURITY CLASSIFICATION OF THIS PAGE	19. SECURITY CLASSIFICATION OF ABSTRACT	20. LIMITATION OF ABSTRACT

A STUDY OF MID-LATITUDE 5577Å OI DAYGLOW EMISSIONS

by

Edward Eugene Hume, Jr.

A dissertation submitted in partial fulfillment
of the requirements for the degree of
Doctor of Philosophy
(Atmospheric and Space Science)
in The University of Michigan
1992

Doctoral Committee:

Research Scientist Vincent J. Abreu, Chairman
Professor Anthony W. England
Professor Timothy L. Killeen
Associate Research Scientist Jeng-Hwa Yee
David C. Cartwright, Associate Director for Research,
Los Alamos National Laboratory

A theory has only the alternative of being right or wrong.
A model has a third possibility: It may be right, but irrelevant.

Manfred Eigen

For my family,
Cheryl, all of my children,
and my parents.

ACKNOWLEDGMENTS

It has been a long journey to this final part of my thesis. There is a large number of people I would like to acknowledge and thank many which I will miss here. First, I have my family to thank for putting up with all of this. My wife, Cheryl, and the children (all of them) have been through as much as I have to get to here. The last few months, they have had to put up with my not being there much of the time and when I was there they endured my grouchiness. It was very difficult to explain to them that I had to work again and I'd see them before they went to bed. Also my parents deserve a lot of credit and thanks. They encouraged me to learn before but then wanted to know when I would be done with school.

I would like to thank many members of the department faculty, both teaching and research. There was a lot to learn and it was well taught, hopefully it will be retained. Special thanks to the "group" members with whom I worked the most. Dr. Vince Abreu, my advisor, who sometimes pusshed and occassionally had to drag me through the stages deserves a lot of credit. Also for the assisitance and advice, Drs. Jeng-Hwa Yee, Wilbert Skinner, and Mark Burrage, are owed thanks. Other groups in the department that deserve mention are the computer and secretarial staffs. For promptly fixing the computer glitches, help with strange bugs and giving advice thanks go to Dave Steinbeck, Gerry Schmitt, and Abe Osman.

The excellent secretarial staff is also deserving of thanks for all the help with trips, papers, copying and just getting things done. Special

thanks to Doug Frayer and Debbie Eddy who gave extra help when needed. Others that deserve special mention are Carol Quinnell, Sue Young, Brenda Gilligan, Erin Morris, and Marti Moon.

There are many students who have contributed to my time at the University. First are those who I have shared office space with at one time or another: Walt Harris, Dave Meyer, Ken Fischer, Matt McGill, Dong Liang Wu, and Darryl Charache. Also one who preceded me out is Dr. Anthony Bucholtz. The other AFIT students who have provided a little stability are Steve Carr, Tom Smith, Pat Purcell, Dick Cannatta, Ken Reese, and Steve Quigley. Other student who deserve some credit are Claudia Alexander, Brian Johnson, Teresa Schultz, Lynn Thomas, and Ned Snell. These students and others have listened to me complain, rant and rave. They also endured endless and tedious descriptions of the work here in various stages.

As a final note, I'd like to thank the entire dissertation committee which besides Drs. Abreu and Yee included Dr. Tim Killeen and Dr. Tony England from the University. Special thanks go to Dr. David Cartwright from Los Alamos National Laboratory for his invaluable advice and for traveling to the University to help with my dissertation.

TABLE OF CONTENTS

LIST OF FIGURES

Figure

LIST OF TABLES

Table

LIST OF APPENDICES

Appendix

CHAPTER I

INTRODUCTION

1.1 Summary of Thesis

The green line (5577Å) is a bright, persistent component of the visible airglow. It is produced by an electric quadrupole transition from the metastable second excited state ($^1S_0$) to the first excited state ($^1D_2$) of atomic oxygen. These two excited states all lie in the same electron shell of the atom and have the same electron configuration as the ground state of $1s^2 2s^2 2p^4$, which is the $^3P_{2,1,0}$.

This emission is present in both the daytime and night airglow and in the aurora, and despite a long history of study it is still not fully understood. The emission in the dayglow and the nightglow is relatively homogeneous spatially and global in coverage. In the aurora, the emission is much brighter than the airglow, highly structured and very localized being restricted to higher latitudes.

The structure of the 5577Å emission with altitude and the chemistry responsible for the production of the emission are complex. The vertical structure for the emission has two distinct layers in the airglow each with

its own set of production and loss mechanisms. The chemistry for either of these layers is not completely known. The auroral emission is not understood either since it overlaps the upper and lower layer altitudes and it tends to contain some parts of the chemistry of both layers as sources and losses.

This thesis addresses the upper layer emission in the dayglow. The chemistry that has been proposed as responsible for this layer is investigated and a photochemical model which describes this emission has been developed. The model is compared to observations from the Atmosphere Explorer satellites to determine the relative importance of the individual reactions. For some of the reactions, the properties of the rate coefficients, branching ratios, and cross sections are not well known or there are large discrepancies between different studies. The model is used to determine the best parameters for some of these reactions based on observations. The model is then applied to the twilight airglow.

The remainder of this chapter gives an extensive account of the history of the discovery of the greenline emission and the determination of the responsible transition. The various proposed chemical reactions for sources and losses are discussed for each of the dayglow layers and the auroral case. In addition, a summary of the observational techniques used to study this emission is presented.

The Atmosphere Explorer (AE) satellite program is discussed in chapter two. The Visible Airglow Experiment (VAE), which was the instrument on the AE spacecraft which measured atmospheric emissions, is described in detail, together with an account of the various data analysis techniques that are applicable to the data. Other instruments on the satellites, which provided measurements of the neutral and ionized

atmospheric constituents that are needed in the various chemical reactions, are also discussed.

Details of the photochemical model are given in Chapter 3. This chapter presents the various atmospheric models that are required by the photochemical model, followed by a description of the photochemical code and the specific reactions that are employed by it.

The next three chapters present the results derived from the photochemical model. Chapter 4 details the calculation of the total rate coefficient for a reaction that is a major source of the $O(^1S)$ at lower altitudes. In Chapter 5, the model is used with the results from Chapter four to determine the effective branching ratio for the energy exchange reaction and the magnitude of the electron impact cross section of atomic oxygen that best represents the observed data. With these parameters determined, Chapter 5 also describes the application of the model to the twilight 5577Å emission. Conclusions and suggestions for further work are given in Chapter six.

1.2 Introduction to the 5577Å OI Emission

The 5577Å green line is produced by an electronic transition in atomic oxygen from the ^1S to the ^1D state. This is an electric quadrupole transition which has a radiative lifetime of about 0.75 sec in the upper state (Kernahan and Pang, 1975). This emission is predominant in the aurora and is one of the brightest emissions in the visible nightglow. Figure 1.1 is an energy diagram for atomic oxygen showing the OI transitions.

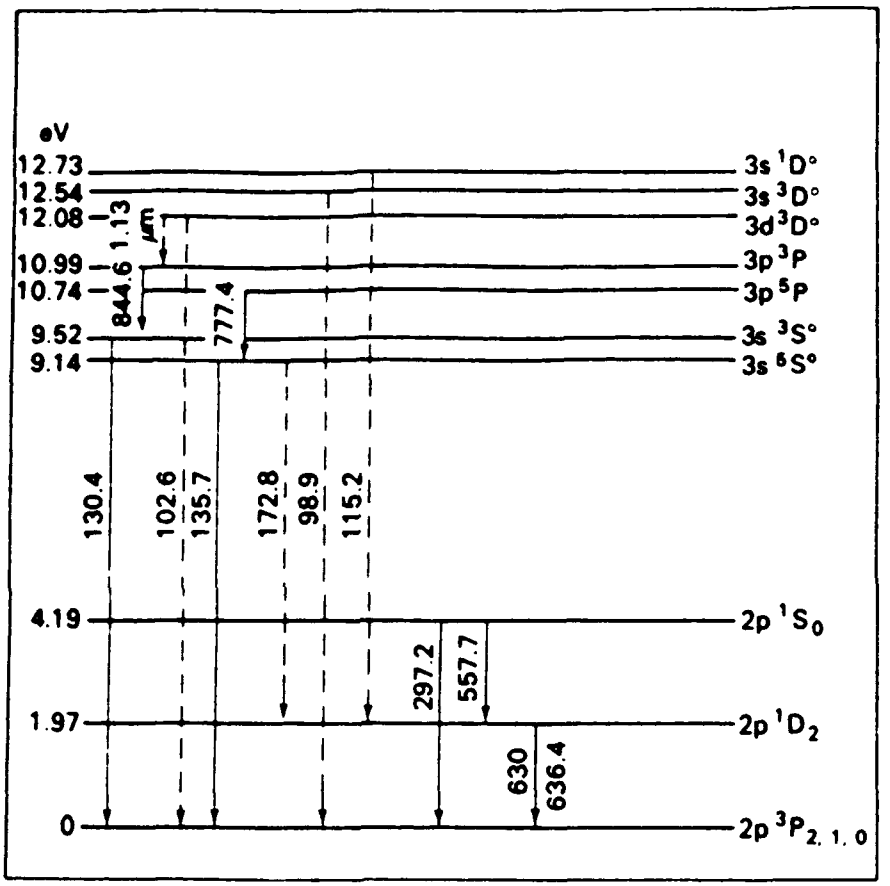

Figure 1.1 Energy level diagram of atomic oxygen, showing potential and observed transitions. Solid arrows are observed transitions, dashed arrows have not been observed. Wavelengths are in nanometers except as noted. (After Rundle, 1971).

In the atmosphere, the 5577Å dayglow emission occurs in two distinct layers. The lower layer is at about 95 km, while the upper layer peaks at about 150 km. These two layers are shown in Figure 1.2. The green line has been studied more than any other airglow emission, and previous investigations have been reviewed by Bates (1978) and Torr and Torr (1982).

The present investigation concentrates on the upper layer which peaks in the dayglow at approximately 150 km and has a complex photochemical processes for production. The majority of the past studies were focused on the auroral regions and in the nightglow (Sharp *et al.*, 1979; Sharp and Torr, 1979; Rees, 1984; Yee and Killeen, 1986; McDade and Llewellyn, 1986, Gerikova and Shepherd, 1988). A study of the 5577 Å airglow including modeling of the dayglow was carried out by Frederick *et al.* (1976) using observations from the Visible Airglow Experiment (VAE) on board the Atmosphere Explorer satellites. Since then, many new laboratory and observational results have improved our understanding of the 5577Å dayglow and the complex chemical processes which produce the $O(^1S)$ metastable state. This section will give a history of the 5577Å emission and discuss the physical processes and morphology of the emission. Also the different techniques that can be used to measure the emission will be described.

1.2.1 History

The green line at 5577Å has been studied more than any other emission. As the brightest emission in the visible nightglow and the dominant color visible in the aurora, it attracts much attention. Despite

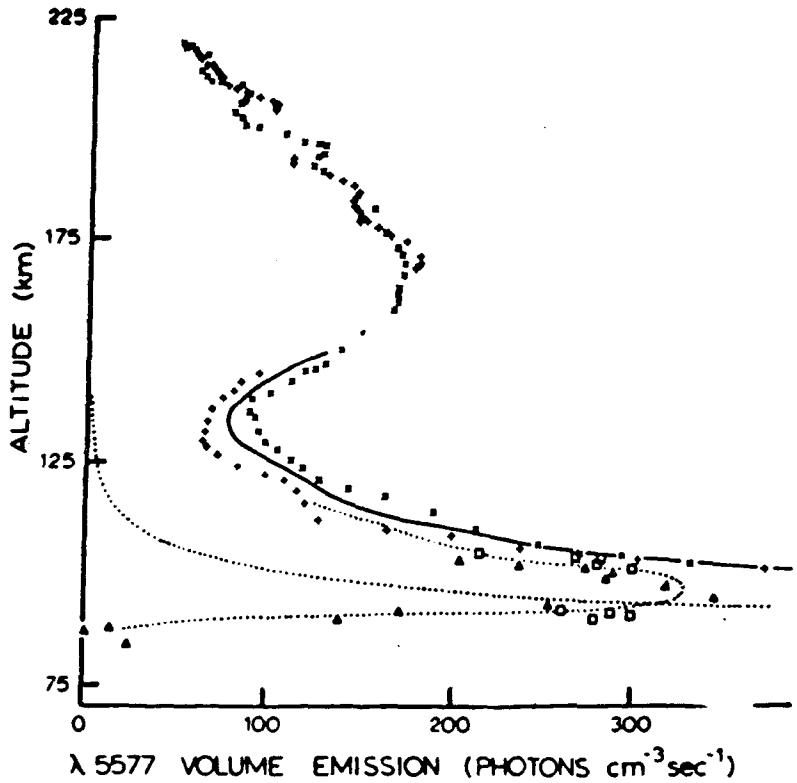

Figure 1.2 The 5577Å volume emission rate profile by Wallace and McElroy (1966). Low altitudes are corrected for Rayleigh scattering as indicated by squares and triangles.

extensive studies, the major processes responsible for the emission are not completely resolved. In this section, an account of the various suggested mechanisms for this emission will be given along with an historical perspective. Since the emission is found in all parts of the sky (aurora, nightglow, and dayglow), no attempt is made here to distinguish the emission in the dayglow alone. This will be done in later chapters.

Studies of the "auroral" green line date back to 1868 when Anders. J. Ångstrom (1814-1874) began making quantitative spectral studies of the aurora. Before this only visual color studies of the aurora were performed. Ångstrom (1868) determined the wavelength of the green emission in the aurora as 5567Å but was unable to determine its source. It was suggested the green line emission would be present even though the aurora was not visible (Ångstrom, 1868; Vogel, 1872, and Wiechert, 1902).

It was noted by Campbell (1895) and Fath (1908) that the "auroral" green line emission was present in the entire sky at all times. This was confirmed by Slipher (1919) using a large number of green line spectrograms. This was termed the permanent aurora by Yntema (1909) or the nonpolar aurora by Rayleigh (1924). The terms airglow and Nightglow were not introduced until the early 1950's (Elvey, 1950; Roach and Pettit, 1951).

Early spectroscopic work by Vegard (1913) placed the green line emission near 5577Å. Using photographs of the green line interference fringes of the night sky from a Fabry-Perot etalon, Babcock determined the wavelength of the emission to be 5577.350±0.005 Å with a maximum width of 0.35 Å. The results of these measurements led to the conclusion that the auroral and nightglow green line emission had a common source.

Sorting out the contributions to the night sky from various terrestrial and extra-terrestrial sources was a significant problem, as pointed out by Fabry (1919,1921). These sources included the stellar background, scattering of sunlight by the interplanetary gas and dust, and the atmospheric emission. Polarization of the night sky was found to be almost non-existant (Rayleigh, 1919; Babcock, 1919). In the plane of the azimuth of the sun, Dufay (1928, 1929) found a polarization of 2-4%, which led to the conclusion that about 15% of the light in the night sky was from the zodical light.

During his investigations of the spectrum of the night sky, Rayleigh (1922a, 1922b, 1923, 1928, 1931) concluded that the terrestrial component of the night sky was quantitatively different from the aurora. The night sky lacked the negative bands of nitrogen seen in the aurora, and the green line showed no consistent enhancement toward the auroral regions. The first absolute measurements of green line brightness were reported by Rayleigh (1930). These measurements in terms of surface brightness led to the photometric unit named after him (Hunten *et al.*, 1956).

Even though the bright green line emission was predominant in all parts of the sky, its source was not known. There were several sources proposed and then discarded in the process of determining the mechanism for the emission. At the turn of the century, it was suggested that krypton gas was responsible for the green line. Krypton gas does have a line at 5570.3Å along with several others close to prominent nitrogen lines, and it was proposed that krypton could explain the entire auroral spectrum (Ramsay, 1919).

An unknown gas called geocoronium was suggested by Wegener (1911) as the source of the green line. This gas was supposed to be lighter

than nitrogen, originated in the solar atmosphere and was transported to the earth (Henriksen and Egeland, 1988). This hypothesis did not last when the implied characteristics of the gas were compared to the aurora. If the gas was lighter than nitrogen, then the fall off of the green line with height would be smaller than that for the nitrogen emissions (Vegard, 1923a). Also, Vegard pointed out that there was no place in the periodic table for such an element.

In the early 1920's, it was suggested by Vegard (1923a, 1923b, 1924) that the source of the green line emission was solid nitrogen. He found that bombarding frozen nitrogen crystals with accelerated electrons produced a series of emissions coinciding with an auroral spectrum (Vegard, 1924). Also, he found a broad feature around the 5577Å emission. This broad feature was found to consist of emissions at 5556Å, 5572Å, 5610Å and 5654Å but a line at 5577Å was not observed (McClennan and Shrum, 1924). Further experiments by McClennan and Shrum (1925) and McClennan and McLeod (1927) found that the green line was due to atomic oxygen via a previously unknown transition.

The nature of this unknown transition was first hinted at by Bowen (1927, 1928) through his studies of the spectra of planetary nebula. He invoked the idea of forbidden transitions and in the following quote set up a key premise in the development of thermospheric photochemistry.

> In the spectra of gaseous nebulae several very strong lines are formed which have not been duplicated in any terrestrial source. Many lines of evidence point to the fact that these lines are emitted by an element of low atomic weight. Since the spectra of light elements as excited in terrestrial sources are well known, this leads to the conclusion that there must be some condition, presumably low density, which exists in the nebulae, that causes additional lines to be emitted.

From studies of the Zeeman pattern it was concluded that the 5577Å emission was from a forbidden and previously unknown (1D-1S) transition of atomic oxygen (McLennan, McLeod, and McQuarrie, 1927; McLennan, McLeod, and Ruedy, 1928; McLennan, 1928; and Sommer, 1928). Frerichs and Campbell (1930) confirmed the identification of the green line as arising from an electric quadrupole transition. Frerichs (1930) used the ultraviolet spectrum of oxygen to predict the energy of the $^1D_2$ and $^1S_0$ states. With the identification of the source and transition for the green line emission, the next issue was to determine the mechanisms that produce O(^{1}S) in the upper atmosphere.

1.2.2 Physical Processes

After the identification of the source of the 5577Å emission as being due to the (1D-1S) transition of atomic oxygen, Chapman (1931) made the first attempted theoretical explanation for the feature using a process first proposed by Frank in 1929 (as cited by Bates, 1981). Chapman noted that McLennan (1930) and Rayleigh (1931) observed that the emission at 5577Å is essentially constant throughout the night. This meant that the energy involved is comparable to the estimate of the energy needed to ionize the upper layer. Chapman (1931) argued that to maintain the emission at a constant level throughout the night, the number of transitions producing 5577Å photons must be small compared to the number of precursor particles.

Chapman looked to the reservoir of energy from the dissociation of O_2 as the source of O(^{1}S). He first noted that the O_2 association energy of 5.03 eV was sufficient to provide the excitation energy of 4.2 eV for O(^{1}S). It is clear from his description, although he never explicitly wrote the reaction,

that the three-body reaction that has become known as the Chapman mechanism (Equation [1.1]) was responsible, i.e.

$$O(^3P) + O(^3P) + O(^3P) \xrightarrow{\gamma_1} O_2 + O(^1S)\,, \qquad [1.1]$$

where γ_1 is the reaction rate coefficient.

Based on the estimated density for the $O(^3P)$, the height of the emission due to the Chapman mechanism was placed at about 100 km. This altitude was not supported by many observations using the van Rhijn method (van Rhijn, 1921; see Chamberlain, 1961), which placed the altitude much higher. The van Rhijn method makes use of the fact that the precise changes in intensity with zenith angle depend on the height of the emitting layer. The method makes the assumptions of an optically and linearly thin emitting layer that is homogeneous and spherically symmetric. There is no provision for extinction in the lower atmosphere for the emission in the method. The invalidity of any of these assumptions cause the van Rhijn method to give widely varying results.

The van Rhijn method was shown later to be unreliable for height determinations, but the matter was not resolved for many years. Phillips (1956) used a Fabry-Perot interferometer to determine the Doppler width of the 5577Å emission, and found it would correspond to a temperature of 155 to 231 K, which is consistent with altitudes of about 100 km. This was followed by rocket observations that placed the peak of the layer between 90 and 102 km (Berg et al., 1956; Koomen et al., 1956; others summarized by Nardi, 1991).

The rocket measurements of Wallace and McElroy (1966) established that the green line actually had two distinct layers. In addition to the layer

at about 95 km, there is an upper F-region layer. Figure 1.2 shows the results of their rocket flight. The rest of this section will discuss these two layers separately beginning with the lower layer. For completeness, a discussion of auroral mechanisms will be presented last.

Lower-altitude component. The Chapman mechanism as the source of $O(^1S)$ was not seriously questioned for some time. The estimation for the rate coefficient, γ_1, is difficult to make by either experiment or theory. Also, it was believed that only a small number of the associations formed would need to produce $O(^1S)$ to give the measured intensity. Nicolet (1959) deduced that only one in one thousand associations need produce a 5577Å photon to account for the measurements of Rayleigh (1930). At this time quenching of $O(^1S)$ was thought to be unimportant due to the investigation by Kvifte and Vegard (1947) that gave the rate, β_2, for the equation

$$O(^1S) + O_2 \xrightarrow{\beta_2} O(^3P) + O_2 \ , \qquad [1.2]$$

to be 4.0×10^{-15} $cm^3\ s^{-1}$ and β_3 for

$$O(^1S) + O(^3P) \xrightarrow{\beta_3} O(^3P \text{ or } ^1D) + O(^3P \text{ or } ^1D), \qquad [1.3]$$

as $4. \times 10^{-13}$ $cm^3\ s^{-1}$.

As interest in the airglow emission grew, other sources of $O(^1S)$ were suggested. The choices were limited by the need to provide 4.2 eV excitation energy to $O(^3P)$. Excess vibrational energy was suggested as a source by Krassovsky (1958) in the reactions

$$O_2^* + CO \xrightarrow{\gamma_4} CO_2 + O(^1S) \qquad [1.4]$$

$$OH^* + OH \xrightarrow{\gamma_5} H_2O + O(^1S)\ , \qquad [1.5]$$

where O_2^* and OH^* are vibrationally excited. This was also the case for the reaction

$$NO^* + N \xrightarrow{\gamma_6} N_2 + O(^1S)\ , \qquad [1.6]$$

proposed by Young and Clark (1960). These were refuted by Dalgarno (1963) mainly on the grounds that the vibrational energy would mostly be converted to translational energy in atom-molecule collisions (Bates, 1955).

Problems with the Chapman mechanism as the source of the lower $O(^1S)$ layer surfaced due to two developments. The first was that most of the oxygen association was found to be due to the catalytic action of hydrogen (Nicolet, 1964, 1971; Thomas and Bowman, 1972), and the density of atomic oxygen in the region was less than supposed. This would make the number of associations with oxygen as the third body considerably larger. The second was of more importance. The rate coefficient for Reaction [1.1] (γ_1) was determined to be less than 8.0×10^{-38} cm^6 s^{-1}, and quenching of $O(^1S)$ by O_2, Reaction [1.2], was 2.7×10^{-15} cm^3 s^{-1} (Barth and Hildebrandt, 1961). The agreement with the value from Kvifte and Vegard (1947) for the quenching rate gave some confidence in the value for γ_1, which is lower than the value required to explain the nightglow emission.

These problems with the Chapman mechanism led to the suggestion of a two step mechanism with excited O_2 (Barth, 1961, 1962, 1964). The two step process starts with an association reaction,

$$O(^3P) + O(^3P) + M \xrightarrow{\gamma_7} O_2^* + M \,. \qquad [1.7]$$

This reaction would then be followed by an excitation transfer process,

$$O_2^* + O(^3P) \xrightarrow{\beta_8} O_2 + O(^1S) \,. \qquad [1.8]$$

The excited O_2 from Equation [1.7] is thought to be in one of four possible states: $c^1\Sigma_u^-$, $A'^3\Delta_u$, $A^3\Sigma_u^+$, or $^5\Pi_g$. These states have been debated in several reviews (see Bates, 1978, 1981, 1988; Torr and Torr, 1982) and will be discussed later.

The loss of O_2^* given in Equation [1.8] is in competition with several other loss mechanisms. The radiative loss is given by,

$$O_2^* \xrightarrow{A_9} O_2 + h\upsilon \,. \qquad [1.9]$$

Other quenching losses would be given by

$$O_2^* + M \xrightarrow{\beta_{10}} O_2 + M \,, \qquad [1.10]$$

where M is not $O(^3P)$ and

$$O_2^* + O(^3P) \xrightarrow{\beta_{11}} O_2 + O(^3P \text{ or } ^1D) \,. \qquad [1.11]$$

This set of reactions allows an effective production rate for $O(^1S)$ to be determined as $\gamma_B[O]^3$ where γ_B is ,

$$\gamma_B = \frac{\gamma_7\beta_8[M]}{(\beta_8 + \beta_{11})[O] + \beta_{10}[M] + A_9} , \qquad [1.12]$$

as given by Bates (1979).

The greenline photon emission rate is less than the excitation rate from either the Chapman or Barth mechanisms due to collisional deactivation of the $O(^1S)$. Particular attention was given by Atkinson and Welge (1972) to

$$O(^1S) + N_2 \xrightarrow{\beta_{13}} O(^3P \text{ or } ^1D) + N_2 \quad \text{and} \qquad [1.13]$$

$$O(^1S) + O_2 \xrightarrow{\beta_{14}} O(^3P \text{ or } ^1D) + O_2 . \qquad [1.14]$$

They found β_{13} to have an upper limit of $5. \times 10^{-17}$ cm^3 s^{-1}, in agreement with Young, Black, and Slanger (1969). For β_{14} they determined a value of

$$\beta_{14} = 4.9 \times 10^{-12} \exp\left(\frac{-1700}{RT}\right) cm^3 s^{-1} , \qquad [1.15]$$

which is consistent with the value found by Zipf (1967) at 300 K of 2.1×10^{-13} cm^3 s^{-1}. This was confirmed by Slanger, Wood, and Black (1972) with a value of

$$\beta_{14} = 4.0 \times 10^{-12} \exp\left(\frac{-1730}{RT}\right) cm^3 s^{-1} . \qquad [1.16]$$

Slanger and Black (1981) identified the state of the O_2 in the quenching reaction to be $O_2(^1\Delta_g)$.

Deactivation of $O(^1S)$ by $O(^3P)$ was proposed by Olsen (1973) to occur mainly by

$$O(^1S) + O(^3P) \xrightarrow{\beta_{17}} O(^1D) + O(^1D) + 2.55\ eV\ . \qquad [1.17]$$

While the earlier measurements by Kvifte and Vegard, 1947) gave a value of 4×10^{-13} $cm^3\ s^{-1}$ regardless of the state of the products, Felder and Young (1972) found the rate to be 7.5×10^{-12} $cm^3\ s^{-1}$ at 300 K. Measurements by Slanger and Black (1976a) for Equation [1.17] gave β_{17} to be

$$\beta_{17} = 5.0 \times 10^{-11} \exp\left(\frac{-610}{RT}\right) cm^3\ s^{-1}\ , \qquad [1.18]$$

which agrees well with a single measurement made by Lorents and Huestis (1975).

On the basis of measured profiles of $O(^3P)$ and laboratory rate coefficients, Slanger and Black (1977) concluded that only the Barth mechanism would reproduce the observed $O(^3P)$ data. A study by Thomas et al. (1979) supported these conclusions and a theoretical study led Bates (1979) to present arguments supporting the Barth mechanism over the Chapman mechanism. The study of Thomas (1981) used simultaneous nighttime measurements of atomic oxygen densities, 5577Å greenline emission and the Hertzberg I bands of O_2 to support the Barth mechanism and show that $O(^3P)$ may not be the predominant quencher of $O(^1S)$.

Since the Barth mechanism is the generally accepted method of production of the $O(^1S)$ in the lower thermosphere, attention has been given to determining which of the four possible O_2^* states is produced in Equation [1.7]. Of these states, Thrush and Stott (1987) have evidence which shows that $O_2(A,v\geq6)$ can be a precursor for $O(^1S)$ but $O_2(A,v<6)$ and $O_2(A',v=2,3,4)$ are not. This along with the oxygen-argon afterglow studies of Slanger and Black (1976b) precludes these two states as being possible precursors for $O(^1S)$. The measurements of Slanger and Black (1976b) indicate support for $O_2(c)$ as the precursor in the afterglows and are consistent with it being the nightglow precursor.

The $O_2(^5\Pi_g)$ state is favored as the precursor by Wraight (1982) and Krasnopolsky (1986). The $O_2(c)$ state is thought to be the precursor since it can produce $O(^1S)$ for $O_2(c,v\geq2)$. In comparison, the Venus atmosphere where the greenline emission is very weak, $O_2(c)$ is in the $v = 0$ level. But, $O_2(^5\Pi_g)$ can meet the requirements for the precursor in the atmospheres on Venus and the Earth if the quenching for the precursor by CO_2 is very effective (Krasnopolsky, 1986). While $O_2(^5\Pi_g)$ is not significant as a precursor in the afterglows of Slanger and Black, its importance in the nightglow as a precursor of $O(^1S)$ is not known and has no obvious difficulty except the lack of positive evidence (Bates, 1988).

The Photodissociation of O_2 by radiation short of 1334Å could provide an additional source of $O(^1S)$ in the dayglow. Early estimates for the dayglow were given as 5 Rayleighs (R) (Bates and Dalgarno, 1954), with an upper limit of 15 R (Walker, 1965). Wallace and McElroy (1966) using data from Metzger and Cook (1964) placed the resulting luminosity below 150 km. Hays and Sharp (1973) found better agreement between 120 km and 150

km for twilight rocket data by using this additional source. This source will be discussed further in the section on the upper layer of 5577Å emission.

Higher-altitude component. The higher altitude layer of the 5577Å emission peaks in the F-region of the ionosphere. In addition to being much higher than the lower peak it is weaker and much broader, especially at night. Unlike the lower layer, which is attributed to a single source mechanism, the higher layer has several source mechanisms that are effective over various altitude ranges. Each of these proposed reactions will now be discussed.

Photoelectron impact on atomic oxygen,

$$O(^3P) + e_p \xrightarrow{\gamma_{19}} O(^1S) + e_p \,, \qquad [1.19]$$

is an important source of $O(^1S)$ in the thermosphere (Wallace and McElroy, 1966). In fact, this is a dominant source of $O(^1S)$ in the dayglow. The production rate for this reaction is a function of atomic oxygen density, [O] , given by:

$$P_{19} = [O] \int f_e(E_e) \sigma(E_e) dE_e \,. \qquad [1.20]$$

The integral over electron energy E_e contains the photoelectron flux, f_e, and σ, the cross section for electron impact, both of which are functions of electron energy.

Feldman *et al.* (1971) used simultaneous rocket measurements of photoelectrons and the 5577Å emission made by Doering *et al.* (1970), and showed this reaction to be minor below 250 km and to account for half of the emission above 250 km. Twilight studies by Hays and Sharp (1973) showed

the electron impact source to be important above 190 km and dominant above 260 km. This was also supported by Frederick *et al.* (1976) using multiparameter Atmosphere Explorer Satellite observations.

The cross section for electron impact excitation of $O(^1S)$ has been measured by Shyn *et al.* (1986) and Doering and Gulcicek (1989). The magnitudes of the cross section obtained by Shyn *et al.* are higher than the previous theoretical results (Smith *et al.*, 1967; Henry *et al.*, 1969; Thomas and Nesbet, 1975 and Vo Ky Lan *et al.*, 1972) by a factor of about 2, while those by Doering and Gulcicek (1989) are higher by a factor of approximately 1.5. Parameterized values of the cross section for the excitation of $O(^1S)$ determined from the values by Smith *et al.* (1967) and later supported by Henry *et al.* (1969) have been given by Green and Stolarski (1972). Recent theoretical calculations by Berrington and Burke (unpublished data) are in good agreement with those of Henry *et al.* (1969) and have uncertainties of 10-20% (Berrington, 1991). Figure 1.3 is a plot of the theoretical and laboratory values of the electron impact cross sections for atomic oxygen.

The dissociative recombination reaction for O_2^+,

$$O_2^+ + e_t \xrightarrow{\gamma_{21}} O(^1S) + O \ , \qquad [1.21]$$

is known to be an important contributor to the green line emission at higher altitudes and the only source in the nightglow. Dissociative recombination was suggested as an important process to explain the observed nightglow spectrum by Kaplan (1931). The general mechanism for this reaction was discussed by Bates and Massey (1947), who described the observed electron recombination rates. The importance to 5577Å emission in the thermosphere was suggested by Nicolet (1954).

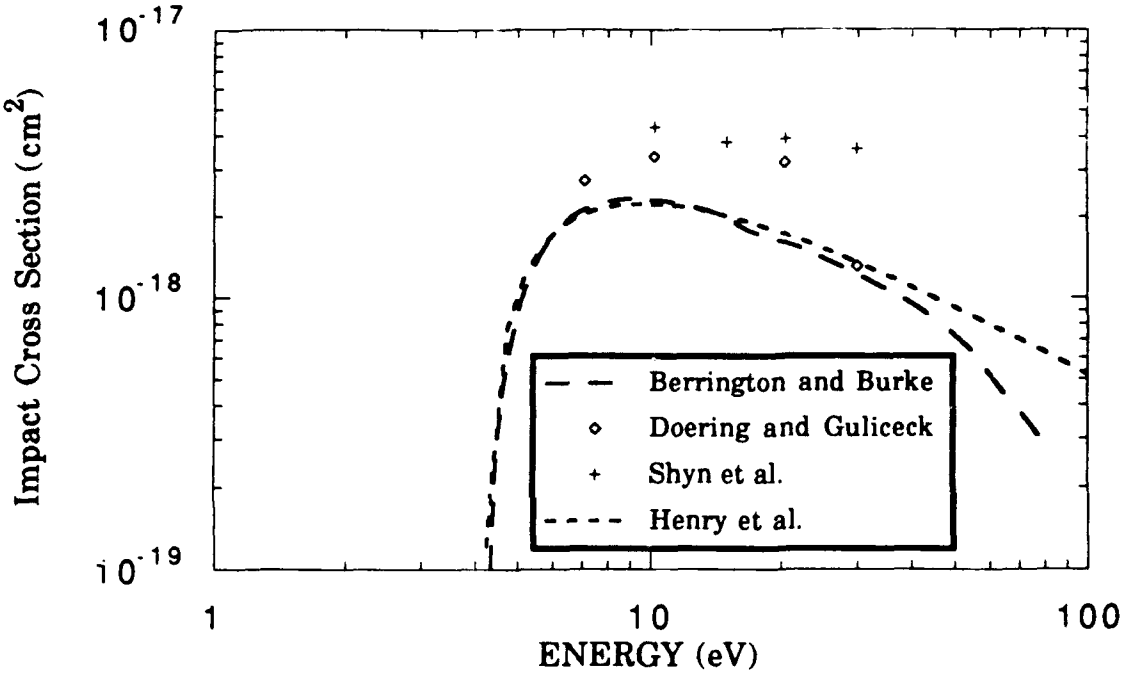

Figure 1.3 Various cross sections for electron impact on atomic oxygen. Lines are theoretical determinations while symbols are experimental.

This reaction has been studied extensively in the past by using thermospheric nightglow measurements (Hernandez, 1971; Hays and Sharp, 1973; Frederick *et al.*, 1976; Kopp *et al.*, 1977; Sharp and Torr, 1979; O'Neil *et al.*, 1979; Zipf, 1979; Abreu *et al.*, 1983; Killeen and Hays, 1983; Yee and Killeen, 1986; Yee *et al.*, 1989; Takahashi *et al.*, 1990) where it is the only production mechanism for 5577Å emission. Numerous laboratory studies have been carried out for this mechanism (Mehr and Biondi, 1969; Walls and Dunn, 1974; Zipf, 1980; Bates and Zipf, 1980; Guberman, 1987; Rowe and Queffelec, 1989; Queffelec *et al.*, 1989; Guberman, 1989). The amount of $O(^1S)$ produced by the dissociative recombination is dependent on the vibrational excitation of the O_2^+ and is not conclusively known. The various studies and their findings have been reviewed and summarized by Bates (1990).

The production rate for $O(^1S)$ from this reaction is,

$$P_{21} = \beta_{21} k_{21} [O_2^+][e_t] \ . \qquad [1.22]$$

The total reaction rate as a function of electron temperature,

$$k_{21} = 1.6 \times 10^{-7} \left(\frac{300}{T_e} \right)^{0.55} , \qquad [1.23]$$

is given by Torr *et al.* (1976). This expression, derived from measurements taken by the Atmosphere Explorer Satellite AE-C, has been shown to agree well with the measurements of Walls and Dunn (1974) and other laboratory measurements as discussed by Walls and Dunn (1974). Mul and McGowan (1979) concluded that the total rate coefficient is not substantially affected by the vibrational excitation of the O_2^+ ion.

The branching ratio for this reaction, β_{21}, is not well known. Early results of aeronomical studies under various conditions varied but were typically less than 0.10 (Hernandez, 1971; Hays and Sharp, 1973; Frederick *et al.*, 1976; Kopp *et al.*, 1977; Sharp and Torr, 1979; O'Neil *et al.*, 1979; Zipf, 1979). These determinations of the production of $O(^1S)$ are not in agreement with the *ab intio* calculations of Guberman (1987, 1989) (Zipf, 1988; Yee *et al.*, 1989; Bates, 1990). Paxton (1983) used the values of the branching ratios known on Earth to deduce unknown branching ratios for other channels from observations of the upper atmosphere of Venus.

From theoretical considerations, the major channel for the production of $O(^1S)$ is from the v=2 level of the O_2^+ ion (Guberman, 1987; 1989). This was supported by Killeen and Hays (1983) and Yee and Killeen (1986) from studies using the Fabry-Perot on the Dynamics Explorer satellite to study the nonthermal line profiles of $O(^1S)$. The quantum yield of $O(^1S)$, β_{21}, as a function of the vibrational population of O_2^+, can be expressed in terms of the ratio of electron density to atomic oxygen ,

$$\beta_{21} \propto \frac{[e_t]}{[O]}\left(\frac{300}{T_e}\right)^{0.7} , \qquad [1.24]$$

as discussed in Abreu *et al.* (1983) and Yee *et al.* (1989).

The energy transfer reaction of $N_2(A^3\Sigma_u^+)$ by atomic oxygen,

$$N_2(A^3\Sigma_u^+) + O(^3P) \xrightarrow{\gamma_{25}} N_2 + O(^1S) , \qquad [1.25]$$

can produce a major portion of the $O(^1S)$ at altitudes near the peak in the thermospheric emission layer. First proposed as an auroral source by Vegard and Tonsberg (1937) and later rejected by Vegard (1939), this

reaction was not considered to be important until the laboratory measurements by Meyer *et al.* (1969,1970). As a source of $O(^1S)$, this reaction was considered to be a minor source by Frederick *et al.* (1976). The total rate coefficient used was 3.0×10^{-11} cm^3 s^{-1} (Hunten and McElroy , 1966; Meyer *et al.*, 1970). The value of the branching ratio in Frederick's model was 0.10, which was chosen to be consistent with auroral observations at that time (Frederick *et al.*, 1976).

The N_2 (A) state is produced both directly by photoelectron impact and indirectly by cascading from higher excited states of the nitrogen molecule. The effective rate of production of $O(^1S)$ from this reaction,

$$P_{25} = \beta_{25} k_{25} [N_2(A^3 \Sigma_u^+)][O] , \qquad [1.26]$$

can be expressed as a product of the total rate coefficient for the production of all states of atomic oxygen and the quantum yield or branching ratio for the amount produced in the $O(^1S)$ state. The branching ratio, β_{25}, is not well known and there is still some disagreement in the total rate for this reaction, k_{25}, as well. Table 1.1 is a list of some of the rate coefficients and branching ratios for this reaction that have been determined by previous studies.

Total reaction rates measured by Piper *et al.* (1981) for the quenching of the υ = 0,1 states of $N_2(A)$ by O and recent measurements by Thomas and Kaufman (1985) for the υ = 0,1,2,3 states of $N_2(A)$ show that as the vibrational level increases, the rate constant for the energy transfer reaction also increases. The two production mechanisms of $N_2(A)$ tend to fill different vibrational levels in the excited state. Direct excitation from the ground state of the N_2 molecule by electron impact will preferentially fill the

Total Rate ($\times 10^{-11}$ cm^3 s^{-1})	Branching Ratio	Study	Comments
3.0	0.10	Frederick et al.	Branching ratio set to match auroral determination
υ=0 3.5±0.6 υ=1 4.1±0.5 υ=2 4.6±0.6 υ=3 5.2±0.8		Thomas and Kaufmann	Laboratory study
υ=0 2.8±0.4 υ=1 3.4±0.6	0.75±0.13	Piper et al.	Laboratory study
υ=0 2.8 υ=1 3.3 υ=2 3.6	0.75	De Souza et al.	Laboratory study
0.57	0.30	O' Neil et al.	Artificial Aurora Experiment
12.0	0.30 0.45	Sharp and Torr	For υ=0,1 For υ=0,1,2

Table 1.1 List of various rate coefficients and branching ratios for Reaction [1.25].

higher vibrational levels, while cascading from the $B^3\Pi_g$ state and above tend to populate the lower levels (Ahmed, 1969; Cartwright *et al.*, 1971,1973;Cartwright, 1978). The total rate coefficient for the reaction will depend on the vibrational population distribution of the $N_2(A)$ molecules, regardless of the final state of atomic oxygen produced.

Using laboratory measurements, Piper (1982) determined a branching ratio for the production of $O(^1S)$ of 0.75±0.13 from the $\upsilon = 0,1$ states of $N_2(A)$. This value is supported by laboratory measurements carried out by De Souza *et al.* (1985). Use of the laboratory determined branching ratios under auroral conditions would produce an excessive amount of $O(^1S)$, as pointed out by McDade and Llewellyn (1984). The quantum yield of this reaction of about 0.30 has been deduced by O'Neil *et al.* (1979) for auroral production during the artificial auroral experiment, Precede. Studies by Sharp and Torr (1979) supported this value for the $\upsilon = 0,1$ levels of $N_2(A)$, and by including the $\upsilon = 2$ vibrational level they found the branching ratio increased to 0.45.

Photodissociation of O_2, whose possible importance was pointed out by Bates and Dalgarno (1954),

$$O_2 + h\nu \xrightarrow{\gamma_{27}} O(^1S) + O \ , \qquad [1.27]$$

is a very minor source for the production of $O(^1S)$ at altitudes above 140 km. However, this reaction becomes the dominant source at 120 km (Hays and Sharp, 1973). The cross sections for this reaction have been given by Lawerence and McEwan (1973). The rate for this reaction as a function of O_2 density is,

$$P_{27} = [O_2]\int f(\lambda)q(\lambda)\sigma(\lambda)d\lambda \ , \qquad [1.28]$$

where $f(\lambda)$ is the attenuated solar flux, $\sigma(\lambda)$ is the photodissociation cross section, and $q(\lambda)$ is the quantum yield of $O(^1S)$ all as a function of wavelength, λ. An expression for the attenuated solar flux is

$$f(\lambda) = f_\infty(\lambda)\exp\left(-\sum_i \int \sigma_{ai}(\lambda)n_i(s)\,ds\right) , \qquad [1.29]$$

where s is the distance along the path from the sun to the point in the atmosphere, $f_\infty(\lambda)$ is the unattenuated solar flux, $\sigma_{ai}(\lambda)$ is the total absorption cross section, and $n_i(s)$ is the number density of the ith species along the path. The species included in the solar flux attenuation are atomic oxygen, O_2 and N_2.

Ion-atom interchange between O_2^+ and atomic nitrogen,

$$O_2^+ + N \xrightarrow{\gamma_\infty} O(^1S) + NO^+ \ , \qquad [1.30]$$

was considered by Frederick *et al.* (1976) as the required additional source of $O(^1S)$ at low altitudes. The rate of production for this process is,

$$P_{30} = \beta_{30}\, k_{30}[O_2^+][N] \ . \qquad [1.31]$$

Atomic nitrogen was found to have a diurnal variation that matched the variation of $O(^1S)$ observed at sunset and sunrise (Kopp *et al.*, 1977). A rate coefficient, k_{30}, of 2.5×10^{-11} $cm^3\ s^{-1}$ was used by Frederick *et al.* (1976) for the analysis of the 5577Å dayglow. The uncertainties in the nitrogen density gives a range for the rate coefficient from 1.2×10^{-11} to 5.0×10^{-11}

$cm^3\ s^{-1}$ (Frederick *et al.*, 1976). This reaction may or may not be significant for the production of 5577Å emission depending on the solar flux and the impact cross section for electrons on atomic oxygen.

Another ion exchange reaction, between N^+ and O_2,

$$N^+ + O_2 \longrightarrow NO^+ + O(^1S)\ , \qquad [1.32]$$

was suggested by Strobel *et al.* (1975). It is unlikely that this reaction will produce any appreciable amount of $O(^1S)$ (Tully *et al.*, 1971). The N^+ and O_2 exchange mechanism has a total rate coefficient of 6×10^{-10} $cm^3\ s^{-1}$ (Howorka *et al.*, 1980) and 43 ± 5 % of the reactions form atomic oxygen (Smith *et al.*, 1978; Howorka *et al.*, 1980). However, less than 0.1 % of the atomic oxygen is in the form of $O(^1S)$ (Langford *et al.*, 1986).

Other mechanisms that have been investigated or suggested as possible sources for the upper layer include,

$$N(^2D) + NO \longrightarrow N_2 + O(^1S)\ , \qquad [1.33]$$

which was investigated by Frederick *et al.* (1976) and then rejected since it did not fit the observations. For the region below 120 km, the source responsible for the lower layer was suggested but due to the low densities it is unlikely that either the Chapman or the Barth mechanism will produce any appreciable amount of 5577Å emission. The Chapman mechanism is especially doubtful since it also has a small rate coefficient.

The loss processes of $O(^1S)$ at the level of the thermospheric emission are the radiative transitions to the $O(^1D)$ and $O(^3P)$ states,

$$O(^1S) \xrightarrow{A_{34}} O(^1D) + h\nu(5577\text{Å}) \qquad [1.34]$$

$$O(^1S) \xrightarrow{A_{36}} O(^3P) + h\nu(2972\text{Å}) , \qquad [1.35]$$

with transition probabilities of 1.06 s^{-1} and 0.045 s^{-1}, respectively (Kernahan and Pang, 1975). Losses of $O(^1S)$ due to quenching are not important at the altitudes of the upper thermospheric emission. The same quenching reactions (Equations [1.13], [1.14], and [1.17]) as occur in the lower layer may have some effect below 125km.

Auroral $O(^1S)$. The study of the 5577Å emission in the airglow stemmed from observational investigations of the aurora. The emission in the aurora has similar source reactions to the upper airglow layer also includes the quenching of the lower layer. This section briefly summarizes the auroral emission as it compares to the other airglow reactions.

While electron impact on atomic oxygen is a major source of $O(^1S)$ in the daytime airglow, it is usually of minor importance in aurora. In auroral spectra, both the greenline at 5577Å and the red line at 6300Å of atomic oxygen are strong. In laboratory studies, however, the red line is absent, which led Vegard (1932) to doubt the direct mechanisms for production of $O(^1S)$. Based on the present knowledge of impact cross sections, Gattinger *et al.*, (1985) concluded that direct electron impact (Equation [1.19]) is of minor importance in the aurora.

Dissociative recombination of O_2^+ (Equation [1.21]) was suggested as a small source by Dalgarno and Khare (1967) when it was shown that the loss of slow secondary electrons to thermal electrons in the aurora could compete strongly with Reaction [1.19]. On the basis of two rocket flights,

Donahue *et al.* (1968) found the secondary electron flux to be much too small to account for the measured 5577Å emission. They examined the possible source from fast electron impact dissociation of molecular oxygen,

$$O_2 + e_p \longrightarrow O + O(^1S) . \qquad [1.36]$$

They also found that this reaction would require an unrealistically large cross section of $\sim 10^{-16}$ cm^2, while Zipf had determined the cross section to be less than 2×10^{-17} cm^2 (Vallance Jones, 1974). Donahue *et al.* (1968) concluded that dissociative recombination (Equation [1.21]) was the major source. Using rocket-borne instruments Parkinson et al. (1970) found that Reaction [1.21] could explain the 5577Å emission at the altitude of the F1 layer, but near the peak of the emission there was insufficient O_2^+ to account for the emission.

This led to the consideration of indirect sources of $O(^1S)$. It was shown by Olmholt (1971) that any indirect source will have a time constant of the order of that for radiative decay. Several indirect sources have been investigated and have been shown to be minor sources. The exception to this is the quenching of $N_2(A)$ by atomic oxygen (Equation [1.25]) as discussed above.

Other proposed reactions to produce $O(^1S)$ include the dissociation of O_2 by EUV photons created by the impact of electrons on N_2 (Zipf, 1973). However, laboratory studies of Zipf and McLaughlin (1978) demonstrated that the EUV photons are resonantly trapped by N_2, causing it to predissociate to atomic nitrogen. Also, Park *et al.* (1977) found the auroral intensity between 950Å and 1100Å was inadequate for the $O(^1S)$ production.

Yau and Shepherd (1979) and Solheim and Llewellyn (1979) pointed out that the electron impact cross section for O_2 to the $A^3\Sigma_u^+$, $C^3\Delta_u$, and $c^1\Sigma_u$ states are large (Watson et al., 1967; Konishi et al., 1970; Vallance Jones, 1974) but that the Herzberg bands are not enhanced in the aurora. Yau and Shepherd (1979) suggested that collisional excitation $O(^1S)$ by these states may be important. Until the mechanisms for the quenching of $O(^1S)$ are understood, the importance of this reaction will not be quantified. The source may not be needed to explain the observed profiles of 5577Å emission, or it may just alter the efficiency required for Reaction [1.25].

As can be seen, the complete answer for any one of the three components of the 5577Å emission is not well known. As new information about any of the reactions becomes available, the emission has to be remodeled. This is compounded since a change in the accepted chemistry in one region can affect the accepted chemistry in the others. Any changes in one region must be consistent with the chemistry in the others.

1.2.3 Measurement Techniques

Various instruments and platforms have been used to study airglow emissions. Photometers provide measurements of the relative strength of atomic and molecular emissions, which can be related to the number densities of the source species. A spectrometer can give information on the intensities of vibrational-rotational bands. The relative intensities of the lines in a band can be related to the rotational temperature of the emitter, which if the emitter is a meta-stable species may be directly indicative of the kinetic temperature. Wind velocities can be determined from line position, and temperatures may be derived by the analysis line width with an interferometer. All of these instruments have been used in studies from

ground based observatories, as rocket borne instruments and on numerous satellites. Measurements of the 5577Å "auroral" green line from these various instruments provide a large amount of the information on the lower thermosphere. This section will review the history of observations of the 5577Å emission by these different means.

Observations of the 5577Å airglow emission from the ground naturally extends from auroral observations. Early history of the aurora and visible observations of emissions is given in the monograph by Eather (1980). Estimates of the auroral altitude were given by Cavendish in 1784 and spectral observations were carried out by Ångstrom in 1868, as mentioned earlier. In 1910 Stomer made the first studies of the aurora using the photographic triangulation technique (Vallance Jones, 1974). Visual reports of the aurora were used to augment mapping of the auroral zone as late as 1957-1958 (Millman, 1968).

Ground based studies of the airglow cannot be used to determine altitude variations but can be used in studies of the long term changes and morphology of the greenline. In studying the green line from the ground, the strong emission layer at about 95 km hampers observations of the upper layer in the F-region. Photometric studies from the ground include Smith and Steiger (1968), Wiens and Weill (1973), Fukuyama (1976; 1977a; and 1977b), Misaua and Takeuchi (1978), Freund and Jacka (1979), Armstrong (1982), Takahashi *et al.* (1977, 1984, 1985), and Saito and Kiyama (1988). Photographic and imaging studies have been carried out by Moreels and Herse (1977), Armstrong (1982) and Taylor *et al.* (1987). Freund and Jacka (1979), Cogger *et al.* (1985), Weins *et al.* (1988), and Lloyd *et al.* (1990) have also performed ground based interferometer studies of the 5577Å emission.

Rockets provide the opportunity to gain high resolution data of emission profiles with height. They also make it possible to study the airglow emissions in the daytime and at twilight. Rockets have the advantage over ground based studies of being able to provide in situ measurements of the atmosphere along with the airglow information.

In spite of the short measurement time, rockets have provided many observations of the green line emission. With photometers, rockets can be used to determine variations of the emission with altitude if the rocket is traveling vertically and the emission is stable. Rocket based instruments can be used to scan the emission but the analysis of the data becomes more difficult.

Rockets have been used to observe the 5577Å green line emission in airglow and aurora. Measurements of the nightglow have been reported by Berg *et al.* (1956), Koomen *et al.* (1956), Heppner and Meridith (1958), Tousey (1958), Cooper *et al.* (1960), Packer (1961), Huruhata *et al.* (1962), Tarasova (1963), O'Brien *et al.* (1965), Greer and Best (1967), Baker and Waddoups (1967, 1968), Gulledge *et al.* (1968), Danderkar and Turtle (1971), Offermann and Drescher (1973), Kulkarni (1967), Thomas, L. *et al.* (1979), Thomas, R. J. (1981), Lopez-Moreno *et al.* (1982), Greer *et al.* (1986) and Kita *et al.* (1988). Twilight and dayglow measurements of the OI 5577Å have been presented by Silverman *et al.* (1964), Wallace and Nidey (1964), Wallace and McElroy (1966), Lloyd *et al.* (1968), Dandekar (1969), Feldman, Doering and Zipf (1971), Schaffer *et al.* (1972) and Hays and Sharp (1973). Coordinated satellite and rockets measurements for aurora were reported in a series of papers by Rees *et al.* (1977), Sharp *et al.* (1979), and Sharp and Torr (1979). Some characteristics of these rocket measurements are summarized in Table 1.2.

Date	Time UT	Lat (deg)	Long. (deg)	Alt (km)	Emission (R)	VER (ph/cc-s)	Reference	Notes
		32.4 N	106 W	92.5			Berg *et al.*, 1956	1
17NOV 55	0900	32.4 N	106 W	96			Koomen *et al.*, 1956	1
		32.4 N	106 W	97			Heppner and Meredith, 1958	1
		32.4 N	106 W	98			Tousey, 1958	1
6 NOV59		32.4 N	106 W	96			Cooper *et al.*, 1960	1
		32.4 N	106 W	97			Packer, 1961	1
23SEP60	0056	mid USSR		90			Tarasova, 1963	1
30OCT61		39.57 N	140 E	98			Huruhata *et al.*, 1962	1
7APR64	1413	32.4 N	106 W	95/170		300/175	Wallace and McElroy, 1966	
9JUL64	0413	37.8 N	75 W	94.5			O'Brian *et al.*, 1965	1
18OCT65	1123	30.96 N	137 E	94.8			Greer and Best, 1967	1,2
23OCT65	1300	32.4 N	106 W	97	~280	360	Gulledge *et al.*, 1968	1
28 APR66	2049	32.4 N	106 W	102	~200	145	Baker and Waddoups, 1967	1

10DEC66		31.5 N	131 E	93	~120	78	Huruhuta *et al.*, 1967	1
20AUG68	0900	59 N	94 W	86			Dandekar, 1972	1
22MAY69	1300	22.02 N	159 W	99	210	200	Dandekar and Turtle, 1971	1
13OCT70	0108	39.6 N	9 E	97.5	~160	177	Offerman and Drescher, 1973	1,2
2FEB73	1935	8 N	76.6 E	102	62	49	Kukarni, 1976	1
23JAN74	0610	58.4 N	94.1 W	90			Deans and Shepherd, 1978	
20MAR74	0413	58.4 N	94.1 W	110			Sharp *et al.*, 1979	
		57.6 N		97	~80	90	Thomas *et al.*, 1979	1
		32.4 N		96	90	140	Thomas and Young, 1981	1
		37.08 N		102	160	195	Lopez-Moreno *et al.*, 1982	1,2
		57.6 N		98, 97	121,165	140,190	Greer *et al.*, 1986	1
		31 N		95	72	75	Kita *et al.*, 1988	1
1NOV86	0159	5.8 S	35.2 W	230	52	9	Takahashi *et al.*, 1990	

1 From Nardi, 1991.
2 Contains summaries of rocket studies.

Table 1.2 Summary of rocket observations of 5577Å emissions.

Satellite observations of airglow can provide data on large scale global emission features. Satellites have the capability to provide observations equivalent to thousands of rocket launches and give the spatial coverage of hundreds of ground observatories. Due to atmospheric drag which would shorten their lifetime, satellites are not able to provide the in-situ measurements of rockets. Information can be obtained about atmospheric conditions above the satellite.

Satellites have provided measurements of the airglow emissions since the late 1960's (O'Brien, 1967; Warnecke *et al.*, 1969; Deehr and Egeland, 1972;) as cited by Vallance Jones (1974). Reed and Chandra (1975) presented measurements from the Orbiting Geophysical Observatory-4 (OGO-4) satellite. OGO-6 observations were presented by Thomas and Donahue (1972), Donahue *et al.* (1973, 1974), Donahue (1975) and Wasser and Donahue (1979). The International Satellites for Ionospheric Studies-2 (ISIS-2) satellite used simple photometers to produce scans of the aurora and airglow (Anger *et al.*, 1973; Shepard *et al.*, 1973; Cogger and Anger, 1973; Cogger and Murphee, 1980; Cogger *et al.*, 1981; Elphinstone, 1986). The Atmosphere Explorer (AE) satellite program studied aurora and airglow emissions for a period from near solar minimum to solar maximum. This satellite program is discussed in detail in Chapter 2.

The two satellite Dynamics Explorer (DE) program used a Fabry-Perot interferometer (Hays *et al.*, 1981) to measure airglow and auroral emission (Killeen and Hays, 1983). The High Resolution Doppler Imager (HRDI) on the recently launched Upper Atmosphere Research Satellite (UARS) carries a combination instrument that contains a photometer and a triple etalon Fabry-Perot that can measure 5577Å emissions (described by

Satellite	Launch Date	Instrument	Start of Data	End of Data	Orbit Inclination
OGO-4	28JUL67	Photometer	30AUG67	10JAN68	86
OGO-6	5JUL69	Photometer	9JUN69	24JUL70	~82
ISIS-2	1APR71	Photometer	23APR71	31DEC71	
AE-C	16DEC73	Photometer	16DEC73	11DEC78	~58
AE-D	6OCT75	Photometer	6OCT75	29JAN76	~90
AE-E	20NOV75	Photometer	21NOV75	07JUL81	~20
DE-2	3AUG81	Fabry-Perot	4AUG81	18FEB83	90
Intercosmos Bulgaria 1300	7AUG81	Photometer			81.9
UARS	12SEP91	Photometer/ Fabry-Perot			~58

Table 1.3 Satellite measurements of 5577Å emission.

Bucholtz, 1991). Table 1.3 summarizes some characteristics of these programs.

1.3 Statement of Thesis Problem

The major purpose of this thesis is to provide the details of the photochemical model developed for the upper layer of the 5577Å airglow emission. In presenting the background and history of the emission, the many potential source and loss mechanisms have been discussed. The relative importance of some of these reactions has not been conclusively determined. This research provides information on which reactions are required to reproduce the observations of the 5577Å dayglow made by the Atmosphere Explorer satellites.

Two reactions have been shown to be major sources of the emission in the upper layer. The photoelectron impact source [Reaction 1.19] is important at the higher altitudes of the layer, and energy transfer from Equation [1.25] becomes more important at the lower part of the layer. Both of these reactions have parameters that have not been conclusively established.

The impact cross section for Reaction [1.19] has as much as a factor of two difference in magnitude between theory and laboratory measurements. The magnitude of the cross section that best reproduces the observed data will be determined. Also, Reaction [1.25] has both a total rate coefficient and the branching ratio for the production of $O(^1S)$ that are not well known. Determinations of the branching ratio in auroral studies give relatively low values of 0.10 to 0.30, while laboratory determinations

place the value at 0.75. The model is used to determine those parameters that best reproduce the observed values of the emission.

The model is then used to study the 5577Å emission in the twilight. The model has been run for the conditions in the terminator and the results compared to the observations of the Atmosphere Explorer satellites. The output of the model is integrated to provide models of the integrated brightness which can then be compared to those observed by the satellite.

CHAPTER II

ATMOSPHERE EXPLORER SATELLITE OBSERVATIONS

2.1 Overview

The Atmosphere Explorer satellites (AE-C, -D, and -E) were used to provide measurements both of the 5577Å airglow and of atmospheric parameters to be used for the modelling of the emissions. This chapter begins with a brief history and overview of the satellite program. Next, the Visible Airglow Experiment (VAE) is described and data handling for the instrument is presented. A general discussion of the inversion methods to derive Volume Emission Rate (VER) profiles from the brightness observations is also included. The chapter concludes with a discussion of the AE instruments used to make *in situ* measurements of neutral and ionized atmospheric composition.

The Atmosphere Explorer satellite program has a rich history. The satellite program has been summarized by Burgess and Torr (1987). This review places the emphasis on the later missions, which were the first examples of problem-dedicated missions. In this case, a team approach was used to study the system of the incoming solar flux, the neutral

atmosphere and the resulting ionization. The Atmosphere Explorer team consisted of theorists and investigators making the correlated measurements required to understand this complex region of the atmosphere.

In the mid 1960's, NASA launched Explorer 17 and Explorer 32, also called AE1 and AE2. The lower thermosphere was largely unknown and the need to study this region specifically led to the Atmosphere Explorer Program. The program consisted of three satellites designated AE3, AE4, and AE5 (or AE-C, -D, and -E).

The purpose of the Atmosphere Explorer program was to provide simultaneous measurements of the parameters needed to study the physical processes that govern the lower thermosphere and ionosphere. Three satellites were required to provide the measurements, each with different orbital characteristics. The spacecraft were to occupy elliptical orbits during the first year with perigee as low as 135 km and apogee about 4000 km, and subsequently the orbits were to be circularized. Each satellite had a propulsion system that would maintain the orbit both during the elliptical phase and during the circular phase where the altitude could be adjusted. Table 2.1 is a listing of the history of the orbital altitudes for the satellites. Even during the circular phase, the altitude of the satellites could vary by a few kilometers during a single orbit.

The orbital inclinations of the three satelites were chosen to provide different spatial and temporal coverages. The inclination of AE-C was to be at about 68, degrees which allowed measurements of low and midlatitudes for a range of local times. AE-D was a polar orbiting satellite with an inclination near 90 degrees. Where AE-C could study the thermosphere with good local time coverage, AE-D's high inclination allowed a complete

Dates	AE-C		AE-D		AE-E	
	Orbit Type	Perigee (km)	Orbit Type	Perigee (km)	Orbit Type	Perigee (km)
12/73-11/74	Elliptical	150				
12/74-9/75	Circular	250				
10/75-11/75	Circular	300	Elliptical	150		
12/75-1/76	Circular	300	Elliptical	150	Elliptical	150
2/76-10/76	Circular	300			Elliptical	150
11/76-2/77	Circular	270			Circular	250
3/77-12/77	Circular	400			Circular	270
1/78-11/78	Circular	350			Circular	350
12/78-12/79					Circular	450
1/80-12/80					Circular	400
1/81-5/81					Circular	300

Table 2.1 Orbital history of the Atmosphere Explorer satellites. Perigee altitudes are approximate. Elliptical orbital eccentricities are between 0.05 and 0.25, Apogees from 400 to 2200 km.

latitudinal coverage. AE-E was placed in an orbit of about 20 degrees, which allowed continuous measurements at low latitudes to be used in correlative studies with the incoherent backscatter station at Arecibo, Puerto Rico. The effects of perigee drift for each satellite as a function of local time and latitude is illustrated in Figure 2.1.

The satellites each carried a variety of instruments for remote sensing and in-situ measurements of the atmosphere. These instruments included various spectrometers, photometers and ion probes. Listed in Table 2.2 is the various instruments used on the different satellites. These instruments are reviewed in a special issue of Radio Science (Volume 8, Number 4, 1973). The satellites were initially launched with a minimum design lifetime of one year. AE-C and AE-E exceeded this by many years, but AE-D failed totally after a few months and never reached the circular phase of the mission. Table 2.3 is a summary of the orbital characteristics for each satellite.

The satellites were spin stabilized and could be used in either a spinning or despun mode. In the spinning mode, the satellite rotated with a period of 15 seconds, with the spin vector either parallel or antiparallel to the orbit normal. This mode enabled the instruments to sweep through all angles of attack within each spin period. In the despun mode, the satellite would rotate once per orbit in order to maintain the same attitude for the instruments relative to the local horizon.

A major achievement for the Atmosphere Explorer program was the handling of the data stream from the spacecraft. The Data was received from the spacecraft and processed in near real time to allow investigators to modify the mission plans quickly in order to take advantage of any observations that were found to address particular aeronomic problems.

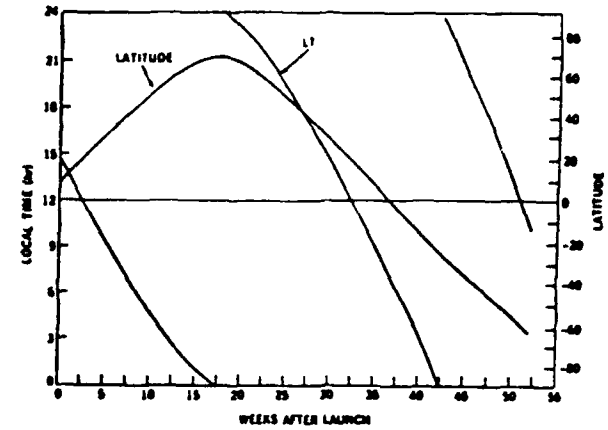

AE-C

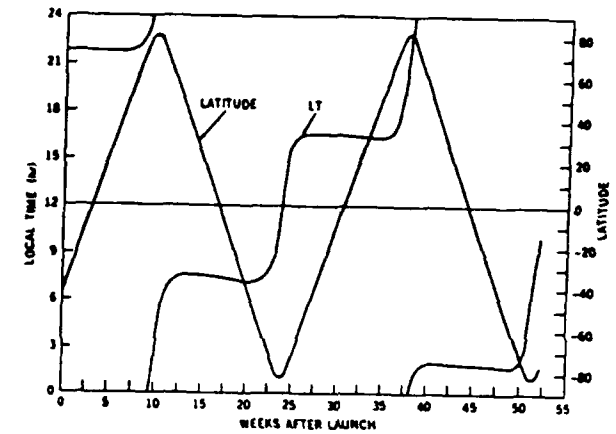

AE-D

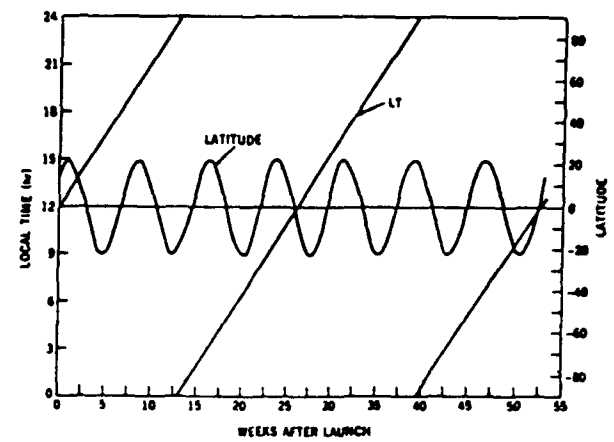

AE-E

Figure 2.1 Perigee drifts for the Atmosphere Explorer satellites. Altitudes ranged from 150 to 4000 km. (From Dalgarno et al., 1973)

Instrument	Acronym	Satellite	Detector	Parameters
Solar EUV Spectrometer	EUVS	C,D,E	Channel Electron Multipliers	140 to 1850 Å
Solar EUV Filter Photometer	ESUM	C,D,E	Spiraltron Electron Multitpiers and EUV diodes	40 to 1300Å
UV Nitric Oxide	UVNO	C,D	Photomultiplier Tubes	2150 to 2190Å
Visible Airglow Photometer	VAE	C,D,E	Photomultiplier Tubes	6300,5577,4278,3371, 5200,7319 to 7330Å
Open Source Neutral Mass Spectrometer	OSS	C,D,E	Electron Multiplier	1 to 46 AMU
Closed Source Neutral Mass Spectrometer	NACE	C,D,E	Electron Multiplier	1 to 46 AMU
Neutral Atmospheric Temperature Experiment	NATE	C,D,E	Electron Multiplier	T_g, N_2, V_w
Atmospheric Density Accelerometer	MESA	C,D,E	Accelerometer	Neutral Density
Planar Ion Trap	RPA	C,D,E	Electrometer	T_i, N_i, M_i, Drift Velocity
Cylindrical Electrostatic Probe	CEP	C,D,E	Electrometer	T_e, N_e, N_i, M_i
Magnetic Ion Mass Spectrometer	MIMS	C,D	Electron Multiplier	1 to 64 AMU
Positive Ion Mass Spectrometer	BIMS	C,E	Electrometer	0.5 to 72 AMU
Low Energy Electron Experiment	LEE	C,D	Spiraltron Electron Multipliers	0.2 to 25 keV
Photoelectron Spectrometer	PES	C,D,E	Johnson Electron Multiplier	Photoelectron Spectra
Capacitance Manometer		C,D,E	Electrometer	Pressure
Cold Cathode Ion Gage Range		C,D,E	Diaphragm	Pressure
Temperature Alarm		C,D,E	Grid Wire	Aerodynamic Heating

Table 2.2 Instrument package lists for the Atmosphere Explorer satellites.

Satellite	Launch Date	Re-entry date	Circular Phase	Orbital Inclination
C	13DEC73	12DEC78	DEC74	68
D	6OCT75	12MAR76	-	90.1
E	20NOV75	10JUN81	NOV76	19.9

Table 2.3 Satellite mission parameters for Atmosphere Explorer.

The data from the Atmosphere Explorer program is available in different formats. The complete database known as the Unified Abstract database contains 15 second averages of the data from all of the various instrument and other important geophysical parameters. This database is available on tapes provided by the National Space Science Data Center (NSSDC) or through the Space Physics Analysis Network (SPAN). Higher resolution databases are available for each of the instruments on magnetic tape and/or in some cases on microfilm plots. These databases and their applicability to the airglow model will be discussed later.

The Atmosphere Explorer satellites were very successful. Most of the instruments provided data for much longer than the expected lifetime of the satellites, and due to the built-in redundancy failures could be replaced by other instruments. The knowledge of the structure, chemistry and dynamics of the upper atmosphere was greatly advanced by this program and provided the opportunity for correlative observations by hundreds of rockets flights and several other satellite programs. The data from the Atmosphere Explorer satellites is still used to study the upper atmosphere and is still being published. The AE measurements have also been employed by semi-empirical models like the Mass Spectrometer and Incoherent Scatter (MSIS) model.

2.2 The Visible Airglow Experiment

2.2.1 Instrument Description

The Visible Airglow Experiment (VAE) was flown on all three of the Atmosphere Explorer satellites and has been described by Hays *et al.* (1973)

and by Burgess and Torr (1987). The instrument consisted of a simple two channel filter wheel photometer similar to that flown on the ISIS-B program (Burgess and Torr, 1987). It was designed to monitor dayglow, nightglow and auroral emissions in the upper atmosphere. The results of previous studies using the VAE instrument have been summarized by Hays *et al.* (1988).

In the VAE instrument, shown in Figure 2.2, the two channels were perpendicular to each other and oriented in the satellite such that in the despun mode channel 1 was pointed back along the satellite track and channel two looked either up (radially out from the Earth) or down (radially in) depending on whether the satellite was in the normal or inverted position, respectively. When the satellite was in a spinning mode, the two channels turned in the plane of the orbit, with channel one always *leading channel two by 90 degrees.* When the satellite was in the normal position and spinning it would have a "skidding" motion, while the inverted position would give a rolling motion. The orientation of the instrument and the motion is shown in Figure 2.3.

The two photometer channels of the VAE instrument were essentially the same with a combination of single-objective lens and field stop used to define two different fields of view for the detectors. The channel 1 photometer had a half angle cone of 0.75° and was used to measure dayglow and nightglow horizons and to observe auroral features with strong spatial gradients. Channel 2 was a high-sensitivity instrument with a 3° half angle cone that could be used to measure nightglow, dayglow above the satellite and other weak emissions but without information on spatial gradients. The integration periods for the two channels were matched to the spin rate of the satellites so that the field of view was roughly equal to

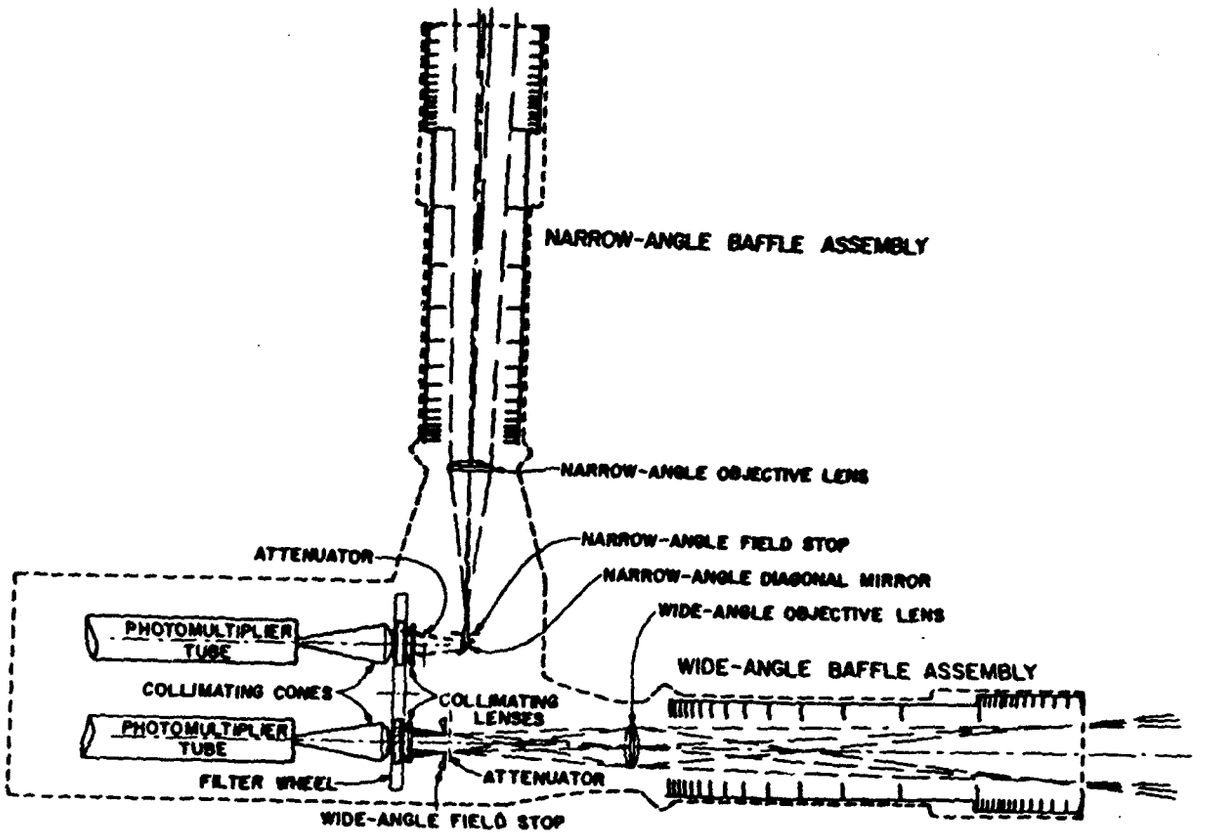

Figure 2.2 Schematic diagram of the Visible Airglow Experiment instrument used on the Atmosphere Explorer satellites.

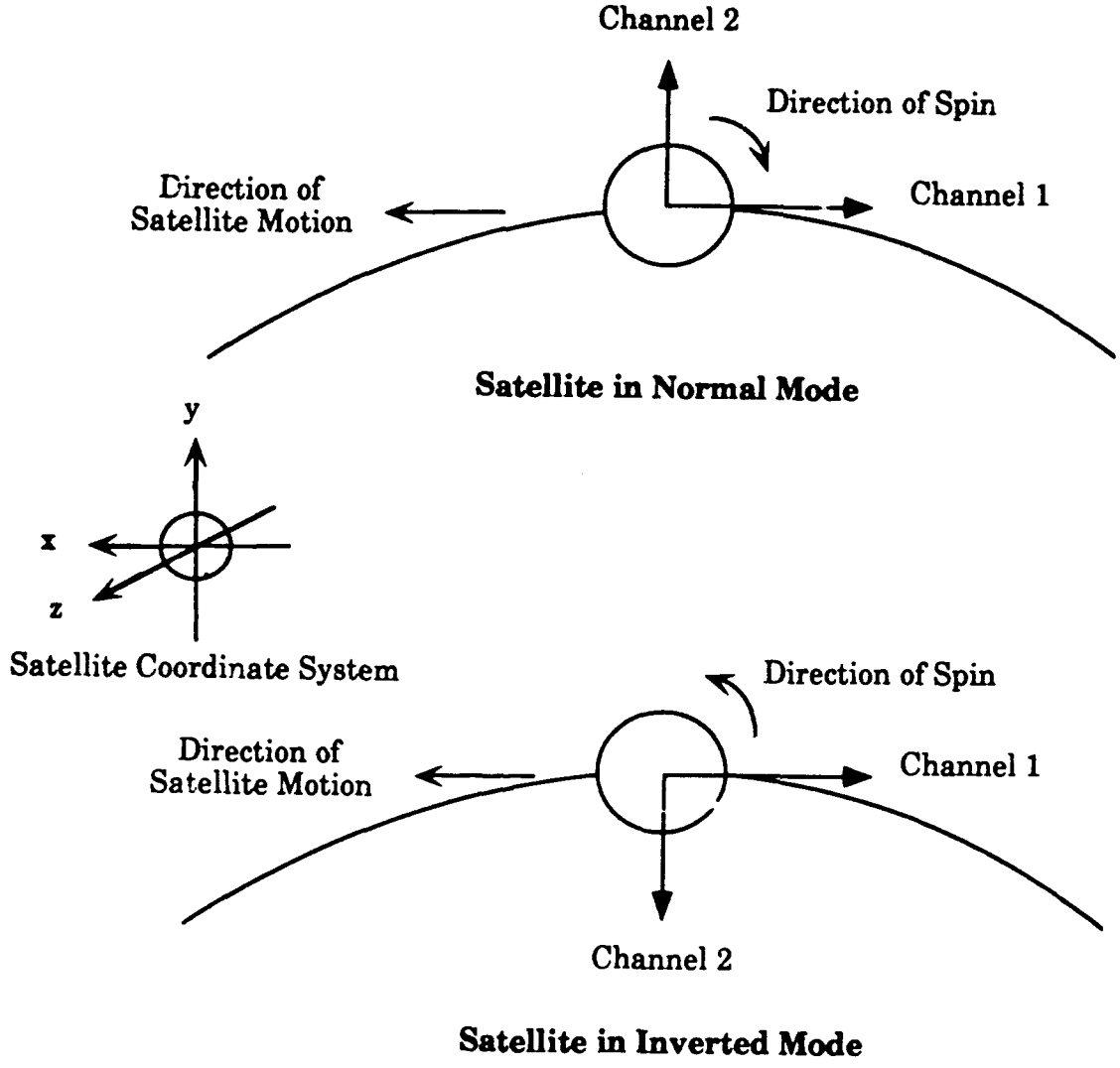

Figure 2.3 Illustration of VAE photometer orientation and spin directions for normal and inverted modes.

the angular interval of the measurement. Channel 1 was integrated for 0.031 second to give a sensitivity of about 20 Rayleighs/count/integration. For Channel 2 the resolution was about 0.3 Rayleighs/count/integration with an integration time of 0.125 seconds.

The two channels of the VAE instrument shared a common filter wheel. The filter wheel contained six interference filters with spectral resolution of 15 to 30Å, a dark count position and a phosphor calibration source position. The different satellites carried filters for different emissions as well as some common emission filters. The emissions and the source on each satellite are listed in Table 2.4. The filter wheels could be operated in either a fixed mode, or in a stepping mode that would change the filter of the channels every 4, 8 or 16 seconds. Because of the large spectral range of the filters, photon contamination from sources other than those of Table 2.4 could be detected by the photometers.

The photometers in the VAE instrument were protected from high dynode currents, which is the primary cause of failure, by two methods. The first was a 1/100 attenuator that acts to extend the dynamic range by 2 orders of magnitude when the count rate exceeds an upper threshold. The second system was a "squint" mechanism. This system used a secondary counting system with a 1.0 msec integration period that adds a bias voltage to the cathode when the count rate exceeds an upper threshold. The back bias would decay slowly to normal and the instrument would "squint" repeatedly until the count rate was below a critical value. This mechanism was used to prevent damage arising from the passage of the sun through the instrument field of view or from the bright dayside of the Earth. With these systems, the VAE instrument could measure a dark feature within 120.0 msec after directly viewing the sun.

Satellite	Emission (Å)	Source
C	6300	$OI(^3P-^1D)$
	5577	$OI(^1D-^1S)$
	7319-7330	$OII(^2D-^2P)$
	5200	$NI(^4S-^2D)$
	3371	$N_2I(B^2\Pi_g, v=0-C^3\Pi_u, v=0)$
	4278	$N_2II(X^2\Sigma_g^+, v=1-B^2\Sigma_u^+, v=0)$
D	6300	$OI(^3P-^1D)$
	5577	$OI(^1D-^1S)$
	7319-7330	$OII(^2D-^2P)$
	5200	$NI(^4S-^2D)$
	4278	$N_2II(X^2\Sigma_g^+, v=1-B^2\Sigma_u^+, v=0)$
	4861	$HI(n=2-4)$
E	6300	$OI(^3P-^1D)$
	5577	$OI(^1D-^1S)$
	7319-7330	$OII(^2D-^2P)$
	5200	$NI(^4S-^2D)$
	2802	$MgII(^2S-^2P)$
	6563	$HI(n=2-3)$

Table 2.4 Emissions measured by the Visible Airglow Experiment on the Atmosphere Explorer satellites with the emission sources.

As noted before, there can be sources of photons that can pass through the interference filters other than those listed in Table 2.4. In addition to the photons from other emissions that fall within the bandpass of the filters, there may be other non-airglow optical contamination. The problem of vehicle glow, from spacecraft atmosphere interaction, can be severe near perigee, especially during elliptical phases, and is most pronounced toward the red end of the spectrum. This source of contaminationhas been discussed for the Atmosphere Explorer satellites by Yee and Abreu (1983). The contribution from galactic and zodical background or from a planet in the field of view can be another source of contamination. The third source of spurious signal is from scattering by the optical baffle systems of the telescopes. This is a particular problem when observing near the bright limb of the Earth. Curves showing valid regions of dayglow limb observations were given by Fesen (1981). The influence of these contamination sources on this work will be discussed later.

2.2.2 Analysis of Visible Airglow Data

The data gathered by the Visible Airglow Experiment is not a direct measure of the volume emission rate at a point in the atmosphere. The recorded quantity is the integrated surface brightness along the path of the observation in Rayleighs. A Rayleigh is a unit of surface brightness equal to $1x10^6$ photons / (cm^2 [column] sec). For the satellite observations, the column is along the line of sight of the instrument. To turn the measured surface brightness into a volume emission rate (VER) the data is inverted by different techniques, depending on the type of orbit. Inversion methods recover a set of physical quantities from a set of integral measurements. The term inversion refers to the inverse transform which is sought to undo

the effects of the measurement process. In this section, some of the techniques that have been used to recover volume emission rates from the measurements made by the Atmosphere Explorer satellites will be discussed. The list will not be exhaustive but will serve to present some of the various classes of the techniques.

Since the Atmosphere Explorer satellites employed several different types of orbits (spinning or de-spun and elliptical or circular), there are several "inversion" processes that may be used to recover volume emission rates from the brightnesses. As ordered here these techniques fall into three basic categories. The first group is not actual inversion techniques but uses different mathematical methods to determine the volume emission rate profiles from brightnesses. The other two groups are analytical inversion methods and linear inversion methods. Examples of methods in each group these will be discussed in terms of the type of orbit and geometry to recover the desired data.

One of the simplest means to recover the volume emission rate from elliptical, de-spun orbits is to use data from channel two looking radially out from the Earth in a technique similar to that used for rocket data. This technique uses a series of brightnesses as the satellite crosses various layers of the atmosphere (see Figure 2.4). The brightness profile generated this way can be differentiated to produce volume emission rate profiles. This technique requires the emission to be homogeneous and spherically distributed. Another restriction is that the background does not change appreciably between two successive measurements. These conditions can usually be met by restricting the data to midlatitudes and away from the terminators. This technique may be used on spinning elliptical orbits by

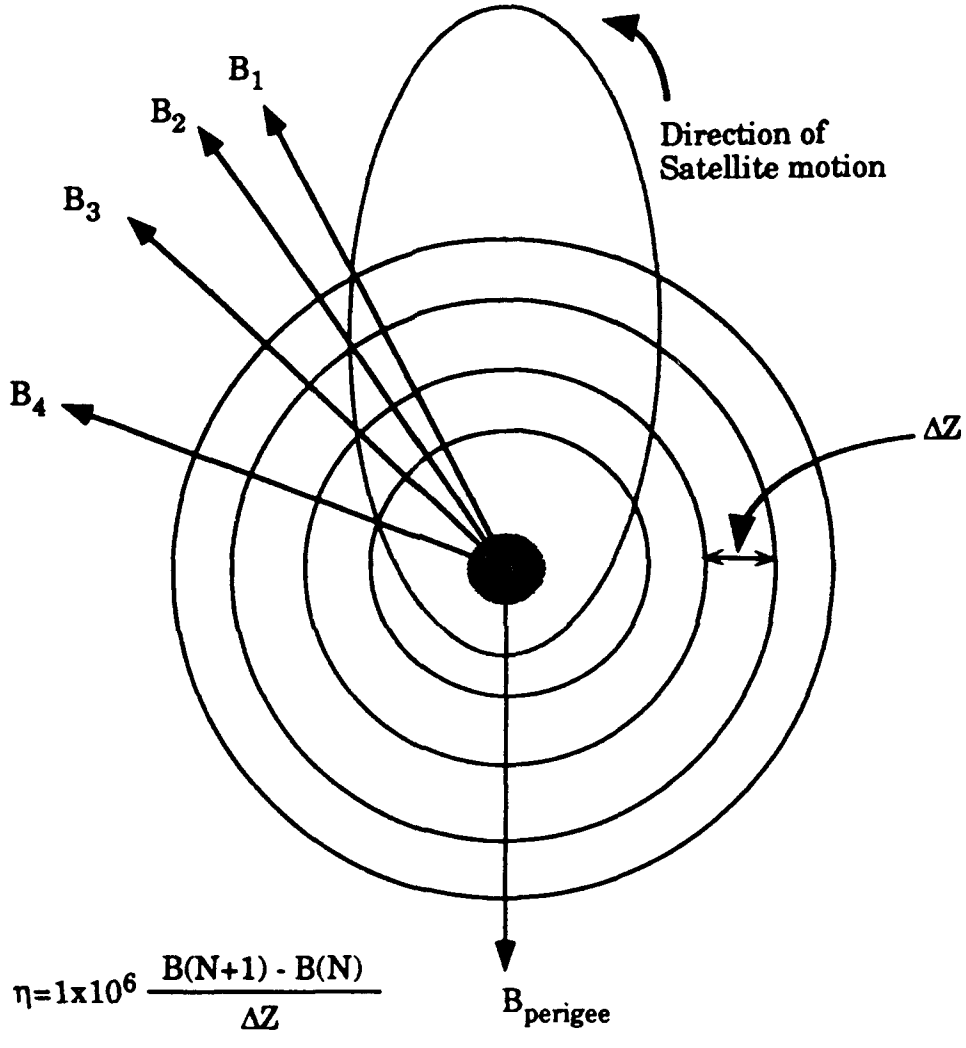

Figure 2.4 Geometry of differential "inversion" used in despun normal modes.

using measurements when the photometer is pointing radially out within some small angle.

A technique that uses circular spinning orbits for the brightness measurements but is not an inversion in the true sense is the chord subtraction technique (Abreu *et al.*, 1983; Yee and Abreu, 1987). The basic geometry of this technique is shown in Figure 2.5. When the satellite is spinning, measurements are made with the photometer looking in the same direction for different positions in the orbit. These measurements are subtracted and divided by the path length to determine the VER along the chord. The same calculation is carried out for another chord and the two are averaged to give the VER at the point desired. This technique corrects for the background since the difference in the measurements is just the emission along the chord bounded the satellite orbit if the background changes slowly compared to the time between the observations.

Another technique which is similar to the chord subtraction method is the "onion peeling" method (Fesen, 1981; Fesen and Hays, 1982). It is a two dimensional inversion that finds a non-iterative solution to the limb scan data. Figure 2.6 shows the inversion geometry and parameters. The method uses the nature of the limb scan and orbit in the algebraic domain by starting at the top and working down through the atmosphere. By starting at the satellite, the contribution to the emission from the first layer below the satellite is found. This is then used to determine the contribution from the second layer, and knowledge of both contributions is then applied tot the next layer. This procedure is continued down through the atmosphere, but to prevent oscillations from occurring, a smoothness constraint is applied.

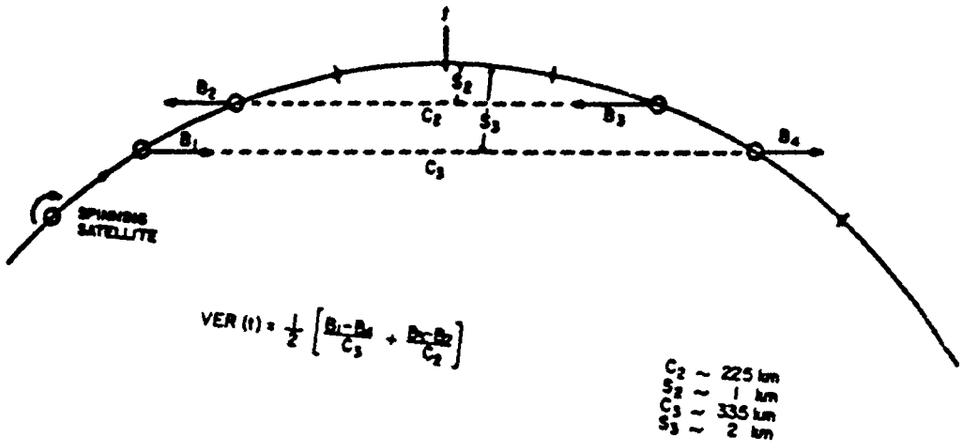

$$VER(t) = \frac{1}{2}\left[\frac{B_1 - B_4}{C_3} + \frac{B_2 - B_3}{C_2}\right]$$

Figure 2.5 Geometry of chord subtraction "inversion" and calculation method used with spinning orbits.

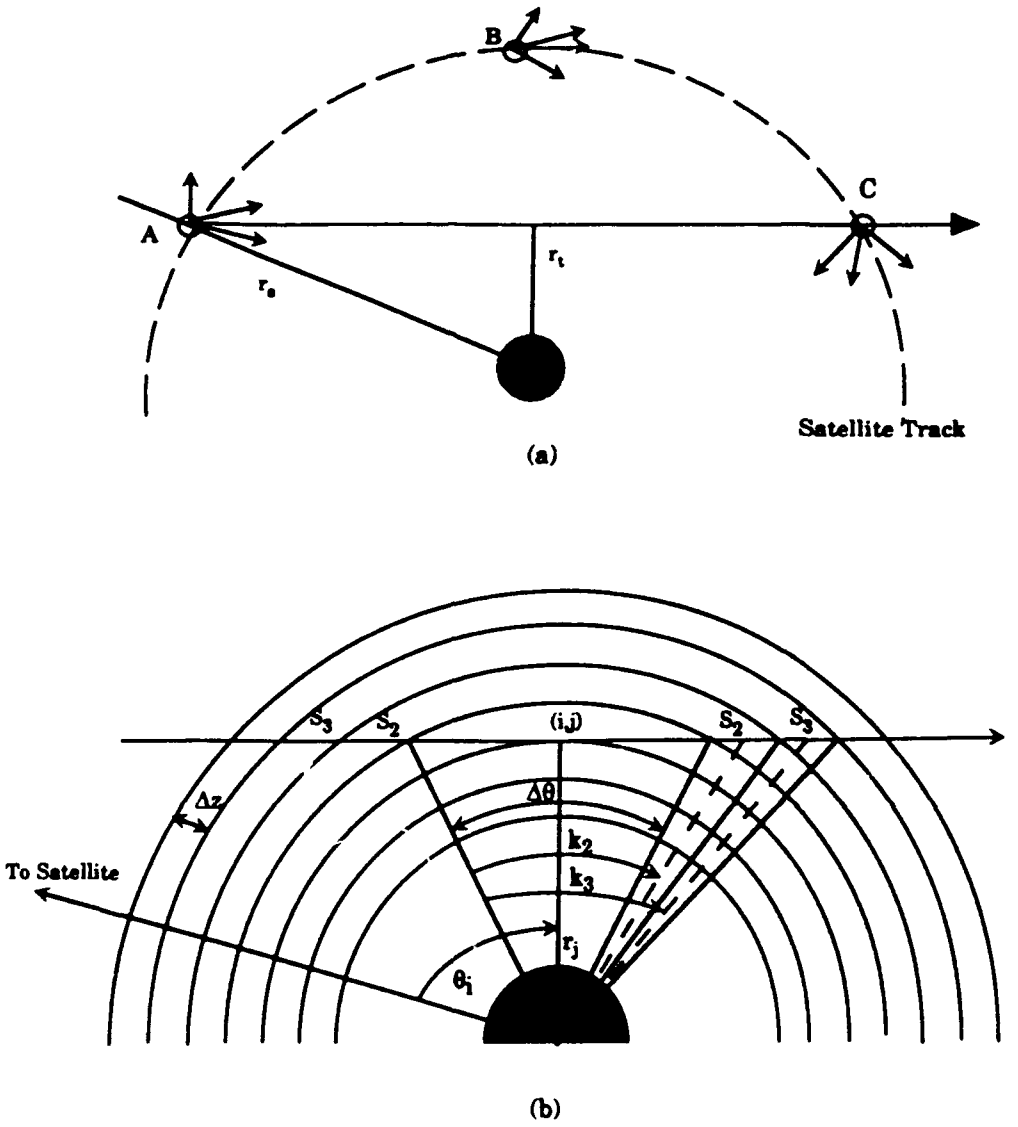

Figure 2.6 Observational sequence for several spins (a) and two-dimensional inversion geometry (b).

The majority of the inversion techniques are based on brightness measurements from circular spinning orbits. The general geometry for this type of observation is shown in Figure 2.7. The measured brightness is the integral of the volume emission rates along the line of sight. The basic equation for this is

$$B(r_t) = \int_{-\infty}^{\infty} \eta(s)\, ds, \qquad [2.1]$$

where B is the measured brightness along a path with a tangent height r_t and η is the volume emission rate along the pathlength s. Using the geometry shown in Figure 2.8 for a single path, equation [2.1] can be re-written as

$$B(r_t) = 2\int_{r_t}^{r_s} \frac{\eta(r)\, r}{\left(r^2 - r_t^2\right)^{\frac{1}{2}}}\, dr. \qquad [2.2]$$

In this case, r_s is the satellite height and the volume emission rate is expressed as a function of height. Equation [2.2] is the basic equation used in most of the inversion processes.

The Abel inversion (Roble and Hays, 1972) was the first inversion applied to VAE data from spinning orbits. The Abel inversion is loosely a tomographic inversion since it can be considered as a one dimensional case of the Cormack inversion where only variation in altitude is allowed. The geometry for the Abel inversion is shown in Figure 2.9. Equation [2.2] is essentially one of a pair of equations that make up the Abel Transform. This equation has an analytical solution which may be expressed in first or second derivative form. The first derivative form of the inverse is,

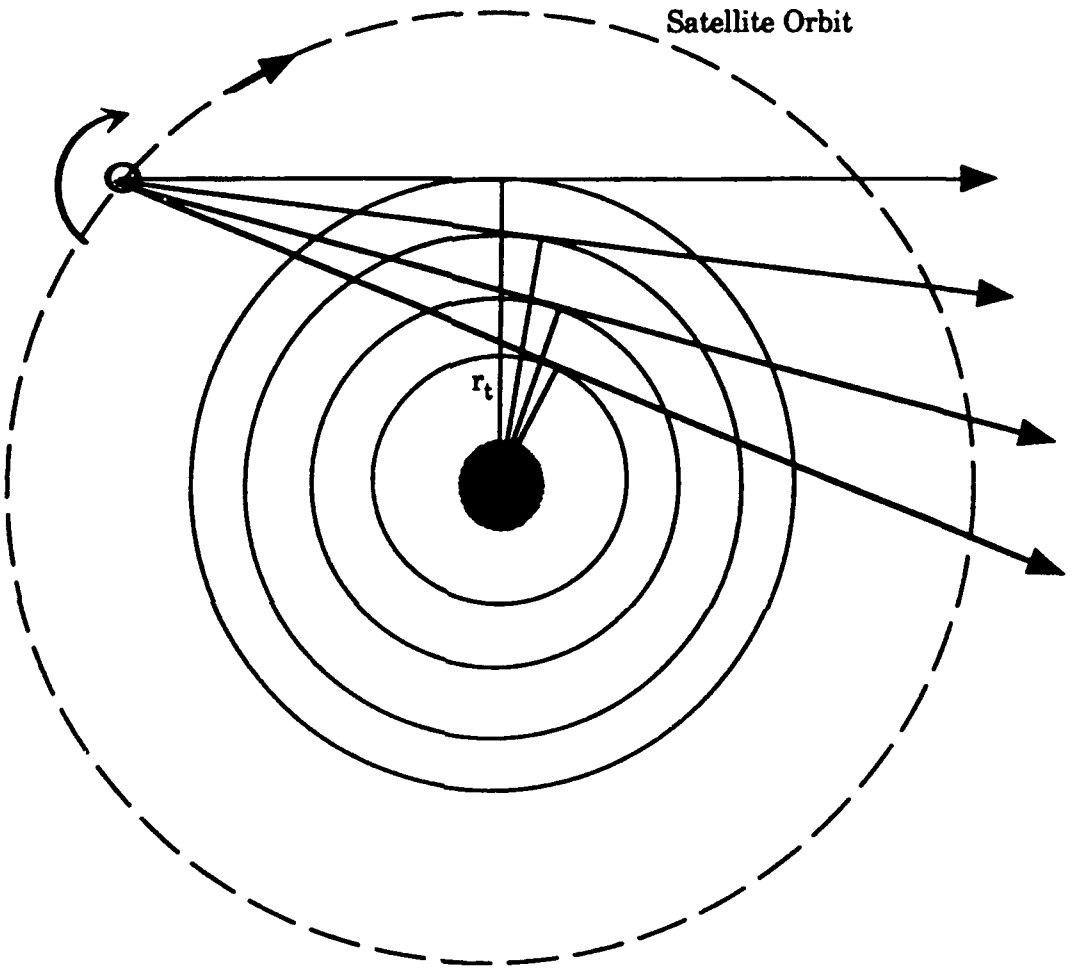

Figure 2.7 Tangent ray heights of surface brightness measurements during a single spin of the satellite.

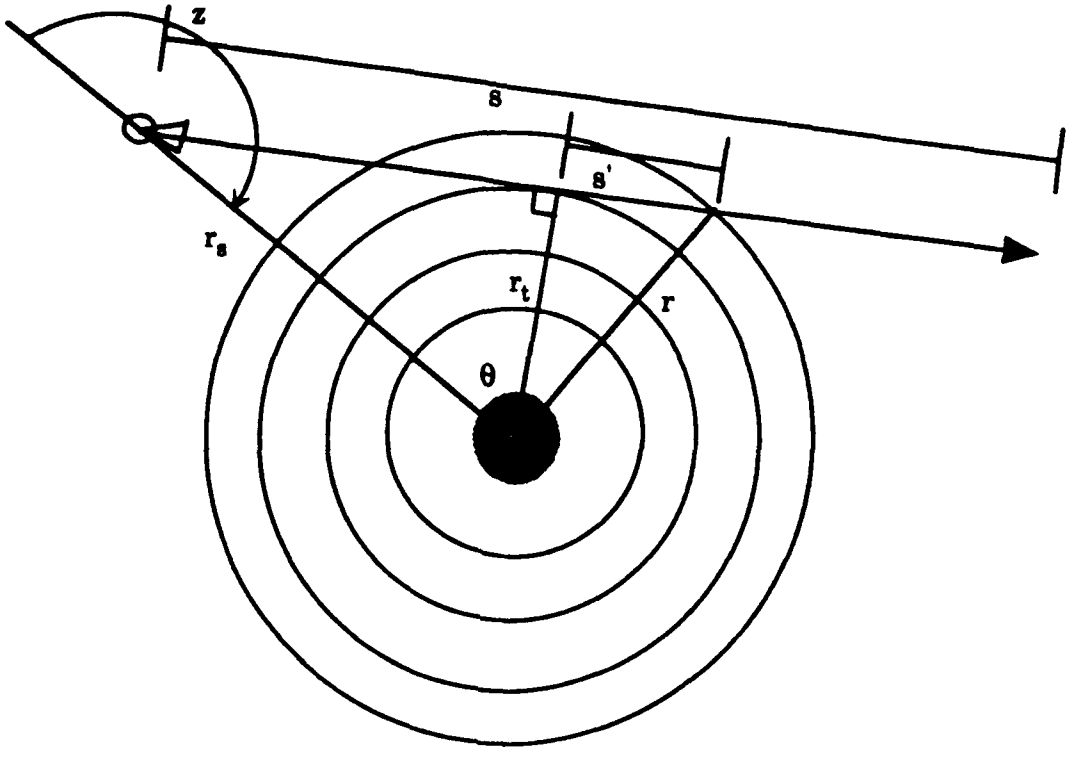

Figure 2.8 Geometry of a single surface brightness measurement from satellite at height r_s and photometer zenith angle z.

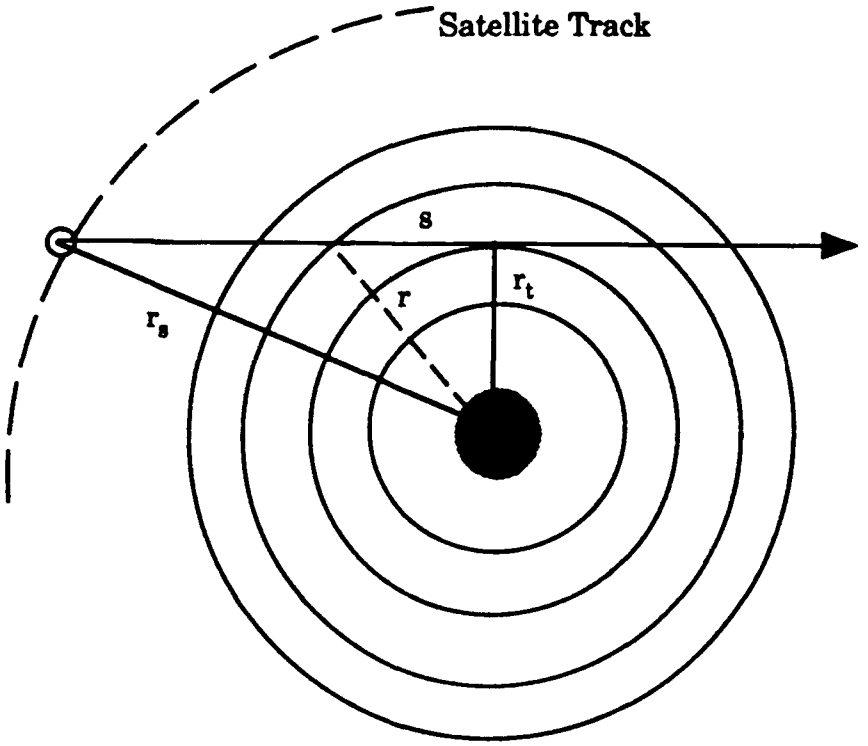

Figure 2.9 Geometry for the Abel inversion showing one brightness measurement.

$$\eta(r) = -\frac{1}{\Pi}\int_{r}^{r_s}\frac{d}{dr_t}\left\{\frac{B(r_t)}{\left(r_t^2 - r^2\right)^{\frac{1}{2}}}\right\}dr_t\,, \qquad [2.3]$$

from r to r_s, the satellite altitude. The second derivative form of the inverse equation is,

$$\eta(r) = \frac{1}{\Pi}\int_{r}^{r_s}\left(r_t^2 - r^2\right)^{\frac{1}{2}}\frac{d}{dr_t}\left\{\frac{\frac{d}{dr_t}B(r_t)}{r_t}\right\}dr_t\,, \qquad [2.4]$$

over the same limits of integration.

The Cormack inversion is a two dimensional inversion that has many applications in different fields (Cormack, 1963; 1964; 1973). It was developed for use in the medical fields and is also known as tomography. In 1963, A. M. Cormack solved the problem of obtaining two dimensional density function from multiple x-ray measurements by estimating the function from knowledge of line integrals. The problem had been solved differently much earlier by Radon (1917) but was forgotten since it would be an academic interest at the time (Berry and Gibbs, 1970). The Abel inversion is a special case of the Cormack inversion. In the Abel case the horizontal gradients are assumed to be small. For the Cormack inversion the spatial dependance is allowed to vary. Figure 2.10 shows the geometry for the Cormack inversion.

The Cormack equation, which is similar to that for the Abel inversion, is

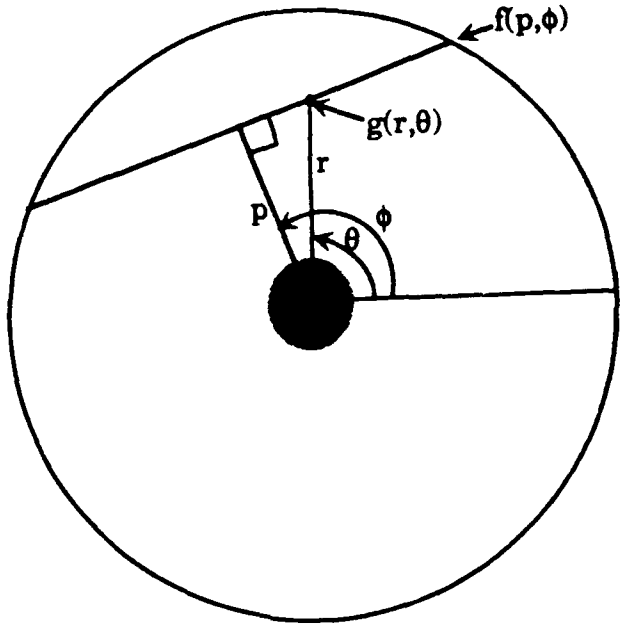

Figure 2.10 Geometry of the Cormack inversion. Every line integral f is the sum of all $g(r,\theta)$ is specified by distance p and angle ϕ.

$$F_n(r_t) = 2\int \frac{G_n(r)T_n\left(\frac{r_t}{r}\right)r}{(r^2 - r_t^2)^{\frac{1}{2}}}\,dr\,, \qquad [2.5]$$

$T_n \equiv n^{th}$ Chebyshev Polynomial

$F_n \equiv$ Fourier Series Expansion of Brightness

$G_n \equiv$ Fourier Series Expansion of Volume Emission Rate

The inverse of the Cormack equation is,

$$G_n(r) = -\frac{1}{\Pi}\int \left\{\frac{d}{dr_t} F_n(r_t)\, T_n\left(\frac{r_t}{r}\right)\right\}\left(r_t^2 - r^2\right)^{\frac{1}{2}} dr_t\,, \qquad [2.6]$$

Discussion of the application of this technique to satellite data has been given by Solomon *et al.* (1984, 1985); Solomon (1987); Abreu *et al.* (1989). The Cormack inversion is particularly useful in the cases where there is a high degree of spatial variability of the emission as in aurora.

Equation [2.2] can itself be re-written into a matrix representation,

$$\vec{G} = A\,\vec{F}\,. \qquad [2.7]$$

In this case, the observed brightness is the vector $\vec{G}$ and the corresponding volume emission rates are in the vector $\vec{F}$. The matrix A contains the weighting function or kernel which relates the two vectors,

$$A = \frac{r}{\left(r^2 - r_t^2\right)^{\frac{1}{2}}}\,. \qquad [2.8]$$

In the case of limb scans, the kernel gives the contribution of each layer of the atmosphere to the integrated brightness due to the geometry of the

observation. Figure 2.11 is an example of the weighting functions at three tangent heights for the geometric kernel.

The task of the inversion is to find a matrix B such that

$$\vec{\mathbf{F}} = B\,\vec{\mathbf{G}}\,, \qquad [2.9]$$

where B can be identified as the inverse of A, if A is a square matrix or can be made square. Only in the simplest cases can the matrix be inverted directly. The weighting functions must be sharp and not have significant overlap to be useful in the inversion process. In typical remote sensing applications, the measurement $\vec{\mathbf{G}}$ contains some errors and the matrix A is nearly singular. The matrix becomes singular when some of the weighting functions are so broad that there is significant overlap between tangent heights. If this occurs the rows of the matrix may not be linearly independant. Finding $\vec{\mathbf{F}}$ in this case may lead to large oscillations. The mathematical explanation of this is that if the eigenvalues of A are small (the matrix is nearly singular) then the eigenvalues of B will be large; this will lead to instability in the calculation of $\vec{\mathbf{F}}$ (Twomey, 1977; Menke, 1989).

By using various linear methods, the problem of solving Equation [2.7] in less than the ideal cases can be reduced. In remote sensing applications the number of measurements is larger than the number of values to be recovered. This will cause the problem to be over determined but it can be made solvable by linear methods by forming the least square solution which is,

$$\vec{\mathbf{F}} = \left(A^{*}A\right)^{-1}A^{*}\,\vec{\mathbf{G}}\,, \qquad [2.10]$$

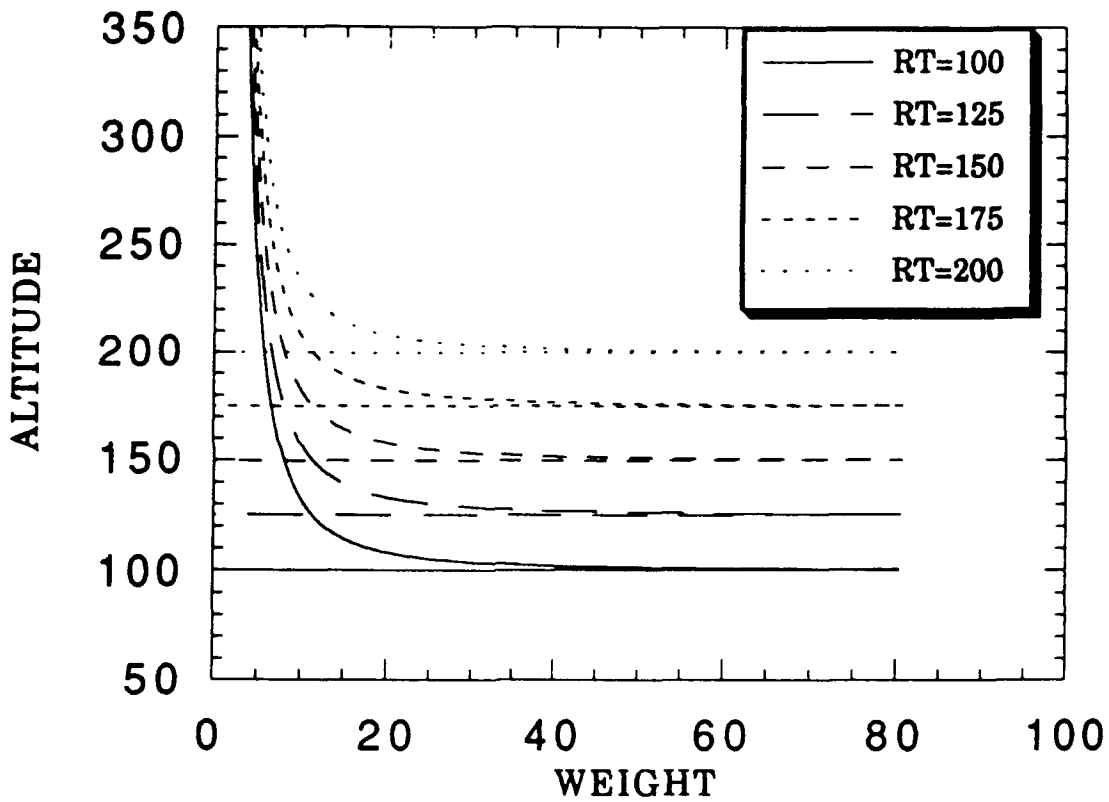

Figure 2.11 Geometric weighting kernels for the tangent height measurements used by the Abel inversion method.

where A * is the transpose of the matrix.

Since Equation [2.10] allows for the solution of non-square matrix equations it will allow for the solution to be constrained by adding more equations to the system. A smoothness constraint may be applied in this manner. The solution to Equation [2.7] is now,

$$\vec{\mathbf{F}} = \left(A^{*}A + \gamma H\right)^{-1} A^{*}\,\vec{\mathbf{G}} \,. \qquad [2.11]$$

In this solution, γ is the weight applied to the constraint and H is the matrix constructed by the differences that will give the desired level of smoothness.

Another form of the solution for Equation [2.7] is one that allows for the system to be constrained to *a priori* information such as a model or climatology. When allowing for the measurements and the constraint to have errors the solution to the system becomes,

$$\vec{\mathbf{F}} = \left(A^{*}E^{-1}A + \gamma I\right)^{-1}\left(A^{*}E^{-1}\,\vec{\mathbf{G}} + \gamma H\right) . \qquad [2.12]$$

In this solution, γ is the weight applied to the constraint and E is the covariance matrix of the measurements. I is the covariance matrix of the *a priori* information and **H** is the *a priori* information vector.

A final linear method that can be applied to the measurements of the Atmosphere Explorer satellites is from optimal estimation theory or sequential estimation (Rodgers, 1976; Houghton *et al.*, 1984; Rodgers, 1990). Using optimal estimation, the solution to Equation [2.7] becomes,

$$\hat{\vec{\mathbf{F}}} = \vec{\mathbf{F}}_0 + S_x A^{\mathrm{T}}\left(AS_x A^{\mathrm{T}} + S_\varepsilon\right)^{-1}\left(\vec{\mathbf{G}} - A\vec{\mathbf{F}}_0\right) \qquad [2.13]$$

$$\hat{S} = S_x - S_x A^T \left(A S_x A^T + S_\varepsilon \right)^{-1} A S_x \,, \qquad [2.14]$$

where $\hat{\vec{\mathbf{F}}}$ is the returned volume emission rate and $\hat{S}$ is the covariance of the returned volume emission rate. The *a priori* estimate for the volume emission rate and its covariance is given by $\vec{\mathbf{F}}_0$ and S_x respectively. The error covariance for the measured values is S_ε. Since these equations can be solved sequentially, it is not necessary to perform a matrix inversion or solve simultaneous linear equations to retrieve a volume emission rate. Besides the savings in computer time, the concept of sequential estimation allows the use of continuity along an orbit to improve the accuracy of the retrievals.The application of this method has been discussed by Rodgers (1976) and Houghton *et al.* (1984). This method has been used to analyze Atmosphere Explorer data by Abreu *et al.* (1991).

There are numerous techniques to recover the volume emission rate from the measured surface brightnesses. The choice of inversion method is primarily determined by the type of orbit used to measure the data. The methods described here have been applied to data taken by the Visible Airglow Experiment data on the Atmosphere Explorer satellites. In the next section of this chapter, instruments used for other measurements from the Atmosphere Explorer satellites needed for the modelling of the O(^{1}S) emission will be described.

2.3 Other Atmospheric Parameters

The various instruments on the Atmosphere Explorer satellites were able to provide *in-situ* measurements of several important atmospheric parameters. The neutral and ion densities were measured along with their

associated temperatures. In most cases each of these parameters were determined by more than one instrument. In this section, these parameters are broken down into neutral measurements and ion measurements. Each of these are discussed separately, as are the individual instruments and the inter-relationship between the instruments.

2.3.1 Neutral Measurements

The neutral atmospheric parameters that are important to the production of 5577Å emission are the molecular nitrogen density, atomic oxygen density, and neutral temperature. These were measured by a combination of three instruments on the satellites, the Open-Source Neutral-Mass Spectrometer (OSS), the Neutral-Atmosphere Composition Experiment (NACE), and the Neutral-Atmosphere Temperature Experiment (NATE). Each of these instruments and their operation will be briefly discussed below.

Open-Source Neutral-Mass Spectrometer. On the Atmosphere Explorer satellites the Open-Source Neutral-Mass Spectrometer provided measurements of the molecular nitrogen density and atomic oxygen density. Open-source spectrometers can best detect reactive species such as oxygen and hydrogen but have difficulty detecting particles that are not approaching along the instrument axis. This instrument has been described by Neir *et al.* (1973) and Burgess and Torr (1987). It is a double-focusing Mattauch-Herzog magnetic-deflection instrument that is similar to those flown on earlier sounding rockets. This type of instrument was chosen for compactness and low power consumption.

The major components of the spectrometer are the ion source, the electric and magnetic analyzers and the ion collection system. The ambient gas enters through a series of grids that isolate the electric and magnetic fields of the ion chamber from the ambient gas. The last of these grids acts to prevent any ions formed in the chamber from exiting through the grids. An electron beam in the ion chamber produces positive ions which are focussed, accelerated and collimated before entering the electric and magnetic analyzing region. The ions pass through the electric and then the magnetic analyzers where energy focusing and mass separation takes place. The two detectors of the OSS would give mass ranges in the ratio of 1:8. The same multiplier detectors were used for each region. The high mass range multiplier would be turned off a low altitudes and a grid and electrometer would be used to determine the high mass density. This collector system allowed the density measurements to be made over a large dynamic range caused by the low perigee orbits.

Neutral-Atmosphere Composition Experiment. The Neutral-Atmosphere Composition Experiment is a closed source instrument that complements the OSS instrument described above. For 5577Å emission, the same constituents measured by the OSS are measured by the NACE. It produces precise measurements of non-reactive species and total oxygen (atomic+molecular) due to surface recombination of the atomic oxygen. The NACE can provide measurements over the entire forward hemisphere independent of the side energies. The NACE instrument was described by Pelz *et al.* (1973) and Burgess and Torr (1987). The system was based on the previously flown instruments of the Orbiting Geophysical Satellite (OGO-6) and the San Marco-3 satellites. The spectrometer had a mass range from one to 46 amu with a better than 1 amu resolution.

The NACE instrument consisted of an inlet system, an ion chamber, a quadrupole analyzer, an electron multiplier and a vacuum pump system. The vacuum pump was not used during flight but was used to maintain a vacuum in the instrument prior to launch. During flight, the antechamber and ion source are connected to the ambient atmosphere by a knife-edge orifice. After the ambient gas is thermalized in the antechamber, it passes into the ion chamber. After ionization, the gas is focused and accelerated into the quadrupole analyzer. The ions are decelerated and separated by their charge to mass ratio. The ions are then accelerated into the electron multiplier. The count rate is proportional to the chamber density of the selected gas. An additional feature of the NACE instrument was a contaminant cover for the orifice to prevent exhaust products from the hydrazine motors from entering the instrument during maneuvering.

Neutral-Atmosphere Temperature Experiment. The Neutral-Atmosphere Temperature Experiment was used to provide the inputs to allow calculation of the temperature of the neutral atmosphere at the location of the satellite and the density of molecular nitrogen outside the spacecraft. The instrument was based on those developed for the San Marcos-3 and AEROS programs. The instrument and the calculation of the temperature and density are discussed by Spencer et al. (1973) and Burgess and Torr (1987).

The NATE instrument was very similar to the NACE. The NATE featured different modes of operation that allowed the determination of the velocity distribution of the ambient gas either by using the spinning motion of the satellite or in the despun mode by using a baffle that could be stepped across the orifice. The method of density and temperature determination is given by Spencer *et al.* (1973). While the main atmospheric constituent used

by the instrument was N_2, oxygen and hydrogen were studied as possible constituents to be used at high altitudes to determine temperature.

2.3.2 Ion Measurements

The ionic atmospheric parameters that are important to the production of 5577Å emission are total ion or electron density, electron and ion temperature and singly ionized molecular oxygen. A combination of four instruments on the satellites provided overlapping measurements of these parameters, the Bennett Ion-Mass Spectrometer (BIMS), the Magnetic Ion-Mass Spectrometer (BIMS), the Retarding-Potential Analyzer (RPA), and the Cylindrical Electrostatic Probes (CEP). Each of these instruments are briefly described below. Also, the inter-calibration between these instruments will be discussed.

Bennett Ion-Mass Spectrometer. The Bennett Ion-Mass Spectrometer as flown on the Atmosphere Explorer satellites was derived from those used on the Orbiting Geophysical Observatories and the Atmosphere Explorer-B satellites. The instrument made measurements of thermal positive ions between 1 and 72 amu in combinations of three ranges with densities between 5 and 5 million ions per cubic centimeter densities. The ion densities measured by the instrument were calibrated by correlation with the RPA and CEP instruments on the satellite. The instrument was described by Brinton *et al.* (1973) and Burgess and Torr (1987).

The Bennett Ion-Mass Spectrometer was located on the forward-looking part of the satellite. The ions are drawn in from the ambient gas by a negative electric field at the orifice. The ions are then accelerated through the spectrometer gaining energy from the radio frequency fields,

passing through a retarding potential to the collector. The flow through the instrument was enhanced by two features, the use of a multigrid ion current collector instead of a solid plate and the venting at the rear of the instrument. The venting was especially important at low altitudes by reducing the ram buildup in the instrument.

Magnetic Ion-Mass Spectrometer. The Magnetic Ion-Mass Spectrometer was designed to measure the abundance of the ambient positive ions at the satellite location. The spectrometer flown on the Atmosphere Explorer satellites was similar to the one flown on the International Satellite for Ionospheric Studies (ISIS-2) spacecraft. It was a magnetic deflection-type spectrometer with a mass range of 1 to 90 amu. Like the BIMS, the MIMS was calibrated in-flight to the RPA and CEP instruments. This instrument has been described by Hoffman *et al.* (1973) and Burgess and Torr (1987).

The MIMS instrument was a small magnetic deflection system consisting of an entrance aperture, a magnetic analyzer and a detector system. The entrance was positioned normal to the spin axis and looking forward in the despun mode. The entrance slit formed the inlet port to the instrument and used ram pressure with a large vent to minimize internal pressure. This venting was adequate to allow operations down to 120 km. The instrument had three detectors that could collect ions in the ratio of 1:4:16. The detectors could be used to study specific mass ions or could study the spectrum of ions by sweeping the voltage.

Retarding Potential Analyzer. The Retarding Potential Analyzer was included on all of the Atmosphere Explorer satellites. It is also known as a planar ion trap and was an improved version of an instrument used on the Orbiting Geophysical Observatory and in high altitude sounding

rockets. Primarily intended to measure ion temperature and ion concentrations on the Atmosphere Explorer satellites, it also was used to measure ion drifts and energy spectra of the thermal and supra-thermal electrons. For the 5577Å emission, the RPA provided electron densities and ion temperatures. The other ion instruments on the satellites were cross calibrated with this instrument. The RPA has been described by Hanson *et al.* (1973) and Burgess and Torr (1987).

The instrument consisted of four sensors, each of which was a series of grids along a small cylinder and a solid detector. Sensor heads one and four were located forward-facing when the satellite was despun and sensor heads two and three were at 110 and 130 degrees, respectively. The grids in the sensors could be controlled to screen the different particles entering the detector. All of the sensors were essentially the same with just a few minor differences. Collector four was called the ion drift meter and was segmented to measure off axis flows. On sensors two and three, an extra grid was used to protect the sensors from ion bombardment when measuring electrons. In addition, the heads could be slightly positively biased to measure thermal electrons.

Cylindrical Electrostatic Probes. The Cylindrical Electrostatic Probes were a continuation of the use of Langmuir probes used since 1947 on high-altitude sounding rockets and numerous satellites, including Tiros, Atmosphere Explorers A and B, and the International Satellite for Ionospheric Studies. The instrument was used to measure the temperature and concentrations of electrons. It consisted of two independent probes, one mounted parallel to the velocity vector and the other perpendicular to it. This instrument was described in detail by Brace *et al*, (1973) and Burgess and Torr (1987).

The method of using the probe to measure temperatures and densities was described by Brace *et al*, (1973). The probes were modified for the different environment the satellite would encounter at low altitudes. The length of the probe was reduced by a factor of three compared to previous probes to minimize the induced voltages from the motion of the instrument through the geomagnetic field. The diameter of the probes were increased by the same amount to add a heating element to drive off any exhaust contaminants from the hydrazine motors. A new collector material of highly oriented tungsten crystals was used to improve the surface potential and reduce energy smearing.

Instrument inter-calibration. The calibration of the various ion measuring instruments is important for using the measurements from the Atmosphere Explorer satellites. Since the instruments provided some redundancy in the measurements, if a parameter from a given instrument was not complete another instrument could be substituted in its place if the inter-calibration was known. The normalization between the instruments was based on using the Retarding Potential Analyzer as ground truth and then determining the factors for the other instrument to make their measurements match those of the RPA.

Prior to this study, the normalization factors were determined as a single parameter fit for the instruments on satellite AE-E (Yee, Private Communication). These factors were determined using a ten day period in the satellite lifetime. The normalization factors for AE-C and AE-D instruments were assumed to be the same as for AE-E. Since AE-E did not have a MIMS instrument, the normalization for the BIMS from AE-E was used on the other satellites. These factors were multiplied by the

Satellite	RPA	CEP	BIMS	MIMS
C	1.000	1.46	2.48	2.48
D	1.000	1.46	-	2.48
E	1.000	1.46	2.48	-

Table 2.5 The single parameter normalization factors for the Atmosphere Explorer ion measurements. All values except CEP and BIMS for AE-E are assumed.

appropriate satellite measurement to get a corrected value to match the RPA and are shown in Table 2.5.

For this study, these normalization factors were recalculated separately for each satellite. This eliminates the assumption that each of the instruments on the three satellites had the same inter-calibration. The RPA instrument on each satellite was assumed to be the correct measurement. Measurements from each of the other instruments were then compared to the RPA as shown in Figure 2.12, and a straight line was fit to the logarithm of the values. Table 2.6 shows the new normalization factors determined for the various satellites and instruments. The two parameters are used in equation [2.15],

$$\log_{10}(M_C) = S[\log_{10}(M_U)] - I, \qquad [2.15]$$

where M_c is the corrected measurement and M_u is the uncorrected measurement. These correction factors were calculated for the elliptical period of each satellite. The normalization factors change over the life of the satellite as shown by Figure 2.13 for the instruments on satellite AE-E. If data is to be used from other periods, the normalization factors will have to be updated for the appropriate period.

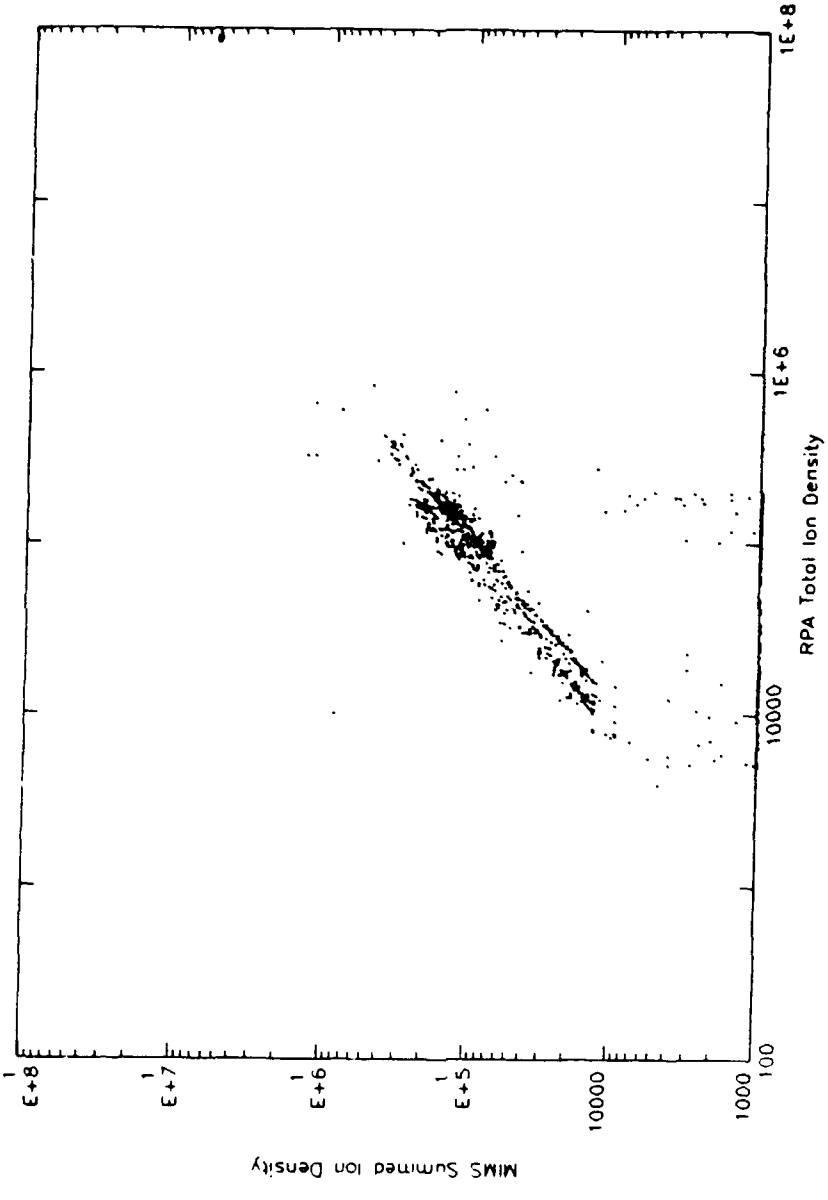
MIMS Summed Ion Density
1E+8
1E+7
1E+6
1E+5
10000
1000
100
100
1000
10000
1E+6
1E+8
RPA Total Ion Density

(a) MIMS-v8-RPA

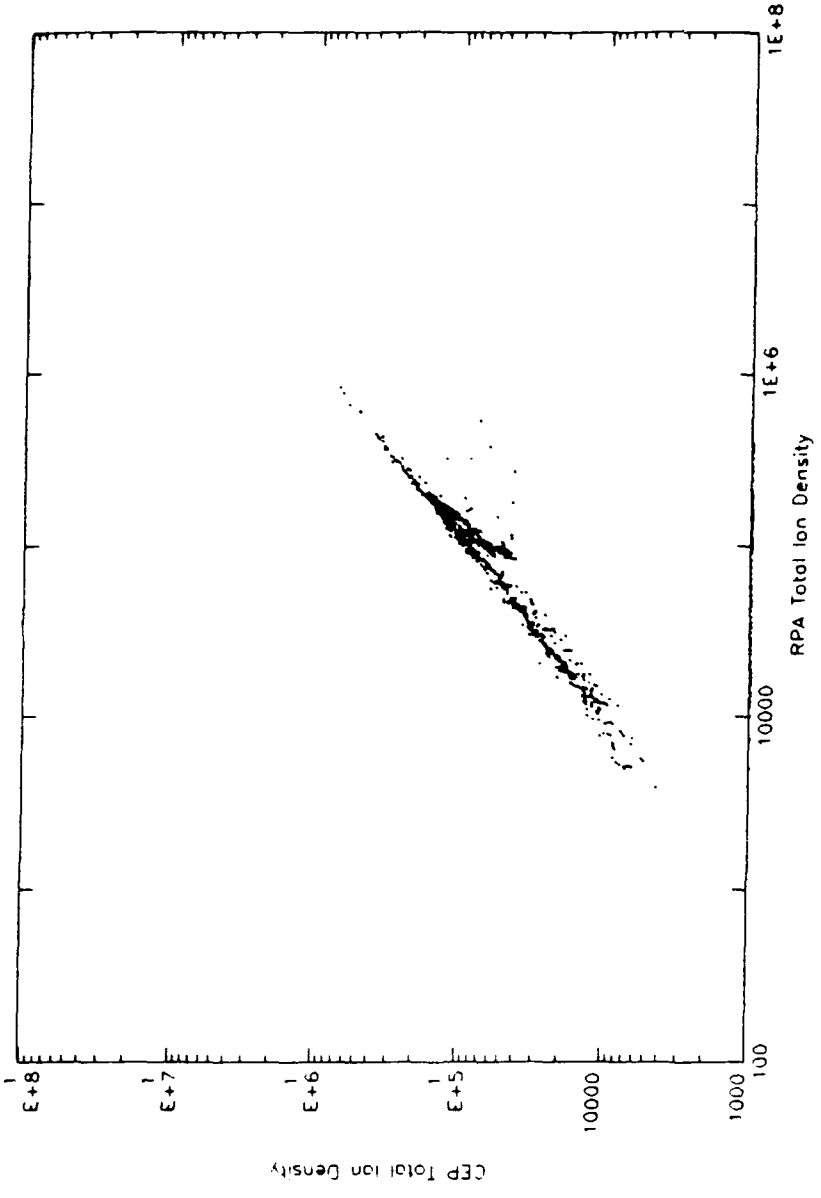
CEP Total Ion Density
1E+8
1E+7
1E+6
1E+5
10000
1000
100
1000
10000
1E+6
1E+8
RPA Total Ion Density

(b) CEP-vs-RPA

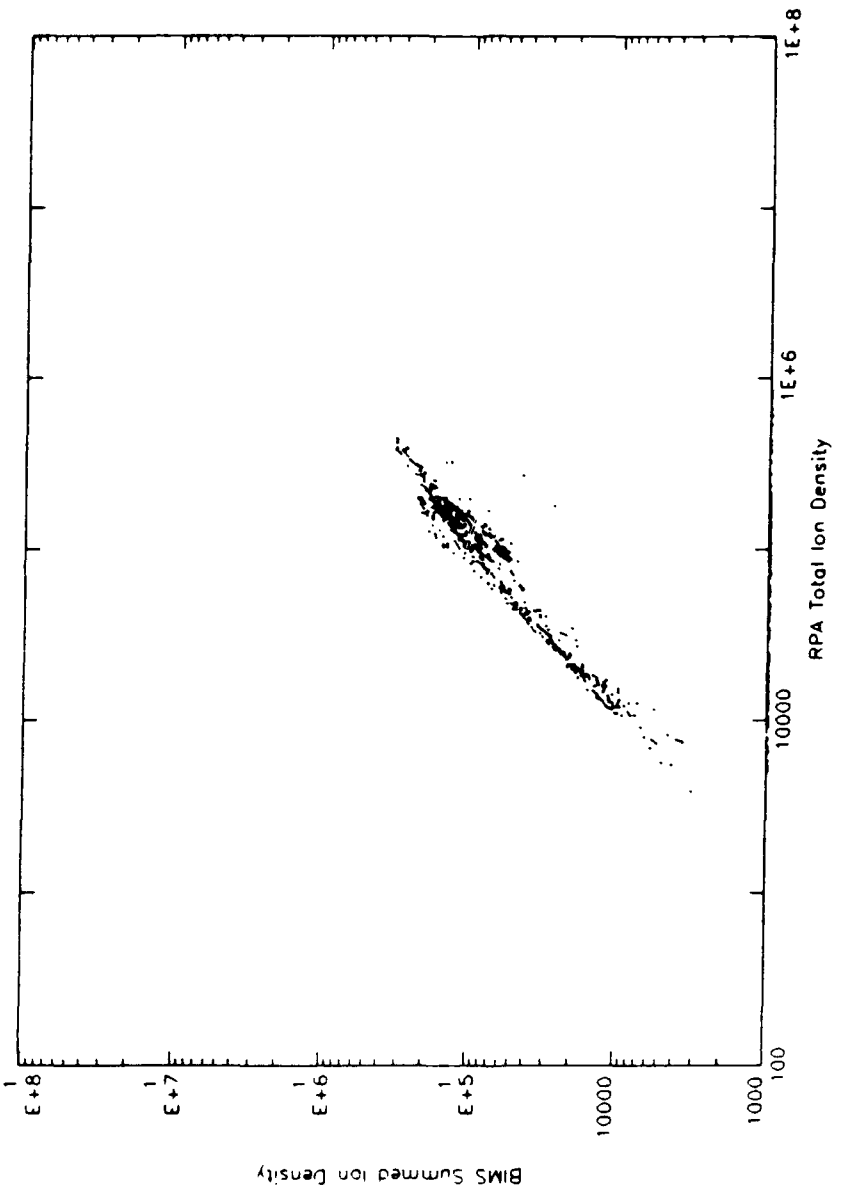

(c) BIMS-v8-RPA

Figure 2.12 Normalization plots for satellite C for a single day of orbits.

Satellite	Dates (Beg/End)	Instrument	Number of Points	S	I
C	74026/ 74280	CEP	57754	0.856328	0.675934
		BIMS	49754	0.981889	0.0383857
		MIMS	60283	0.896835	0.523747
D	75331/ 76029	CEP	161171	0.738625	1.19673
		MIMS	168700	0.807566	0.953168
E	75345/ 76291	CEP	50824	0.910671	0.875266
		BIMS	51548	0.947073	0.04620

Table 2.6 Linear normalization factors for the Atmosphere Explorer ion measurements during the elliptical phase.

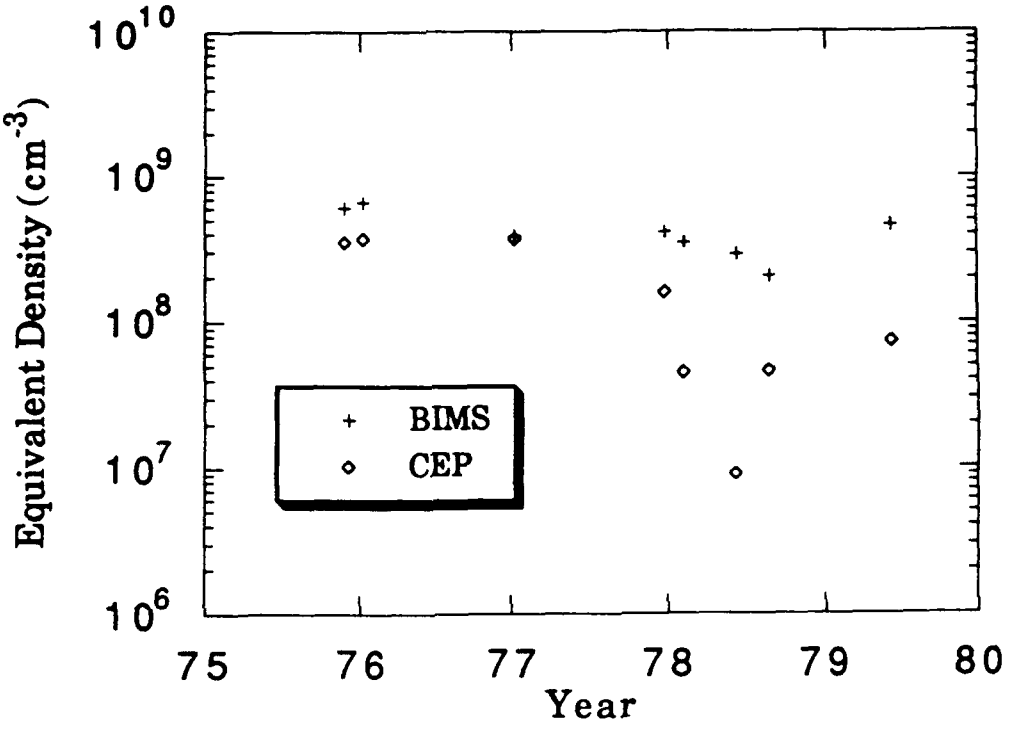

Figure 2.13 Equivalent RPA densities over life time of AE-E. Assumed measurement is $1x10^9$ cm^{-3} by the indicated instrument. Each point uses normalization for a 15 day period.

CHAPTER III

THEORETICAL MODEL OF 5577Å OI EMISSION

3.1 Introduction

In this chapter the development of a theoretical model for the production of $O(^1S)$ will be discussed. The model will be constructed to use data from the Atmosphere Explorer satellites if available to calculate volume emission rate profiles. The simulated volume emission rate (VER) profiles will be used to study the various sources of $O(^1S)$ in order to determine their importance to the dayglow emission. The model will also be used to study the individual reactions themselves.

The photochemical model requires some inputs that are not available from the satellites. These inputs are produced by other models and include solar flux, neutral, and ionic parameters. The models used have been developed for and used in a number of investigations and can be used to fill in gaps in the satellite data, as well as, provide vertical profiles of densities and temperatures. Figure 3.1 gives a general flow for the various models used in the production of $O(^1S)$.

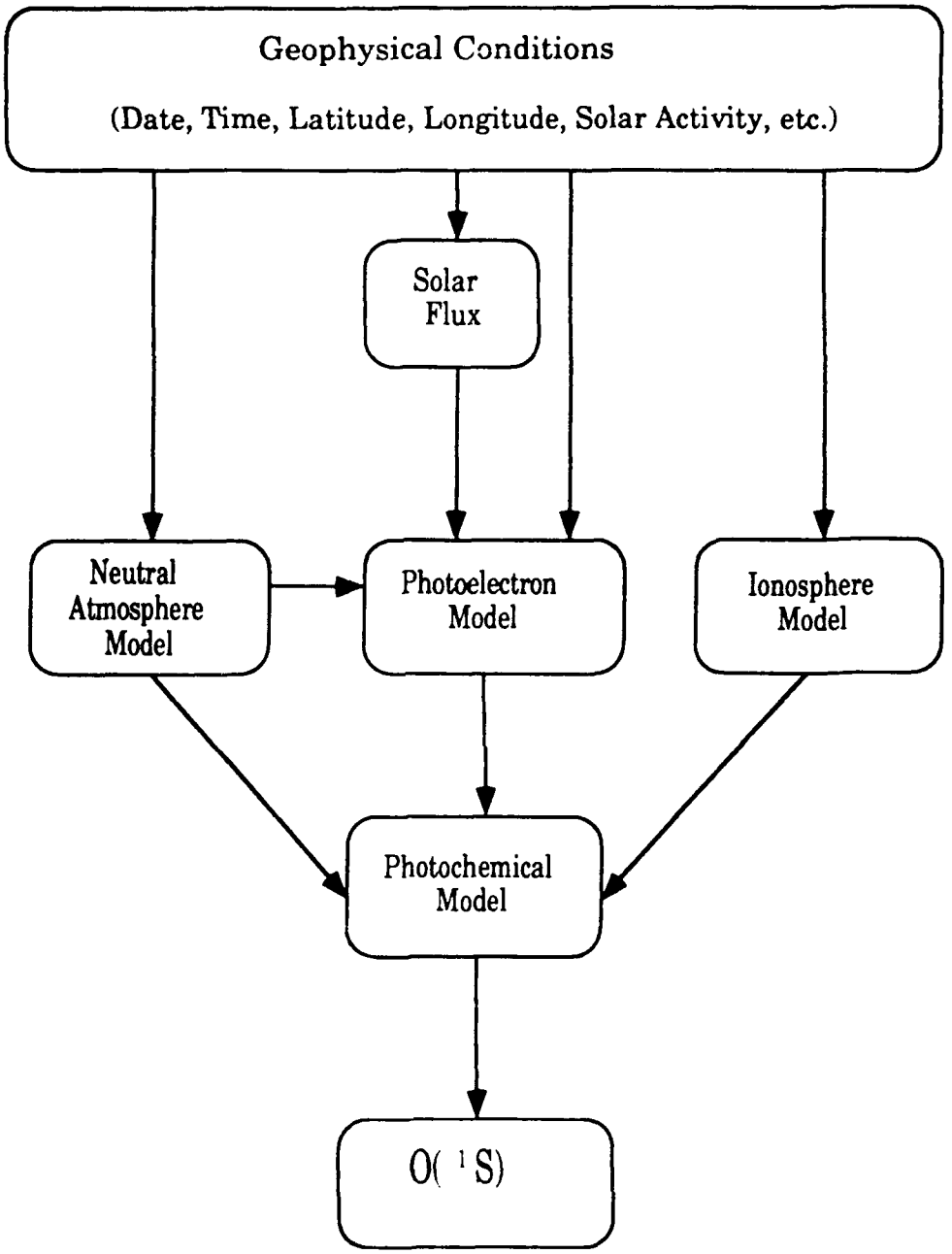

Figure 3.1 Simple flow diagram showing the models used with the satellite data to calculate the production of $O(^1S)$.

Each of the individual models will be discussed separately in this chapter. The general model will be covered and examples of the outputs shown. The use of the individual model sources to supplement or replace the satellite data will be covered in Section 3.3. As seen in Section 1.2, there are numerous reactions that may be applicable to the 5577Å dayglow emission. The selection of the reactions for production and losses in the photochemical model of 5577Å emission will also be discussed in Section 3.2.

3.2 Photochemical Modelling of 5577Å OI Emission

The various source and loss reactions that have been suggested for the production of the $O(^1S)$ in the upper atmosphere were discussed in Chapter I. The reactions were discussed from a historical standpoint. To produce the photochemical model, the reactions were examined to determine those that would be applicable to the thermospheric 5577Å emission. The reactions concluded of possible importance are listed in Table 3.1. These source and loss reactions will be briefly reviewed then the use of the reactions in the photochemical model will be discussed.

The major source of upper thermospheric $O(^1S)$ in the dayglow is direct excitation of $O(^3P)$ by photoelectron impact (Wallace and McElroy, 1966),

$$O(^3P) + e_p \xrightarrow{\gamma_1} O(^1S) + e_p \,. \qquad [3.1]$$

The production rate for this reaction is a function of atomic oxygen density, [O], given by

	Sources	
R 3.1	$O(^3P) + e_p \Rightarrow O(^1S) + e_p$	See Text
R 3.3	$O_2^+ + e_t \Rightarrow O(^1S) + O$	Torr and Torr (1981)
R3.7	$O(^3P) + N_2 (A^3\Sigma_u^+) \Rightarrow O(^1S) + N_2$	See Text
R 3.9	$O_2 + h\nu \Rightarrow O(^1S) + O$	Lawerence and McEwan (1973)
R 3.12	$O_2^+ + N \Rightarrow O(^1S) + NO^+$	Frederick *et al.* (1976)
	Losses	
R 3.14	$O(^1S) \Rightarrow O(^1D) + h\nu$ (5577Å)	Kernahan and Pang (1975)
R 3.15	$O(^1S) \Rightarrow O(^3P) + h\nu$ (2972Å)	Kernahan and Pang (1975)

Table 3.1 List of proposed source and loss reactions for the upper layer $O(^1S)$.

$$P_1 = [O]\int f_e(E_e)\sigma(E_e)dE_e. \qquad [3.2]$$

The integral over electron energy E_e contains the photoelectron flux, f_e, and σ, the cross section for electron impact, both of which are functions of electron energy.

As discussed in Chapter 1, the cross section for excitation of $O(^1S)$ by electron impact has been studied by using laboratory measurements (Shyn *et al.* ,1986; Doering and Gulcicek, 1989) and from theoretical calculations (Smith *et al.*, 1967; Henry et al., 1969; Thomas and Nesbet, 1975 and Vo Ky Lan *et al.*, 1972; Berrington, 1991). The theoretical cross sections are lower than the measurements of Shyn *et al.* (1986) by a factor of approximately 2 and those by Doering and Gulcicek (1989) by a factor of about 1.5.

Since this is the dominant source of $O(^1S)$ in the dayglow, it is important to know the magnitude of the cross-section for this reaction. Over the energy range of 1 to 100 eV, a correction factor for the magnitude of the parameterized cross sections of Green and Stolarski (1972) will be determined by doing a least squares fit to the VAE observations. This derived cross section will then be compared to those determined by the previous studies.

The dissociative recombination reaction for O_2^+,

$$O_2^+ + e_t \xrightarrow{\gamma_3} O(^1S) + O\ , \qquad [3.3]$$

is an important source of green line emission at night and at higher altitudes in the dayglow but is a minor source near the peak of the emission. The production rate for $O(^1S)$ from this reaction is,

$$P_3 = \beta_3 \gamma_3 [O_2^+][e_t]. \qquad [3.4]$$

The total reaction rate as a function of electron temperature,

$$\gamma_3 = 1.6 \times 10^{-7} \left(\frac{300}{T_e} \right)^{0.55}, \qquad [3.5]$$

is taken from Torr *et al.* (1976). The amount of $O(^1S)$ produced by the dissociative recombination is dependant on the vibrational excitation of the O_2^+ and is not conclusively known. Mul and McGowan (1979) concluded the total rate coefficient is not substantially affected by the vibrational excitation of the O_2^+ ion. The quantum yield of $O(^1S)$, β_3, is a function of the vibrational population of O_2^+ and can be expressed in terms of the ratio of electron density to atomic oxygen,

$$\beta_3 = \frac{[e_t]}{[O]} \left(\frac{300}{T_e} \right)^{0.7}, \qquad [3.6]$$

as discussed in Abreu *et al.* (1983) and Yee *et al.* (1989).

The energy transfer reaction of $N_2(A^3\Sigma_u^+)$ by atomic oxygen,

$$N_2(A^3\Sigma_u^+) + O(^3P) \xrightarrow{\gamma_7} N_2 + O(^1S), \qquad [3.7]$$

can produce a major portion of the $O(^1S)$ at altitudes near the peak in the thermospheric emission layer. The effective rate of production of $O(^1S)$ from this reaction,

$$P_7 = \beta_7 \gamma_7 [N_2(A^3\Sigma_u^+)][O], \qquad [3.8]$$

can be expressed as a product of the total rate coefficient for the production of all states of atomic oxygen and the quantum yield or branching ratio for the amount produced in the $O(^1S)$ state. As was discussed in Chapter 1, the branching ratio, β_7, is not well known and there is still some disagreement in the total rate for this reaction, γ_7, as well. Table 3.2 is a list of some of the rate coefficients and branching ratios for this reaction that have been determined by previous studies.

As can be seen from the discussion in Chapter 1 and from Table XXX, this reaction has been repeatedly accepted and rejected as an important source of $O(^1S)$ in aurora. The importance to the dayglow 5577Å emission has not been conclusively determined. Frederick *et al.* (1976) assumed the values for the total rate coefficient and branching ratios based on auroral studies. Using these values, a small contribution to the total $O(^1S)$ production was found and led to the search for other source reactions in the dayglow.

This reaction will be studied in two parts. First, the total rate coefficient for the quenching of $N_2(A)$ will be determined by a study of the 3371Å emission of N_2 in Chapter 4. The value of the total rate coefficient will be compared with previous values determined. In Chapter 5, this value for the total rate coefficient will be used to find the branching ratio for the production of $O(^1S)$ due to this reaction. An effective branching ratio for the production of $O(^1S)$ from energy transfer from $N_2(A)$ under dayglow conditions will be determined and the results compared to recent laboratory and aeronomical values.

Total Rate ($\times 10^{-11}$)	Branching Ratio	Study	Comments
Laboratory Values			
υ=0 3.5±0.6 υ=1 4.1±0.5 υ=2 4.6±0.6 υ=3 5.2±0.8		Thomas and Kaufmann	
υ=0 2.8±0.4 υ=1 3.4±0.6	0.75±0.13	Piper *et al.*	
υ=0 2.8 υ=1 3.3 υ=2 3.6	0.75	De Souza *et al.*	Branching ratio determined from numerical solution of differential equations
Aeronomical Values			
3.0	0.10	Frederick *et al.*	Branching ratio set to match auroral determination
2.0	0.29	O' Neil *et al.*	Precede artificial aurora experiment using Koneshea *et al.* (1978) atmospheric model
12.0	0.30 0.45	Sharp and Torr	For υ=0,1 For υ=0,1,2

Table 3.2 Summary of previous values of the total rate coefficient and branching ratios used for Reaction [3.7].

Photodissociation of O_2 whose possible importance was pointed out by Bates and Dalgarno (1954),

$$O_2 + h\nu \xrightarrow{\gamma_9} O(^1S) + O, \qquad [3.9]$$

is a very minor source for the production of $O(^1S)$ at altitudes above 140 km. However, this reaction becomes the dominant source at 120 km. The cross sections for this reaction have been given by Lawrence and McEwan (1973). The rate for this reaction as a function of O_2 density is,

$$P_9 = [O_2] \int f(\lambda) q(\lambda) \sigma(\lambda) d\lambda, \qquad [3.10]$$

where $f(\lambda)$ is the attenuated solar flux, $\sigma(\lambda)$ is the photodissociation cross section, and $q(\lambda)$ is the quantum yield of $O(^1S)$ all as a function of wavelength, λ. An expression for the attenuated solar flux is

$$f(\lambda) = f_\infty(\lambda) \exp\left(-\sum_i \int \sigma_{ai}(\lambda) n_i(s)\, ds \right), \qquad [3.11]$$

where s is the distance along the path from the sun to the point in the atmosphere, $f_\infty(\lambda)$ is the unattenuated solar flux, $\sigma_{ai}(\lambda)$ is the total absorption cross section, and $n_i(s)$ is the number density of the ith species along the path. The species included in the solar flux attenuation are atomic oxygen, O_2 and N_2. At or above perigee for the AE satellites, the attenuation of the flux for this reaction is small.

Ion-atom interchange between O_2^+ and atomic nitrogen,

$$O_2^+ + N \xrightarrow{\gamma_{12}} O(^1S) + NO^+, \qquad [3.12]$$

was considered by Frederick *et al.* (1976) as the required additional source of $O(^1S)$ at low altitudes. The rate of production for this process is,

$$P_{12} = \beta_{12}\,\gamma_{12}[O_2^+][N]. \qquad [3.13]$$

A rate coefficient, γ_{12}, of 2.5 x 10^{-11} cm^3 s^{-1} was used in Frederick's model for the analysis of the 5577Å dayglow. The uncertainties in the nitrogen density gives a range of the rate coefficient from 1.2 x 10^{-11} to 5.0 x 10^{-11} cm^3 s^{-1} (Frederick *et al.*, 1976). This reaction may or may not be significant for the production of 5577Å emission depending on the solar flux and the impact cross section for electrons on atomic oxygen.

The loss processes of $O(^1S)$ at the level of the thermospheric emission are the radiative transitions to the $O(^1D)$ and $O(^3P)$ states,

$$O(^1S) \xrightarrow{A_{14}} O(^1D) + h\nu(5577Å), \qquad [3.14]$$

$$O(^1S) \xrightarrow{A_{15}} O(^3P) + h\nu(2972Å), \qquad [3.15]$$

with transition probabilities of 1.06 s^{-1} and 0.045 s^{-1}, respectively (Kernahan and Pang, 1975). Losses of $O(^1S)$ due to quenching are not important at the altitudes of the thermospheric emission. Quenching of $O(^1S)$ by $O(^3P)$ has a reaction rate of 2 x 10^{-14} cm^3 s^{-1} (Krauss and Neumann, 1975) and can be ignored in modeling. The quenching by N_2 rate of about 5 x 10^{-17} cm^3 s^{-1} as noted in Chapter 1 and that by O_2 is a very small factor above about 125 km.

A photochemical model was developed using the reactions discussed in the introduction as the sources and losses initially. Some of the reactions

discussed were later removed from the model since they could not produce enough $O(^1S)$ to be of any consequence in the dayglow. The model developed includes the following reactions. The sources of $O(^1S)$ are photoelectron impact on atomic oxygen (1), quenching of $N_2(A)$ by atomic oxygen (7), dissociative recombination of O_2^+ (3), and photo dissociation of O_2 (9). The only losses are the radiative transitions from $O(^1S)$ to either $O(^1D)$ or $O(^3P)$. Using these reactions the production of $O(^1S)$ is

$$\left[O(^1S)\right] = \frac{\{P_1 + P_3 + P_7 + P_9\}}{\{A_{5577} + A_{2972}\}} . \qquad [3.16]$$

Where A_{5577} and A_{2972} are the Einstein transition probabilities for the radiative loss processes and P_1, P_3, P_7, and P_9 are the production rates previously discussed. Ion-atom interchange process in Reaction [3.12] is included in the model, Equation [3.16] becomes,

$$\left[O(^1S)\right] = \frac{\{P_1 + P_3 + P_7 + P_9 + P_{12}\}}{\{A_{5577} + A_{2972}\}} , \qquad [3.17]$$

where P_{12} is the production of $O(^1S)$ from the reaction. The importance of this reaction to the 5577Å dayglow emission will be discussed in Section 3.4.

The photochemical model calculates the volume emission rate at each given point in space. A schematic diagram of the model is presented in Figure 3.2 and shows the general flow of the photochemical model. The

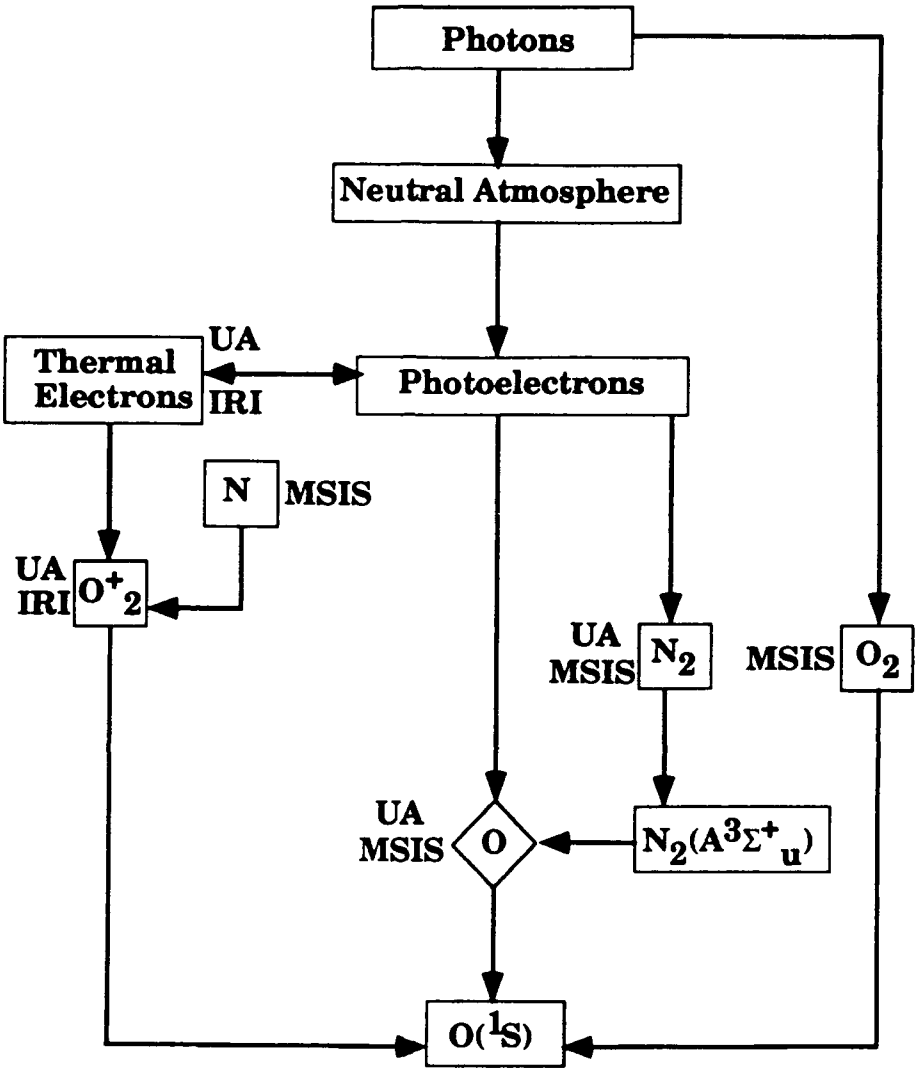

Figure 3.2 Schematic diagram of the photochemical model showing the various possible sources of the atmospheric constituents used to calculate the population of $O(^1S)$.

schematic (Figure 3.2) indicates the sources for the constituents required for the chemical reactions. The model employs in-situ atmospheric composition measurements from the AE satellites when they are available. The instruments used to collect the data were discussed in Chapter II. Data were obtained for most of the chemical species from more than one instrument to insure the most complete measured profiles possible. Atomic oxygen and N_2 densities were measured by the Open-Source Spectrometer (OSS) (Nier *et al.*, 1973) and the Neutral-Atmosphere Composition Experiment (NACE) (Pelz *et al.*, 1973). The Neutral-Atmosphere Temperature instrument (NATE) (Spencer *et al.*, 1973) provided temperature measurements. Ion composition data were collected by the Bennett Ion-Mass Spectrometer (BIMS) (Brinton *et al.*, 1973) and the Magnetic Ion-Mass Spectrometer (MIMS) (Hoffman *et al.*, 1973). Electron temperatures are from the Cylindrical Electrostatic Probes (CEP) (Brace *et al.*, 1973) and electron densities were obtained from the Retarding Potential Analyzer (RPA) (Hanson *et al.*, 1973). To avoid possible inconsistencies between the data from the various sources, the ion composition measurements were normalized to those made by the RPA. This was done by performing a least squares fitting of the data between the RPA and the ion mass spectrometers individually over the elliptical phase of the satellite's lifetime.

When an in-situ measured parameter is not available, the photochemical model employs the Mass Spectrometer and Incoherent Scatter model (MSIS-86) (Hedin, 1987) to provide neutral densities and temperatures and the International Reference Ionosphere (IRI) (Belitza, 1986; 1990a) for plasma densities and temperatures. When these model

parameters are used, they are normalized to the available in-situ satellite measurements.

Since both of the important reactions being studied are dependant on the solar flux, the model employs a solar flux spectrum based on the Hinteregger Reference Spectra (Hinteregger *et al.*, 1981) and is scaled by the level of solar activity. The solar flux below 250Å is corrected by a factor of two as discussed by Richards and Torr (1984). The photoelectron spectrum is produced using the photoelectron model based on the two stream approximation (Nagy and Banks, 1970). The photoelectron model is used to calculate the production of $O(^1S)$ from direct excitation of atomic oxygen and the $N_2(A)$ population due to both direct excitation and cascading from the higher excited states of the nitrogen molecule.

For a given model run, measured or modeled values for the atmospheric parameters are obtained at 15 second intervals along the orbit, as the satellite moves towards and then away from perigee. At each point along a satellite orbit where the volume emission rate is determined, a complete profile in 5 km steps between 80 and 500 km is generated by the MSIS-86 and IRI models which are scaled by the in-situ measurements made at the point the volume emission rate is being determined. These vertical profiles are used to produce the photoelectron fluxes and direct excitations used by the model to determine the volume emission rate at the point of measurement. This procedure compensates for the variation in photoelectron production as the satellite moves along the path to different latitudes, longitudes and solar zenith angles. Once the profiles are constructed, the model determines the volume emission rate at 5577Å for that point using the measured in-situ constituent data. This procedure is repeated at each point where in-situ measurements are made. Since each

point is calculated independently, a profile of the model volume emission rate can be constructed from a series of constituent measurements along the satellite track.

As mentioned before, the model is constructed to be run if some of the satellite data are not available. The photochemical model will use various atmospheric model to fill the data gaps from the satellite. These models can also supply all of the needed inputs to the photochemical model to allow it to run independant of the satellite. These various models will be discussed individually in the next section. Examples of the model output will be given in section 3.4. These examples will give the results both with and without satellite data. This model will be used to examine the major reactions responsible for producing the 5577Å dayglow emission. In Chapter VI, the model will be used to examine the emission profile during twilight conditions.

3.3 Models for Atmospheric Parameters

The photochemical model of the thermospheric 5577Å emission requires inputs that either are not available from the satellite observations or are missing at a given point in the orbit This is also required if the model is to be used without satellite input. These parameters are supplied by separate models which have been incorporated into the photochemical model. Where possible these inputs are scaled to fit the observed parameters. The models used, discussed in this section separately, include a solar flux model, the Mass Spectrometer and Incoherent Scatter (MSIS) model, the International Reference Ionosphere (IRI) model, and a photoelectron/electron transport model.

3.3.1 The Solar Flux Model

During the daytime at midlatitudes, the upper atmospheric process are dominated by those that are either directly or indirectly by the sun. The solar radiation is absorbed by the gasses of the atmosphere which are then either excited, ionized or dissociated. The result of the energy deposited in the upper atmosphere is heating of the upper atmosphere. The part of the solar spectrum that is most important to the thermosphere is the x-ray and ultraviolet regions below about 2000Å. The bulk of this radiation is absorbed above 100 km.

The solar radiation shorter than 1000Å has enough energy to ionize the predominant species in the atmosphere. While the region between 1000Å and 2000Å is almost completely absorbed in the dissociation of O_2. This short wavelength radiation is a small part of the total radiation flux from the sum, less than 1 part in 10^5 (Ratcliffe, 1972; Wallace and Hobbs, 1977). But, the mass of the absorbing part of the atmosphere is a small fraction of the total atmospheric mass, so the input of energy per unit mass is extremely large. This energy input becomes even larger during solar disturbances when wavelengths less than about 1000Å can increase by orders of magnitude. The changes in solar flux due to solar activity are shown in Figure 3.3.

To model the 5577Å dayglow emission it is necessary to have the solar flux as a direct or indirect input to several of the reactions. The model used here gives the solar EUV and FUV flux at the top of the atmosphere in the range of 1 to 1750Å based on a specification of the level of solar activity. This solar flux is used to calculate the direct excitation of $O(^1S)$ as well as various ions and the photoelectrons that can be used to produce $O(^1S)$. The solar

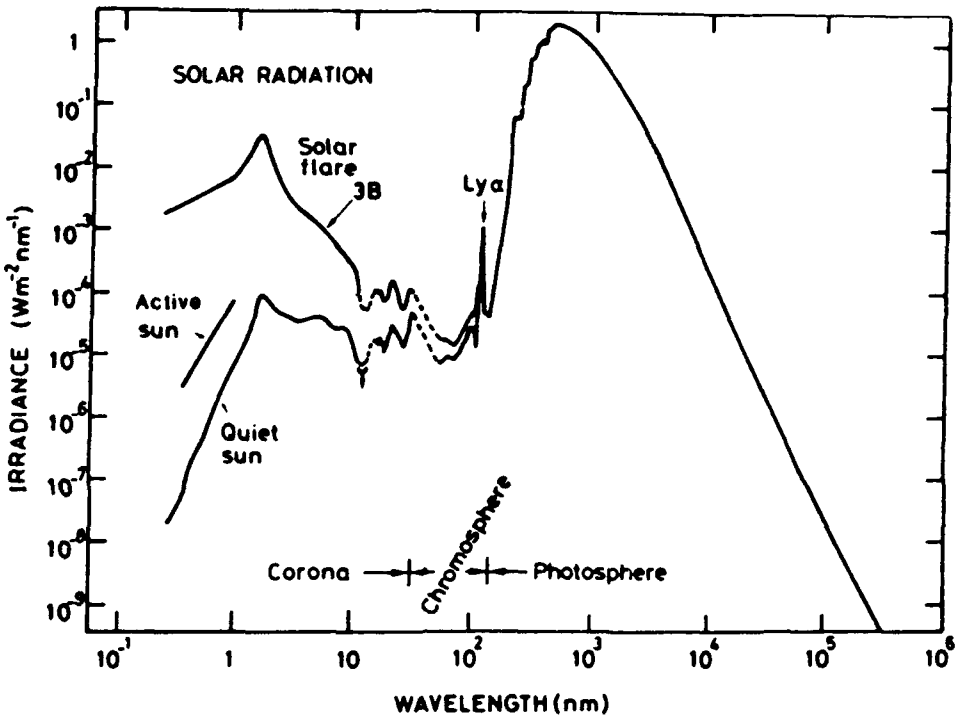

Figure 3.3 Spectral distribution of the solar irradiance and its variation with solar activity. This representation emphasizes the x-ray and EUV contribution (After Smith and Gottleib, 1974).

flux is input to other models, which will be discussed later, to produce the desired quantities for modelling the 5577Å emission.

The model has several methods of estimating the solar flux depending on the level of solar activity. each of these methods will be briefly described here. Details of these methods are given in the listing in Appendix A along with the various data sets used by the different methods. After the different methods are described, examples of the models will be shown for different activity cases.

In the first case, the flux is scaled using parametrization methods based on the daily 10.7 cm radio flux and the 81 day centered average 10.7 cm flux. For the ionizing EUV flux, Hinteregger's contrast ratio method (Hinteregger *et al.*, 1981) is used, based on the Torr and Torr (1985) bin structure for reference spectrum SC#21REFW. The 1026Å (Hydrogen Lyman Beta) and 335Å (Iron XVI) enhancement ratios are calculated from Hinteregger's formula. The flux spectrum is then calculated from these emissions using Hinteregger's method. For Hydrogen Lyman alpha line at 1216Å, the correlation relationship derived from SME data by Tobiska and Barth (1990) is used. For the Schumann-Runge continuum, the Torr *et al.* (1980) 50Å bin structure is used but the coefficients have been adjusted to reflect SME and LASP rocket data (Rottman, 1981, 1988; Mount and Rottman, 1983, 1985).

Another method of determining the solar flux is by linear interpolation between high and low activity spectra. This method is based on daily 10.7 cm radio flux alone. It is assumed that the low activity spectrum corresponds to a 10.7 cm flux of 68 and the high activity spectrum to 243. The Hinteregger SC#21REFW and F79050 spectra as binned by Torr & Torr (1985) are used for ionizing EUV. For the 1050Å-1350Å region, the

SC#21REFW spectrum for low solar activity is scaled by the contrast ratios to obtain the high activity spectrum. For Lyman alpha and the Schumann-Runge continuum, linear interpolation is essentially the same parametrization as above.

The next two methods do not cover the spectral range of the previous methods. To keep the range the same these methods use one of the above methods and then replaces the values for their spectral range. The first of these methods is the model by Tobiska and Barth (1990) which uses the linear interpolation method to complete the spectrum of solar fluxes and model the spectrum between 32Å to 1050Å. The procedure involves using 10.7 cm flux and the Hydrogen Lyman alpha flux, considered as representative of the coronal/transition region and the chromospheric emissions, respectively. The chromospheric fluxes are calculated from a linear correlation relationship with the Hydrogen Lyman alpha flux. While the coronal fluxes are calculated from a combination of 10.7 cm flux and a "modeled" 10.7 cm flux based on Hydrogen Lyman alpha flux. The coronal and chromospheric scaled fluxes are then summed to obtain the value of the solar flux.

The last method uses the Hinteregger contrast ratio method for the spectrum and the Woods and Rottman rocket spectrum for 10 November, 1988 for the region from 300-1050Å. None of the above models extends shortwards of 18Å. An amalgam of sources are used to estimate the flux in this region, e.g., DeJager, 1964; Smith & Gottlieb, 1974; Manson, 1977; Kreplin *et al.*, 1977; Horan and Kreplin, 1981; Wagner, 1988. For the first two methods, the EUV fluxes between 250Å and 50Å are normalized upwards (after Richards and Torr, 1984). The EUV normalization coefficient is 2.0 for a 10.7 cm flux of 68 and reduces linearly to 1.0 for a 10.7

cm flux of 243. Examples of the solar flux are shown in Figure 3.4 for different solar conditions and each of the methods above.

3.3.2 The Neutral Atmosphere Model

As can be seen from Figures 3.1 and 3.2, the modelling of $O(^1S)$ requires a neutral atmosphere model. The model serves two roles, the first is to provide density and temperature profiles for use in the photoelectron model discussed below. These profiles are scaled to match the satellite measurements where possible. The model is also used to fill in for the satellite when some of the parameters normally measured are missing. The neutral model can also be used to calculate the profiles of emission above and below the satellite or in cases when the satellite is not used.

The neutral atmosphere model used is the Mass Spectrometer and Incoherent Scatter (MSIS) model of Hedin (1983, 1987). The MSIS-86 model uses data collected by satellites, rocket measurements and ground based incoherent scatter radars to produce a composite model of the densities for selected species and temperatures. Table 3.3 is a summary of the data sources used in the production of the MSIS-86 model. The MSIS-86 model is an extension of the MSIS-83 model into the polar regions using the additional data from the Dynamics Explorer satellite and the addition of atomic nitrogen as an output species.

In the MSIS model, data are fit to equations for the temperature and density by least squares methods. The fitting equations are spherical harmonic expansions in terms of local time and geographic latitude. The coefficients for the equations are dependant on solar and magnetic activity as well as season (Hedin *et al.*, 1974). The temperature profile is created by joining a Bates (1959) temperature profile for the upper thermosphere to an

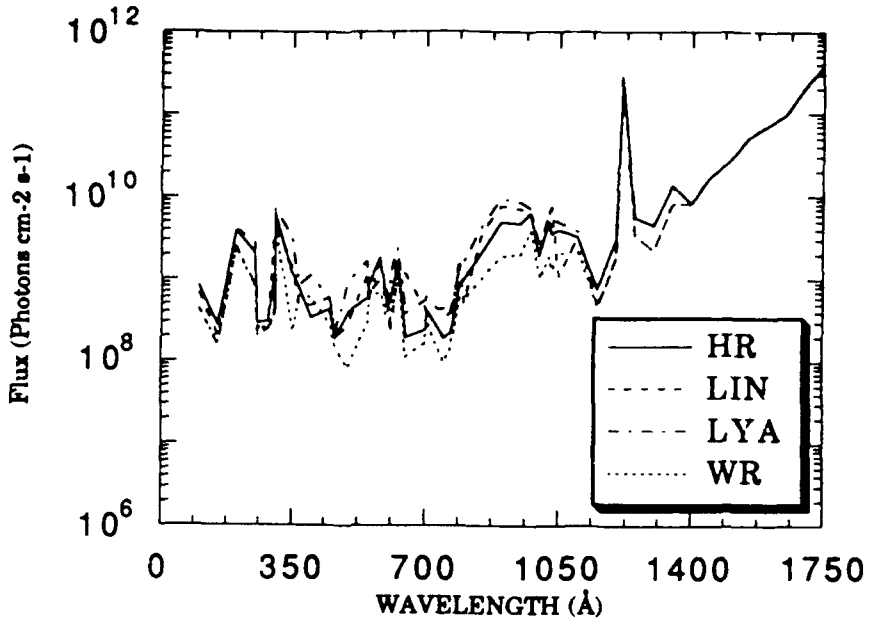

(a)

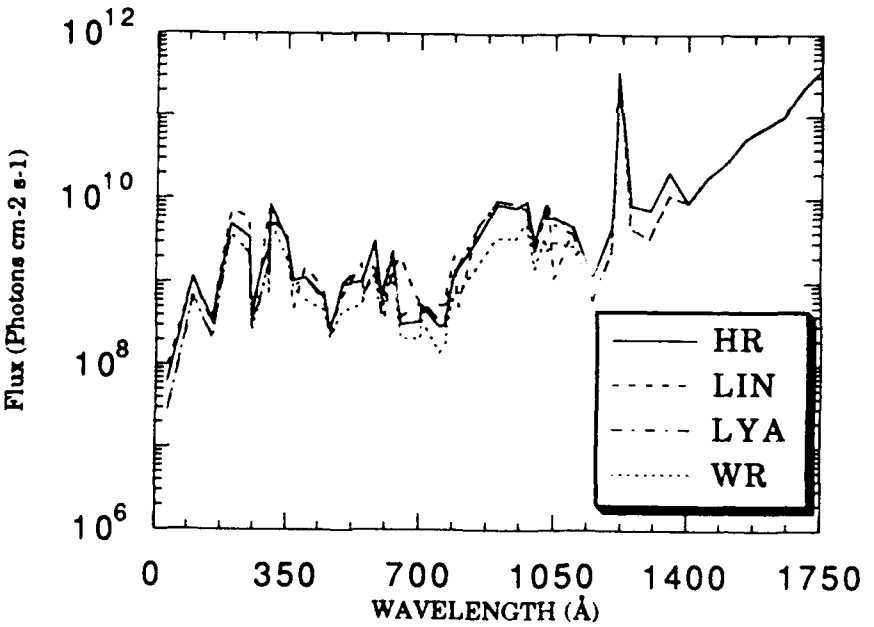

(b)

Figure 3.4 Model solar flux from the various methods for (a) low solar activity and (b) high solar activity. [HR- Hinteregger Contrast Ratio; LIN- Hinteregger Linear Interpolation; LYA- Lyman α scaling of Tobiska and Barth; WR- Woods and Rottman Rocket Spectrum]

SOURCE	MEASUREMENT								
	N2	O	He	H	N	O2	Ar	Tp	Rho
Satellites									
OGO-6	X	X	X						
San Marcos-3	X	X	X				X		
AEROS-A	X	X	X				X		
AE-C	X	X	X	X	X	X	X	X	
AE-D	X	X	X		X	X	X	X	
AE-E	X	X	X	X	X	X	X	X	
ESRO-4	X	X	X				X		
DE-B	X	X	X		X		X		
Rocket									
MS	X					X	X	X	
Absorp						X			
Guage								X	X
Falling Sphere								X	X
Grenade								X	X
Radars									
Millstone Hill								X	
St. Santin								X	
Arecibo	X							X	
Jicamarca								X	
Malvern								X	

Table 3.3 List of data sources used to produce the Mass Spectrometer and Incoherent Scatter model (After Hedin,1983,1987).

inverse polynomial profile for the lower thermosphere (Hedin, 1983). These profiles are joined at 116.5 km by matching the temperature and the temperature gradient.

Using the temperature profiles and and average density that is a function of location and solar and magnetic activity, the densities are determined. Using functional forms of the temperature profiles, the hydrostatic equation is integrated exactly to give an expression for the density in terms of the average density. To account for the homopause near 100 km, the models give density profiles that are sums of mixed and diffusive densities. The sum is multiplied by one or more factors to allow for changes due to chemistry and dynamics for each species. Details of the methods of calculation for these parameters and the expansion coefficient data sets are given in Hedin (1983, 1987) and are based on the methods of the OGO-6 model of Hedin *et al.* (1974).

The MSIS model produces densities for N_2, O_2, He, O, H, Ar, and N at a given altitude. It also produces two temperatures, the exospheric temperature and the neutral temperature at the altitude desired. Comparison of the model to subsets of the data used to produce the model show reasonably good agreement (Hedin, 1983, 1987). While the model densities can vary from the measurements by as much as 20% and the temperatures by as much as 40 K, an average error of about 10% in the density and about 15 K in temperature can be assumed. Figure 3.5 gives examples of the various density profiles for low and high solar activity.

3.3.3 The Ionospheric Model

Several of the possible source reactions for $O(^1S)$ require knowledge of temperatures and densities of the ionosphere. These include thermal

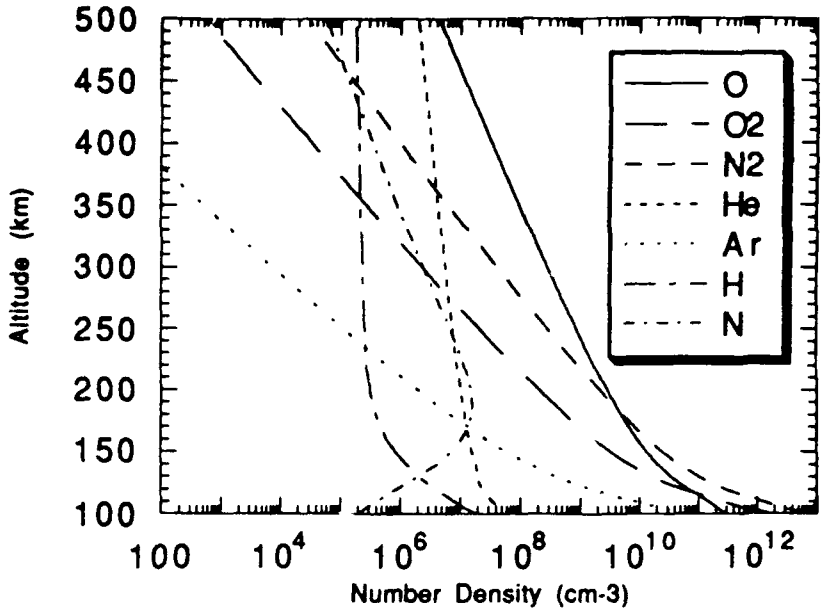

(a)

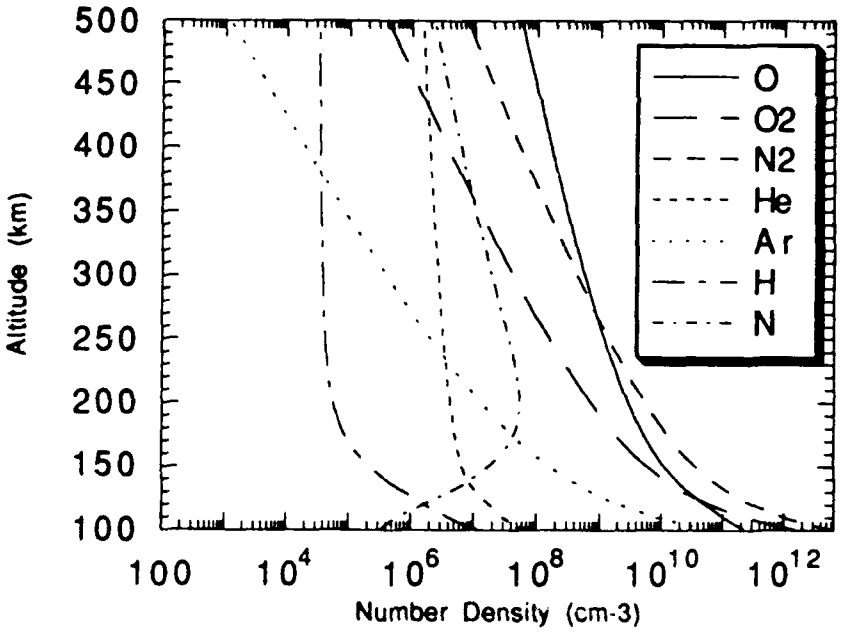

(b)

Figure 3.5 Neutral constituents from the MSIS model for (a) low solar activity and (b) high solar activity.

electron density and temperature and ionic species densities. As discussed before this information is available from the Atmosphere Explorer satellites but a model is needed if the information is not available. The model profiles can also be also be used to calculate the $O(^1S)$ production above and below the satellite track.

To provide this information, the International Reference Ionosphere (IRI) model is used. The IRI model describes monthly averages of the electron density, electron temperature and ion composition in an altitude range from 50 to 1000 km. The model is designed to operate under magnetically quiet conditions in non-auroral regions. The IRI model has been described by Rawer et al. (1981). Since its development the model has been extended and improved by the addition of ground and space data as described in a series of issues of Advances in Space Research (see Volume 2, No. 10, 1982; Volume 4, No. 1, 1984; Volume 5, No. 7 and No. 10, 1985; Volume 7, No. 6, 1987; Volume 8, No. 4, 1988; Volume 10, No. 8 and No. 11, 1990). The newest version of the model has been described by Belitza (1990a). Table 3.4 gives a summary of the various data sources used in the development of the IRI model.

The IRI model can be separated into three parts, the electron density profile, the temperature profiles and the ion density profiles. Each of these will be discussed below. The model uses a variety of analytical functions and expressions to represent the variations of the densities and temperatures. In most cases, these are in the form of spherical harmonic function. A group of functions known as the Epstein family have been used to represent the additional variations and other special latitudinal and diurnal features as described by Rawer (1987, 1988). The approach of

Data Sources	Measurement
Ionosondes	Peak Plasma Frequencies
Incoherent Scatter Radars Jicamarca Arecibo St. Santin Millstone Hill Malvern	E Valley F2 Peak Height F2 Bottomside, Topside Electron and Ion Temperature
Allouette 1 & 2	Topside Sounder Measurements
Atmosphere Explorer C	Electron Temperatures
ISIS 1 & 2	Electron temperatures
AEROS	Electron and Ion Temperatures Ion Composition
Various Rocket Measurements	D & E Region Electron Density and Ion Composition
Beacon Satellites	Ionospheric Electron Content Testing
Ground Based Absorption	D & E Region Variability

Table 3.4 Data sources used in the development of the International Reference Ionosphere model (After Belitza, 1990).

Booker (1977) is used to construct the altitude profiles. Both the Epstein functions and the Booker application are discussed in Appendix B.

The electron density profiles have 1000 km as an upper limit and either 60 or 80 km as a lower limit for daytime or night respectively. It is built from six sub-regions. These sub-regions are joined using the Booker approach. The middle ionosphere is determined by various layer parameters such as peak densities and heights, thicknesses, and valley parameters (Bilitza and Rawer, 1990).

The temperature profiles extend from 120 km to 1000 km in the IRI model. At the lower boundary, thermal equilibrium is assumed between the neutral species, ions and electrons. As altitude increases, temperatures are maintained with the electron temperature greater than the ion temperature which is greater than the neutral temperature. Neutral temperatures are derived from the CIRA-72 model. Both the ion and electron temperature profiles are constructed of sub-intervals which are defined using Booker functions. The methods of determining the electron temperatures are discussed by Bilitza (1984, 1990) and the ion temperatures in Bilitza (1990).

IRI determines the ion density profiles as percentages relative to the total ion density or the electron density profile. The model uses the Booker approach to determine the O^+ and O_2^+ profiles and fills the rest of the ionosphere with NO^+ at lower altitudes and uses H^+ and He^+ at higher altitudes. At higher altitudes, it is assumed that He^+ is 10% and H^+ is 90% of the remaining ions. The ion density parameters have variation with solar zenith angle during the daytime but because of the database limitations has no variations if the solar zenith angle is greater than 90 degrees. Details of the ion composition calculations is given by Bilitza

(1990a, 1990b). Variations of temperatures are not explicitly included in the model but may occur through the CIRA neutral temperatures.

The IRI model is designed to give ionospheric parameters in non-auroral, magnetically quiet times. IRI has been shown to give reasonable results for total electron content (TEC) for mid-latitude stations but underestimates daytime low latitude TEC (McNamara, 1984). IRI was tested along with other various ionospheric models by Brown *et al.* (1984). It was shown that IRI gives reasonable results for solar minimum conditions but consistently over estimates TEC during solar maximum. Temperatures from IRI are in good agreement with observations with most discrepancies attributed to the insufficient description of changes with season and solar activity (Buonsanto, 1989; Bilitza and Hoegy, 1990). The following Figures 3.6 and 3.7 show profiles of densities and temperatures for electron and ion species from the IRI model for various conditions.

3.3.4 The Photoelectron Model

During the daytime, the upper atmosphere is dominated by solar driven processes. The solar flux interacts with the upper atmosphere having three possible consequences: photodissociation of molecules, photoexcitation of atoms and molecules, and photoionization of atoms and molecules. The photelectrons produced by the ionization processes have sufficient energy to in turn dissociate, excite or ionize the neutral atmosphere further. This cascading process of photoelectrons is shown schematically in Figure 3.8.

The photoelectron model used is essentially the one described by Solomon (1987), Solomon *et al.* (1988), and Solomon and Abreu (1989). It uses the two stream electron transport model of Nagy and Banks (1970) to

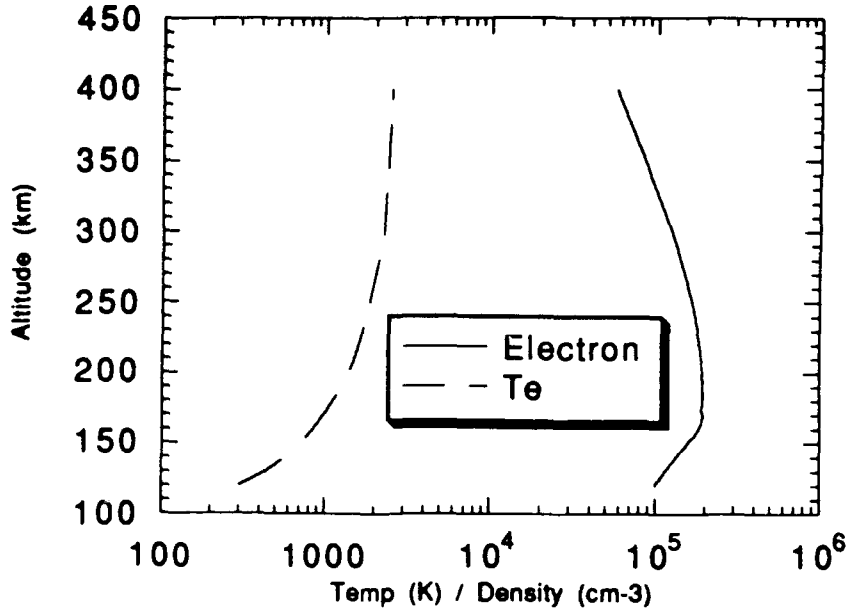

(a)

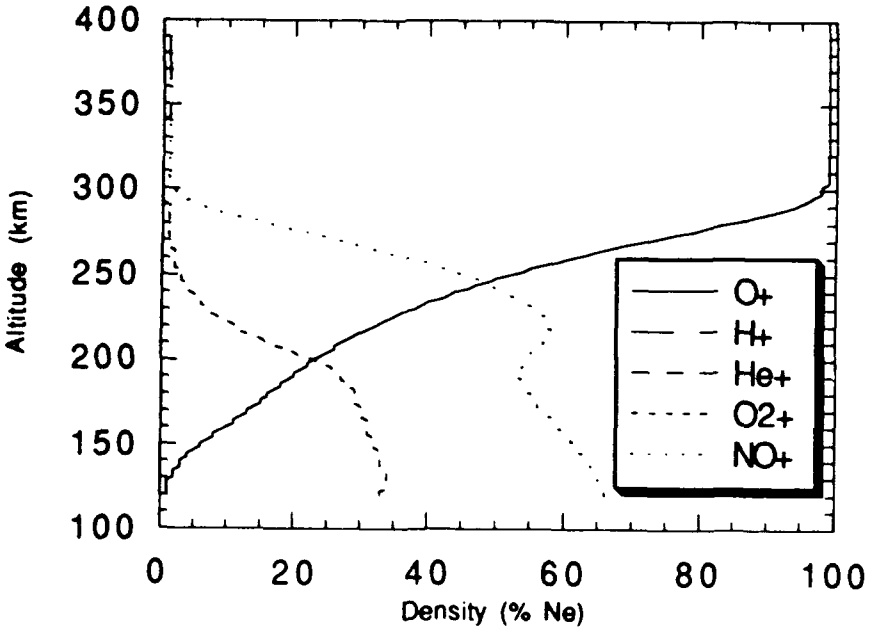

(b)

Figure 3.6 Results for the IRI model (a) electron temperature and number density and (b) Ion densities for low solar activity.

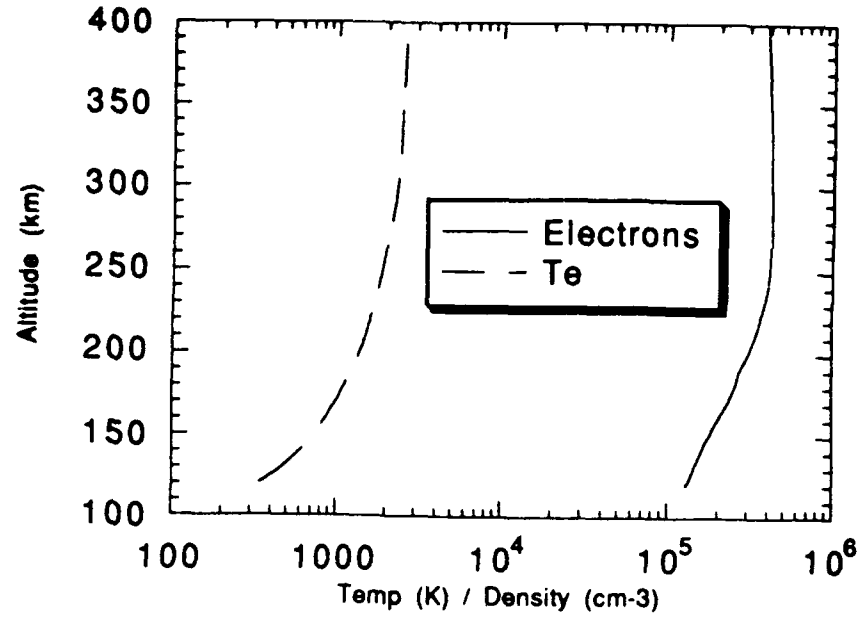

(a)

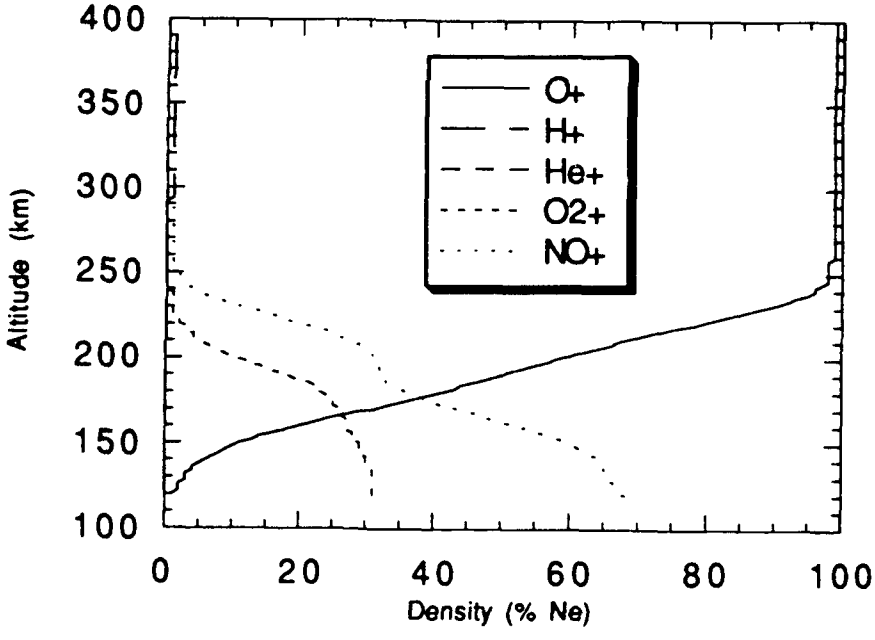

(b)

Figure 3.7 Results for the IRI model (a) electron temperature and number density and (b) ion densities for high solar activity.

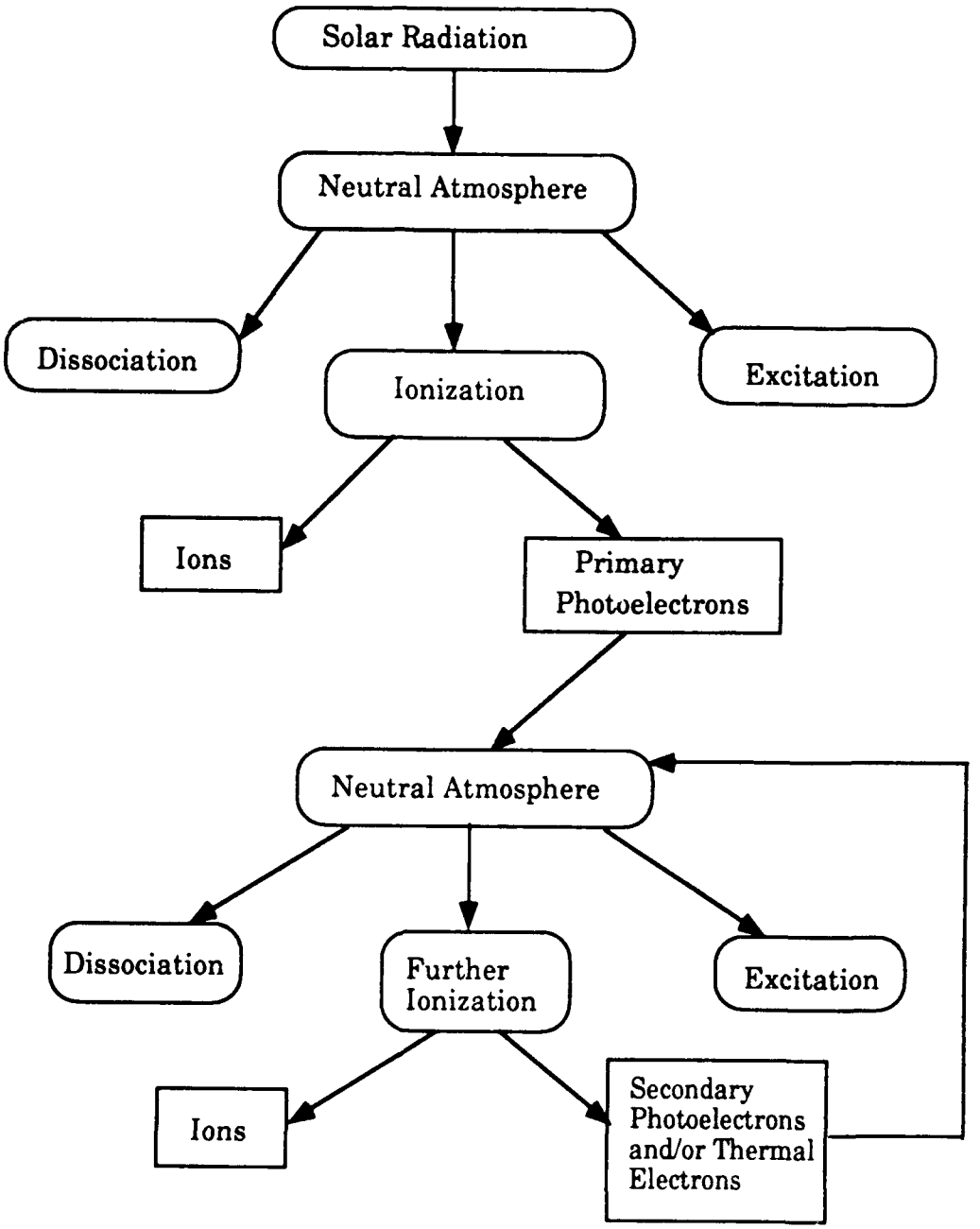

Figure 3.8 Simple flow diagram illustrating the cascading of photoelectrons from photoionization of the neutral atmospheric constituents.

calculate the photoelectron fluxes. The solar flux model described above is used as an input at the top of the atmosphere and is attenuated to a given altitude. The MSIS-86 model can be used to generate the density profiles for the major neutral species for attenuation of the solar flux and for ionization, dissociation, and excitation calculations. The photoionization cross sections are from Samson and Pareek (1985) and Kirby (1979). The electron impact cross sections are those used by Solomon (1988) and were calculated using the analytic fit parameters of Green and Stolarski (1972) and Jackman et al. (1977). Appendix C is a detailed discussion of the model and has tables showing the cross section parameters used.

The electron flux is calculated for the upward and downward hemispherical fluxes along a magnetic field line as a function of energy and altitude. The effects of gravity and electric and magnetic fields are neglected. The model does not allow for variations in the pitch angle, so the value of 0.577 was assumed for the average cosine of the pitch angle to characterize the transport as recommended by Banks *et al.* (1974). Discrete energy losses from inelastic collisions and elastic collisions with the neutral atmosphere are considered. The backscatter ratios for the inelastic collisions were assumed to be equal to those for elastic collisions.

To calculate the electron fluxes at a given point in the atmosphere, the electrons are binned according to energy in variable sized energy bins. Starting with the highest energy electrons, the secondary and degraded primary electrons are computed and added to the electron flux at each altitude and each bin of lower energy. The excitation and ionization due to this energy of electrons is also found. Then the next highest energy bin is calculated and the results added to those below it in energy. This process is

repeated until the lowest energy bin is reached. Figure 3.9 gives examples of the modeled fluxes.

3.4 Model Simulations of 5577Å Dayglow Emission

In the previous sections of this chapter the photochemical model of the 5577Å dayglow emission was described. Also, details of several subsiderary atmospheric models used in the photochemical model. In this section some examples of the output from the model will be presented. These examples will use data from the Atmosphere Explorer satellites. The model output will also be shown using input profiles from the atmospheric models in place of the *in-situ* measurements of the satellites under the same geophysical conditions. Figure 3.10 shows the relative importance of the selected reactions in a typical model run. Reaction [3.12] is included in this figure.

The atmospheric constituent profiles for the *in-situ* measurements are shown in Figures 3.11 and 3.12 for the up and down legs from AE-C orbit 0584 and AE-D orbit 0912 respectively. Orbit AE-C 0584 varied in solar zenith angle from 75 to 41 degrees during the down and up leg of the orbit respectively with an F10.7 of 80.0 and an Ap of 10.0. For AE-D 0912, the solar zenith angle changed from 54 degrees to 85 degrees and the f10.7 and Ap was 72.0 and 7.0 respectively. The resulting 5577Å emission from the various reactions are shown in Figures 3.13 and 3.14 for the photochemical model output from the *in-situ* data.

As discussed before, the production from the two major reactions in the dayglow has not been conclusivly established. The cross sections for electron impact on atomic oxygen varies by as much as a factor of two

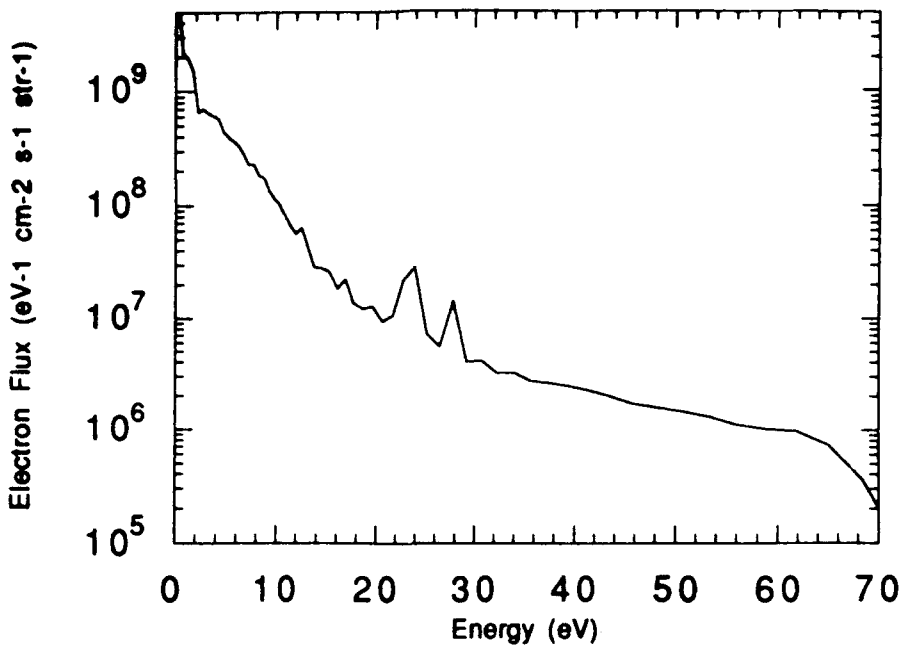

(a)

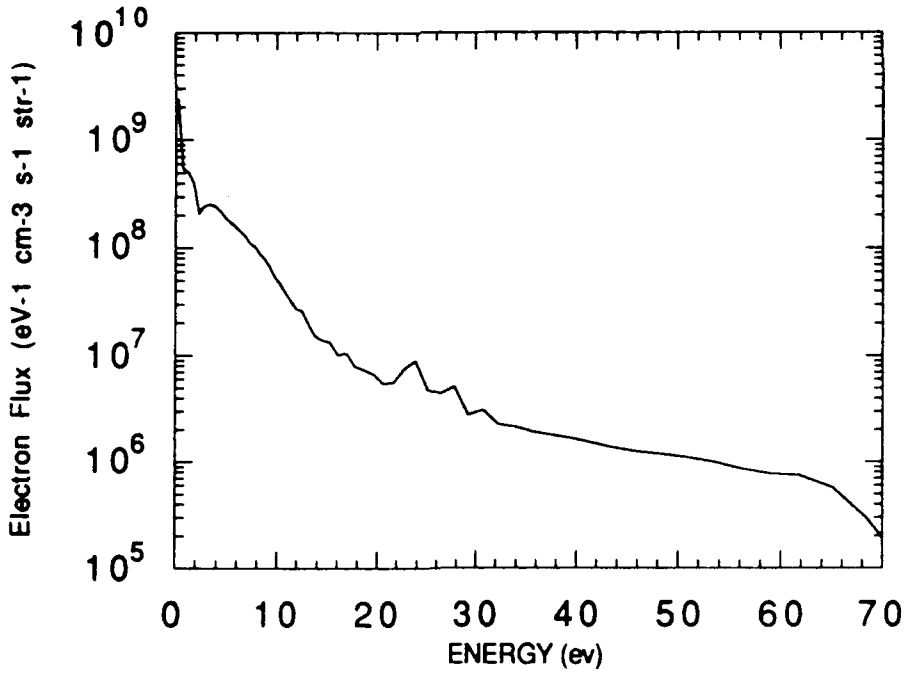

(b)

Figure 3.9 Sample spectrum of the modelled photoelectron flux at 300 km for (a) low activity and (b) high activity.

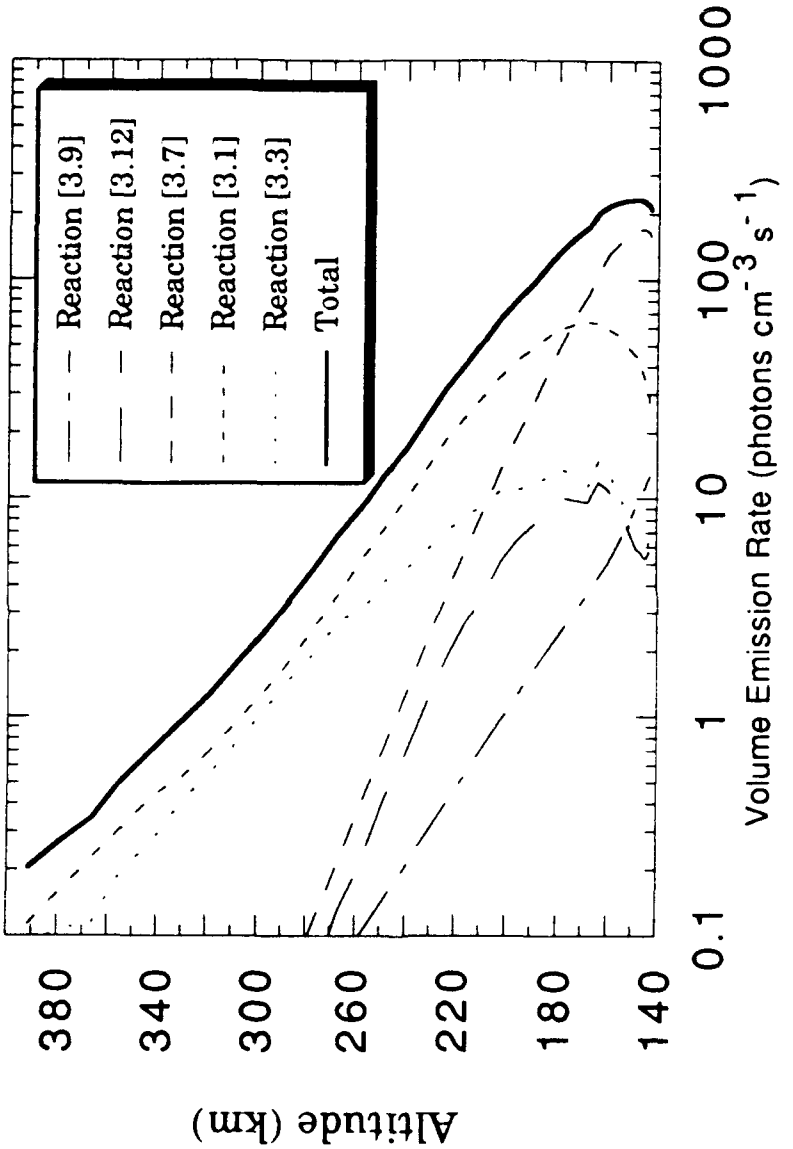

Figure 3.10 Plot of the model output based on constituent profiles provided by the subsidiary models showing the emission due to the various production reactions of $O(^1S)$.

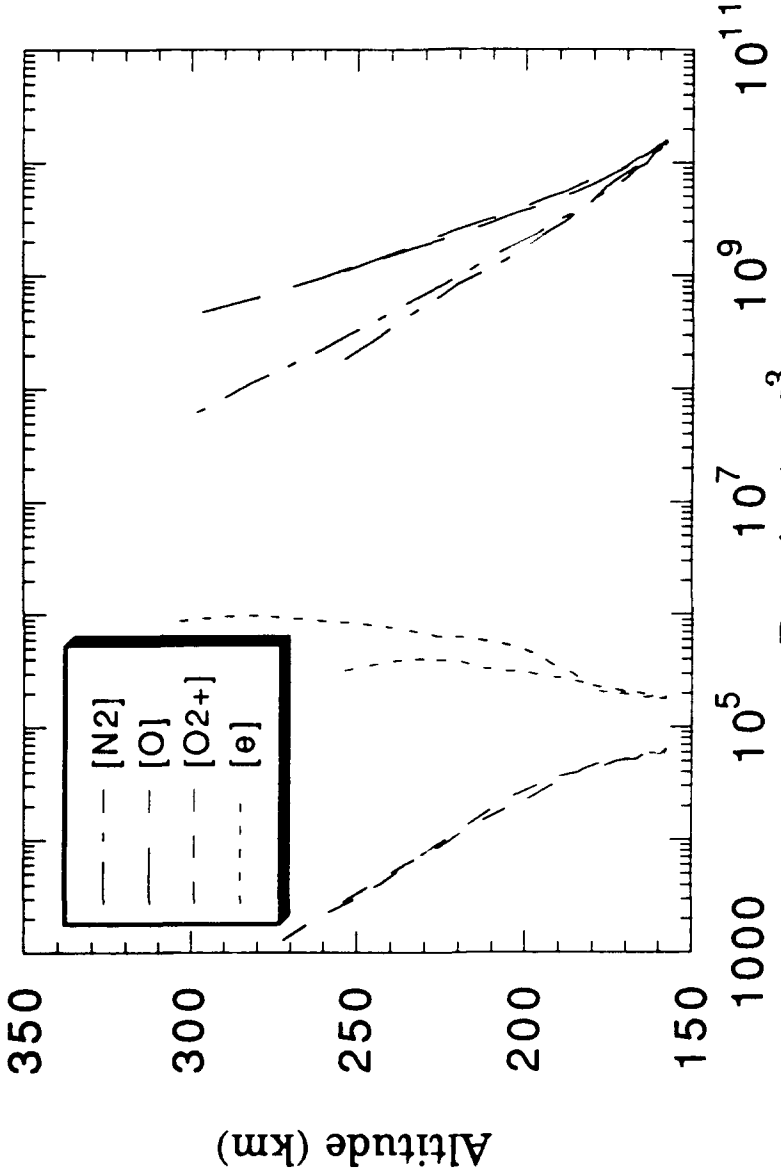

Figure 3.11 *In-Situ* measurements of atmospheric constituents provided by the various instruments for orbit AE-C 0584 up and down leg of the orbit.

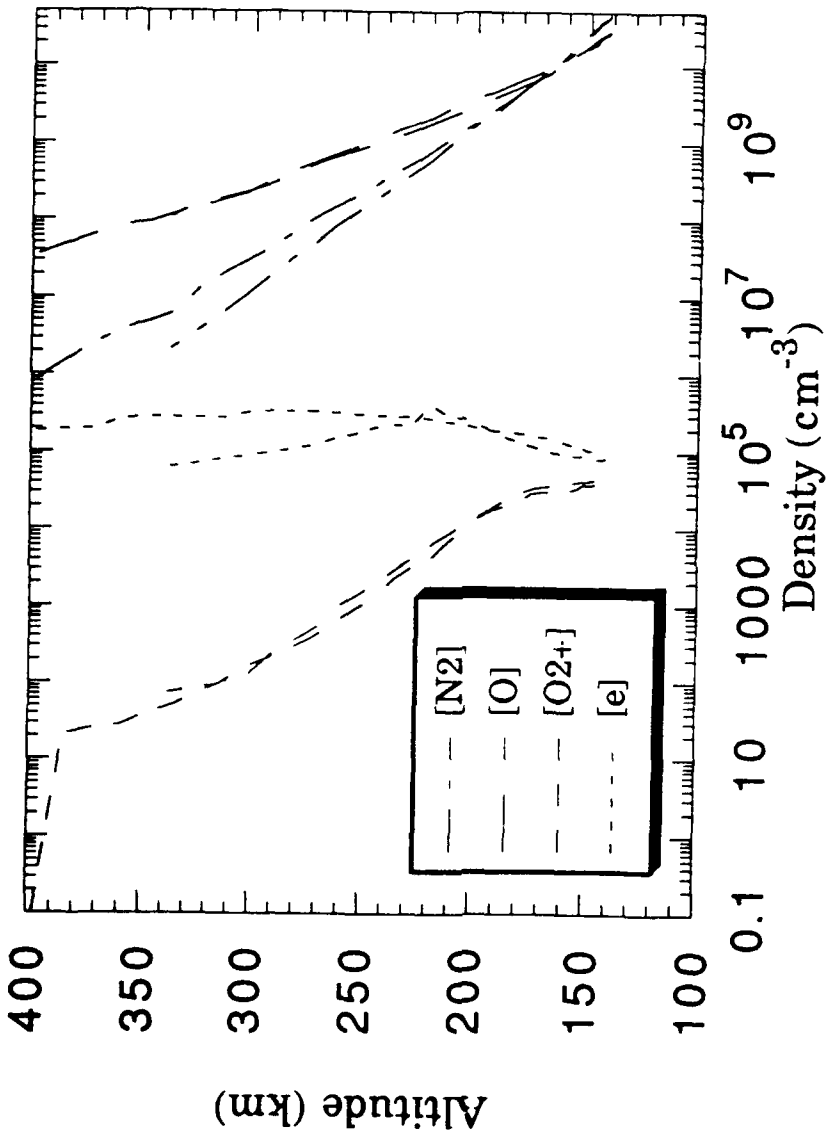

Figure 3.12 *In-Situ* measurements of atmospheric constituents provided by the various instruments for orbit AE-D 0912 up and down leg of the orbit.

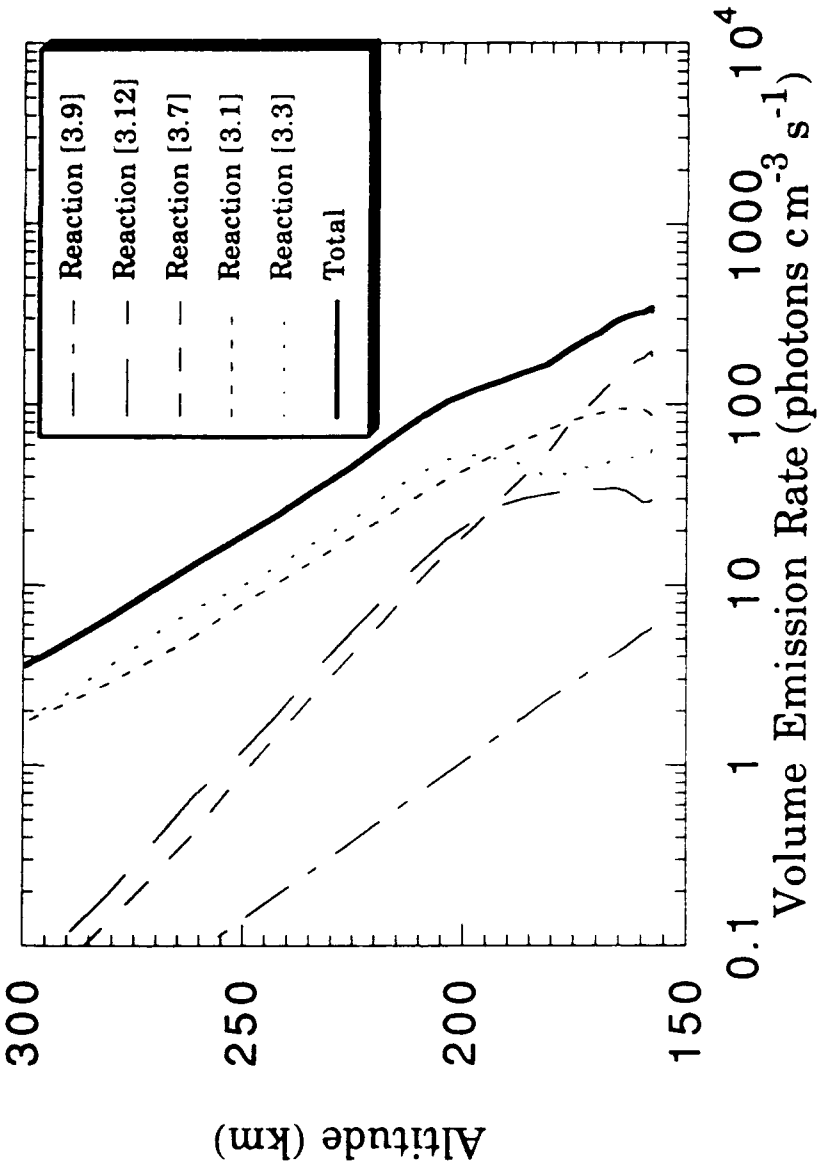

Figure 3.13 Plot of the model output for orbit AE-C 0584 based on constituent profiles provided by the *in-situ* measurements in Figure 3.11.

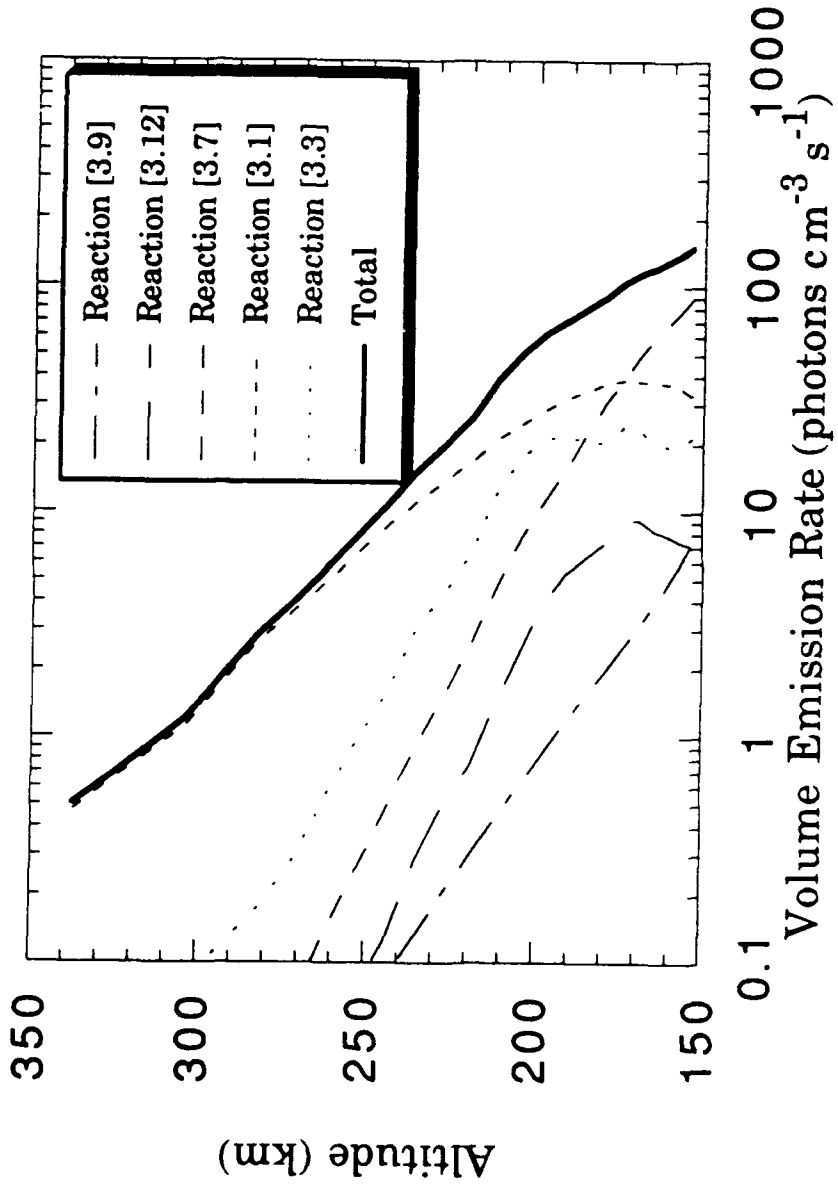

Figure 3.14 Plot of the model output for orbit AE-D 0912 based on constituent profiles provided by the *in-situ* measurements in Figure 3.12.

between the theoretical and experimental values. The quenching of $N_2(A)$ by atomic oxygen has both the total rate coefficient and the $O(^1S)$ branching ratio in question. In Chapter 4, the total reaction rate for the quenching reaction (Reaction [3.7]) will be discussed in more detail. Chapter 5 will deal with the cross section of electron impact (Reaction [3.1]) and the branching ratio of Reaction [3.7] using the total rate coefficient determined in Chapter 4.

CHAPTER IV

RATE FOR ENERGY EXCHANGE FROM $N_2(A)$ BY $O(^3P)$

4.1 Introduction

As shown by this study, one of the important mechanisms for the production of $O(^1S)$ near the peak of the dayglow is the energy transfer reaction,

$$N_2(A^3\Sigma_u^+) + O(^3P) \xrightarrow{\gamma_1} N_2 + O(^1S). \qquad [4.1]$$

There is disagreement about the value of the total rate coefficient for this reaction and for the branching ratio of the $O(^1S)$ channel. Details of the reaction and the rate coefficient and branching ratio were given in Chapters 1 and 3. In this chapter, a separate study of this reaction is done using a model that gives the vibrational distribution of the excited triplet states of N_2. This model is used in conjunction with a band model of N_2, the photoelectron model discussed in Chapter 2 and observations from the Atmosphere Explorer satellites. The value of the total rate coefficient is

determined for the reaction in Equation [4.1] and will be used in the rest of this work.

The $N_2(A^3\Sigma_u^+)$ state is the lowest excited triplet state of N_2 with a threshold energy of 6.5 eV. Figure 4.1 shows the N_2A state and other excited triplet states which are important to the N_2A state. This state is populated by two mechanisms, direct excitation from the ground state of N_2 and by cascading from the higher N_2 triplet states, involving the $B^3\Pi_g$, $W^3\Delta_u$, $B'^3\Sigma_u^-$, and $C^3\Pi_u$. These population processes tend to fill different vibrational levels of the N_2A state (Ahmed, 1969; Cartwright *et al.*, 1971; Cartwright, 1978). The direct mechanism fills the higher vibrational levels of the N_2A state while the cascading processes fill the lower levels.

The N_2A is a metastable state with a lifetime of 1.36 to 2.6 s (Shemansky and Carleton, 1969; Shemansky, 1969). The emission due to this state going to the ground state is known as the Vegard-Kaplan (VK) bands and is weak in the dayglow. The loss of N_2A is due to quenching by O, O_2, N_2 (Cartwright, 1978). Above about 120 km, quenching by $O(^3P)$ would be an important removal mechanism for N_2A. Figure 4.2 shows altitude profiles of the direct and cascading sources for N_2A and the loss by radiation and quenching with O.

The determination of the rate coefficient for this mechanism requires knowledge of the distribution of the vibrational population of the N_2A state. The rate coefficient for the energy transfer reaction has been determined by Piper (1982) for the $v = 0,1$ vibrational levels and by Thomas and Kaufmann (1985) for $v = 0,1,2,3$. Both studies show the rate coefficient tends to increase as the population of higher vibrational levels increases.

In addition to the radiation and quenching losses of the N_2A state, the vibrational levels can have processes that will affect the population

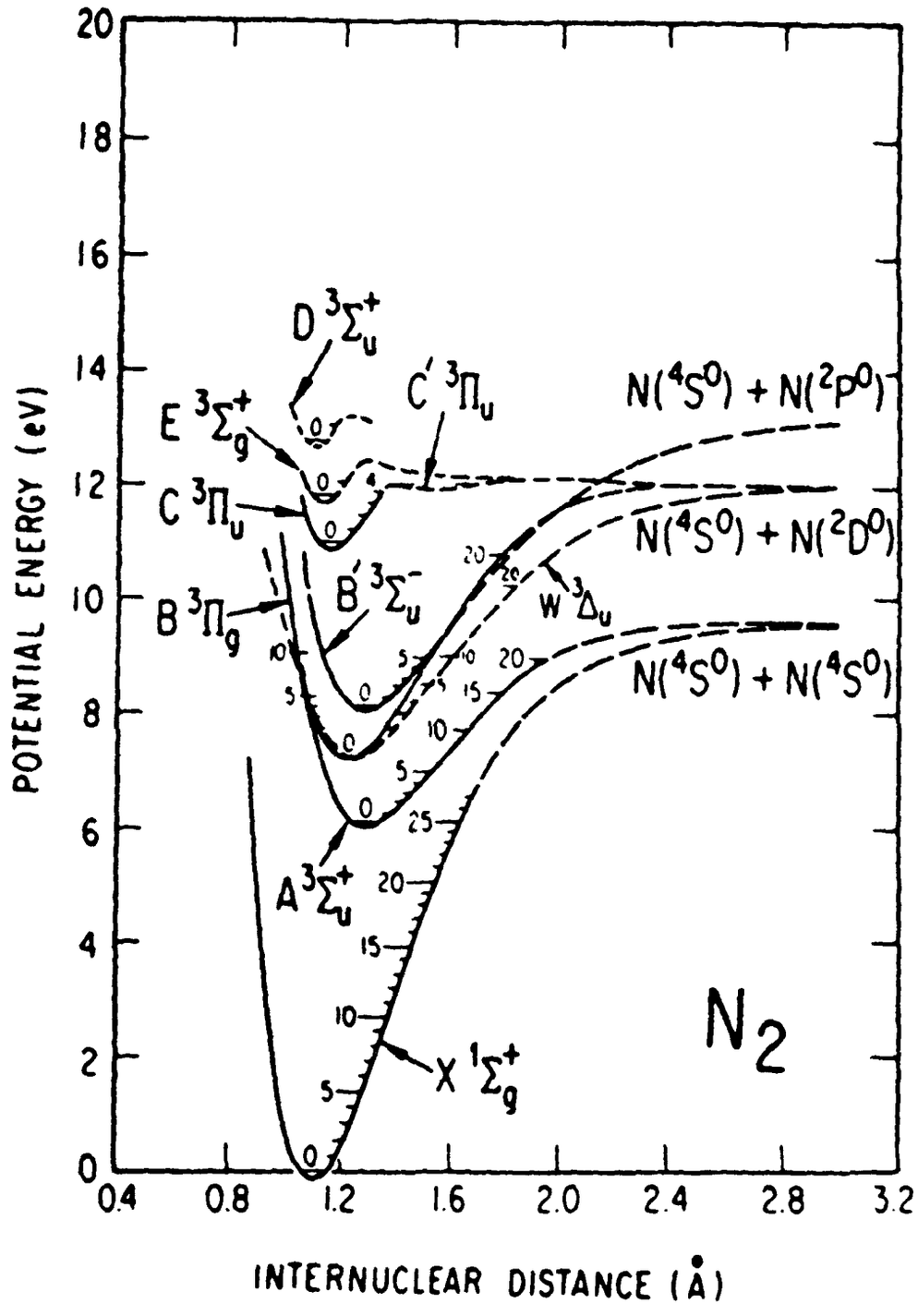

Figure 4.1 Potential energy curves for the lowest triplet states of N_2.

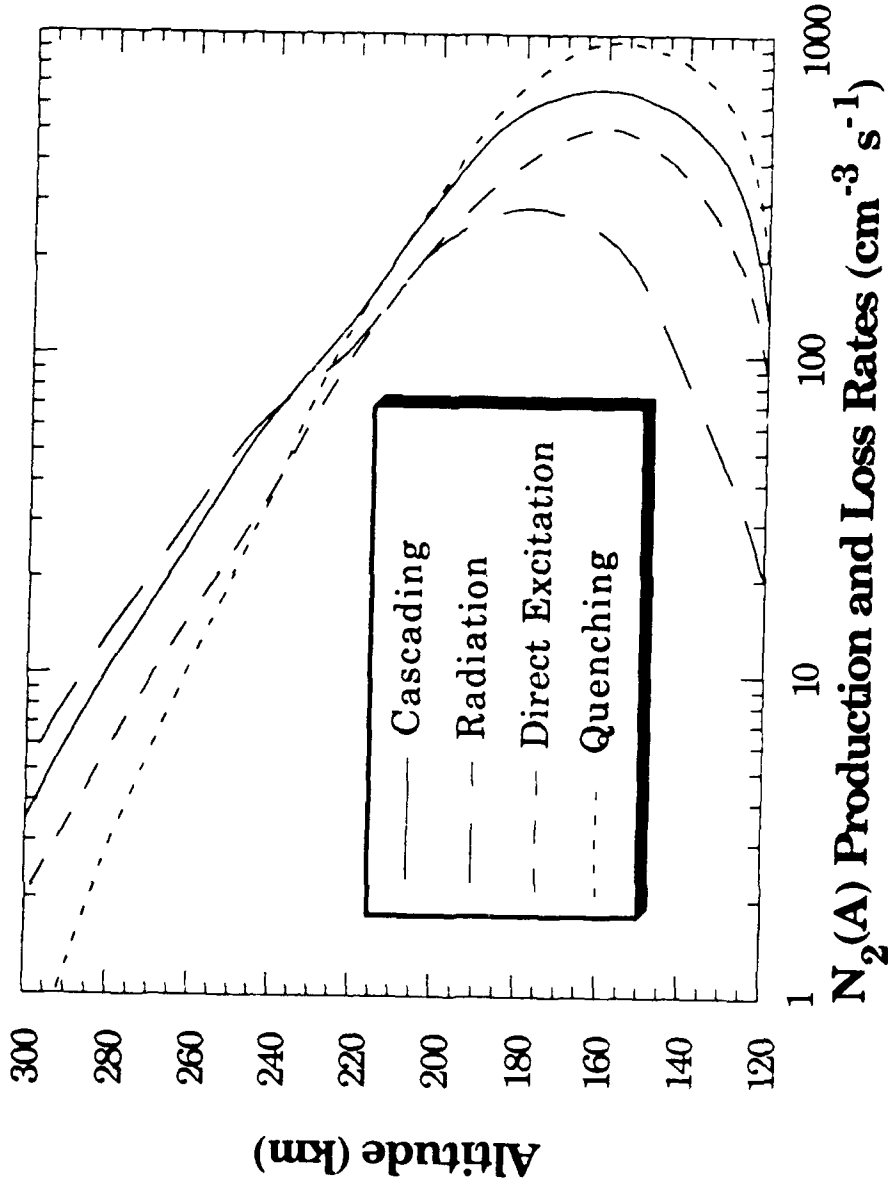

Figure 4.2 Sources and sinks of $N_2(A)$ in the thermosphere.

distribution of the N_2A state. For vibrational levels higher than 7, an inverse transition to the $N_2(B^3\Pi_g)$ has been suggested by Campbell and Thrush (1967) and Gilmore (1969). This mechanism can account for the lack of emissions from the N_2A states higher vibrational levels even though these levels are preferably populated by the direct excitation mechanism as discussed above. This mechanism would tend to remove the population from the higher vibrational levels of the N_2A state and return it into the lower vibrational levels by cascading from the $B^3\Pi_g$ state. This transition can be either a cascading process or may be induced by collisions as in Equation [4.2],

$$N_2(A^3\Sigma_u^+), \upsilon = 7 + N_2 \leftrightarrow N_2(B^3\Pi_g), \upsilon = 0 + N_2 + \Delta E. \qquad [4.2]$$

This reaction is spin allowed and should be a fast process that will have ΔE=-0.0156 eV (Dreyer and Perner, 1973). The modelling of the inverse transition mechanism has been done by Cartwright *et al.* (1971) and Cartwright (1978).

Another method which can redistribute the vibrational population of N_2A is a relaxation process that could follow the reaction in Equation [4.3],

$$N_2(A), \upsilon_i \geq 2 + N_2(X), \upsilon = 0 \leftrightarrow N_2(A), \upsilon_i - 2 + N_2(X), \upsilon = 1, \qquad [4.3]$$

as described by Dreyer and Perner (1973). Setser *et al.* (1970) suggested a two quanta process to account for the observations of emissions from only the v = 0 and 1 levels at elevated pressures of N_2 which would correspond with a rapid relaxation of the bands from higher vibrational levels. The fundamental vibration of the ground state $N_2(X^1\Sigma_g^+)$ is 2330.7 cm-1 which

is nearly equal to an energy difference of $\Delta v = 2$ for N_2A and the resonance becomes a better match as the vibrational level increases (Dreyer and Perner, 1973). This process may become important at lower altitudes.

4.2 Modelling of N_2 Triplet States

The model for the vibrational population of the N_2 triplet excited state is adapted from the model used by Cartwright *et al.* (1971,1973) and Cartwright (1978) for the auroral studies of the molecular nitrogen emissions. In this section, the model will be briefly described and a discussion of the application of the model to determine the total rate coefficient for reaction [4.1]. Examples of the output from the model will be shown in general and for the N_2A state in general.

The vibrational population model takes into account the excited states lying within 13 eV of the ground state. The cross sections for excitation to energies of higher states become very small. Using this energy level as a cutoff gives seven excited triplet states to be considered ($A^3\Sigma_u^+$, $B^3\Pi_g$, $W^3\Delta_u$, $B'^3\Sigma_u^-$, $C^3\Pi_u$, $E^3\Sigma_g^+$, and $D^3\Sigma_u^+$) which are shown in Figure 4.1. The population mechanisms for the excited states are direct excitation from the ground electronic state ($X^1\Sigma_g^+$, $v=0$) and by various intrasystem cascading processes. Collisional transfer excitation can be neglected above 100 km but may become important at lower altitudes (Hays and Oskam, 1973; Cartwright, 1978).

The vibrational population model has been described by Cartwright *et al.* (1971,1973) and Cartwright (1978). In this model the populations of the triplet states are governed by statistical equilibrium as the entire system cannot be characterized by a kinetic temperature. By assuming the only

direct excitation to the triplet states is from the ground state v=0, the statistical equilibrium equation for the relative number density (n_i^{α}/n_0^{X}) of the v' vibrational level of the α excited state can be written as,

$$k_{v'0}^{\alpha} + \sum_{\beta}\sum_{i} A_{iv'}^{\beta\alpha} \frac{n_i^{\beta}}{n_0^{X}} = \left\{ \sum_{\delta}\sum_{r} A_{v'r}^{\alpha\delta} + Q_{v'}^{\alpha} \right\} \frac{n_i^{\alpha}}{n_0^{X}} , \qquad [4.4]$$

where n_0^X is the number density of the ground state N_2 (Cartwright, 1978). The Greek and Arabic symbols denote the excited electronic states and vibrational levels respectively. The first term on the left is the direct excitation to the v' level of the α excited state from the ground state with $k_{v'0}^{\alpha}$ being the excitation rate from electron impact in s^{-1}.The second term on the left represents the cascading transitions from the i^{th} vibrational level of the β^{th} state to to the v' vibrational level of the a state with $A_{ij}^{\beta\alpha}$ as the Einstein transition probability between levels and states. The terms on the right side of Equation [4.4] represent the losses of the population of the v' level of the α state. These are the spontaneous transitions to the r^{th} level of the δ^{th} state and the collisional quenching of the α^{th} state, by species such as O, n, O_2, NO, and N_2, $Q_{v'}^{\alpha}$.

The population of each vibrational level for certain excited states are coupled to those in some other electronic state by dipole allowed intrasystem cascading terms of Equation [4.4]. A set of 93 coupled equations is produced when each level is expressed as a separate equation given by Equation [4.4]. This set of equations may be solved iteratively for the populations relative to the ground state lowest level. Iteration is used to solve the equations since the states are initially populated by direct excitation and then allowed to evlove into steady state populations by intrasystem cascading. To solve the set of equations, knowledge of the photoelectron flux which is assumed to

change slowly compared to the time it takes the system to reach steady state populations, the excitation cross sections, the Einstein transition probabilities, and the quenching rates are required. Each of these items will be briefly discussed below.

The calculation of direct excitation rate from the ground state can be expressed as,

$$k^{\alpha}_{v'0} = q^{\alpha}_{v'0} \int_0^{\infty} f(e)\sigma^{\alpha}_{v'0}(e)de, \qquad [4.5]$$

where $q_{v'0}{}^{\alpha}$ is the Franck-Condon factor between the ground state v=0 and the v' level of the α^{th} state, f(e) is the photoelectron flux as a function of energy, $\sigma_{v'0}{}^{\alpha}(e)$ is the rotationally averaged excitation electron impact cross section for the v' level of the α^{th} state.

The Franck-Condon factors between the electronic states are those used by Cartwright (1970; 1978); Cartwright *et al.*(1971, 1973). By using the v=0 of the ground state as the only source level for the direct excitations, the use of the Franck-Condon approximation is accurate to better than 10% (Miller and Krauss, 1967; Cartwright, 1970).

The photoelectron spectrum used by the vibrational population model is generated by the photoelectron model discussed in Chapter 3. The upward and downward fluxes are summed to give the total photoelectron flux from 0 to 245 eV and are binned in continuously variable sized bins ranging from 0.50 to 11.93 eV. The range of photoelectrons more than adequately covers the energies for the impact cross sections for excitation of the triplet states which peak between 10 and 20 eV and fall off quickly beyond 30 eV.

The electron impact excitation cross sections for the excited states are those used by Cartwright (1978). These cross sections, obtained by Cartwright *et al.* (1977), do not contain contributions from cascading processes. This allows the cascading contribution to be separated from the direct process for individual study (Cartwright, 1978). For this work the impact cross section for the $D^3\Sigma_u^+$ state is assumed to be the same as the cross section for the $E^3\Sigma_g^+$, both being small relative to the lower state cross sections since they are the lowest Rydberg states for N_2.

The transition probabilities used in this work are the same as those used by Cartwright (1978). Thirteen sets of probabilities are used including three for the inverse intrasystem transitions. The ground state is only connected to the triplet excited states through the $A^3\Sigma_u^+$ level which give rise to the Vegard-Kaplan bands and are of interest here. The transitions used for the triplet states are shown in Figure 4.3. In Figure 4.3, the three inverse transitions are shown as dashed lines.

The quenching of the excited N_2 triplet states is well known only for the $A^3\Sigma_u^+$ and the $B^3\Pi_g$ states. Estimates can be made of the effects of quenching on the populations of the other excited states based on orbital similarities (Cartwright, 1978). For this work, quenching is only important for $N_2(A^3\Sigma_u^+)$ since it is a metastable state but it is also important for the $W^3\Delta_u$ state. Of the species available for quenching, only O is important for quenching since the densities of the other species is low above 130 km, especially for N and NO. Along with decreasing densities, O_2 has a quenching rate an order of magnitude smaller than that of O. N_2 may be important at lower altitudes for vibrational relaxation of the N_2A state as discussed before but for low vibrational levels the quenching rate is very small.

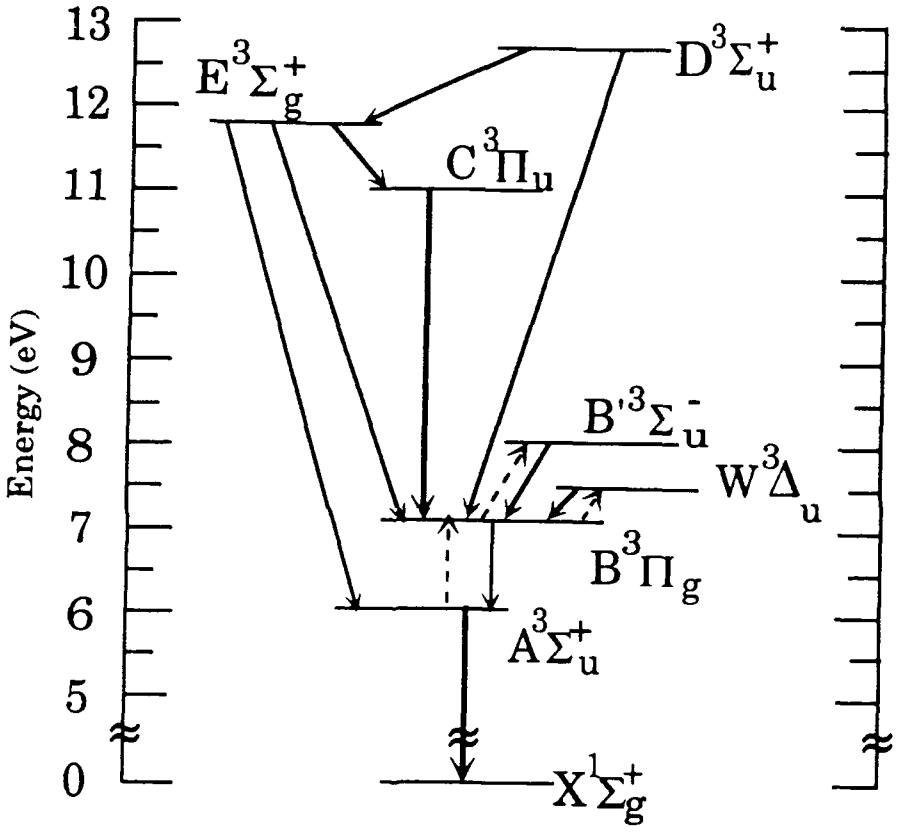

Figure 4.3 Transitions of the triplet states of N_2 in the vibrational population model. Inverse transitions are shown as dashed lines.

Figure 4.4 shows the general flow of the vibrational population model in the dayglow. The figure indicates the sources of the input data at the various steps. Typical resultant populations of the three lowest triplet states is shown in Figures 4.5-4.7. In Figure 4.5, the N_2A state shows the population is primarily in the lowest vibrational levels. Also in this figure, the inverse transition to the N_2B state is seen at vibrational levels above 6. The shapes of the N_2A and N_2B states (shown in Figure 4.6) are determined by both direct production and cascading processes while the N_2C state in Figure 4.7 is only due to direct excitation.

4.3 Determination of Total Rate Coefficient

4.3.1 Background

The determination of the total rate coefficient for Equation [4.1] is approached by a study of the 3371Å emission from the second positive transition of $N_2(C^3\Pi_u, \upsilon=0)$ to $N_2(B^3\Pi_g, \upsilon=0)$. The 3371Å emission was measured by the Visible Airglow Experiment on the Atmosphere Explorer satellites. The measurements of the 2^{nd} positive transitions were contaminated by the Vegard Kaplan bands, primarily due to the (0-9) transition. Figure 4.8 is a low resolution spectrum of the N_2 dayglow emission from 3000 to 4000Å. The overlap of the bands at 3371Å is shown.

The sources of the population of the $N_2(A)$ state were discussed above. The $N_2(C)$ state in the dayglow has photoelectron excitation as the only source with minimal cascading from higher states. Since the second positive transitions are dipole allowed, quenching is not important to the $N_2(C)$ state. The use of 3371Å emission is ideal to study N_2 densities and as

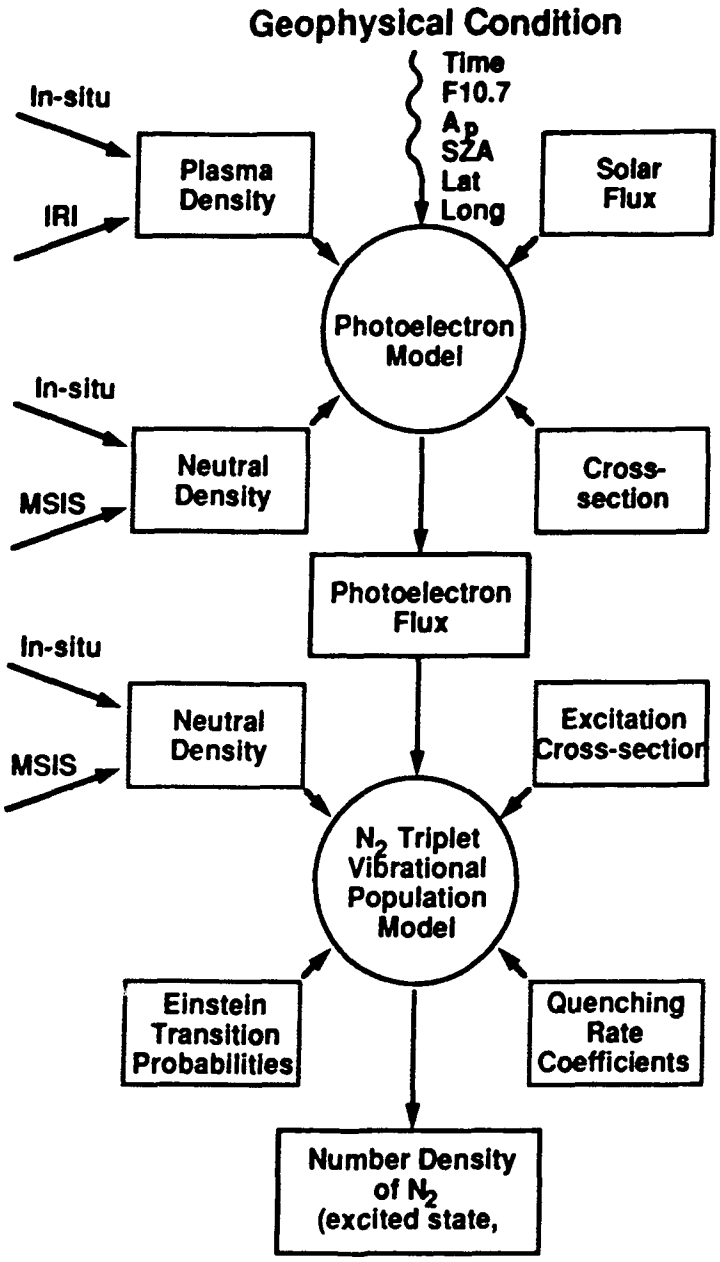

Figure 4.4 Diagram showing the general flow of the vibrational population model with the various inputs and sources of data.

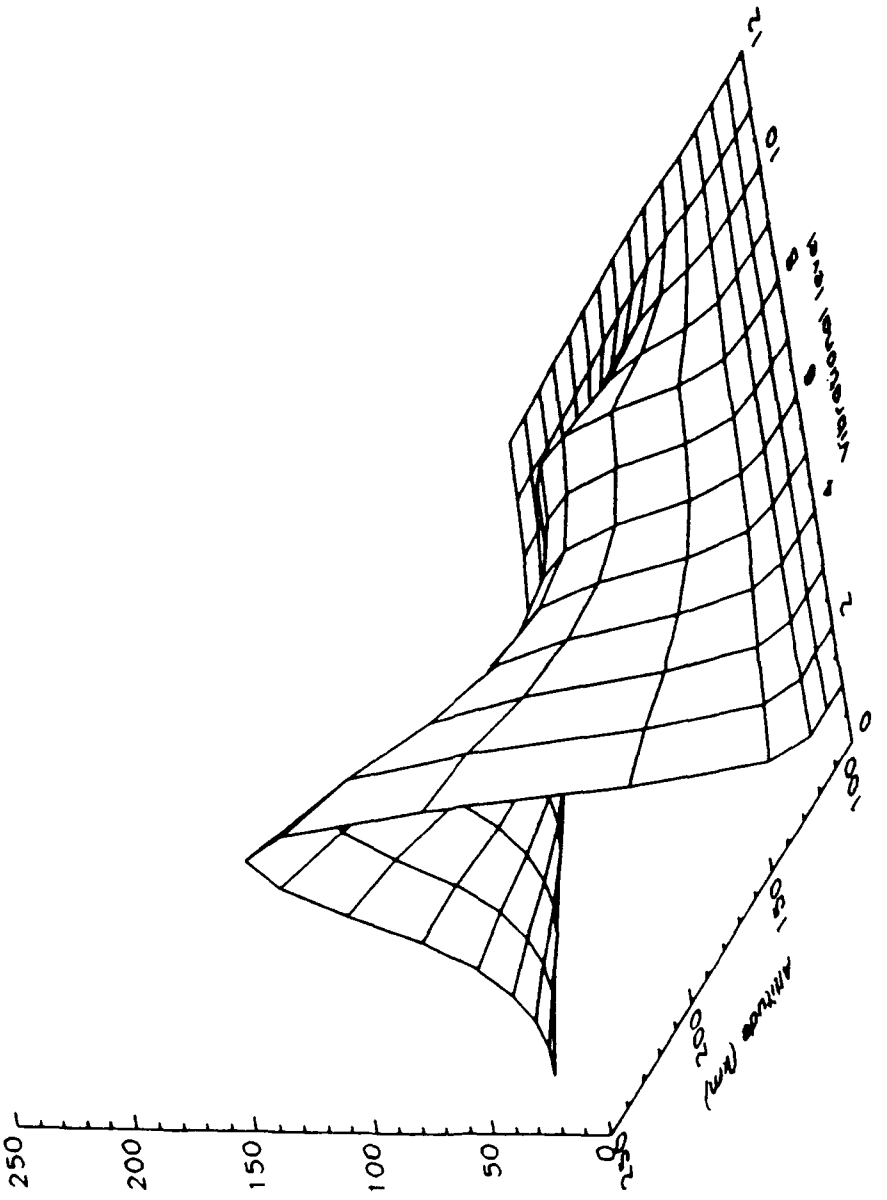

Figure 4.5 Resultant population of the $N_2(A)$ state for the vibrational levels less than 12 from the model.

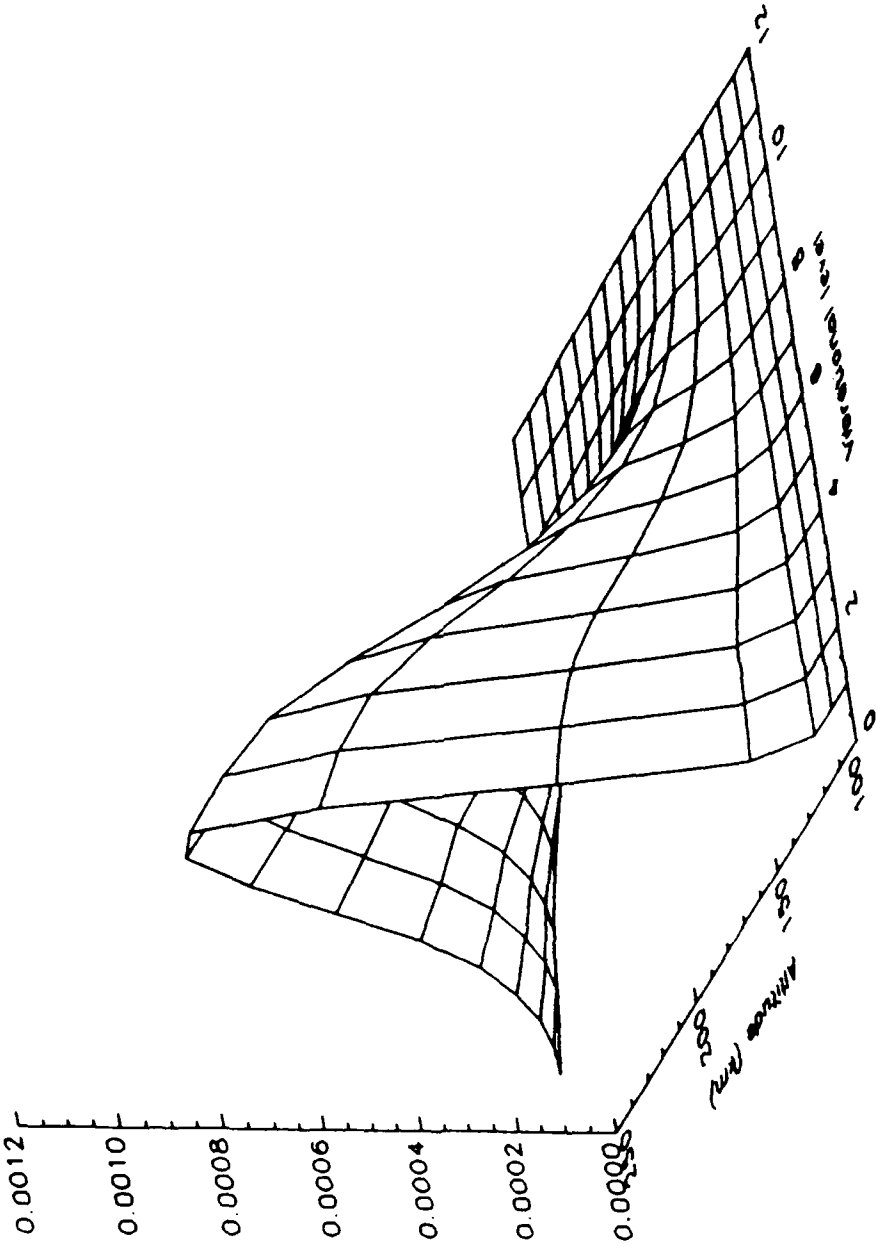

Figure 4.6 Resultant population of the $N_2(B)$ state for the vibrational levels less than 12 from the model.

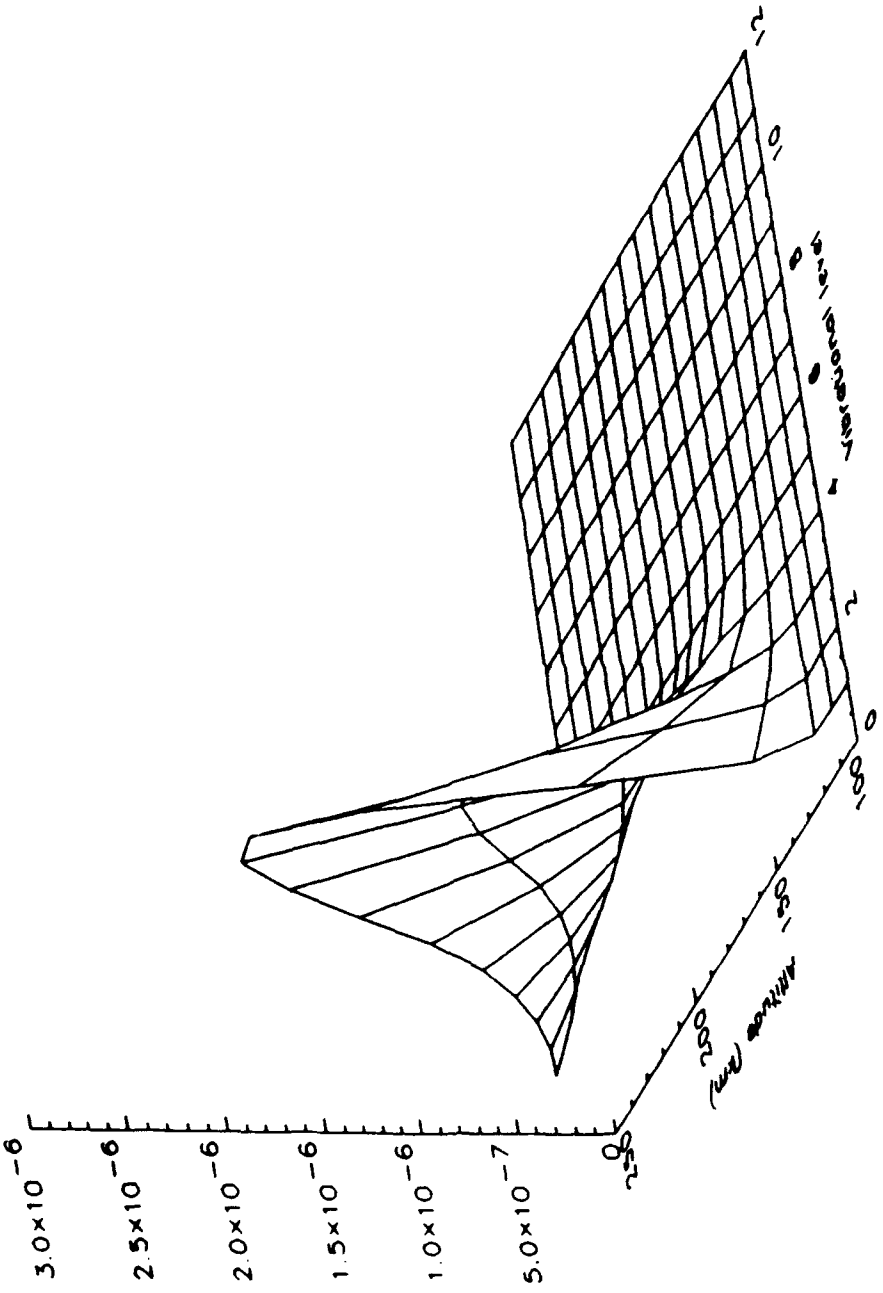

Figure 4.7 Resultant population of the $N_2(C)$ state for the vibrational levels less than 12 from the model.

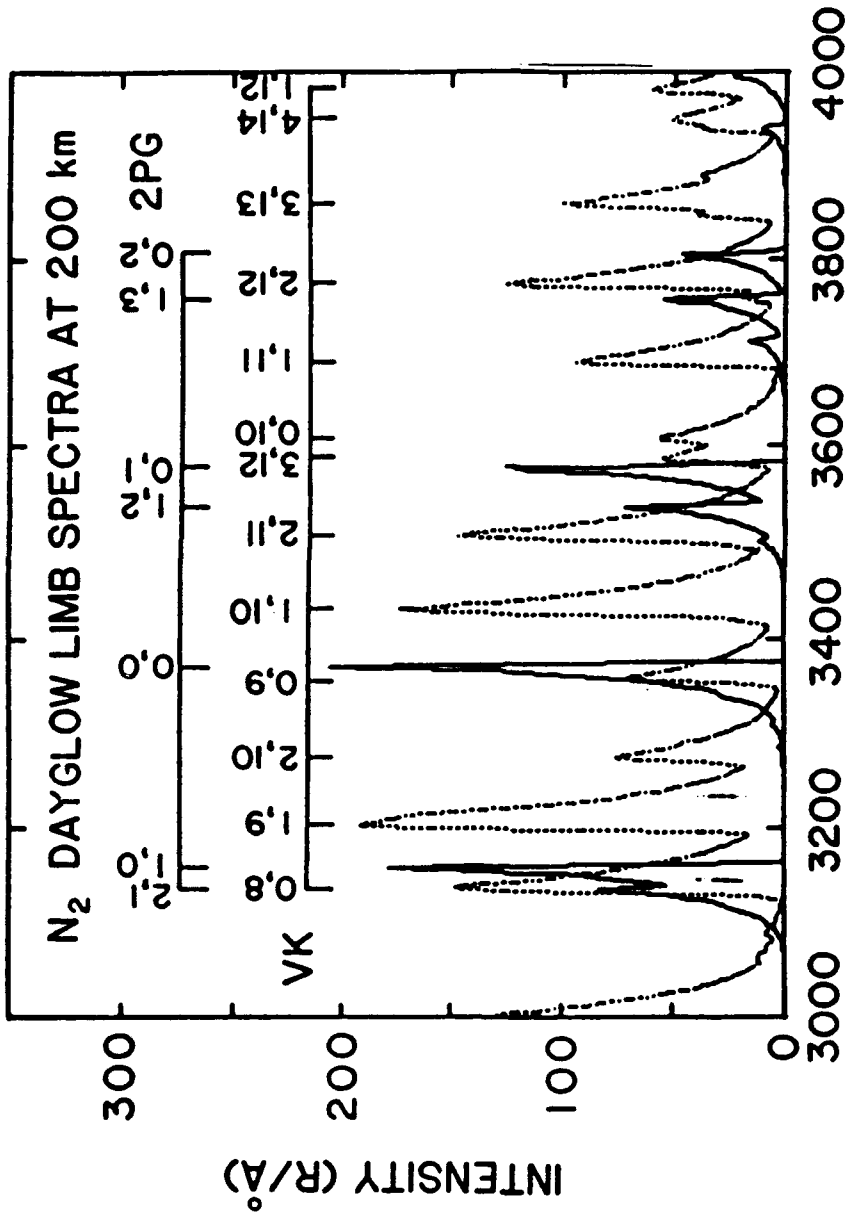

Figure 4.8 Low resolution spectrum from 3000 to 4000 Å with the Second Positive and Vegard-Kaplan bands (After Conway and Christensen, 1984).

an indicator of the photoelectron fluxes (Kopp *et al.*, 1977; Hernandez *et al.*, 1983; Conway,1983; Conway and Christensen, 1985). Both Kopp *et al.* (1977) and Hernandez *et al.* (1983) concluded that the observations by the Atmosphere Explorer satellites consistently overestimated the modelled emission at 3371Å (Conway, 1983).

By using the model for the vibrational population for N_2 described above and a band model for the nitrogen molecule, simulated brightnesses for the 2nd positive and Vegard-Kaplan (0-9) emissions can be made and the results compared with the measured brightnesses of the AE satellites. Since atomic oxygen will be the only important quencher for the $N_2(A)$ state, by adjusting the quenching rate the modelled emissions can be made to agree with those measured by the instrument. This will give the total rate coefficient in the dayglow for Equation [4.1].

4.3.2 Method of Determination

The measurements of 3371Å emission by the VAE instrument also contained emission from the (0-9) Vegard-Kaplan band. Using these measurements, the quenching of the $N_2(A),\upsilon=0$ state may be determined by separating the Vegard-Kaplan band contribution from the 3371Å brightness. For this purpose, orbits were selected in which the satellite was despun with channel two of the VAE instrument oriented radially outward from the earth. Data were limited to orbits which remained south of auroral latitudes to climinate sources for the $N_2(C)$ state other than photoelectron impact.

The 3371 Å brightness data were taken using channel 2 (wide angle) of the Visible Airglow Experiment (VAE) on Atmosphere Explorer satellite (AE-C) (Hays et al., 1973) which was described in Chapter 2. The center of

the transmission was at 3371 Å for a filter temperature of 19.3 °C and shifted to longer wavelengths by 0.1577 Å per °C. The transmission of the filter, which peaks at 46.4%, is shown in Figure 4.9 along with each of the two bands normalized to give a total intensity of 1.0. Atomic oxygen and molecular nitrogen densities were acquired from the Open Source Mass Spectrometer (OSS) (Nier et al., 1973) aboard AE-C.

Using a band model for molecular nitrogen, the second positive and Vegard-Kaplan bands can be produced for a given rotational temperature. These synthesized bands are shown in Figure 4.10 with the total intensity of both of the bands normalized to 1.0 for a rotational temperature of 500 K. Increasing the rotational temperature broadens the band structure and will alter the contribution of the bands to a measurement of the 3371Å emission. Since the transmission function of the filter shifts with its temperature, the fractional contribution of the bands to a given measurement can be written as,

$$\phi(T_{fil}, T_{rot}) = S\left\{\int_i T(\lambda_i, T_{fil}) f_{2PG}(\lambda_i, T_{rot}) d\lambda_i + \int_j T(\lambda_j, T_{fil}) f_{VK}(\lambda_j, T_{rot}) d\lambda_j\right\}, \quad [4.6]$$

where S is the sensitivity of the instrument, T is the filter transmission function of the filter at the filter temperature, and f is the line intensity for the band. T_{fil} and T_{rot} are the filter and rotational temperatures respectively. Figures 4.11 and 4.12 show the contribution factors of the N_2 second positive and Vegard-Kaplan bands which are observed as a function of filter and rotational temperatures from the two terms in Equation [4.6].

The vibrational population model for the N_2 triplet states described above provides the steady-state populations for the $N_2(A),\upsilon=0$ and $N_2(C),\upsilon=0$

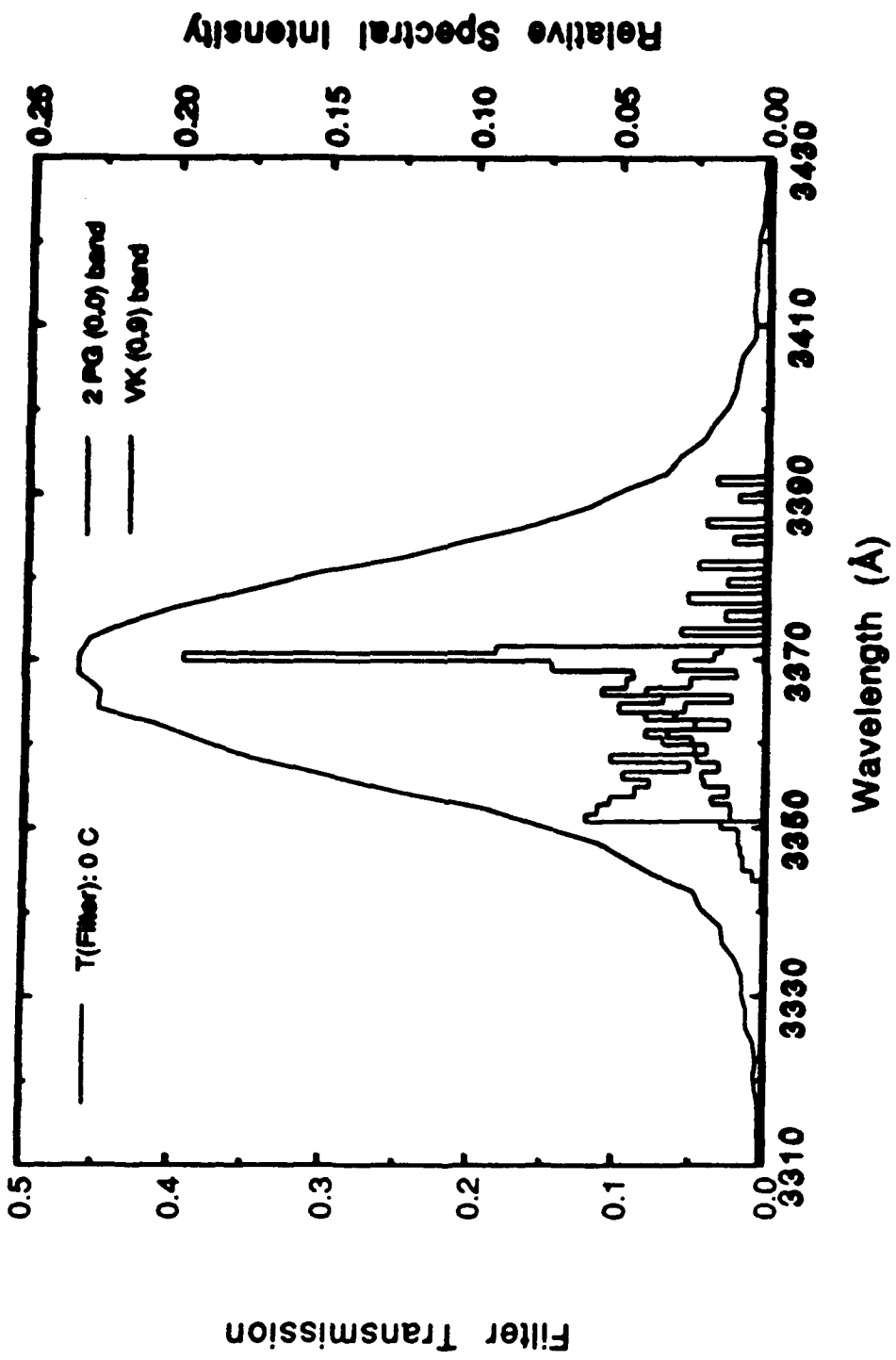

Figure 4.9 The VAE 3371 Å filter transmission for AE-C with the Second Positive and Vegard-Kaplan bands shown normalized to 1.

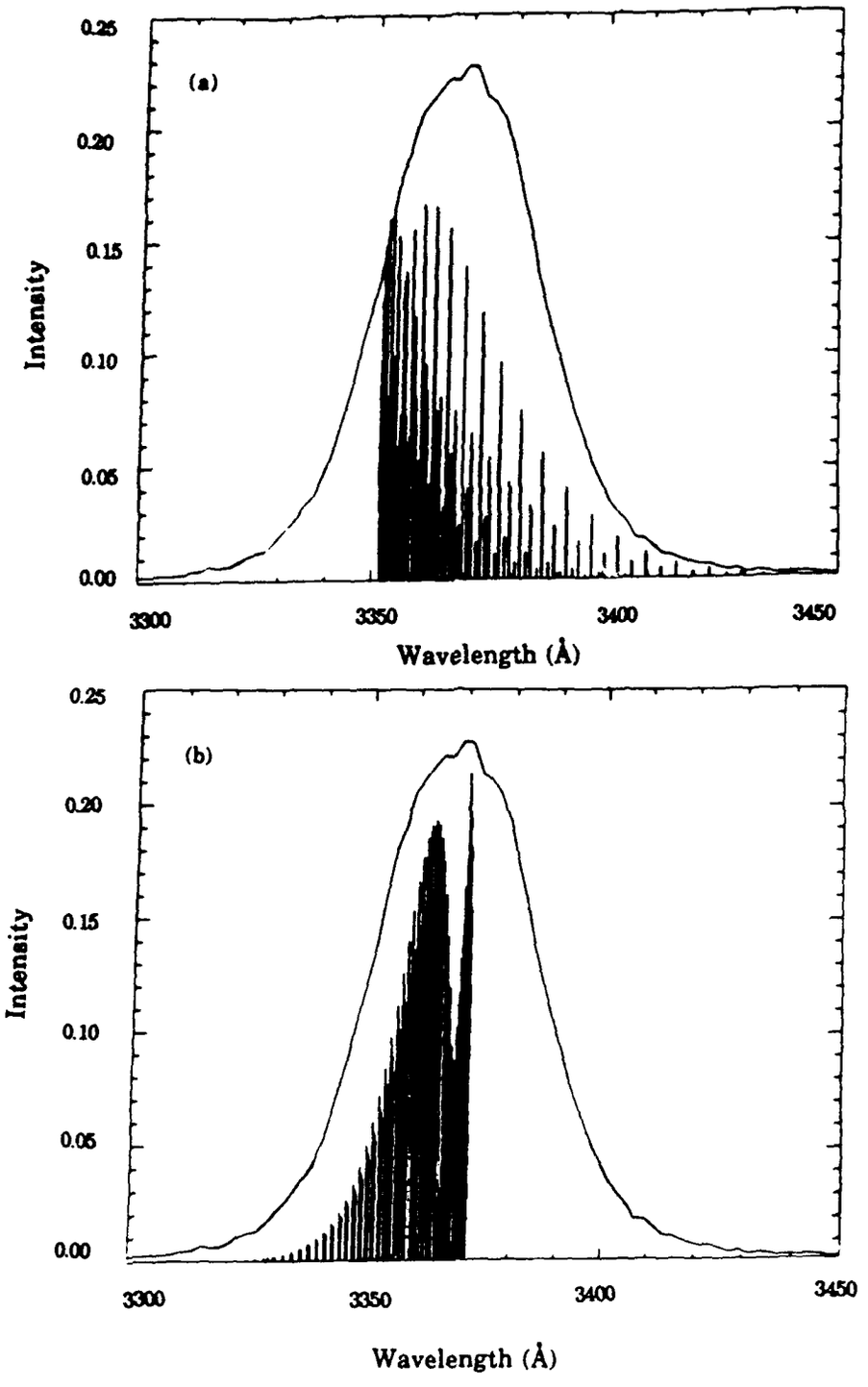

Figure 4.10 The results of the band model for molecular nitrogen for the two bands normalized to 1 at a rotational temperature of 500 K. (a) V-K (0-9) (b) 2PG (0-0).

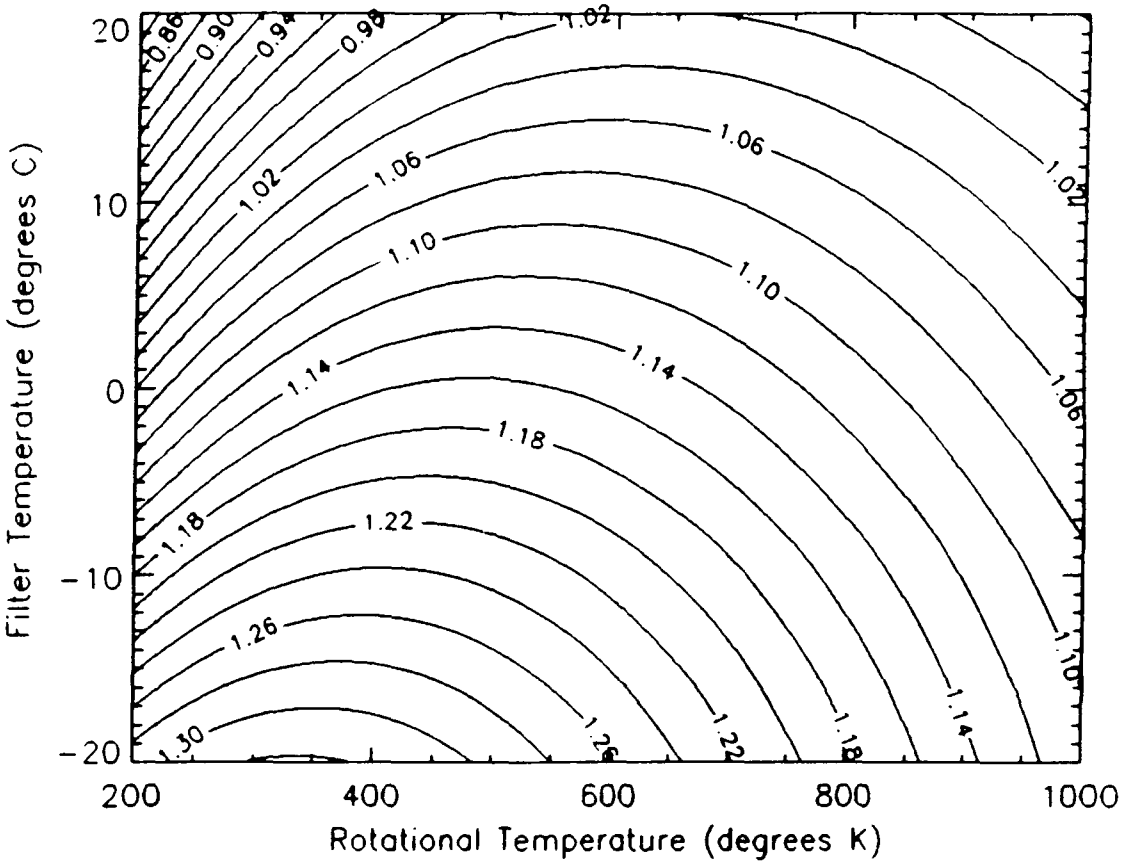

Figure 4.11 Contribution factors for the Vegard-Kaplan (0-9) band as a function of rotational temperature and filter temperature.

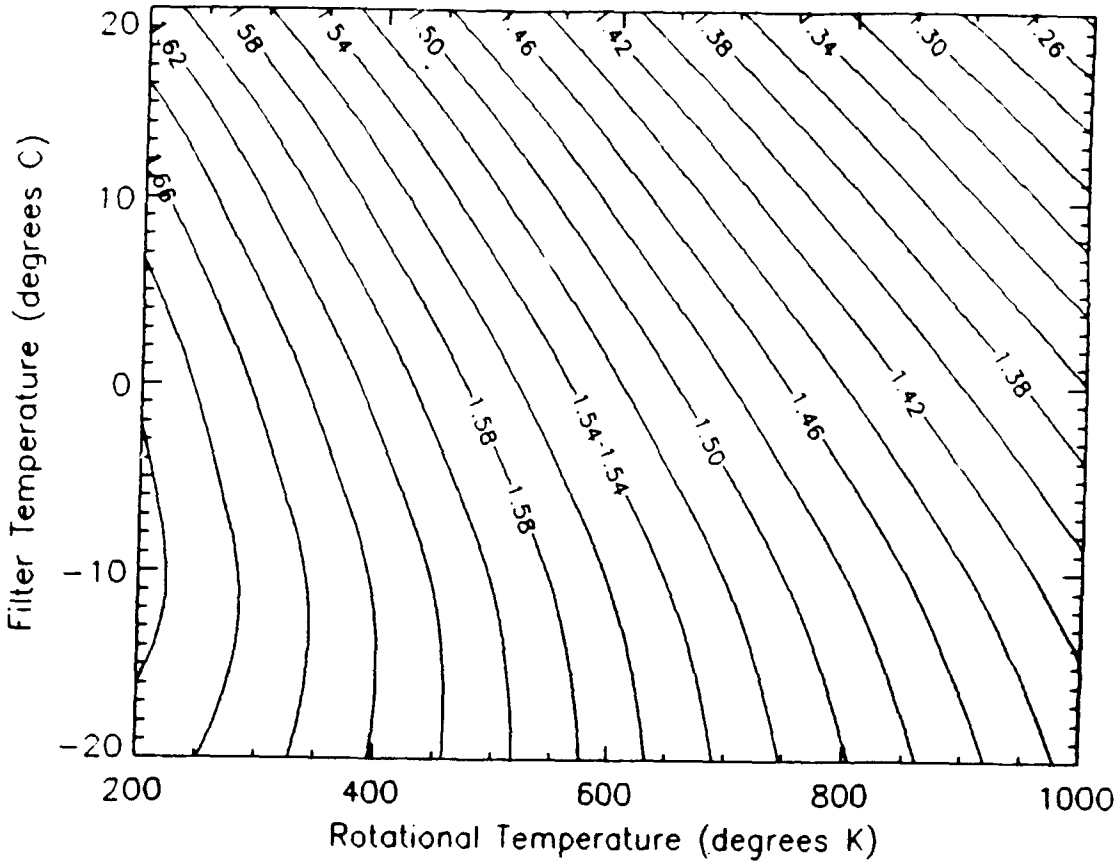

Figure 4.12 Contribution factors for the Second Positive (0-0) band as a function of rotational temperature and filter temperature.

excited states. These populations can be used to determine the emission rate as a function of altitude for the particular transitions of interest (VK 0-9 and 2PG 0-0). The emission rates can be combined with the terms for the contribution for each band in Equation [4.6] and integrated along a line of sight path to calculate the observed brightness as measured by the VAE instrument,

$$\Phi(T_{fil}, T_{rot}) = S\int_{l}\left\{\int_{i}\varepsilon_{2PG}T(\lambda_i)f_{2PG}(\lambda_i)d\lambda_i + \int_{j}\varepsilon_{VK}T(\lambda_j)f_{VK}(\lambda_j,)d\lambda_j\right\}dl. \qquad [4.7]$$

In Equation [4.7], Φ is the integrated surface brightness, ε is the emission rate for the bands from the vibrational population model, and the integral would be from the satellite to infinity along the line of sight of the instrument. The other variables are defined as in Equation [4.6].

The rate for quenching of the $N_2(A)$ state by atomic oxygen can be found by using Equation [4.7] to model the 3371Å observations from the VAE instrument. The quenching will affect only the contribution from the Vegard-Kaplan emissions to the integrated brightness. By adjusting the modelled brightness to best reproduce the observations the quenching rate may be determined.

The value of the quenching rate may be determined by finding the value that will give the minimum χ^2 between the data and modelled emission. The data for the χ^2 calculation was taken from four orbits from satellite AE-C, with the altitudes between 150 and 165 km. This altitude range was selected to avoid data from higher altitudes where the quenching is not important and the lower altitudes where vheicle glow contamination may be included in the data. This contamination problem will be briefly

covered later. The results of the determination will be discussed in the next section and comparisons with previous values will be given. The rate coefficient will be used in Chapter 5 to determine the branching ratio for the production of $O(^1S)$ by Equation [4.1].

4.3.3 Results

Orbits from the AE-C satellite were used to determine the quenching rate of the $N_2(A)$ state. Using the vibrational population model for these orbits, Figures 4.13 and 4.14 show the altitude profiles of the emissions rate for the Vegard-Kaplan (0-9) and the Second Positive (0-0) bands. The quenching rates used for the $N_2(A)$ υ=0 level shown in the figures are from Beiting and Feldman (1979) and Piper and Caledonia (1981). The effects of the quenching rate on the $N_2(A)$ state can be seen by the change in emission in the two figures.

The results of the χ^2 minimization is shown in Figure 4.15 with a total rate coefficient of 2.75×10^{-11} cm^3 s^{-1}. The observed 3371Å emission is simulated using these emission profiles in Figures 4.13 and 4.14. These have been compared to the observations from AE-C for orbits 457 and 1911 as shown in Figures 4.16 and 4.17. The smaller quenching rate which agrees with the values of Piper and Caledonia (1981) gives the best fit to the observations.

The model tends to under predict the emission at low altitudes near perigee for orbit 1911. The discrepancy may be due to vehicle glow which has been studied for the Atmosphere Explorer satellites (Yee et al., 1984) and recently for the Space shuttle (Viereck et al., 1991). The residual of the brightness for orbit 1911 is a linear function of $[N_2]^2[O]$ (private communication Yee) as shown by Figure 4.18. The vehicle glow reactions

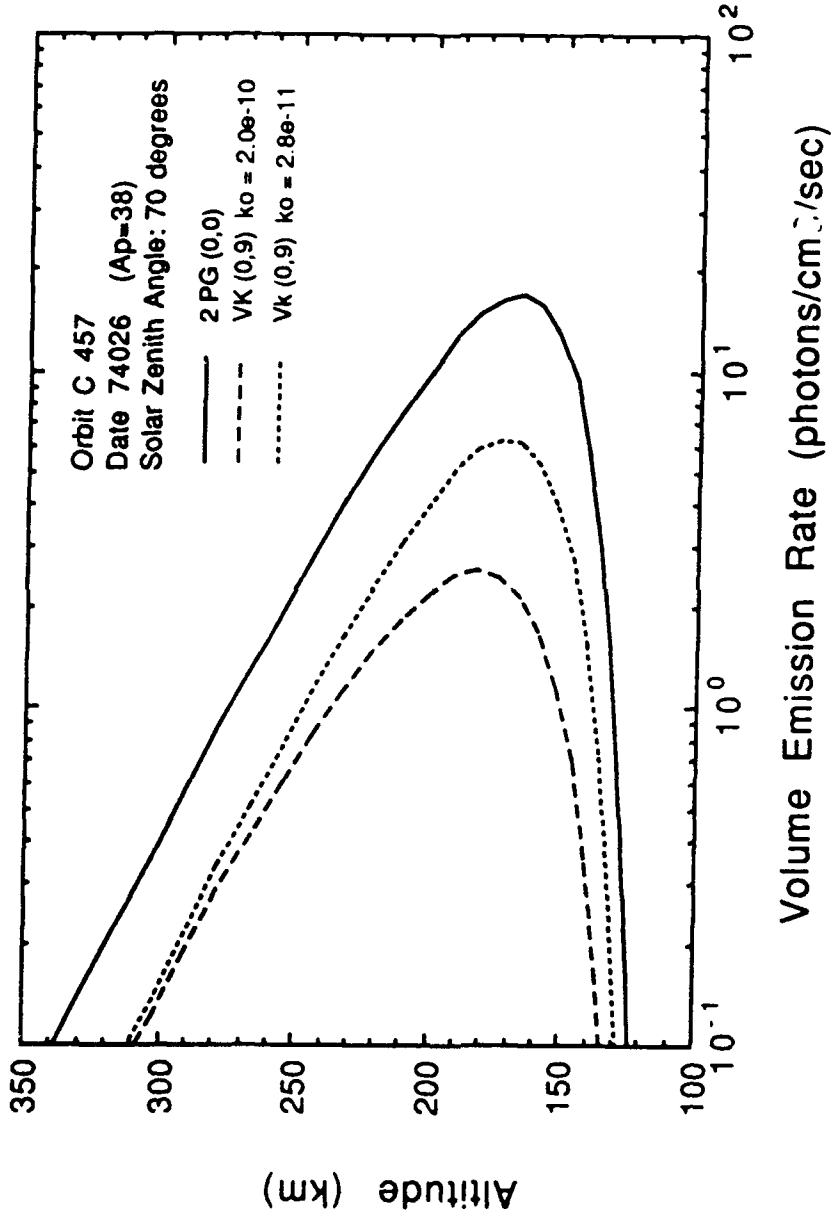

Figure 4.13 Plot of emission rates from the model for orbit AE-C 0457 based on perigee conditions for the two bands. The effects of the change in quenching for the VK (0-9) is shown.

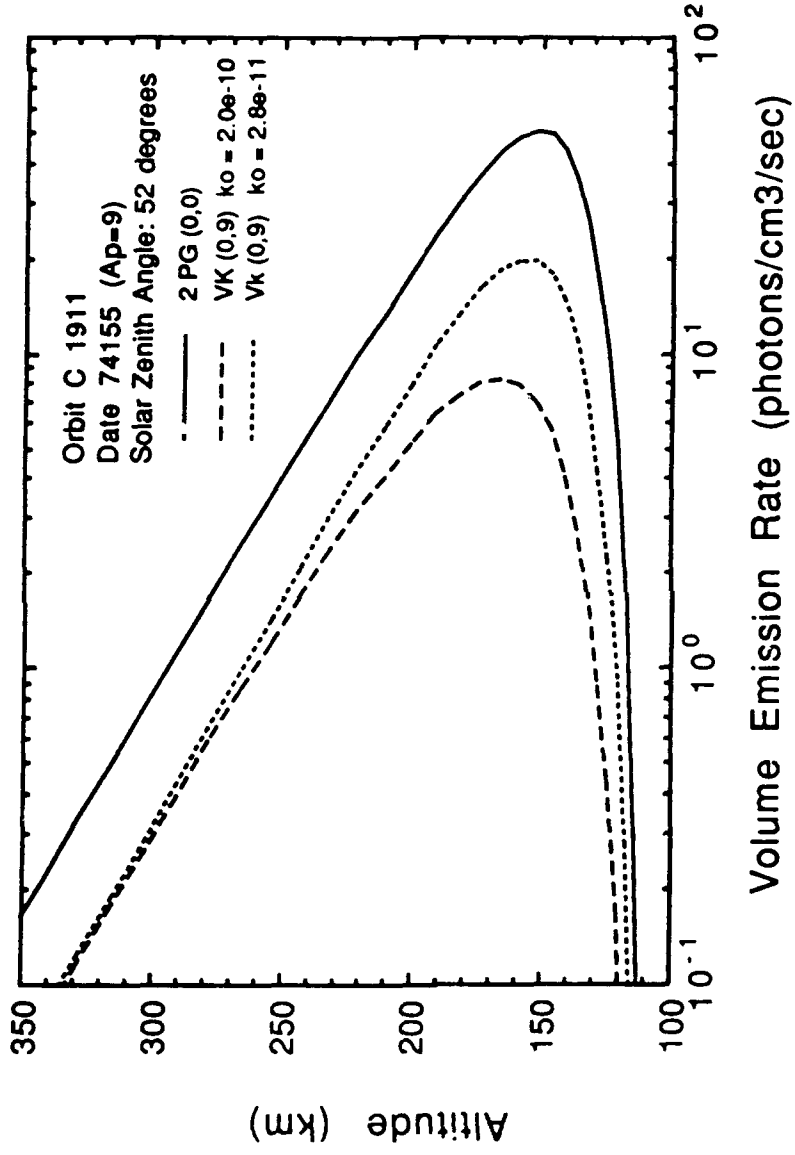

Figure 4.14 Plot of emission rates from the model for orbit AE-C 1911 based on perigee conditions for the two bands. The effects of the change in quenching for the VK (0-9) is shown.

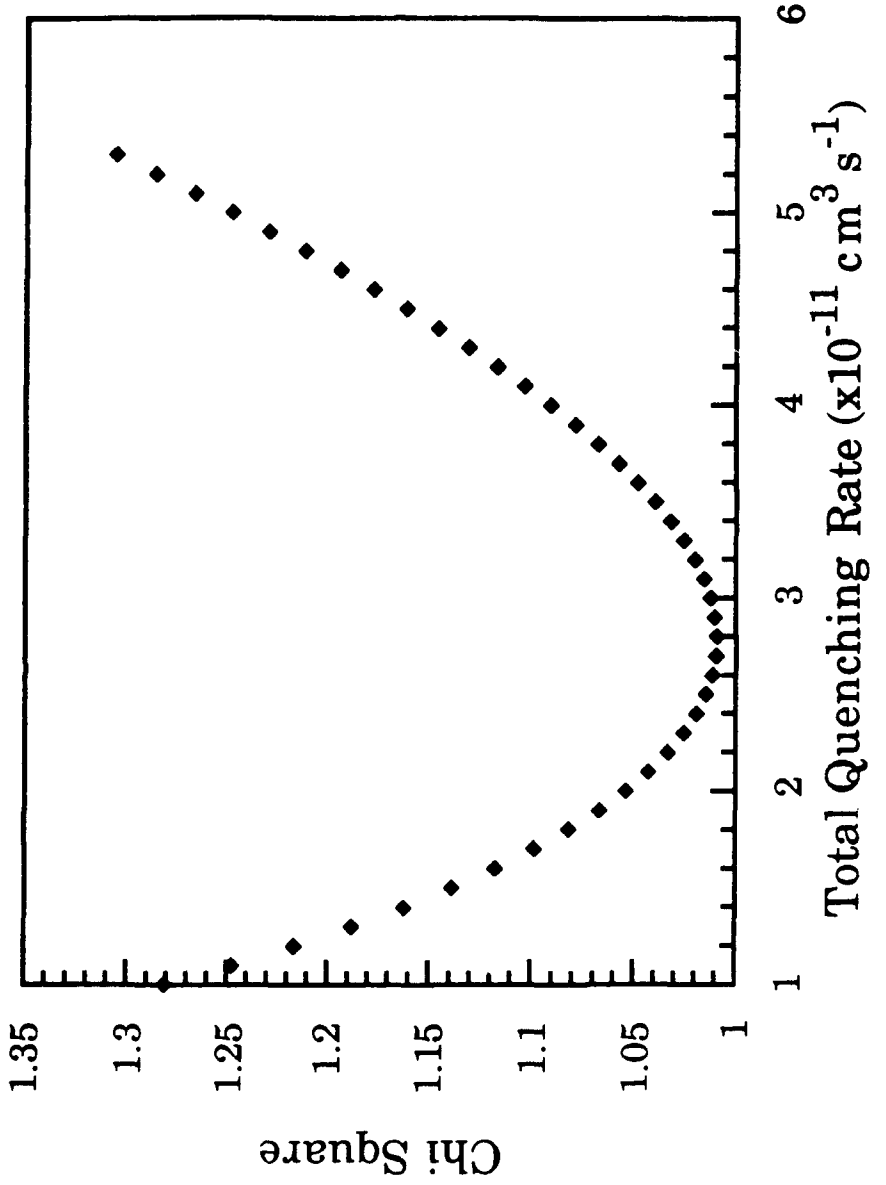

Figure 4.15 The results of the χ^2 determination of the total rate coefficient for Reaction [4.1].

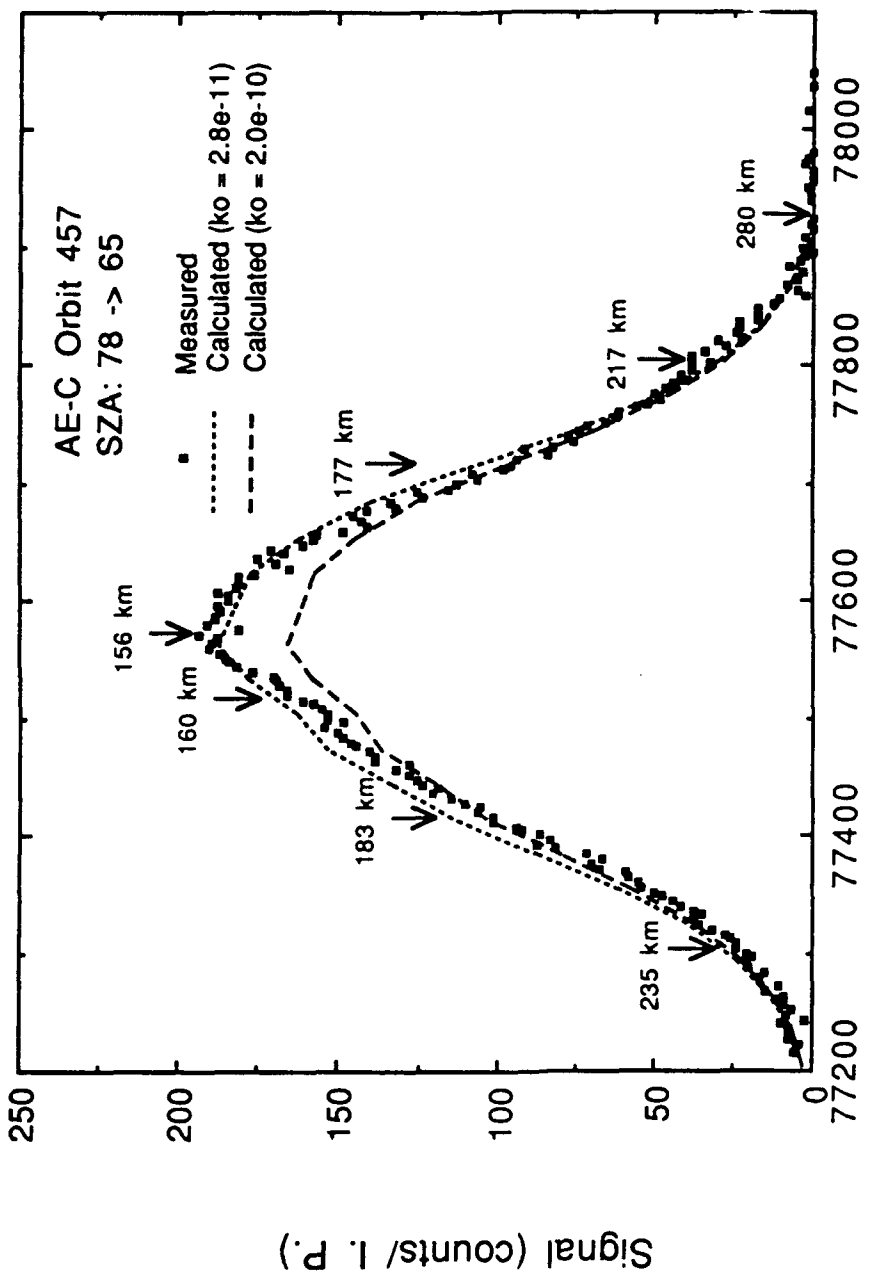

Figure 4.16 Plot of integrated brightness measurements from the model and as measured for orbit AE-C 0457. The effects of the change in quenching for the VK (0-9) on the integrated brightness is shown.

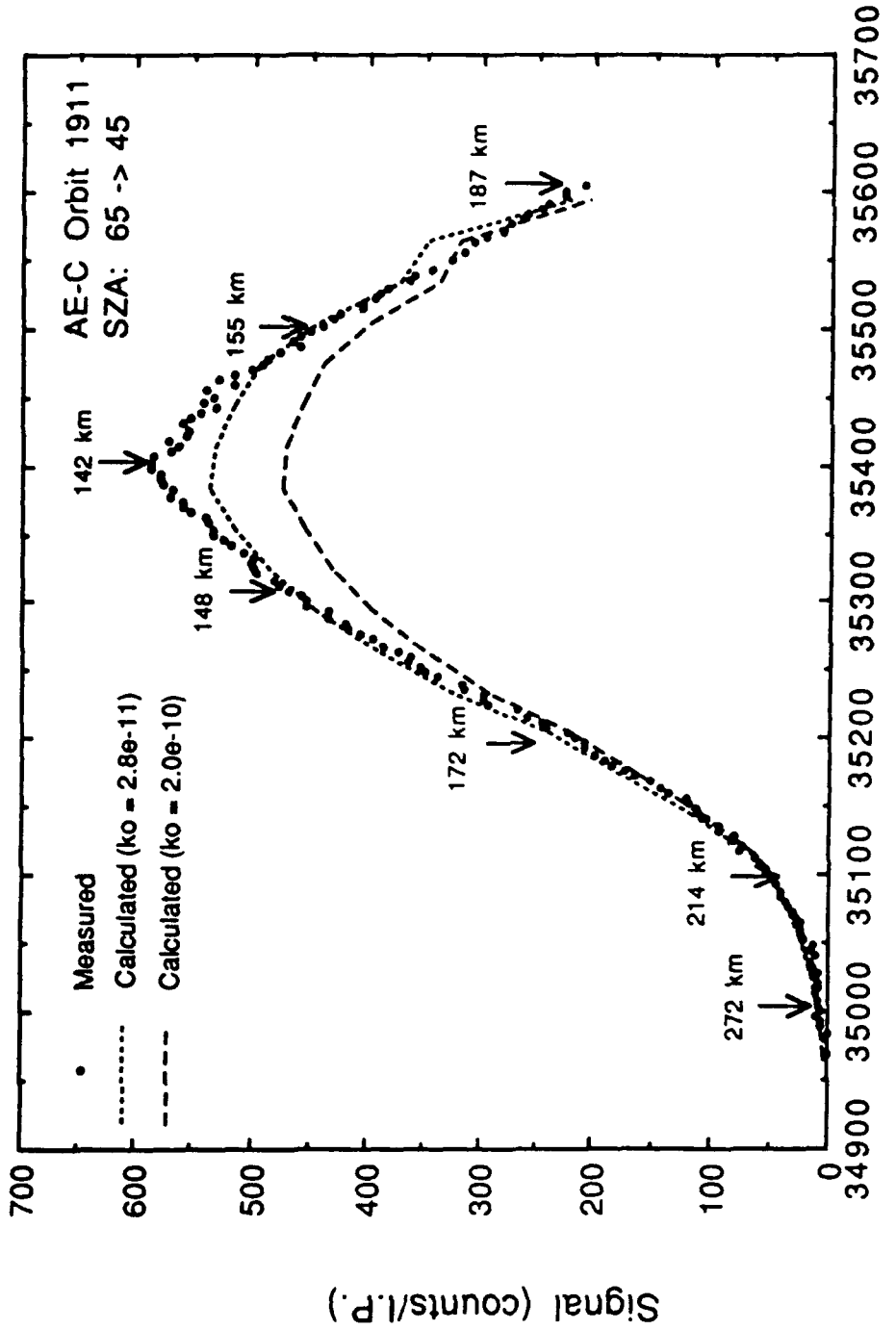

Figure 4.17 Plot of integrated brightness measurements from the model and as measured for orbit AE-C 1911. The effects of the change in quenching for the VK (0-9) on the integrated brightness is shown.

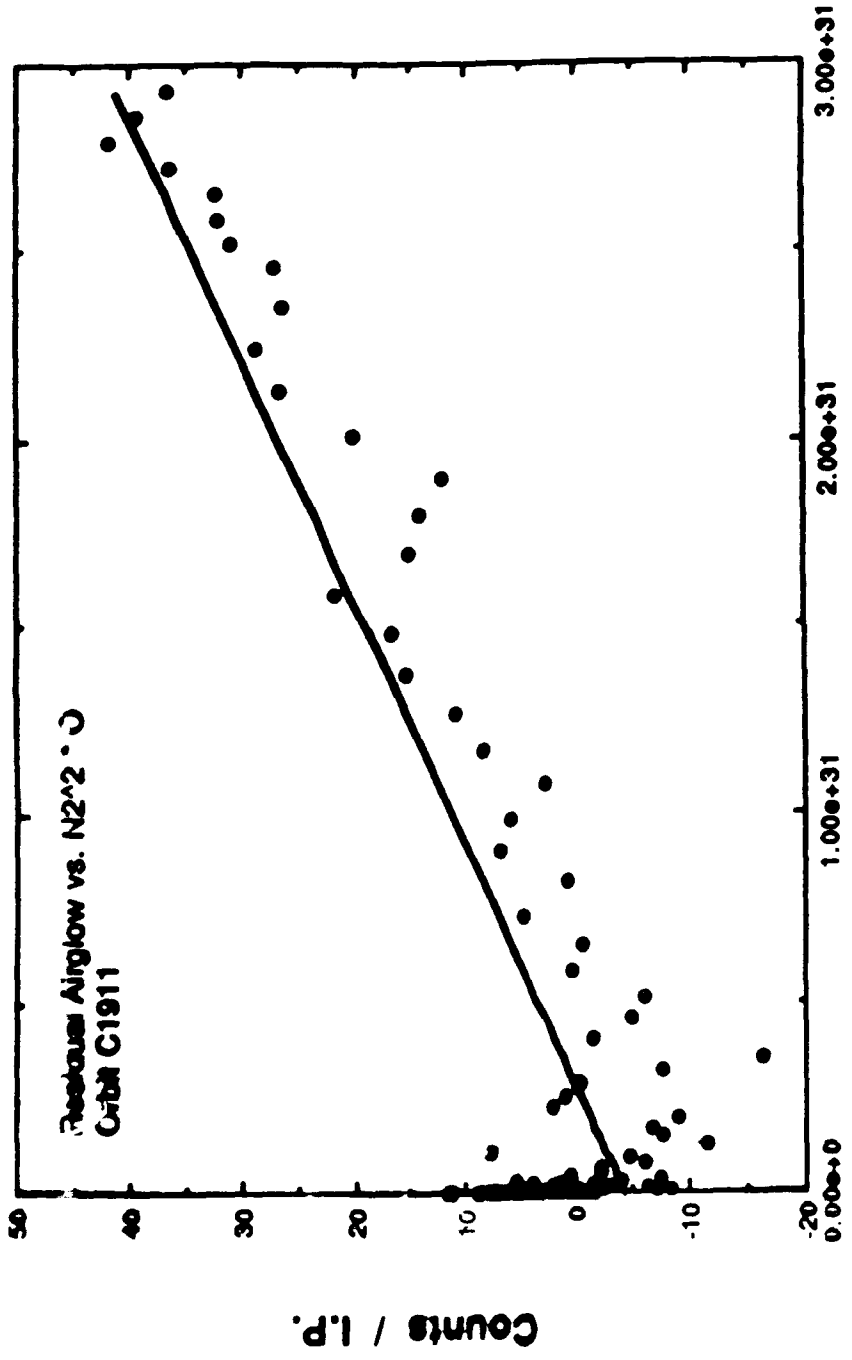

Figure 4.18 Comparison of the residual airglow brightness versus the $[N_2]^2[O]$.

have not been confirmed but this dependance would support the suggested reactions for vehicle glow suggested by Green (1984) and Green et al. (1986) and is similar to the results of Meyerott and Swenson (1990).

The rate of quenching for Equation [4.1] determined by this study supported the value of 2.8×10^{-11} cm^{-3} s^{-1} as determined by Piper and Caledonia (1981) and DeSouza et al. (1985) for the $\upsilon=0$ vibrational level. This value will be used in the following chapters to determine the cross section for electron impact on atomic oxygen and the branching ratio of Equation [4.1] for the production of $O(^1S)$.

CHAPTER V

ANALYSIS OF 5577Å OI DAYGLOW EMISSION

5.1 Introduction

As was discussed in Chapters 1 and 3, the major reactions for production of $O(^1S)$ in the dayglow have parameters which are not known well. The total rate coefficient for the quenching of $N_2(A)$ by $O(^3P)$ (Reaction [4.1]) was determined in Chapter 4 from observations of the 3371 Å emission by the Visible Airglow Experiment on AE-C. The electron impact cross section of atomic oxygen (Reaction [3.1]) and the branching ratio for the quenching reaction (Reaction [4.1]) have large variations between various studies of these reactions. In this chapter, these two parameters will be determined by a study of the 5577Å dayglow emission.

The model developed in Chapter 3 will be used to determine the magnitude of the electron impact cross sections for atomic oxygen and the branching ratio for the quenching of $N_2(A)$. The total rate coefficient for the quenching reaction from Chapter 4 will be used. Observations of the $O(^1S)$ emission by the Atmosphere Explorer satellites are used with the photochemical model to determine the two parameters by least squares

techniques. The effect of the vibrational population of the $N_2(A)$ state on the production of $O(^1S)$ will be discussed. Since the chemistry for the production of O(1S) in the dayglow must extend into the twilight, in the final part of this chapter the values for the various reactions determined for the dayglow will be used to model the 5577Å emission in the twilight.

5.2 Determination of Reaction Parameters

5.2.1 5577Å Dayglow Model

The photochemical model was developed in Chapter 3 using some of the reactions discussed in Chapter 1 as the sources and losses. Some of the reactions discussed in Chapter 1 were not used in the model since their production of $O(^1S)$ was not of any consequence in the dayglow. The model developed for the dayglow includes the following reactions. The sources of $O(^1S)$ are photoelectron impact on atomic oxygen (Reaction [3.1]), dissociative recombination of O_2^+ (Reaction [3.3]), quenching of $N_2(A)$ by atomic oxygen (Reaction [3.7]), photo dissociation of O_2 (Reaction [3.9]), and ion-atom exchange (Reaction [3.12]). The only losses are the radiative transitions from $O(^1S)$ to either $O(^1D)$ or $O(^3P)$. Using these reactions the production of $O(^1S)$ is

$$[O(^1S)] = \frac{\{P_1 + P_3 + P_7 + P_9 + P_{12}\}}{\{A_{5577} + A_{2972}\}}. \qquad [5.1]$$

Where A_{5577} and A_{2972} are the Einstein transition probabilities for the radiative loss processes and P_1, P_3, P_7, P_9, and P_{12} are the production rates previously discussed in Chapter 3.

The photochemical model calculates the volume emission rate at each given point in space. A schematic diagram of the model as used in Equation [5.1] is presented in Figure 5.1 for the source reactions of $O(^1S)$ used in this Chapter. The schematic (Figure 5.1) indicates the constituents required for the chemical reactions and the possible by products that result from the reactions. The model employs in-situ atmospheric composition measurements from the AE satellites where possible.

Data were obtained for most of the chemical species from more than one instrument to insure the most complete measured profiles possible. These instruments were described in Chapter 2. Atomic oxygen and N_2 densities were measured by the Open-Source Spectrometer (OSS) (Nier *et al.*, 1973) and the Neutral-Atmosphere Composition Experiment (NACE) (Pelz *et al.*, 1973). The Neutral-Atmosphere Temperature instrument (NATE) (Spencer *et al.*, 1973) provided temperature measurements. Ion composition data were collected by the Bennett Ion-Mass Spectrometer (BIMS) (Brinton *et al.*, 1973) and the Magnetic Ion-Mass Spectrometer (MIMS) (Hoffman *et al.*, 1973). Electron temperatures are from the Cylindrical Electrostatic Probes (CEP) (Brace *et al.*, 1973) and electron densities were obtained from the Retarding Potential Analyzer (RPA) (Hanson *et al.*, 1973).

When an in-situ measured parameter is not available, the photochemical model employs the Mass Spectrometer and Incoherent Scatter model (MSIS-86) (Hedin, 1987) to provide neutral densities and temperatures and the International Reference Ionosphere (IRI) (Belitza, 1986) for plasma densities and temperatures. These models were discussed in Chapter 3. When these model parameters are used, they are scaled to the available in-situ satellite measurements.

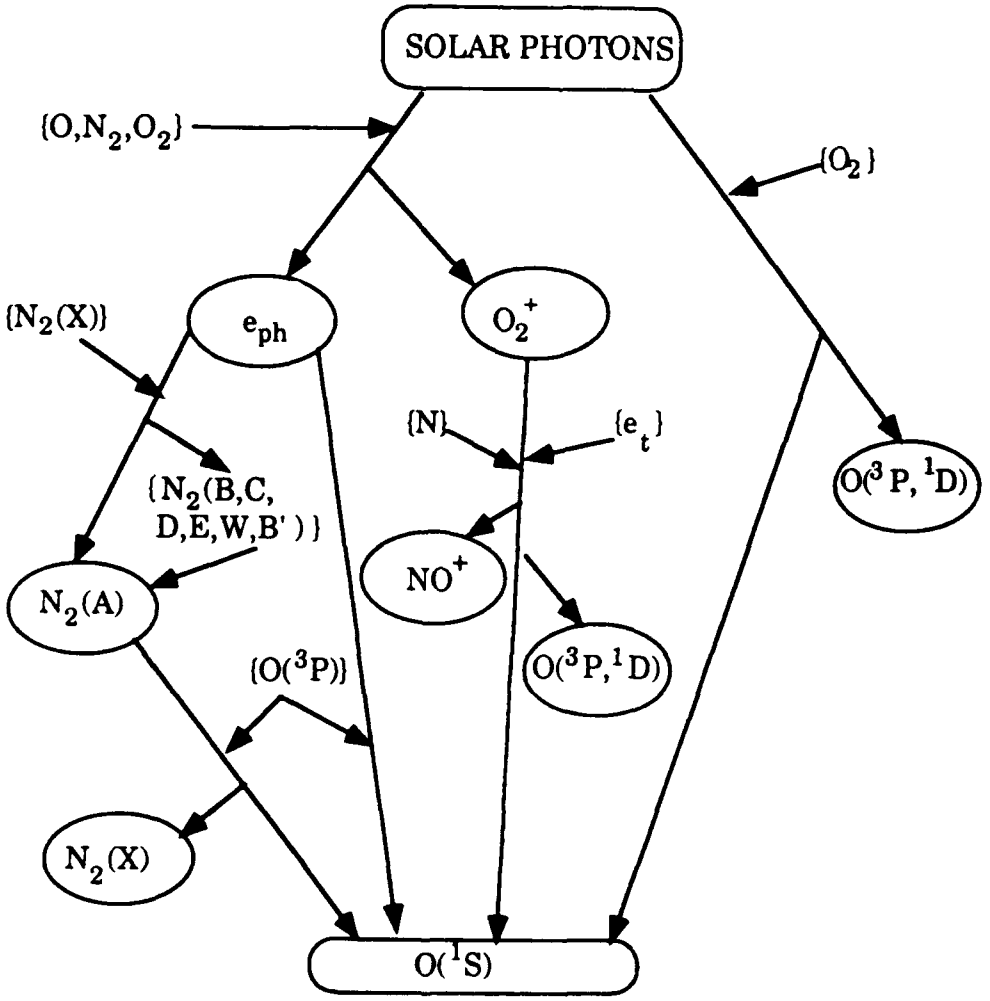

Figure 5.1 Schematic of the photochemical model showing the various inputs and products in the production of $O(^1S)$.

Since both of the important reactions being studied are dependant on the solar flux, the model employs a solar flux spectrum based on the Hinteregger Reference Spectra (Hinteregger *et al.*, 1981) and is scaled by the level of solar activity. The solar flux below 250Å is corrected by a factor of two as discussed by Richards and Torr (1984). The photoelectron spectrum is produced by a model based on the two stream approximation (Nagy and Banks, 1970). The photoelectron model is used to calculate the production of $O(^1S)$ from direct excitation of atomic oxygen and the $N_2(A)$ population due to both direct excitation and cascading from the higher excited states of the nitrogen molecule. The solar flux model was described in Chapter 3 along with the photoelectron model which was described by Solomon *et al.* (1988) and by Solomon and Abreu (1989).

For a given model run, measured or modeled values for the atmospheric parameters are obtained at 15 second intervals along the orbit, as the satellite moves towards and then away from perigee. At each point along a satellite orbit where the volume emission rate is determined, a complete profile in 5 km steps between 80 and 500 km is generated by the MSIS-86 and IRI models which are scaled by the in-situ measurements made at the point the volume emission rate is being determined. These vertical profiles are used to produce the photoelectron fluxes and direct excitations used by the model to determine the volume emission rate at the point of measurement. This procedure compensates for the variation in photoelectron production as the satellite moves along the path to different latitudes, longitudes and solar zenith angles. Once the profiles are constructed, the model determines the volume emission rate at 5577Å for that point using the measured in-situ constituent data. This procedure will be repeated at each point along the satellite path where in-situ

measurements are made. Since each point is calculated independently, a profile of the model volume emission rate can be constructed from a series of constituent measurements along the satellite track.

5.2.2 Observations of 5577Å Dayglow

The observations of the 5577Å emission were taken by the Visible Airglow Experiment (VAE) photometer on the Atmosphere Explorer (AE) satellites (Hays *et al.*, 1973) which were described in Chapter 2. The measurements of the 5577Å airglow employed in this study were obtained by the AE-C and -D satellites, which occupied elliptical orbits during the first year of their lifetimes. Selected orbits from this period provide the emission data which were used in the development and validation of the photochemical model.

Data were selected for elliptical orbits, when the spacecraft was de-spun. For the de-spun normal mode, the high-sensitivity channel (channel 2) of the VAE instrument pointed radially out from the Earth as the satellite moved along its track. This orientation allowed the measurements to be made without significant contamination from either vehicle glow or by Rayleigh scattered light from below the satellite (Yee and Abreu, 1983). In an elliptical orbit it is possible to obtain a profile of the emission as the satellite intersects layers of the atmosphere at different altitudes. Data were selected for mid-latitude and equatorial, daytime conditions (latitude between ±60 degrees and solar zenith angle < 85 degrees).

Volume emission rates were calculated from the brightness measurements in steps of 4 km from the satellite perigee altitude up to 400 km. It was assumed that the emission layer is horizontally homogeneous and there are no changes in galactic background intensity between two

successive measurements by the instrument. The measurements of the column brightness made in this fashion can be inverted by a simple derivative technique schematically illustrated in Figure 5.2 which was discussed in Chapter 2.

An example of the measurements of the 5577Å emission and the inverted volume emission rate profile from the derivative "inversion" technique are presented in Figure 5.3. The figure shows the measured surface brightness for AE-C orbit 0455 as the satellite moves away from perigee. As the satellite moves away from perigee the latitude changes from 30° N to 15° N and the solar zenith angle changes from 69° to about 66°.

5.2.3 Method of Determination

Photochemical model simulations have been carried out using orbits from the AE satellites to determine the magnitude of the impact cross-section of electrons on atomic oxygen (Reaction [3.1]) and the branching ratio for $O(^1S)$ by quenching of $N_2(A)$ by atomic oxygen using the total rate from Chapter 4 (Reaction [3.7]) that will best reproduce the measured 5577Å emission profiles. Table 5.1 is a list of the orbits used along with some orbital characteristics. All of the orbits were used to find the parameters for Reactions [3.1] and [3.7] that will best represent the emission profile for $O(^1S)$ using data between perigee and 250 km. Above 250 km, dissociative recombination (Reaction [3.3]) becomes as important as Reaction [3.1] for the production of $O(^1S)$. The best fit is determined by finding the parameters that will give the minimum χ^2 deviation for the orbits listed. The equation for χ^2 is

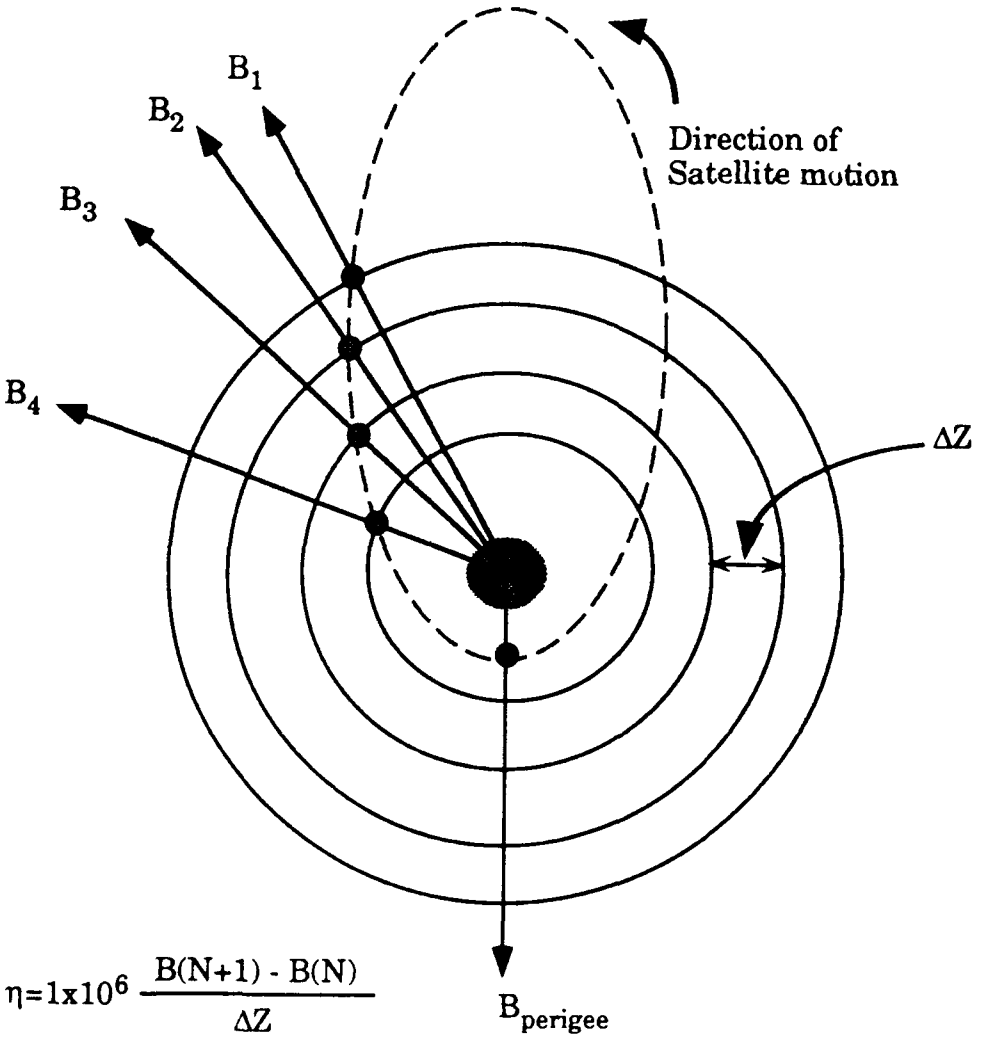

Figure 5.2 The geometry used for the brightness measurements of the 5577Å emission.

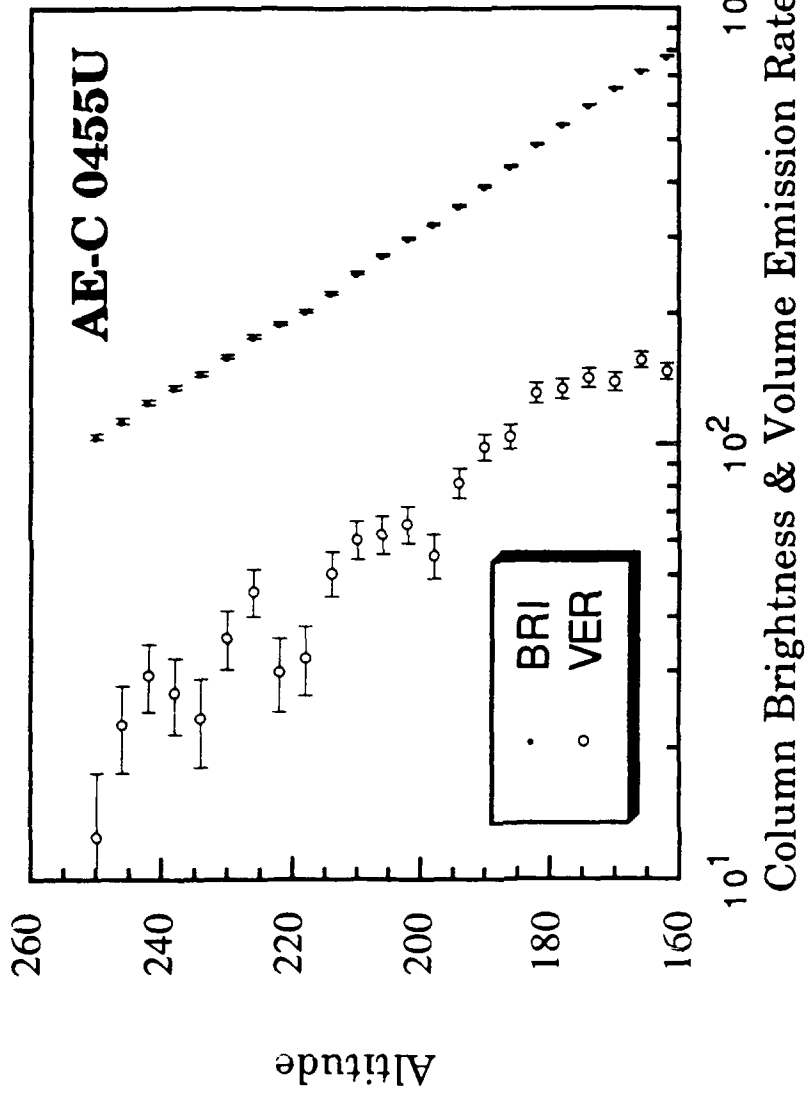

Figure 5.3 Example of the measured brightness and the inverted volume emission rates for AE-C 0455U.

Satellite	Orbit	Date	Alt	LST	Diplat	Leg
C	455	74026	155.5	15.17	34.0	U/
C	584	74038	157.8	12.90	41.8	U/D
C	606	74040	158.2	12.54	42.2	U/D
C	628	74042	158.5	12.13	44.3	D
C	650	74044	159.0	11.75	45.4	D
C	656	74044	159.0	11.64	56.0	U/D
C	3354	74269	135.3	7.36	-21.1	U
C	3410	74273	136.1	6.36	-28	U
D	672	75337	142.5	9.39	57.1	D
D	814	75349	142.8	8.53	26.5	D
D	816	75349	143.0	8.52	22.6	D
D	818	75349	143.0	8.51	37.3	D
D	846	75351	141.8	8.43	20.	D
D	912	75357	141.6	7.94	0.4	D
D	918	75357	141.6	7.90	8.0	D
D	942	75359	142.0	7.76	4	D
D	984	75363	143.0	7.50	-14.2	U/D
D	1021	76001	144.6	7.27	-13.5	U/D
D	1045	76003	146.0	7.13	-23.5	U/D
D	1069	76005	147.4	.99	-32.9	U/D
D	1094	76007	149.3	6.84	-27.2	U/D
D	1190	76015	142.0	6.28	-45.0	U
D	1192	76015	142.2	6.27	-35.9	U

Table 5.1 List of orbits used from Satellites AE-C and AE-D in this study along with some of the parameters.

$$\chi^2 = \frac{1}{n}\sum \frac{[V_s - V_m]^2}{\sigma_s^2 + \sigma_m^2}, \qquad [5.2]$$

where n is the number of data points, σ_S is the error in the VER from the measurements of the satellite, σ_m is the errors attributed to the model, V_S is the VER from the satellite, and V_m is the VER determined by the model. Correction factors for the magnitude of the electron impact cross section and values of the effective branching ratio for the production of $O(^1S)$ by $N_2(A)$ quenching are determined that will best represent the data. The model VER profile was interpolated to be on the same altitude grid as the inverted data, then the total χ^2 deviation for all of the selected orbits were calculated.

The total rate coefficient for Reaction [3.7] determined in Chapter 4 is for the υ=0 vibrational level. This value for the total rate coefficient is in close agreement with the values for υ=0 of Piper (1982) and of Thomas and Kaufman (1985). The branching ratio is varied from 0.0 to 1.0 and the value to give the best fit to the observed data is determined. The effective rate of production of $O(^1S)$ will then be the product of the total rate coefficient and the best fit branching ratio for the reaction from the simulations.

The magnitude of the electron impact cross section for electrons on atomic oxygen was determined by using Equation 5.2. The magnitude of the parameterized cross section of Green and Stolarski (1972) is varied by factors from 0.5 to 3.5 in steps of 0.25. This allows the cross section magnitudes to vary from half the values of Henry *et al.* (1969) to almost twice those of Shyn *et al.* (1986). The value of the multiplying factor that gives the best fit is determined by this method.

The magnitude of the cross section and the yield of $O(^1S)$ from Reaction [3.7] were varied simultaneously to find the best fit parameters by a least squares fitting to the inverted data. The result is a plot of the magnitude of the χ^2 as a function of the multiple factor for the impact cross section and the effective branching ratio for a given assumed total rate coefficient. An example of results for determining of the model parameters are shown in Figure 5.4. The next section will discuss the results of the parameters determined here as they affect the dayglow 5577Å emission.

5.3 Analysis of Results for 5577Å Dayglow

5.3.1 Effects of the Vibrational Population of $N_2(A^3\Sigma_u^+)$

The total rate coefficient for the quenching reaction is dependant on the distribution of the population of the vibrational levels of the $N_2(A)$ state. As noted before, the vibrational levels are preferentially populated by direct and cascading processes. The results from laboratory studies and aeronomical determinations of the total rate coefficient cannot be directly compared unless the vibrational population is taken into account. The effective branching ratio for the reaction can be determined if a value of the total rate coefficient is assumed and the distribution of the vibrational population is known.

The production of $O(^1S)$ by the quenching of $N_2(A)$ from Reaction [3.7] can be expressed as,

$$P[O(^1S)] = \sum_{\upsilon} \beta_{\upsilon} k_{\upsilon} \left[N_2(A)\right]_{\upsilon} \left[O\left(^3P\right)\right] = \beta_{eff} k_{tot} \left[N_2(A)\right]_{tot} \left[O\left(^3P\right)\right], \qquad [5.3]$$

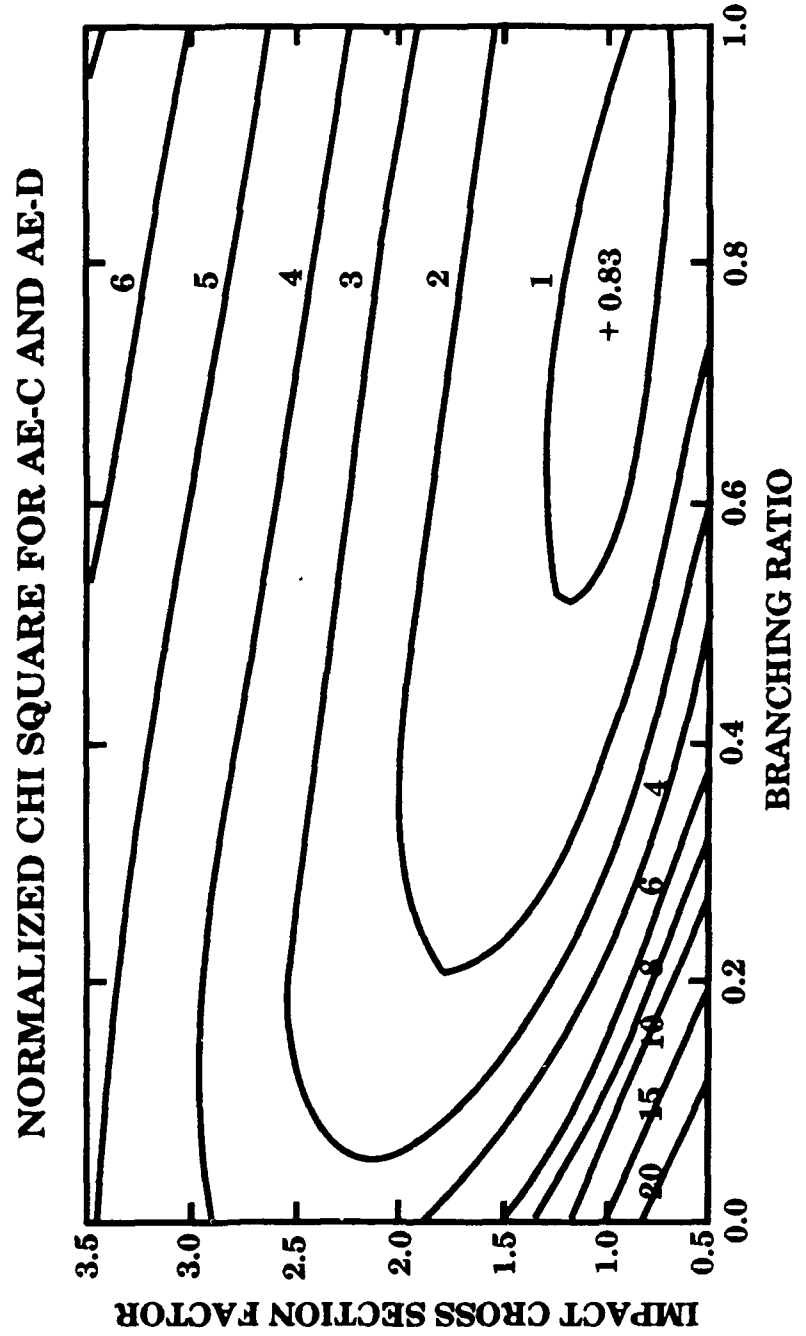

Figure 5.4 Example of the normalized χ^2 for the orbits listed in Table 5.

where β is the branching ratio and k is the rate coefficient for the reaction. Allowing for the change in rate coefficient by vibrational level as shown by Piper *et al.* (1981), De Souza *et al.* (1985), and Thomas and Kaufman (1985), solving Equation [5.3] for the effective branching ratio gives,

$$\beta_{eff} = \sum_{\upsilon} \beta_{\upsilon} f_{\upsilon} r_{\upsilon} \ , \qquad [5.4]$$

where f_{υ} is the fractional population of the υ^{th} vibrational level and r_{υ} is the ratio of the rate coefficient for the υ^{th} level and the total rate coefficient.

The vibrational population of the $N_2(A)$ state was calculated from the model by Cartwright *et al.* (1971, 1973) and Cartwright (1978) which was adapted to used the photoelectron flux spectrum from a two stream model for photoelectron fluxes (Nagy and Banks, 1970). The vibrational population model used statistical equilibrium with both direct and cascading processes to calculate the population of the lowest triplet states of N_2. The photoelectron model was discussed in Chapter 3 and the vibrational population model was described in detail in Chapter 4.

The results for the distribution of the vibrational population of the $N_2(A)$ state at 150 km is shown in Figure 5.5. The figure shows the population is highest for the two lowest vibrational levels. The rapid decrease in population for vibrational levels above υ=7 due to the inverse transition to the $N_2(B)$ state. This population distribution is important in determining the production of $O(^1S)$ due to Reaction [3.7]. Even though the quenching rate increases with vibrational level as shown by Piper (1982) and Thomas and Kaufman (1985) the rapid decrease in population indicates the lowest levels are important for the production of $O(^1S)$.

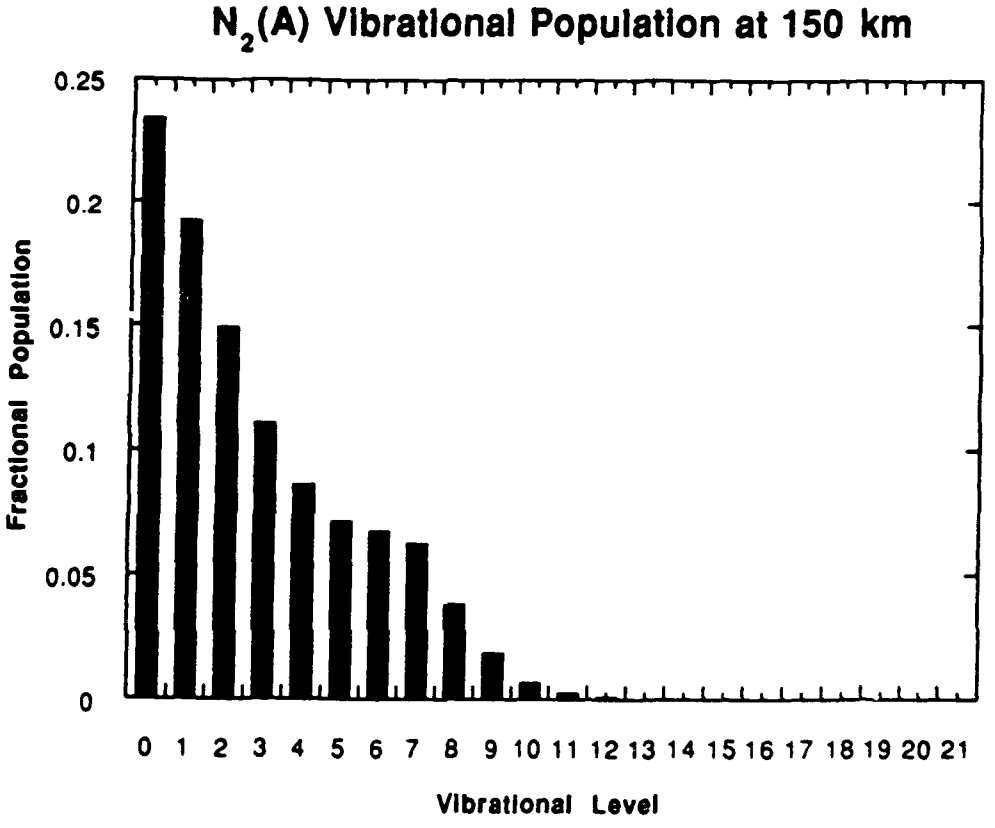

Figure 5.5 Fractional population from the N_2 Triplet model at 150 km.

Using the population levels from Figure 5.5 and the results from Piper *et al.* (1981) and Piper (1982) for the υ=0,1 levels, solving for the effective branching ratio as given by Equation [5.4] gives a value of 0.312. This value does not agree well with the one determined from the χ^2 fitting studies performed in this work. This indicates that the higher vibrational levels are required to fully determine the $O(^1S)$ production from the quenching reaction.

5.3.2 Dependance of the Determined Parameters on Other Reactions

In addition to the major reactions for the production of the 5577Å dayglow, there are several minor sources which could play a role in the determined magnitude of the reactions from above. The two of most importance at the altitude regions of the Atmosphere Explorer observations used in this study are the dissociative recombination of O_2^+ (Reaction [3.3]) and the ion exchange between atomic nitrogen and O_2^+ (Reaction [3.12]). Both of these reactions, which were discussed in detail in Chapters 1 and 3, and will be important to the twilight transition period (discussed in the following section) and the nightglow.

These reactions are used to determine the sensitivity of the determined parameters for Reactions [3.1] and [3.7]. The two parameters are determined for different combinations of the rate coefficient for Reaction [3.12] and the branching ratio for the production of $O(^1S)$ by Reaction [3.3]. For the branching ratio, in addition to the calculated value determined as described in Chapter 3, the value was fixed at 6%, which is a median value of the branching ratio listed in several studies (Zipf ,1970, 1980; Kopp *et al.*, 1977; Abreu *et al.*, 1983; Guberman 1988). The rate coefficient for Reaction [3.12] is not well known. A value of 2.5 $x10^{-11}$ cm^3 s^{-1} was determined by

Frederick *et al.* (1976) within a factor of two due to uncertainty in the actual atomic nitrogen density profile. For this study the value was set at 2.5 x10^{-11} cm^3 s^{-1} and then multiplied by 0, 0.5, 1.0, and 2.0 to remove the reaction from the model completely and allow the rate coefficient to vary over the limits stated by Frederick *et al.* (1976).

The two parameters determined in Section 5.2.3 were found for each case described above. The results of the χ^2 fitting were similar to the one shown in Figure 5.4 with some small variations in the values previously determined. The results are summarized in Figure 5.6 for the eight cases along with the values determined by the previous studies for comparison. These results will be summarized below along with the rest of the model analysis.

5.3.3 Summary of Dayglow Results

The photochemical model we have developed is able to reproduce the observed daytime 5577Å thermospheric emission. Four major source reactions were incorporated into the model of the emission profile. The reactions needed for the model are photoelectron impact on atomic oxygen, dissociative recombination of O_2^+, quenching of $N_2(A^3\Sigma_u^+)$ by atomic oxygen, and photo-dissociation of O_2 which becomes more important below the peak. The ion-exchange reaction between O_2^+ and atomic nitrogen reaction is not needed to explain the 5577Å dayglow emission profile.

In this section, the results of the determination of the magnitude of the impact cross section for photoelectrons on atomic oxygen and the branching ratio for the quenching of $N_2(A)$ will be summarized. The vibrational population distribution of $N_2(A)$ will be discussed as it affects the

production of $O(^1S)$ by the quenching reaction. Some comparisons of the photochemical model to 5577Å dayglow observations will be presented.

The impact of photoelectrons on atomic oxygen is the primary source of 5577Å dayglow emission in the thermosphere. The reaction produces the majority of the $O(^1S)$ even at the peak in the emission layer. As can be seen from Figure 5.4, the observed profiles of 5577Å emission is best reproduced by the impact cross sections of Henry *et al.* (1969) with a multiplying factor of 1.0. The magnitude of the impact cross sections determined by this study are also in good agreement with the latest theoretical impact cross sections determined by Berrington and Burke (1991, Personal Communication) and are about a factor of two smaller than the laboratory cross sections of Shyn *et al.* (1986).

The quenching of $N_2(A)$ by atomic oxygen is an important source of the 5577Å emission at the peak in the layer. While the photoelectron impact is still the largest contributor, this reaction is needed to adequately fill in the peak in the emission layer. This reaction was studied for changes in the contribution to the volume emission by fixing the total rate coefficient to the value determined in Chapter 4 for the $N_2(A)$, υ=0 level. The value for the total rate coefficient used in the study is 2.8×10^{-11} cm^3 s^{-1} which falls between $2.1 \pm 0.4 \times 10^{-11}$ cm^3 s^{-1} from Piper (1982) and $3.5 \pm 0.6 \times 10^{-11}$ cm^3 s^{-1} from Thomas and Kaufman (1985). The effective branching ratio for this reaction determined by this study of 5577Å dayglow observations is 0.75±0.25 for the assumed total reaction rate for quenching. The effective branching ratio for the quenching of $N_2(A)$, υ=0 determined by these simulations tend to support the results from Piper (1982) and De Souza *et. al* (1985) of 0.75±13. When combined with the total rate coefficient, the branching ratio gives a production rate for $O(^1S)$ of 2.01×10^{-11} cm^3 s^{-1}.

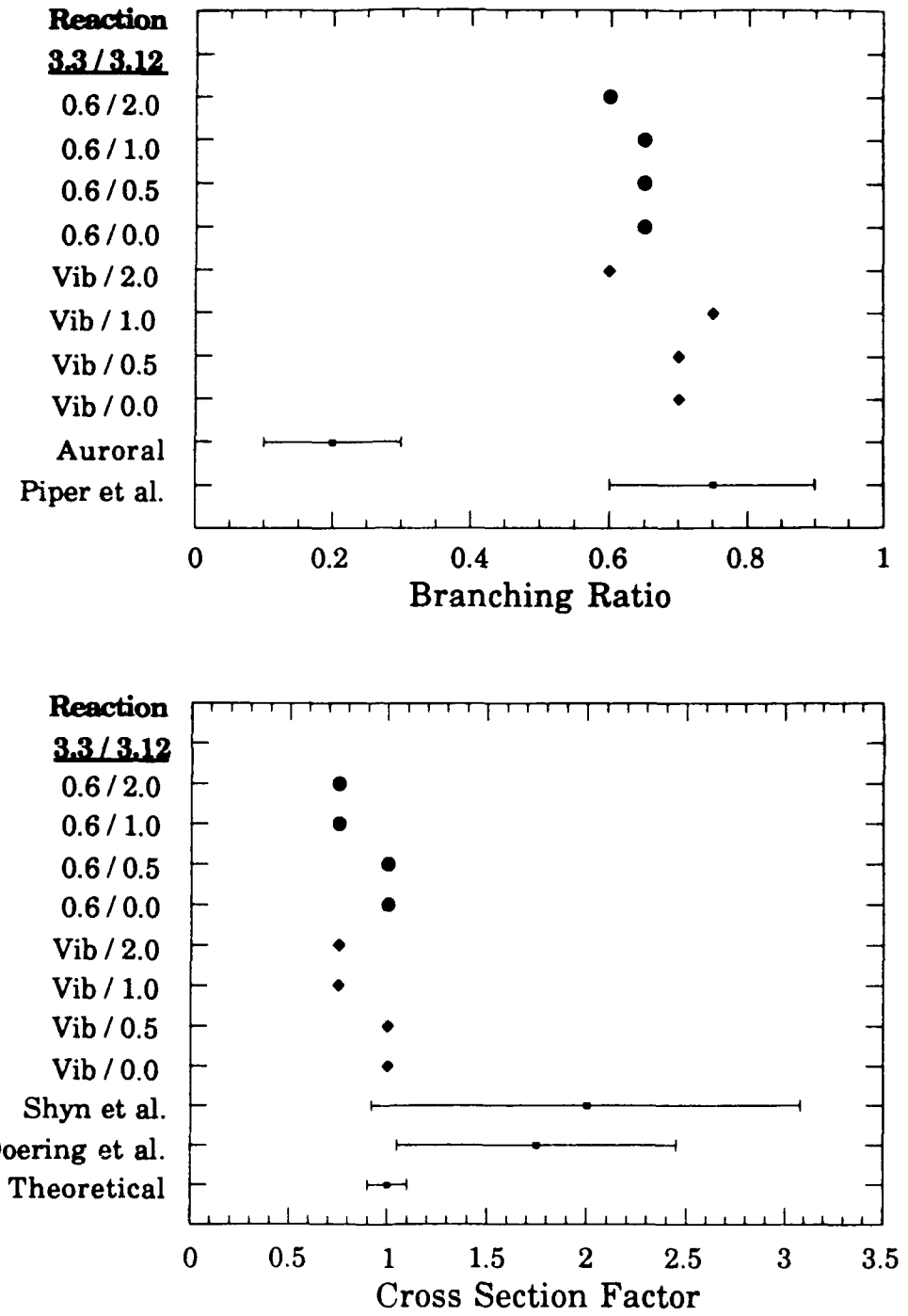

Figure 5.6 Results of the tests of the sensitivity of the major reaction parameters determined here to the values used in the minor sources.

Differences in the vibrational population may account for the discrepancy between the branching ratios determined by aeronomical studies and by laboratory experiment. While the vibrational population in laboratory studies is restricted to a single level, the dayglow will have the population distributed over all vibrational levels. This distribution plays an important part in determining the effective branching ratio for the quenching reaction. Since the rate coefficient has been shown to change with vibrational level, the contribution of each level will depend on the fraction of the population it contains.

The branching ratio determined by Piper (1982) was for the entire population of the $N_2(A)$ in either the $\upsilon = 0$ or the $\upsilon = 1$ level. The effective branching ratio from this study for the $O(^1S)$ dayglow agrees well with the values of Piper (1982) but assumes the population is in the $\upsilon=0$ vibrational level only. In the dayglow, the vibrational population of $N_2(A)$ is not limited to the lowest two levels as was shown in Figure 5.5. By allowing for the distribution of the vibrational population of the $N_2(A)$ state and knowing the dependance of the branching ratio and rate coefficient by vibrational level, the effective branching ratio discrepancy can be resolved. If the $N_2(A)$ vibrational levels responsible for the production of the $O(^1S)$ in the dayglow are mainly the lower levels, then the auroral studies of the effective branching ratios may have better agreement with those from laboratory studies.

Using the magnitude for the impact cross section and the effective rate coefficient for the $N_2(A)$ quenching reaction determined above, the calculated 5577Å volume emission rate from the model can be compared to the inverted emission rate profile on an orbit by orbit basis. Examples of these comparisons are shown in Figures 5.7 and 5.8. The figures show the

relative importance of the source reactions for the production of $O(^1S)$ for the selected conditions. Figure 5.7 shows AE-D 0846 downleg which starts at 3° S latitude and ends at about 13° N and the solar zenith angle changes from about 56° to about 65° along the satellite path. Figure 5.7a shows the individual reactions used in the model and the total emission rate from the model compared to the inverted emission rate along the satellite orbit while 5.7b compares the error of the inverted emission rates to the errors attributed to the model. The area between the two lines is the total of the model ±20%. Figure 5.8 is for AE-D 0912 downleg which travels from 15° S latitude to about 2° N while the solar zenith angle changes from about 57° to about 64°. Figures 5.8a and 5.8b are similar to 5.7a and 5.7b respectively. Electron impact is the dominant source at all altitudes between 250 km and satellite perigee with dissociative recombination a secondary source at higher altitudes and quenching of $N_2(A)$ becoming more important at lower altitudes. Near the peak of the layer, quenching of $N_2(A)$ by atomic oxygen becomes an important source of $O(^1S)$ in the 5577Å dayglow. Further down, below satellite perigee, photodissociation of O_2 (Reaction [3.9]) quickly becomes the major source of 5577Å emission. Though Reactions [3.3] and [3.12] become more important in the twilight and nightglow, they are not important in the dayglow calculations in the photochemical model developed here.

Even though the model is run in equal steps in time and the inverted brightnesses are in equal steps in altitude, good agreement is found between the observations and the model predictions, particularly at high altitudes. At low altitudes, where the satellite is near perigee, the model does not predict the emission layer as well especially in high solar zenith angle cases. This is because the assumption of small horizontal gradients

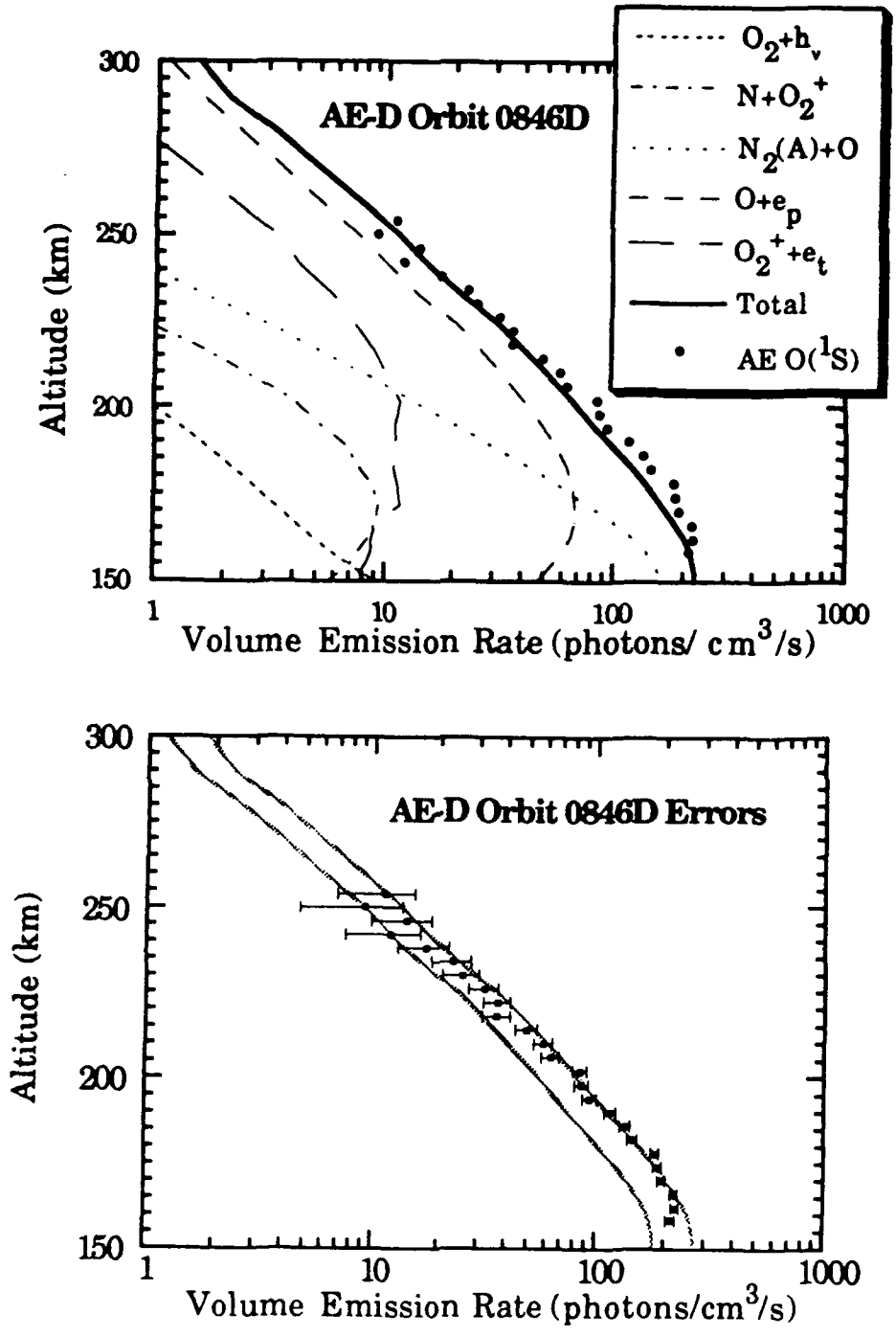

Figure 5.7 Results of the model compared to the inverted profile for AE-D 0846D. (a) the individual reactions and total emission rate from the model and the inverted data. (b) Shows a comparison of the error of the inverted data with the model ±20% (area between lines) .

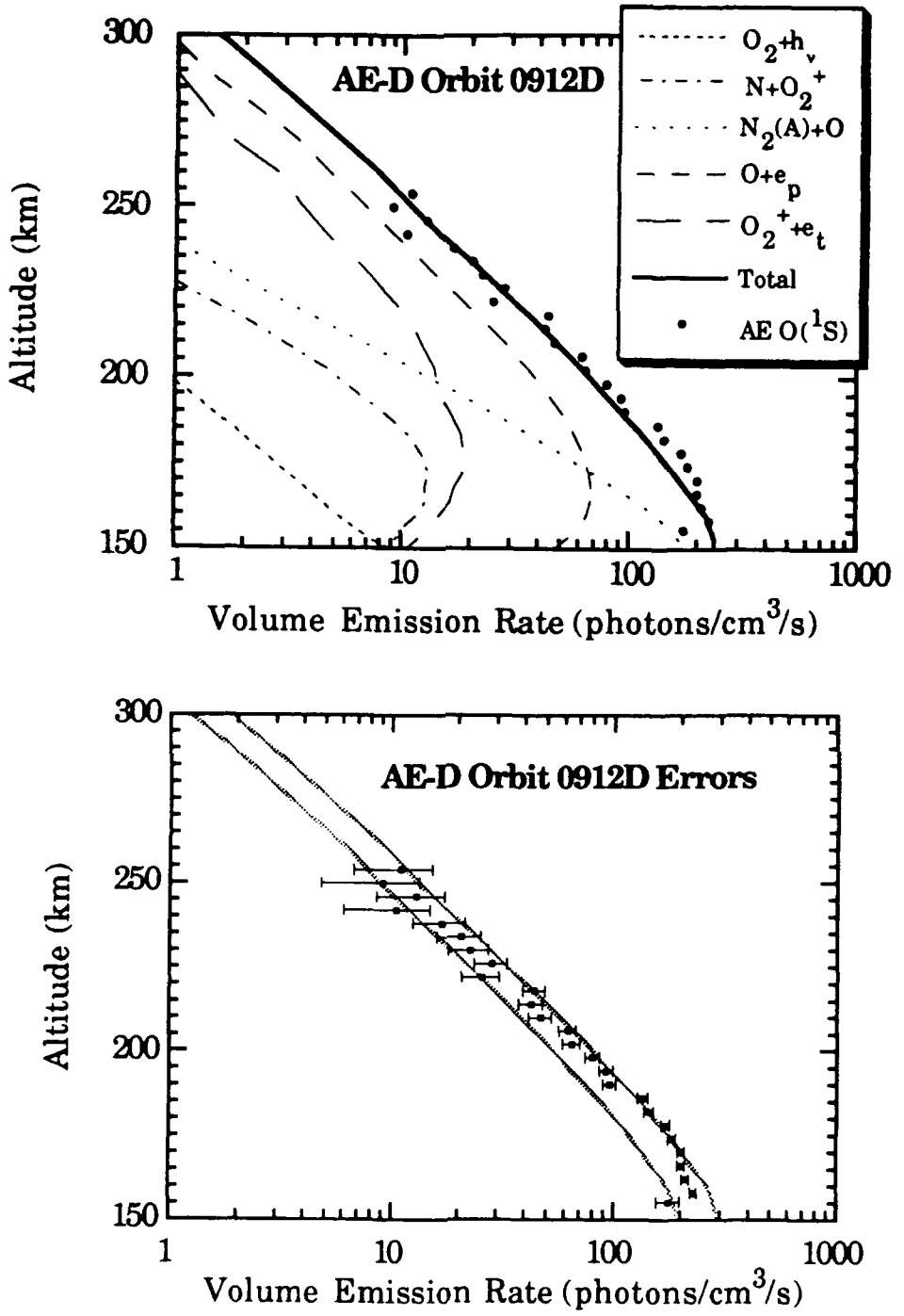

Figure 5.8 Results of the model compared to the inverted profile for AE-D 0912D. (a) the individual reactions and total emission rate from the model and the inverted data. (b) Shows a comparison of the error of the inverted data with the model ±20% (area between lines) .

in brightness is not as valid near perigee. As the satellite approaches perigee, the photometer zenith angle will undergo a larger change in a 4 km step than when at 400 km. The larger photometer zenith angle change means that horizontal gradients in the emission will not be completely corrected for in the inversion technique. Integrating the model volume emission rates and comparing to the measured brightness will not avoid the problem of horizontal gradients. Since the model only predicts the emission at a point from the in-situ measurements, which are along the satellite track, the model volume emission rates are not vertical profiles. Two consecutive measurements of brightness are treated as measurements from a vertical profile for the differentiation to determine the volume emission rate. Integrating vertically will not predict the brightness seen by the photometer looking radially out at any given point.

5.4 5577Å Emission in the Mid-latitude Twilight

At midlatitudes, the upper atmosphere undergoes a rapid, drastic period of change twice daily known as twilight. During this period, the atmosphere is either going from a period of prolonged sunlight (day) to a period of dark (night) or *vice versa*. This transitional state makes the study of the twilight both interesting and difficult. This period has been reviewed by Bates (1960), Chamberlain (1961), Gadsen (1967), and Hunten (1967).

Appendix D contains a discussion of the twilight in general and the 5577Å emission in the twilight. The modeling of the twilight is very difficult and the inversion of the observations in the twilight is not as straight forward as in the dayglow. The photochemical model developed for the dayglow is able to transition to the twilight conditions. As the solar zenith

to transition to the twilight conditions. As the solar zenith angle increases, the various reactions that are driven by the solar flux begin to decrease in importance while those driven by ion chemistry become the dominant sources. This is illustrated in Figure 5.9 which shows the shift in reaction importance as the orbit proceeds into twilight. As the solar zenith angle increases to 90°, the contribution of the quenching reaction for $N_2(A)$ drops rapidly as does the electron impact on atomic oxygen. The two reactions involving O_2^+ also decrease in magnitude but at a much smaller rate than the solar driven reactions. The overall results of the change are shown in Figure 5.10 which shows the change in the total volume emission rate as the solar zenith angle increases. The changes illustrated in the figure occur in less than six minutes of time along the satellite path. This rapid change in chemistry makes inversion and modelling of the twilight very difficult.

5.4.1 Model Results for Twilight Conditions

The photochemical model developed and used in the dayglow as described above should be able to also model the twilight 5577Å emission. The model may be used in a manner similar to the dayglow cases. Elliptical orbits are used to collect the *in-situ* data and measurements of the brightness above the satellite. The model volume emission rates are then integrated vertically above the satellite and the results may be compared to measured brightnesses. Also, the model volume emission rates will be compared to the results of a circular orbit inverted using the sequential estimation method as described in Chapter 2 and applied to Atmosphere Explorer observations (Abreu *et al.*, 1991). Example results using these two methods will be presented and briefly discussed.

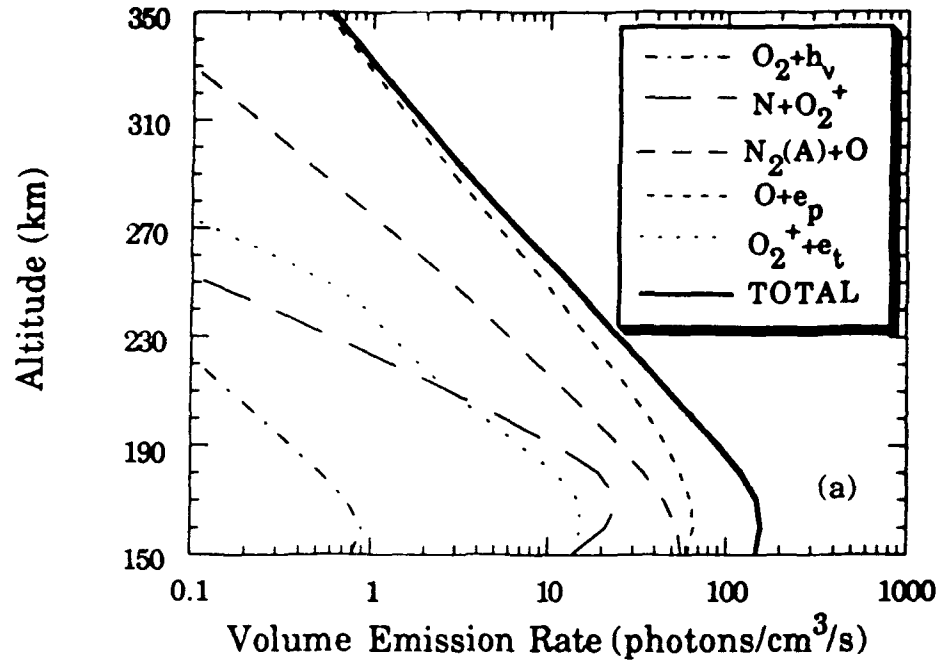
350
310
270
230
190
150
Altitude (km)
0.1
1
10
100
1000
Volume Emission Rate (photons/cm^3/s)
O_2+h_ν
N+O_2^+
N_2(A)+O
O+e_p
O_2^++e_t
TOTAL
(a)

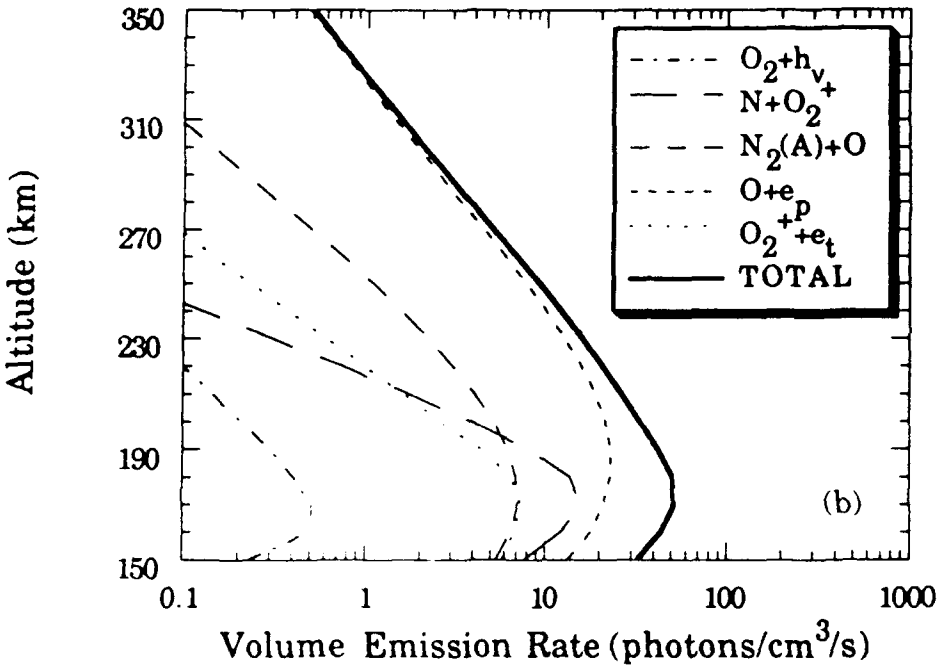
350
310
270
230
190
150
Altitude (km)
0.1
1
10
100
1000
Volume Emission Rate (photons/cm^3/s)
O_2+h_ν
N+O_2^+
N_2(A)+O
O+e_p
O_2^++e_t
TOTAL
(b)

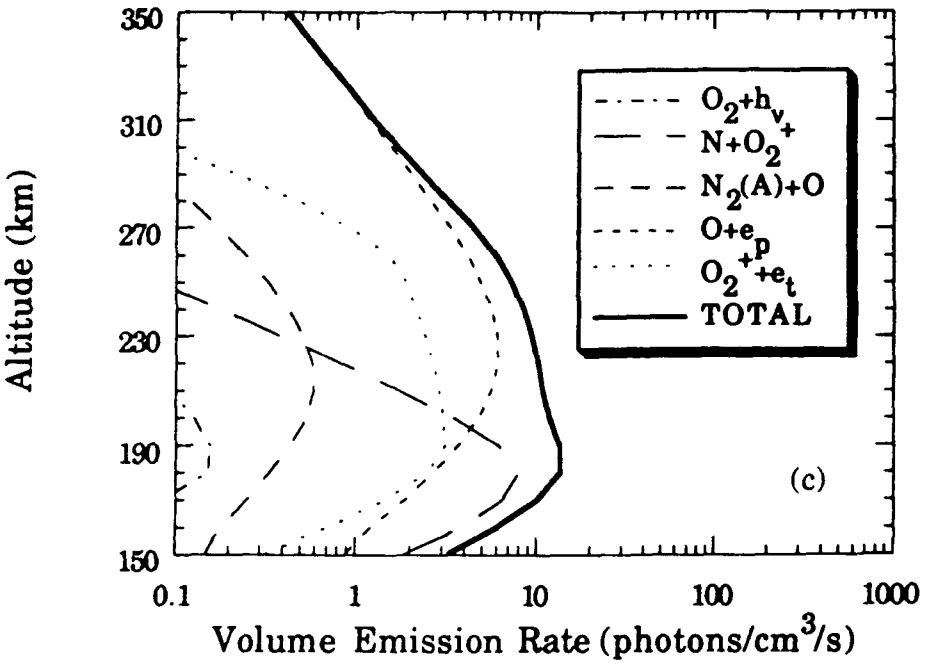

Figure 5.9 Model source reactions for 5577Å emission during twilight. For (a) 70° (b) 80° (c) 90° solar zenith angle.

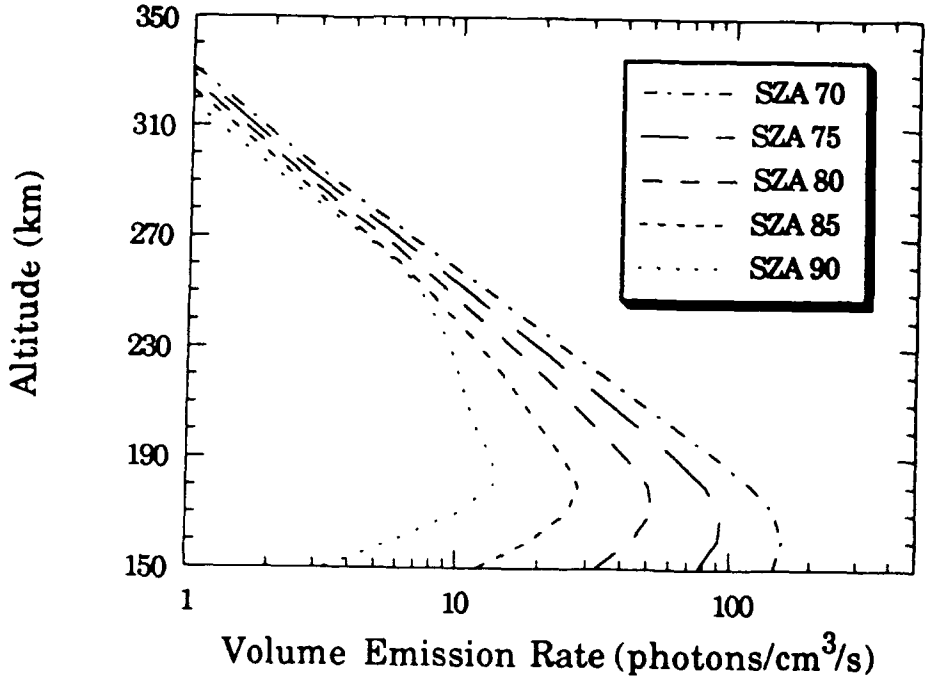

Figure 5.10 Comparison of total emission for the model as satellite proceeds through the terminatior.

The use of the 5577Å dayglow model in twilight is complicated by the high solar zenith angles which affects the calculations of the various parameters in the subsiderary models. The complication due to the assumption of the change in background emission above a given level thatwas present at perigee affects the twilight also. This restriction at perigee is due to the rapid change in photometer zenith angle. As the satellite traverses the twilight it is not the change in photometer zenith angle that changes so quickly, but the rapid change in the emitting layer and background. The use of this method of inversion is not capable of handling the twilight emission.

An example of the problem is shown in Figure 5.11. In this figure the model has error bars of 20%. While those of the measured brightness is set at 20% also, it could be higher due to the changes discussed above. The general features of the observed emission is well represented by the model. The integrated brightness from the model is smaller than the observed but the background is not corrected for above the altitude of the model.

The sequential estimation technique is better suited to the changes in the twilight. Figure 5.12 shows the results of the inversion without the subtraction of Rayleigh scattered light. The inverted emission is shown in Figure 5.13 after the subtraction of the Rayleigh scattering and Figure 5.14 is the model results. As can be seen, the model can reproduce the general features of the transition in the twilight.

The examples and results presented here represent preliminary results of the investigation into the twilight emission using the 5577Å dayglow model. These figures show the 5577Å model as developed here is able to reasonably reproduce the general features of the twilight emission. However, the rapidly changing chemical processes in the twilight are

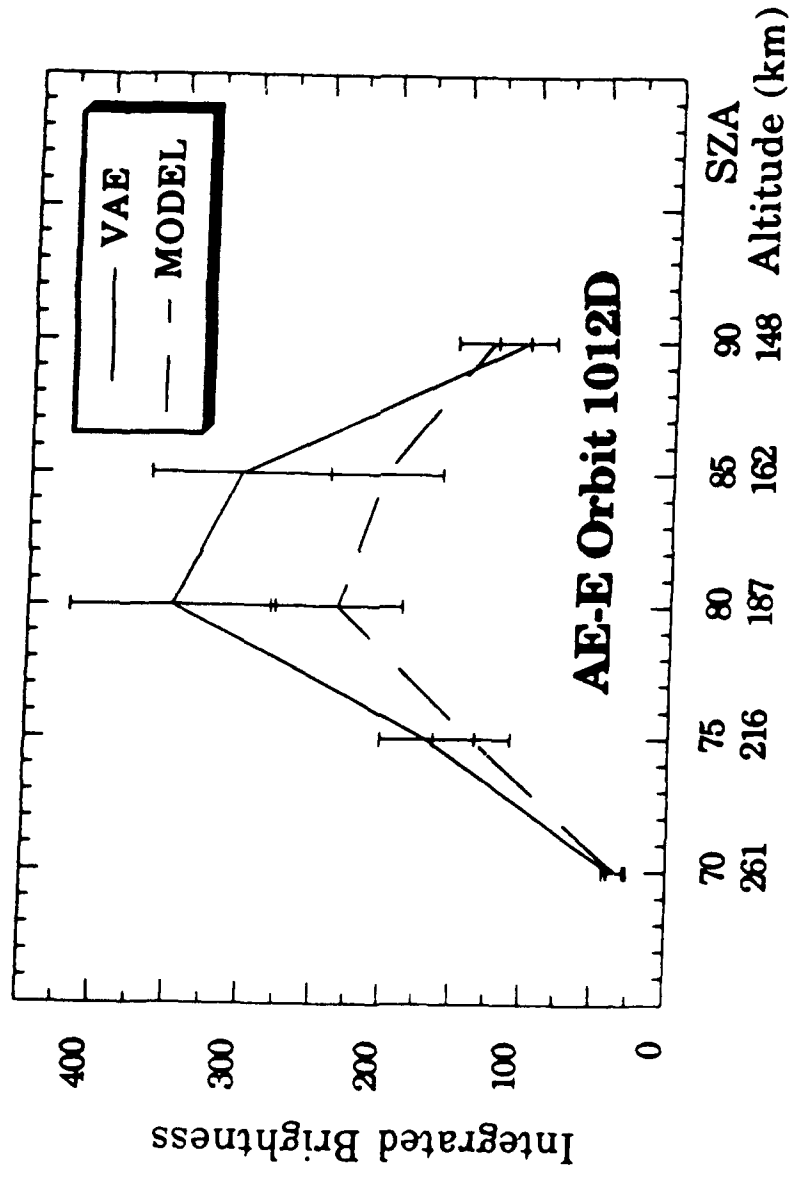

Figure 5.11 Twilight period for AE-E 1012D from integrated model and observed brightness.

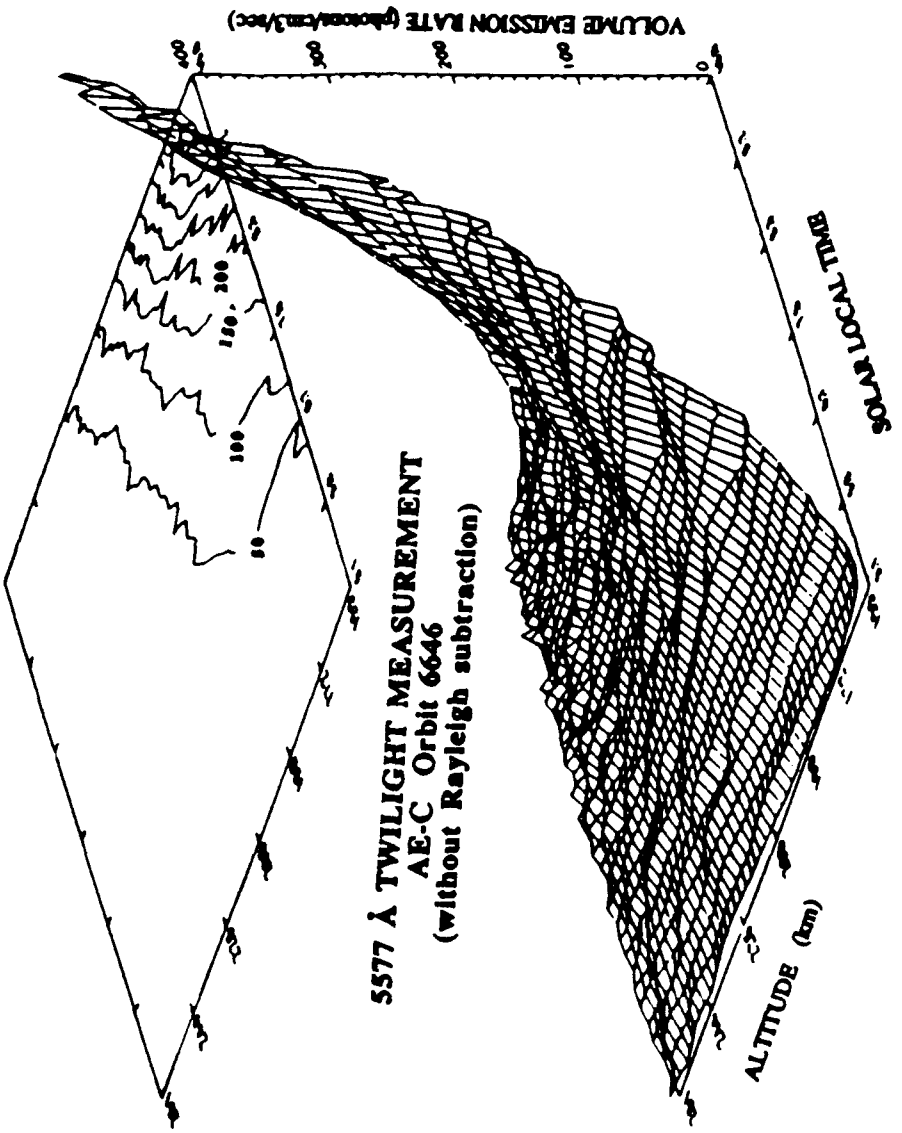

Figure 5.12 AE-C Orbit 6646 inverted 5577Å emission using sequential estimation without subtraction for Rayleigh scattering.

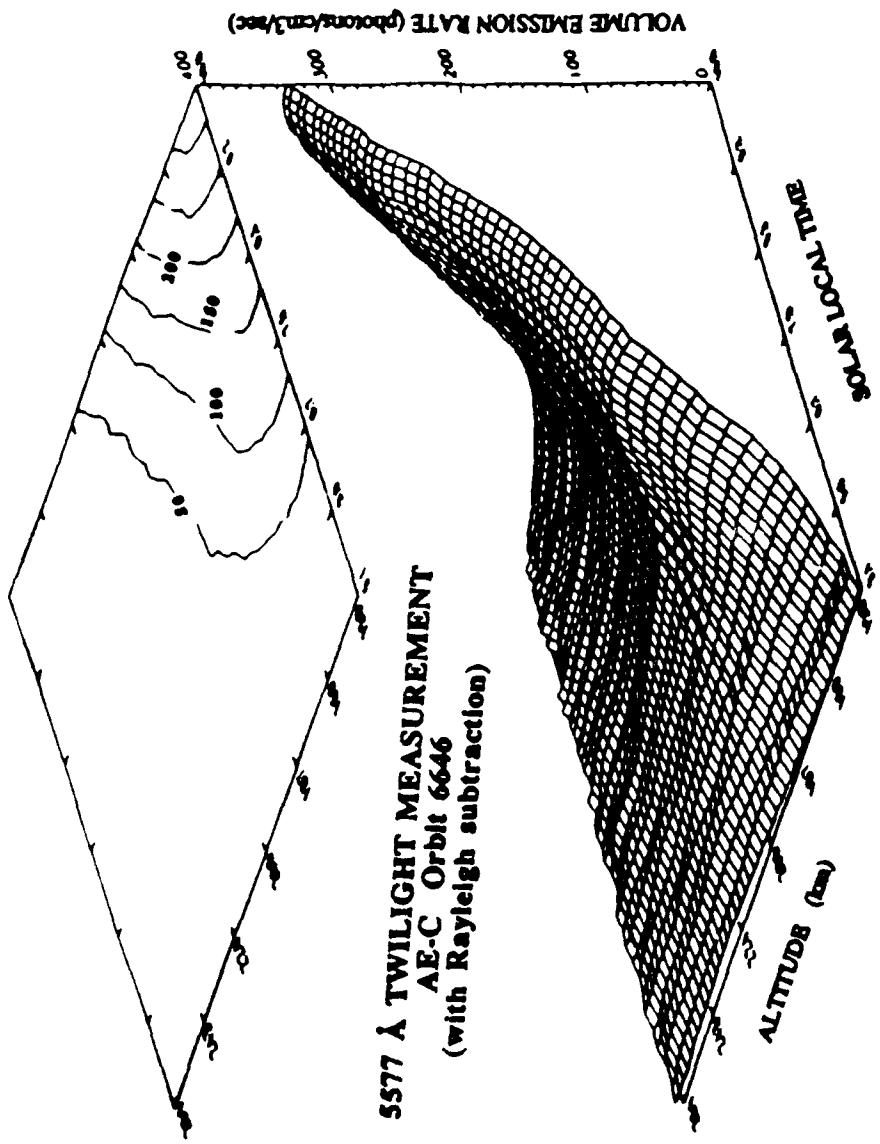

Figure 5.13 AE-C Orbit 6646 inverted 5577Å emission using sequential estimation with subtraction for Rayleigh scattering.

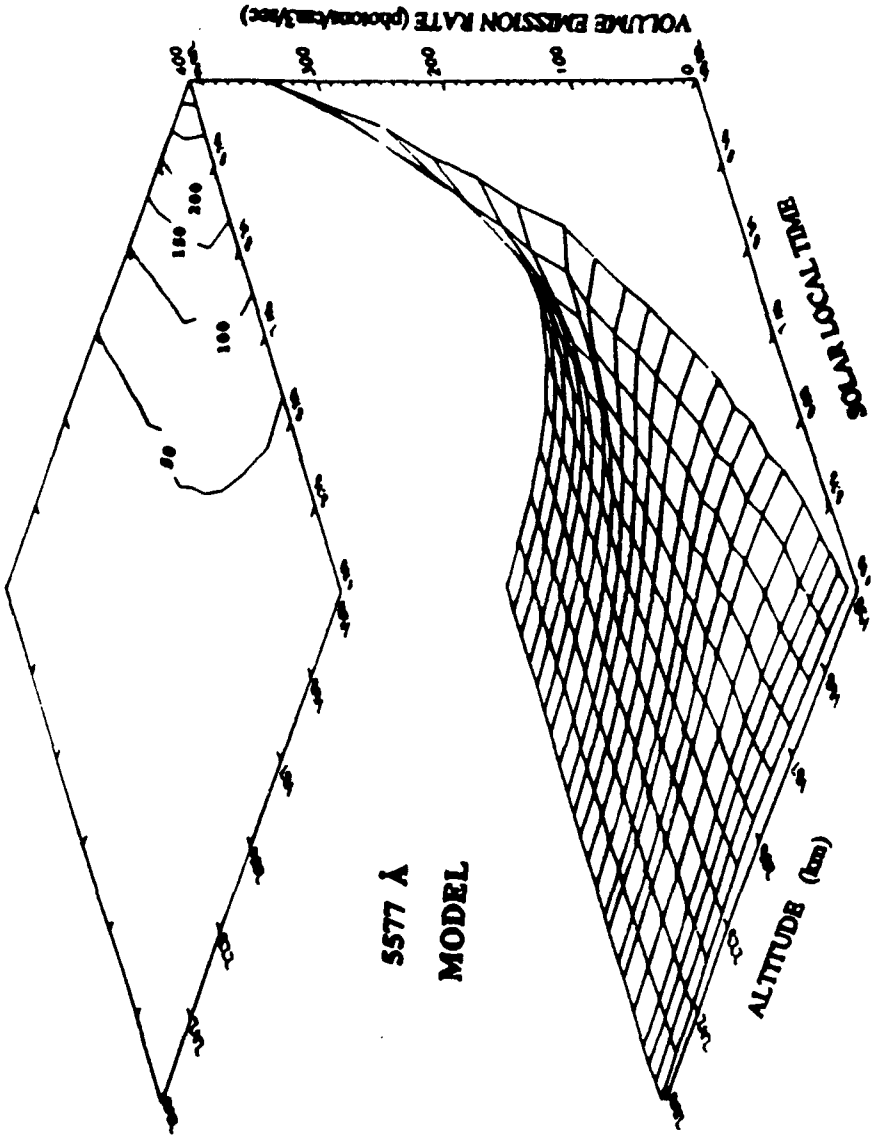

Figure 5.14 Model 5577Å emission for orbit AE-C 6646.

difficult to model and to observe. Work is still needed to study the twilight, both in the model for the rapidly changing twilight conditions and in the inversion methods to be used in the twilight. This research is to be continued at a later date and may be extended to include other emissions as discussed in Appendix D.

CHAPTER VI

CONCLUSIONS

The OI emission at 5577Å has a history that goes back over 100 years since its discovery in the aurora and nightglow. This emission was the central part of the study presented here. As was pointed out in Chapter 1, there are still questions about the various processes that produce the $O(^1S)$ which gives rise to the emission even though it has been studied a long time. The work in this thesis centered on answering some of these questions by using observations of the emission taken by the Atmosphere Explorer satellites.

To study the 5577Å dayglow emission, a photochemical model was developed for the production of $O(^1S)$ and compared with the observations. The description of the satellite instruments and the analysis of the data was given in Chapter 2 and the development of the photochemical model was discussed in Chapter 3. The rest of the thesis describes the two most important reactions to the dayglow production of $O(^1S)$. The results of the study are given in the next section. The continuation of the work on this project is discussed in the last section. Also, work that may be continued from parts of this project that were only briefly started here will be discussed.

6.1 Results

The photochemical model developed here is able to reproduce the observed daytime 5577Å thermospheric emission. Five source reactions are need in the modeling of the emission profile. The reactions needed for the model are photoelectron impact on atomic oxygen, dissociative recombination of O_2^+, quenching of $N_2(A^3\Sigma_u^+)$ by atomic oxygen, ion-exchange reaction between O_2^+ and atomic nitrogen, and photo-dissociation of O_2 which becomes more important below the peak. The ion-exchange reaction between O_2^+ and atomic nitrogen is not a major reaction needed to explain the 5577Å emission profile but does become important in the twilight period.

The impact of photoelectrons on atomic oxygen is the primary source of 5577Å dayglow emission in the thermosphere. The reaction produces the majority of the $O(^1S)$ even at the peak in the emission layer. As can be seen from Figure 5.4, the observed profiles of 5577Å emission is best reproduced by the impact cross sections of Henry *et al.* (1969). The magnitude of the impact cross sections determined by this study are also in good agreement with the latest cross sections determined by Berrington and Burke (1991, Personal Communication) and about a factor of two smaller than the cross sections of Shyn *et al.* (1986) [See Figure 1.3].

The quenching of $N_2(A)$ by atomic oxygen is an important source of the 5577Å emission at the peak in the layer. While the photoelectron impact is still the largest contributor, this reaction is needed to adequately fill in the peak in the emission layer. This reaction was studied for changes in the contribution to the volume emission from varying the branching ratio for $O(^1S)$ production. The value of 2.75×10^{-11} cm^3 s^{-1} for the total rate

coefficient determined in Chapter 4 agreed well with the values of *Piper* (1982) and Thomas and Kaufman (1985) was used in this study. The effective branching ratio for this reaction determined by this study of 5577Å dayglow observations varies from approximately 0.65 to about 0.75. The effective branching ratio for the quenching of $N_2(A)$ determined by these simulations tend to support the results from Piper (1982) and De Souza *et. al* (1985) of 0.75±13 and do not agree with those of earlier studies in auroral cases.

The importance of the vibrational population distribution was demonstrated. The differences in the vibrational population may account for the discrepancy between the branching ratios determined by aeronomical studies and by laboratory experiment. While the vibrational population in laboratory studies is restricted to a single level, the dayglow will have the population distributed over all vibrational levels. This distribution plays an important part in determining the effective branching ratio for the quenching reaction. Since the rate coefficient has been shown to change with vibrational level, the contribution of each level will depend on the fraction of the population it contains.

The branching ratio determined by Piper (1982) was for the entire population of the $N_2(A)$ in either the $\upsilon = 0$ or the $\upsilon = 1$ level. The effective branching ratio from this study for the $O(^1S)$ dayglow agrees well with the values of Piper (1982). In the dayglow, the vibrational population of $N_2(A)$ is not limited to the lowest two levels as was shown in Figure 5.5. By allowing for the distribution of the vibrational population of the $N_2(A)$ state and using the the branching ratio and rate coefficient for the first two vibrational levels from Piper (1982), it was shown that the higher vibrational levels are

needed for about 50% of the production of $O(^1S)$. This points to the need to extend the study of the $N_2(A)$ state to higher vibrational levels.

The production of $O(^1S)$ in the dayglow from these two reactions determined here are not greatly affected by the other reactions in the photochemical model. The effects of changing the reaction rate of Reaction [3.12] and the branching ratio of dissociative recombination of O_2 (Reaction [3.3]) were investigated in Section 5.3.2. This study showed that the variations of these reactions over those given in the literature will not significantly affect the results for the major reactions. The impact cross section does not shift a significant amount toward those determined in the laboratory. Nor does the branching ratio for the energy transfer reaction agree with the values determined in the auroral studies.

The possible errors due to the determination of the atomic oxygen densities by the satellite measurements was also investigated for the effects on the determined parameters. The possible changes due to errors in the atomic oxygen density was tested by assuming an error of ±30%. Increasing the oxygen density is equivalent to measuring the density low, which is the most likely case due to surface recombination. This would make the best fit impact cross sections even smaller, about 0.75 times the theoretical cross sections. This makes the determined branching ratio even larger to get agreement with the peak in the emission layer. If the oxygen density was measured high by 30%, the impact cross section and the branching ratio will be smaller but the change is not sufficient to change the overall results.

The results of applying the 5577Å model to the twilight period demonstrated that the model is able to reproduce general features. The processes in the twilight are difficult to model and to observe so

comparisons are not exact or as clear as in the dayglow. The 5577Å model developed here is able to reasonably reproduce the twilight emission but needs refinining. The ability of the model to follow the changing twilight conditions was shown but also points to the need for improvment in inversion methods for use in the twilight and in the model.

The results of this work tend to support a set of values for the various reactions that were determined in several separate studies. It is not necessarily the final solution to the question of 5577Å emission in the atmosphere. The efforts here provide a basis for the starting point of other investigations that may give these answers. These future investigations are the topic of the final section of this chapter.

6.2 Further Work

The questions about the sources for the greenline emission in the F-region have not been completly answered. The future work on the 5577Å emission based on this study falls into two groups, the work in the dayglow itself and work to expand the greenline into the twilight and auroral regions to build a complete model. Other possible research topics on related subjects will also be presented.

In the dayglow, the major work should concentrate on the two most important reactions as discussed here. For the impact of photoelectrons on atomic oxygen, the discrepancy between the laboratory and the value from this study and theoretical calculations needs to be addressed with detailed laboratory investigations. Improved experimental techniques may help to solve this puzzle. The same can be done for the energy transfer reaction. The rate coefficients and branching ratios need to be determined by

vibrational level past v=0,1 as done by Piper *et al.*, (1982). This can best be accomplished in the laboratory with new techniques that have recently been developed.

Once these two major reactions are more fully understood, a better determination of the contribution by the minor sources can be studied. This is especially true for the ion atom exchange reaction between O_2^+ and atomic nitrogen which is important in the twilight but not well known. The model for the 5577Å can be extended into the auroral regions with modification to the photoelectron model. This can be done as the model is currently used, but improved results from experiments will make the model of the aurora more complete since the same reactions as the dayglow are thought to be important in the aurora. When these steps are completed, the model for $O(^1S)$ emission will be a global model and three dimensional maps of the 5577Å emission can be constructed.

Other possible research based on this study are the continued expansion of the photochemical model to other emissions which has already been started and expand the use of the vibrational population model for molecular nitrogen. The photochemical model can be converted to calculate other emissions based on the same profiles as the 5577Å greenline. The nitrogen vibrational population model contains many transitions that were not used in this study but others have began using them for various studies. The triplet model used here has a companion model for the low lying singlet transions of molecular nitrogen, this model can be converted to the dayglow also. These two models will then be able to describe the complete set of nitrogen transitions in the atmosphere.

APPENDICES

APPENDIX A

SOLAR FLUX MODEL

The subroutine SSFLUX listed here calculates the solar EUV and FUV flux in the range 1 to 1750 Å for a specified level of solar activity. The calling routine supplies a scaling switch, ISCALE; the daily 10.7 cm flux, F107; its 81-day centered average, F107A; and the Hydrogen Lyman-alpha flux, FLYA. The subroutine returns the longwave and shortwave boundaries, WAVE1 and WAVE2, of the wavelength bins (Å), and the solar flux in each bin SFLUX (photons cm^{-2} s^{-1}). The dimension of these arrays must also be supplied by the calling routine (currently 59). One of four methods are used, depending on the value of ISCALE, described as follows.

If ISCALE=0 the flux is scaled using parameterization methods based on F107 and F107A. For ionizing EUV, Hinteregger's contrast ratio method (Hinterregger *et al.*, 1981) is used, based on the Torr and Torr (1985) bin structure for reference spectrum SC#21REFW. The 1026Å (H Lyβ) and 335Å (FeXVI) enhancement ratios are calculated from Hinteregger's formula, using the coefficients which reduce to the reference values at F107=75.4, F107A=71.5. The 'best fit' coefficients are not used as they produce some negative values at low solar activity, but remain in an unused data statement for reference. The rest of the spectrum is then

calculated from these key emissions using Hinteregger's method. Scaling factors are calculated from contrast ratios in the original spectrum data file. For FUV in the 1050-1350Å region, 50Å interval averaging is done based on SC#21REFW, and scaling factors also calculated. For Hydrogen Lyman alpha at 1216Å, which is treated separately as an individual line, the correlation relationship derived from SME data by Tobiska and Barth (1989) is used. For the Schumann-Runge continuum, the Torr *et al.* (1980) 50Å bin structure is used but the coefficients have been adjusted to reflect SME and LASP rocket data (Rottman, 1981 and 1988; Mount and Rottman, 1983 and 1985).

If ISCALE=1 linear interpolation between high and low activity spectra is done, based on F107 alone, and assuming the low activity spectrum corresponds to F107=68 and the high activitiy spectrum to F107=243. The Hinteregger SC#21REFW and F79050 spectra as binned by Torr & Torr (1985) are used for ionizing EUV. For the 1050-1350Å region, the SC#21REFW spectrum averaged into 50Å intervals is used for low solar activity; the high activity spectrum was obtained by scaling this spectrum using the contrast ratios. For the Hydrogen Lyman alpha and the Schumann-Runge continuum, linear interpolation amounts to the same thing as the aformentioned parameterization.

If ISCALE=2, the flux is scaled according to the Tobiska and Barth method (Tobiska and Barth, 1990). The procedure involves using 10.7 cm flux, F107, and the Hydrogen Lyman alpha flux, FLYA, considered as coronal/transition region and chromospheric emissions, respectively. Chromospheric fluxes are calculated from a linear correlation relationship with FLYA. Coronal fluxes are calculated from a combination of F107 and a "modeled" F107 based on FLYA. When no value for FLYA is supplied, it

is calculated from F107 using the SME-derived formula as above, and then used to scale the other fluxes. The coronal and chromospheric scaled fluxes are then summed to obtain the solar flux. The subroutine takes a value of FLYA in photons cm^{-2} s^{-1}, but converts it to ergs cm^{-2} s^{-1} for internal computations. Since the wavelength bins used here extend past those used by Tobiska & Barth for both long and short wavelengths, the linear interpolation method is used for those bins not covered by the Tobiska & Barth model.

If ISCALE=3, the Woods and Rottman rocket spectrum for 10 November, 1988 is employed from 300-1050Å. The entire spectrum of the solar flux is calculated by the contrast ratio method of Hinteregger discussed above. The bins of the woods and Rottman spectrun are then inserted in the calculated spectrum.

The EUV fluxes between 50 and 250Å are normalized upwards (after Richards and Torr, 1984) for both the linear interpolation and the contrast ratio method. The normalization coefficient is 2 at F107=68 and reduces linearly to 1 at F107=243. None of the above models extends shortwards of 18A, so from 1-18 Å an amalgam of sources are used to derive an estimated flux, e.g., DeJager, 1964; Smith & Gottlieb, 1974; Manson, 1977; Kreplin *et al.*,1977; Horan & Kreplin, 1981; Wagner, 1988.

Model Program Listing

```
C Definitions:
C ISCALE  =0 for Hinteregger contrast ratio method,
C       =1 for Hinteregger linear interpolation,
C       =2 for Tobiska and Barth method
C F107    daily 10.7 cm flux (1.E-22 W m-2 Hz-1)
C F107A   81-day centered average 10.7 cm flux (")
C FLYA    H Lyman-alpha flux (photons cm-2 s-1)
C WAVE1   longwave bound of spectral intervals (Angstroms)
C WAVE2   shortwave bound of intervals (= WAVE1 for indiv. lines)
C SFLUX   scaled solar flux returned by subroutine (photons cm-2 s-1)
C LMAX    dimension of above arrays, currently = 59
C WAVEL   = WAVE1
C WAVES   = WAVE2
C RFLUX   low solar activity reference flux
C XFLUX   high solar activity flux
C SCALE1  scaling factors for H LyB-keyed chromospheric emissions
C SCALE2  scaling factors for FeXVI-keyed coronal emissions
C LM      dimension of above arrays, currently = 59
C SRA      'A' value for S-R continuum scaling formula
C SRB      'B' value for S-R continuum scaling formula
C B1      fit coefficients for H LyB
C B2      fit coefficients for FeXVI
C R1      enhancement ratio for H LyB
C R2      enhancement ratio for FeXVI
C SFNORM  normalization factor for scaling flux shortwards of 250A
C CHINT   intercept from chromospheric Ly-a linear correlation
C CHSLP   slope from chromospheric Ly-a linear correlation
C COINT   intercept from coronal F10.7 linear correlation
C COSLP   slope from coronal F10.7 linear correlation
C W1      weighting factor for coronal emissions
C W2      weighting factor for coronal emissions
C WCHR    weighting factor for chromospheric emissions
C WAVEAV  average wvl. for converting T&B flux from ergs to photons
C FLYERG  value of Lyman-a flux in erg cm-2 s-1
C F107MD  modeled F107 value (uses Ly-a in photons)
C FLUXCH  scaled chromospheric flux value based on Ly-a (in ergs)
C FLUXCO  scaled coronal flux value based on F107
C
      SUBROUTINE SSFLUX(ISCALE,F107,F107A,FLYA,WAVE1,WAVE2,SFLUX,LMAX)
C
     PARAMETER (LM=59)
C
      DIMENSION WAVE1(LMAX), WAVE2(LMAX), SFLUX(LMAX),
     +       WAVEL(LM), WAVES(LM), RFLUX(LM), XFLUX(LM),
     +      SCALE1(LM), SCALE2(LM), SRA(8), SRB(8), B1(3), B2(3),
     +       CHINT(LM), CHSLP(LM), COINT(LM), COSLP(LM), W1(LM),
     +       W2(LM), WCHR(LM), FLUXCH(LM), FLUXCO(LM), WAVEAV(LM),
     +      WAR1(LM)
C
C new B's:
```

```
      DATA B1/1.0, 0.0138, 0.005/, B2/1.0, 0.59425, 0.3811/
C
C old B's, commented out:
C     DATA B1/1.31, 0.01106, 0.00492/, B2/-6.618, 0.66159, 0.38319/
C
      DATA WAVEL/ 1750.00, 1700.00, 1650.00, 1600.00, 1550.00, 1500.00,
     +        1450.00, 1400.00, 1350.00, 1300.00, 1250.00, 1215.67,
     +        1200.00, 1150.00, 1100.00, 1050.00, 1031.91, 1025.72,
     +        1000.00, 977.02, 950.00, 900.00, 850.00, 800.00,
     +        789.36, 770.41, 765.15, 750.00, 703.31, 700.00,
     +        650.00, 629.73, 609.76, 600.00, 584.33, 554.37,
     +        550.00, 500.00, 465.22, 450.00, 400.00, 368.07,
     +        350.00, 303.78, 303.31, 300.00, 284.15, 256.30,
     +        250.00, 200.00, 150.00, 100.00,  50.00,  32.00,
     +         23.00,  16.00,  8.00,  4.00,  2.00/
      DATA WAVES/ 1700.00, 1650.00, 1600.00, 1550.00, 1500.00, 1450.00,
     +        1400.00, 1350.00, 1300.00, 1250.00, 1200.00, 1215.67,
     +        1150.00, 1100.00, 1050.00, 1000.00, 1031.91, 1025.72,
     +        950.00, 977.02, 900.00, 850.00, 800.00, 750.00,
     +        789.36, 770.41, 765.15, 700.00, 703.31, 650.00,
     +        600.00, 629.73, 609.76, 550.00, 584.33, 554.37,
     +        500.00, 450.00, 465.22, 400.00, 350.00, 368.07,
     +        300.00, 303.78, 303.31, 250.00, 284.15, 256.30,
     +        200.00, 150.00, 100.00,  50.00,  32.00,  23.00,
     +         16.00,  8.00,  4.00,  2.00,  1.00/
      DATA WAR1/   0.00,   0.00,   0.00,   0.00,   0.00,   0.00,
     +          0.00,   0.00,   0.00,   0.00,   0.00,   0.00,
     +          0.00,   0.00,   3.81,   5.00,   5.34,   6.90,
     +          2.44,   7.33,   8.62,   9.60,   4.54,   1.58,
     +          1.28,   0.53,   0.38,   0.34,   0.61,   0.55,
     +          0.38,   2.37,   1.07,   0.41,   1.74,   0.61,
     +          1.67,   0.95,   0.23,   0.58,   1.14,   0.86,
     +          3.32,   7.24,   1.31,   0.00,   0.00,   0.00,
     +          0.00,   0.00,   0.00,   0.00,   0.00,   0.00,
     +          0.00,   0.00,   0.00,   0.00,   0.00/
      DATA RFLUX/ 370.45, 203.69,  96.00,  69.71,  50.70,  26.67,
     +          17.21,   8.26,  12.86,   4.10,   5.20, 272.00,
     +          2.78,   0.70,   3.07,   3.64,   3.18,   4.38,
     +          1.78,   5.96,   4.22,   4.43,   1.93,   0.87,
     +          0.79,   0.24,   0.20,   0.17,   0.39,   0.22,
     +          0.17,   1.50,   0.45,   0.48,   1.58,   0.80,
     +          0.51,   0.31,   0.18,   0.39,   0.21,   0.74,
     +          0.87,   6.00,   0.24,   0.84,   0.10,   0.27,
     +          0.92,   1.84,   0.13,   0.38, 0.0215, 0.0067,
     +          1.E-3,  2.E-3,  1.E-5,  5.E-8,  1.E-10/
      DATA XFLUX/ 400.00, 226.00, 107.50,  81.20,  58.70,  29.30,
     +          19.40,   9.90,  30.70,  11.20,  12.00, 438.00,
     +          6.50,   1.60,   6.40,   8.66,   9.04,  13.12,
     +          4.42,  13.18,  12.03,  13.29,   5.01,   2.18,
     +          1.59,   0.67,   0.43,   0.43,   0.72,   0.46,
     +          0.48,   3.02,   1.46,   1.02,   4.86,   1.59,
     +          1.57,   1.67,   0.36,   0.99,   2.20,   1.39,
     +          5.63,  11.28,   2.50,   4.14,   3.16,   0.59,
     +          3.70,   4.80,   0.34,   1.15,   0.18,   0.08,
```

```
+        2.5E-2,  5.E-2,  8.E-4,  3.E-5,  5.E-7/
 DATA SCALE1/12573.0, 9220.0, 4820.0, 4694.0, 3227.0, 1090.0,
+        922.00, 671.00, 8009.80, 3186.34, 3033.78, 47555.,
+        1692.09, 405.95, 1516.20, 2731.70, 3314.57, 4375.00,
+        1316.91, 3621.91, 3908.56, 4432.54, 1541.21, 531.73,
+        364.83,  0.00, 116.00, 129.41, 162.48,  94.07,
+        41.29, 709.50,  0.00, 268.47, 1561.05, 367.64,
+        290.06, 184.36,  0.00,  86.15,  7.50,  0.00,
+        0.00, 2220.00,  0.00,  61.00,  0.00,  86.95,
+        206.00, 135.89,  60.35, 157.12,  7.06,  0.75,
+        0.00,  0.00,  0.00,  0.00,  0.00/
 DATA SCALE2/ 0.00,  0.00,  0.00,  0.00,  0.00,  0.00,
+        0.00,  0.00,  0.00,  0.00,  0.00,  0.00,
+        0.00,  0.00,  0.00,  0.00,  0.00,  0.00,
+        0.00,  0.00,  0.00,  0.00,  0.00,  0.00,
+        0.00,  5.34,  0.00,  0.00,  0.00,  0.54,
+        3.30,  0.00,  12.60,  0.00,  0.00,  0.00,
+        5.34,  11.63,  2.28,  5.56,  24.93,  8.16,
+        60.69,  0.00,  28.20,  45.90,  40.80,  1.27,
+        35.47,  42.80,  1.12,  6.19,  1.26,  0.69,
+        0.23,  0.46, 7.6E-3, 2.9E-4, 4.8E-6/
 DATA SRA/  0.169,  0.128,  0.066,  0.064,  0.044,  0.015,
+        0.013,  0.009/
 DATA SRB/  358.5,  195.3,  91.5,  65.6,  48.0,  25.7,
+        16.3,  7.72/
 DATA CHINT/0.00000E+00, 0.00000E+00, 0.00000E+00, 0.00000E+00,
+       0.00000E+00, 0.00000E+00, 0.00000E+00, 0.00000E+00,
+       0.00000E+00, 0.00000E+00, 0.00000E+00, 0.00000E+00,
+       0.00000E+00, 0.00000E+00, 0.00000E+00, 0.18223E-01,
+       -0.14763E-02, 0.13765E-02, 0.10044E-01, 0.48687E-01,
+       0.79848E-02, 0.16334E-02, 0.99890E-02, 0.12362E-01,
+       0.38317E-02, 0.00000E+00, 0.22214E-02, 0.87883E-03,
+       0.65437E-02, 0.20197E-02, 0.11897E-02, 0.25303E-01,
+       0.00000E+00, 0.69859E-02, 0.15090E-02, 0.15679E-01,
+       0.71813E-02, 0.18873E-02, 0.00000E+00, 0.44750E-02,
+       0.43206E-03, 0.00000E+00, 0.00000E+00, 0.24958E+00,
+       0.00000E+00, 0.17434E-03, 0.00000E+00, 0.11585E-01,
+       0.11532E-01, 0.98362E-02, 0.24461E-02, 0.91696E-02,
+       0.86457E-03, 0.00000E+00, 0.00000E+00, 0.00000E+00,
+       0.00000E+00, 0.00000E+00, 0.00000E+00/
 DATA CHSLP/0.00000E+00, 0.00000E+00, 0.00000E+00, 0.00000E+00,
+       0.00000E+00, 0.00000E+00, 0.00000E+00, 0.00000E+00,
+       0.00000E+00, 0.00000E+00, 0.00000E+00, 0.00000E+00,
+       0.00000E+00, 0.00000E+00, 0.00000E+00, 0.13097E-01,
+       0.15670E-01, 0.20808E-01, 0.66142E-02, 0.18084E-01,
+       0.20603E-01, 0.24699E-01, 0.91077E-02, 0.49109E-02,
+       0.79057E-03, 0.00000E+00, 0.73979E-03, 0.83584E-03,
+       0.11269E-02, 0.68429E-03, 0.34588E-03, 0.54965E-02,
+       0.00000E+00, 0.23091E-02, 0.13033E-01, 0.32354E-02,
+       0.27878E-02, 0.17867E-02, 0.00000E+00, 0.10032E-02,
+       0.96861E-04, 0.00000E+00, 0.00000E+00, 0.35650E-01,
+       0.00000E+00, 0.96698E-03, 0.00000E+00, 0.16549E-02,
+       0.44742E-02, 0.38025E-02, 0.23655E-02, 0.10185E-01,
+       0.96072E-03, 0.00000E+00, 0.00000E+00, 0.00000E+00,
```

```
+       0.00000E+00, 0.00000E+00, 0.00000E+00/
 DATA COINT/0.00000E+00, 0.00000E+00, 0.00000E+00, 0.00000E+00,
+       0.00000E+00, 0.00000E+00, 0.00000E+00, 0.00000E+00,
+       0.00000E+00, 0.00000E+00, 0.00000E+00, 0.00000E+00,
+       0.00000E+00, 0.00000E+00, 0.00000E+00, 0.00000E+00,
+       0.00000E+00, 0.00000E+00, 0.00000E+00, 0.00000E+00,
+       0.00000E+00, 0.00000E+00, 0.00000E+00, 0.74083E-03,
+       0.00000E+00, 0.13995E-02, 0.00000E+00, 0.00000E+00,
+       0.00000E+00, 0.13215E-02,-0.52657E-03, 0.00000E+00,
+       0.17231E-03, 0.00000E+00, 0.00000E+00, 0.00000E+00,
+       -0.57828E-02,-0.14201E-01, 0.44921E-02, 0.81510E-03,
+       -0.38050E-01, 0.25868E-01,-0.74031E-01, 0.00000E+00,
+       -0.49781E-01,-0.65154E-01,-0.93662E-01, 0.00000E+00,
+       -0.59300E-01, 0.12726E-01, 0.32644E-02,-0.64290E-02,
+       -0.17720E-01,-0.17972E-01, 0.00000E+00, 0.00000E+00,
+       0.00000E+00, 0.00000E+00, 0.00000E+00/
 DATA COSLP/0.00000E+00, 0.00000E+00, 0.00000E+00, 0.00000E+00,
+       0.00000E+00, 0.00000E+00, 0.00000E+00, 0.00000E+00,
+       0.00000E+00, 0.00000E+00, 0.00000E+00, 0.00000E+00,
+       0.00000E+00, 0.00000E+00, 0.00000E+00, 0.00000E+00,
+       0.00000E+00, 0.00000E+00, 0.00000E+00, 0.00000E+00,
+       0.00000E+00, 0.00000E+00, 0.00000E+00, 0.35613E-04,
+       0.00000E+00, 0.67265E-04, 0.00000E+00, 0.00000E+00,
+       0.00000E+00, 0.71233E-05, 0.45645E-04, 0.00000E+00,
+       0.20078E-03, 0.00000E+00, 0.00000E+00, 0.00000E+00,
+       0.98801E-04, 0.23753E-03, 0.45868E-04, 0.12901E-03,
+       0.64519E-03, 0.20540E-03, 0.17408E-02, 0.00000E+00,
+       0.90311E-03, 0.17093E-02, 0.13948E-02, 0.00000E+00,
+       0.15455E-02, 0.23847E-02, 0.87499E-04, 0.79916E-03,
+       0.34005E-03, 0.31881E-03, 0.00000E+00, 0.00000E+00,
+       0.00000E+00, 0.00000E+00, 0.00000E+00/
 DATA W1/  0.00000, 0.00000, 0.00000, 0.00000, 0.00000, 0.00000,
+       0.00000, 0.00000, 0.00000, 0.00000, 0.00000, 0.00000,
+       0.00000, 0.00000, 0.00000, 0.00000, 0.00000, 0.00000,
+       0.00000, 0.00000, 0.00000, 0.00000, 0.00000, 0.00000,
+       0.00000, 0.00000, 0.00000, 0.00000, 0.00000, 2.22570,
+       5.40850, 0.00000, 0.00000, 0.00000, 0.00000, 0.00000,
+       1.23810, 0.29122, 0.00000, 0.24172, 0.02037, 0.00000,
+       0.00000, 0.00000, 0.00000, 0.18000, 0.00000, 0.00000,
+       0.33750, 1.12500, 1.12500, 0.80000, 0.24000, 0.00000,
+       0.00000, 0.00000, 0.00000, 0.00000, 0.00000/
 DATA W2/  0.00000, 0.00000, 0.00000, 0.00000, 0.00000, 0.00000,
+       0.00000, 0.00000, 0.00000, 0.00000, 0.00000, 0.00000,
+       0.00000, 0.00000, 0.00000, 0.00000, 0.00000, 0.00000,
+       0.00000, 0.00000, 0.00000, 0.00000, 0.00000, 0.00000,
+       0.00000, 1.80579, 0.00000, 0.00000, 0.00000, 0.74191,
+       3.60570, 0.00000, 0.42239, 0.00C00, 0.00000, 0.00000,
+       0.56275, 0.65524, 1.04710, 0.44890, 1.20180, 0.01272,
+       1.13808, 0.00000, 1.17450, 2.07000, 1.05000, 0.00000,
+       1.91250, 1.12500, 1.12500, 1.20000, 1.76000, 2.00000,
+       0.00000, 0.00000, 0.00000, 0.00000, 0.00000/
 DATA WCHR/ 0.00000, 0.00000, 0.00000, 0.00000, 0.00000, 0.00000,
+       0.00000, 0.00000, 0.00000, 0.00000, 0.00000, 0.00000,
+       0.00000, 0.00000, 0.00000, 0.04970, 2.06310, 1.07370,
```

```
     +       0.98260, 1.00000, 1.51570, 1.54410, 1.91970, 0.00000,
     +       10.9300, 1.20380, 2.81790, 2.84590, 0.85290, 2.47300,
     +       1.20190, 0.64480, 0.52800, 1.65450, 0.52580, 0.58410,
     +       2.25100, 0.72810, 0.80550, 3.45310, 1.10184, 0.02540,
     +       1.72600, 0.58730, 1.00000, 1.00000, 1.00000, 1.00000,
     +       1.00000, 1.00000, 1.00000, 1.00000, 1.00000, 1.00000,
     +       0.00000, 0.00000, 0.00000, 0.00000, 0.00000/
      DATA WAVEAV/ 0.000,   0.000,   0.000,   0.000,
     +        0.000,  0.000,  0.000,  0.000,
     +        0.000,  0.000,  0.000,  0.000,
     +        0.000,  0.000,  0.000, 1025.500,
     +       1031.900, 1025.700, 975.500, 977.020,
     +       925.500, 875.500, 825.500, 775.005,
     +       787.710, 770.410, 765.150, 725.500,
     +       703.360, 675.150, 626.930, 629.730,
     +       609.760, 576.985, 584.330, 554.370,
     +       525.000, 476.185, 465.220, 418.920,
     +       377.915, 368.070, 326.580, 303.780,
     +       303.310, 275.300, 284.150, 256.320,
     +       224.600, 174.340, 124.470,  75.255,
     +        39.620,  24.070,   0.000,   0.000,
     +        0.000,   0.000,   0.000/
C
C Hinteregger Method:
C
      IF (ISCALE .EQ. 0 .OR. ISCALE .GE. 3) THEN
       R1 =  B1(1) + B1(2)*(F107A-71.5) + B1(3)*(F107-F107A+3.9)
       R2 =  B2(1) + B2(2)*(F107A-71.5) + B2(3)*(F107-F107A+3.9)
       DO 100 L=1,LMAX
       IF (L .LT. 9) THEN
        SFLUX(L) = SRA(L) * F107 + SRB(L)
      ELSE
        IF (L .EQ. 12) THEN
         SFLUX(L) = (F107 + 218.88) / 1.05453
       ELSE
          SFLUX(L) = (RFLUX(L) + ((R1-1.)*SCALE1(L)
     +                + (R2-1.)*SCALE2(L)) / 1000.)
       ENDIF
      ENDIF
  100  CONTINUE
     ELSE
C
C Linear Interpolation Method:
C
       FRAT = (F107-68.) / (243.-68.)
       DO 200 L=1,LMAX
        SFLUX(L) = RFLUX(L) + (XFLUX(L)-RFLUX(L)) * FRAT
  200  CONTINUE
     ENDIF
C
C Normalize flux from 250 - 16 A (after Richards & Torr):
C
      SFNORM = 2. - 1. * (F107-68.) / (243.-68.)
      IF (SFNORM .LT. 1.0) SFNORM = 1.0
```

```
      DO 300 L=1,LMAX
        IF (WAVEL(L) .LT. 251. .AND. WAVES(L) .GT. 15.)
     +   SFLUX(L) = SFLUX(L) * SFNORM
  300 CONTINUE
C
C Tobiska and Barth Method:
C
      IF (ISCALE.EQ.2) THEN
        IF (FLYA.LT.1.) THEN
        FLYA = (F107 + 218.88) / 1.05453E-9
        F107MD = F107
      ELSE
        F107MD = (1.05453E-9*FLYA) - 218.88
        SFLUX(12) = FLYA/1.E9
      ENDIF
      FLYERG = FLYA*12398.*1.6022E-12/1215.67
      DO 500 J = 16,54
         FLUXCH(J)=CHINT(J)+(CHSLP(J)*WCHR(J)*FLYERG)
         FLUXCO(J)=COINT(J)+COSLP(J)*(W1(J)*F107MD+W2(J)*F107)
       SFLUX(J) = FLUXCH(J) + FLUXCO(J)
       SFLUX(J) = SFLUX(J)*WAVEAV(J)/(12398.*1.6022E-12*1.E9)
  500   CONTINUE

      ENDIF
C
C Woods and Rottman (10 Nov. 1988) spectrum:
C
      IF (ISCALE .EQ. 3) THEN
       DO 550 L=15,45
        SFLUX(L) = WAR1(L)
  550   CONTINUE
      ENDIF
C
C Convert from gigaphotons to photons:
C
      DO 600 L=1,LMAX
       WAVE1(L) = WAVEL(L)
       WAVE2(L) = WAVES(L)
      IF (SFLUX(L) .LT. 0.0) SFLUX(L) = 0.0
      SFLUX(L) = SFLUX(L) * 1.E9
  600 CONTINUE
C
      RETURN
      END
```

APPENDIX B

INTERNATIONAL REFERENCE IONOSPHERE

The Internatiional Reference Ionosphere (IRI) model was described briefly in Chapter 3. There the use of the Booker approach of building profiles was noted (Booker, 1977) along with the use of the Epstein functions to construct layers. This apendix will describe these topics in further details.

The IRI model uses the first three Epstein functions to represent altitudnal variations as well as special variations in latitude and diurnal features. These three functions are defined as:

$$EPS_{-1}(h;HX,SC) = \ln\left(1+e^{x}\right) \qquad [B.1]$$

$$EPS_{0}(h;HX,SC) = 1/\left(1+e^{-x}\right) \qquad [B.2]$$

$$EPS_{1}(h;HX,SC) = e^{x}/\left(1+e^{x}\right)^{2} \qquad [B.3]$$

with:

$$x = \frac{h - HX}{SC} \qquad [B.4]$$

and

$$EPS_{i+1} = \frac{d}{dx} EPS_i \quad . \qquad [B.5]$$

EPS-1 describes a transition, EPS0 a step, and EPS1 a peak at h=HX with width SC. These functions are used in combinations to construct the profiles of the model. The step function can be used as a filter function taking a value of 0 below a certain altitude and a value of 1 above. Rawer (1987) explained how three such filter functions can be used to construct a jiont analytical representation of the electron density profile. The three Epstein functions are shown in Figure B.1.

The Booker function is a single analytical function that is capable of representing simultaneously the principle features of the D-, E-, F1-, and F2-Regions of the ionosphere. In the Booker method (Booker, 1977), several subsections were used to construct a skeleton profile where each subsection is approximated by a straight line. The derivative of this profile function can be representd by a sum of Epstein functions, stepping from subsection to subsection. Integrating from a height h_0 to height h gives the Booker function,

$$y(h) - y(h_0) = (h - h_0)Dy_1 + \sum_{j=1}^{M} (Dy_{j+1} - Dy_j) SC_j \Delta EPS \qquad [B.6]$$

where:

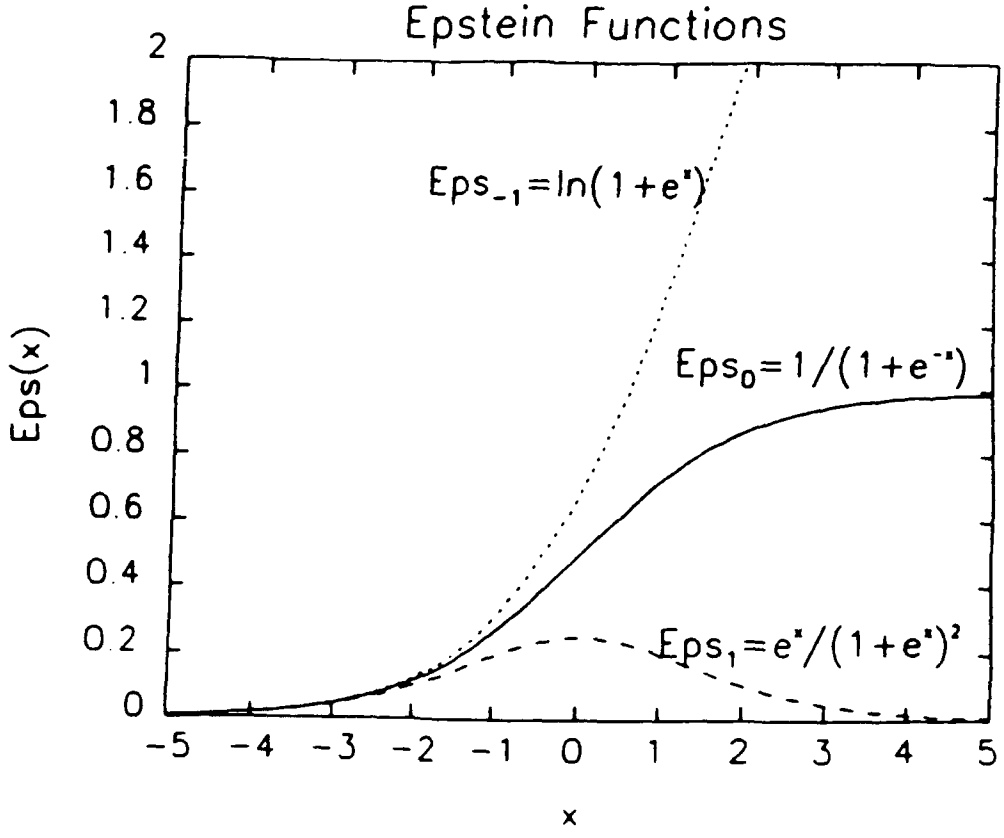

Figure B.1 Plot of the Epstein Functions used in the International Reference Ionosphere model (from Bilitza, 1990a).

$$\Delta EPS = EPS_{-1}(h;HX_j,SC_j) - EPS_{-1}(h_0;HX_j,SC_j) \qquad [B.7]$$

and

M = the number of subsections

Dy = the constant gradients of y in the subsections

HX = the subsection boundaries

SC = the thickness of the transition zones between the subsections.

The selection of SC is critical to the sucess of the function representing an actual profile. If SC is small, the model profile will closly reproduce the skeleton profile. If it is too large, there can be interference between adjacent layers. The best results are achieved when

$$\frac{D}{20} \le SC \le \frac{D}{10}, \qquad [B.8]$$

where D is the height range of the smaller of the two subsections. Also, the choice of h_0 should be in a region where the skeleton and the actual profile are close, ie., outside of any highly variable transitions. These constraint make it difficult to represent layer profiles.

Layers are constructed by using the Epstein transition functions as introduced by Rawer (1984). By combining the Epstein function with a linear term, the layer function is,

$$L(h;h_m,HX,SC) = \Delta EPS - (h - h_m)EPS_0(h_m;HX,SC)/SC \qquad [B.9]$$

where

$$\Delta EPS = EPS_{-1}(h;HX,SC) - EPS_{-1}(h_m;HX,SC). \qquad [B.10]$$

The layer peaks at $h=h_m$. Figure B.2 shows examples of layers for a variety of values of HX and SC.

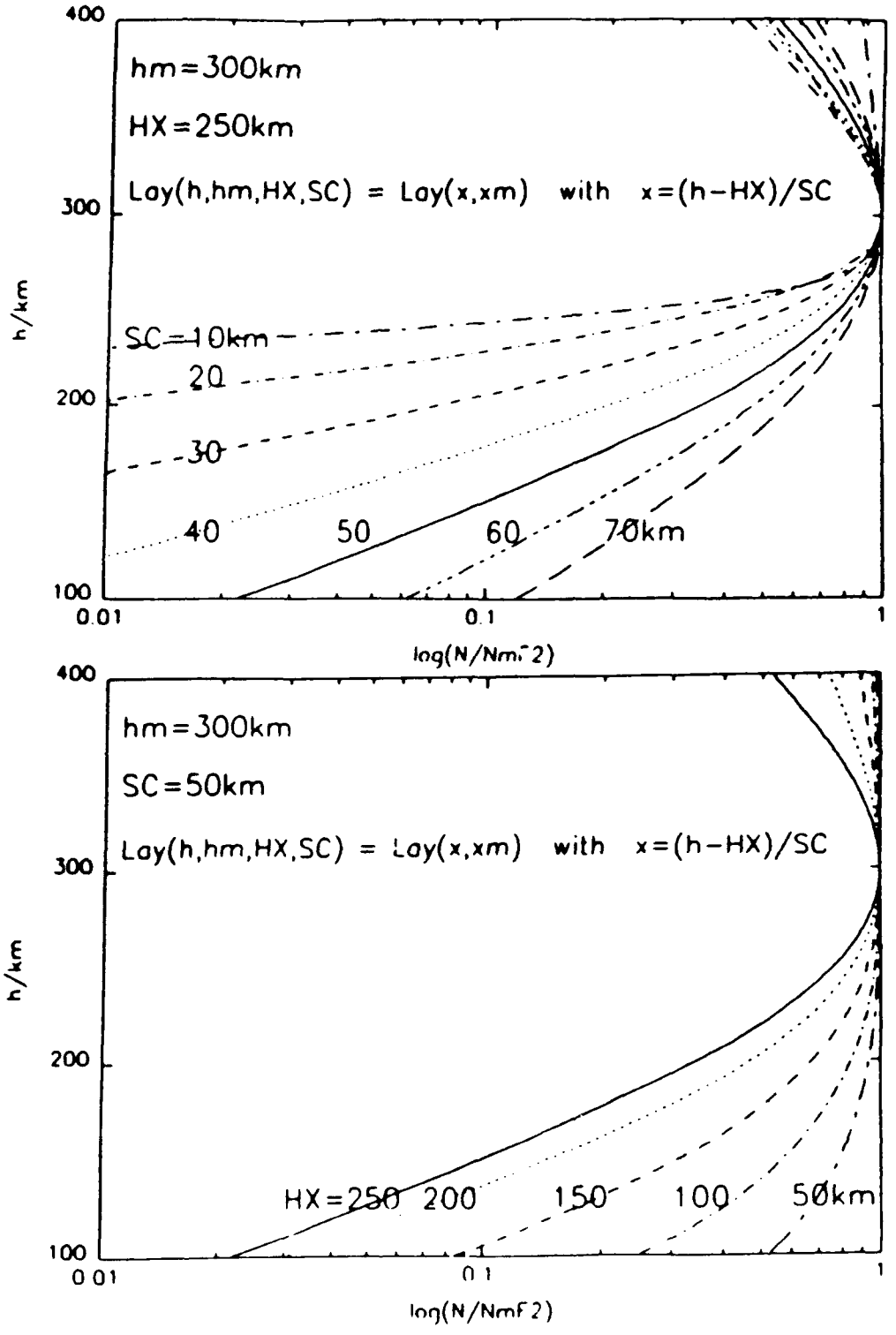

Figure B.2 Examples of the Layer Function used in the International Reference Ionosphere model for a variety of HX and SC values (from Bilitza, 1990a).

APPENDIX C

PHOTOELECTRON MODEL

The model of the photoelectons used in this work is essentially the sam as described in Solomon (1987), Solomon *et al.* (1988), and Solomon and Abreu (1989). Here, a discription of the electron transport equation is given and the impact cross sections for excitation and ionization are listed. The model is discussed in general terms in Chapter 3.

The electron transport calculations used in the model use the continuity equations of Banks *et al.* (1974) for the flux along a magnetic field line. Neglecting gravity, parallel electric fields and magnetic field convergence, thes transport equations are,

$$\frac{d\Phi^+}{ds} = \frac{-1}{\mu}\sum_k n_k\left(\sigma_a^k + p_e^k\sigma_e^k\right)\Phi^+ + \frac{1}{\mu}\sum_k n_k p_e^k\sigma_e^k\Phi^- + \frac{q}{2\mu} + \frac{q^+}{\mu}\ , \qquad [C.1]$$

$$\frac{d\Phi^-}{ds} = \frac{-1}{\mu}\sum_k n_k\left(\sigma_a^k + p_e^k\sigma_e^k\right)\Phi^- + \frac{1}{\mu}\sum_k n_k p_e^k\sigma_e^k\Phi^+ + \frac{q}{2\mu} + \frac{q^-}{\mu}\ , \qquad [C.2]$$

where:

$$q^+(E,s) = \sum_k n_k(s)\sum_{}\left\{R\Phi^-(E',s) + [1-R]\Phi^+(E',s)\right\} \qquad [C.3]$$

$$q^{-}(E,s) = \sum_{k} n_k(s) \sum_{j,\varepsilon>E} \left\{ R\Phi^{+}(E',s) + [1-R]\Phi^{-}(E',s) \right\}, \qquad [C.4]$$

where:

$$R = p_{aj}^{k}(E')\sigma_{aj}^{k}(E' \rightarrow E) \qquad [C.5]$$

and

s=distance along a magnetic field line (positive upward)

$\Phi^{+} = \frac{\Phi_u}{\mu}$ =electron flux upward along s

$\Phi^{-} = \frac{\Phi_d}{\mu}$ =electron flux downward along s

$n_k(s)$ =neutral species number density

$p_e^k(E)$ =elastic backscatter probability

$\sigma_e^k(E)$ =elastic cross section

$q(E,s)$ =secondary electron production rate

$q^{\pm}$ =electron production rate due to cascading

p_{aj}^k =inelastic backscatter probability

σ_{aj}^k =inelastic cross section

$\sigma_a^k = \sum_j \sigma_{aj}^k$

j=process index

k=neutral species index

μ=mean pitch angle cosine (assumed 0.577).

The equations are solved by implicit integration with boundary conditions of the fluxes are equal and near zero at the bottom and specified by an incident electron flux at the top.

To calculate the electron fluxes at a given point in the atmosphere, the electrons are binned according to energy in variable sized energy bins.

Starting with the highest energy electrons, the secondary and degraded primary electrons are computed and added to the electron flux at each altitude and each bin of lower energy. The excitation and ionization due to this energy of electrons is also found. Then the next highest energy bin is calculated and the results added to those below it in energy. The degraded fluxes are filled in the neighboring bins by a weighted distribution method similar to that of Swartz (1985) at allow for the differences between electron energy and bin mean energy.

The cross sections for excitation and ionization of the neutral species were calculated using the analytic fit parameters of Green and Stolarski (1972) and Jackman *et al.* (1977). For the excitation parameters of O, N2, and O2, The Green and Stolarski formula was used,

$$\sigma_a(E) = \left(\frac{q_0 A_0}{W^2}\right)\left(1-\frac{W}{E}\right)^{\nu}\left(\frac{W}{E}\right)^{\Omega}, \qquad [C.6]$$

where q_0 = 6.51 x 10^{-14} cm^2 eV^2, W is the excitation energy, E is the incident electron energy, and A_0, ν,Ω are the fitting parameters. The parameters for the excitation cross sections are given in Table C.1.

For ionization of atomic oxygen, the Green and Stolarski formula was used for the cross section and the Opal *et al.* (1971) description of the secondary electron production spectrum was employed,

$$\sigma_i(E_p) = q_0 A \int_I^{(E_p+I)/2} \frac{\varepsilon^{-\Omega}}{W^2}\left(1-\varepsilon^{-\gamma}\right)^{\nu} dW \qquad [C.7]$$

ν	Ω	W	A	γ	State
Atomic Oxygen					
2.00	1.00	1.96	1.00E-2	1.00	^1D
1.00	1.00	4.17	4.20E-3	0.50	^1S
1.00	2.00	9.15	2.30E-2	1.00	^5S
3.00	0.75	9.53	4.65E-2	1.00	^3S
1.00	0.75	13.5	4.30E-2	2.00	$\Sigma\Delta l=0$, $\Delta s=0$
3.00	0.75	14.2	3.67E-1	1.00	$\Sigma\Delta l=1$, $\Delta s=0$
1.00	2.00	14.7	6.94E-1	1.00	$\Sigma\Delta s=1$
Molecular Oxygen					
1.0	3.00	0.98	5.00E-4	3.00	a
1.0	3.00	1.64	5.00E-4	3.00	b
1.0	0.90	4.50	2.00E-2	3.00	A
2.0	0.75	8.40	2.30E-1	1.00	B
3.0	0.75	9.90	8.00E-2	1.00	9.7-12.1 eV
3.0	0.75	13.5	2.77E 0	1.00	Σ Rydbergs
1.0	0.90	0.25	9.57E-4	1.00	vib.
Molecular Nitrogen					
1.00	3.00	6.14	2.26E-1	1.00	A
1.00	3.00	7.30	1.78E-1	3.00	B
1.00	3.00	11.0	2.80E-1	3.00	C
1.00	1.00	9.10	1.36E-1	1.00	a
3.00	0.75	12.9	6.70E-1	1.00	b
3.00	0.75	14.0	3.30E-1	1.00	b'
3.00	0.75	13.8	2.66E 0	1.00	Σ Rydbergs
9.00	16.0	1.40	1.50E 5	1.00	vib.

Table C.1 Parameters for the Excitation Cross Sections used by the Photoelectron model.

$$S(E_p, E_s) = \frac{2}{\pi \tilde{E}} \frac{\sigma_i(E_p)}{1+(E_s/\tilde{E})}, \qquad [C.8]$$

where I is the ionization potential, E_p is the energy of the primary electron, E_s the energy of the secondary, $\varepsilon = E_p/W$, $\tilde{E}$ is an empirically derived energy degradation coefficient (15.0 eV for atomic oxygen), and A, Ω, γ, ν are the fitting parameters. The atomic oxygen ionization parameters are given in Table C.2.

For the molecules, the Jackman *et al.* formula for the differential cross sections were used,

$$S_i(E_p, E_s) = \frac{A(E_p)\Gamma^2(Ep)}{(E_s - T_0(E_p))^2 + \Gamma^2(Ep)}, \qquad [C.9]$$

where:

$$A(E) = \left(\frac{K}{E_p} + K_B\right) \ln\left(\frac{E_p}{J} + J_B + \frac{J_C}{E_p}\right) \qquad [C.10]$$

$$\Gamma(E_p) = \frac{\Gamma_s E_p}{E_p + \Gamma_b} \qquad [C.11]$$

$$T_0(E_p) = T_s - \frac{T_a}{E_p - T_b}. \qquad [C.12]$$

I_i	A	Ω	ν	γ	State
13.6	0.29	0.85	1.00	0.30	^4S
16.9	0.36	0.85	1.00	0.30	^2D
18.5	0.19	0.85	1.00	0.30	^2P

Table C.2 Ionization parameters for Atomic Oxygen used in the Photoelectron model.

These parameters are given in Table C.3. Figure C.1 shows the electron impact elastic cross sections and backscatter ratios used in the two stream model (After Solomon, 1987).

I_i	K	K_B	J	J_b	J_c	T_s	T_a	T_b	Γ_s	Γ_b	State
Molecular Oxygen											
12.10	0.475	0.00	3.76	0.00	0.00	1.86	1000.0	24.2	18.5	12.1	X
16.10	1.129	0.00	3.76	0.00	0.00	1.86	1000.0	32.2	18.5	16.1	a
16.90	1.129	0.00	3.76	0.00	0.00	1.86	1000.0	33.8	18.5	16.9	A
18.20	1.010	0.00	3.76	0.00	0.00	1.86	1000.0	36.4	18.5	18.2	b
20.00	0.653	0.00	3.76	0.00	0.00	1.86	1000.0	40.6	18.5	20.3	B
23.00	0.950	0.00	3.76	0.00	0.00	1.86	1000.0	46.0	18.5	23.0	c
37.00	0.594	0.00	3.76	0.00	0.00	1.86	1000.0	74.0	18.5	37.0	37 eV
Molecular Nitrogen											
15.58	2.420	0.00	1.74	0.00	0.00	4.71	1000.0	31.16	13.8	15.58	X
16.73	1.060	0.00	1.74	0.00	0.00	4.71	1000.0	33.46	13.8	16.73	A
18.75	0.551	0.00	1.74	0.00	0.00	4.71	1000.0	37.50	13.8	18.75	B
22.00	0.371	0.00	1.74	0.00	0.00	4.71	1000.0	44.00	13.8	22.00	D
23.60	0.371	0.00	1.74	0.00	0.00	4.71	1000.0	47.20	13.8	23.60	C
40.00	0.530	0.00	1.74	0.00	0.00	4.71	1000.0	80.00	13.8	40.00	40 eV

Table C.3 Ionization parameters for molecular oxygen and nitrogen used by the Photoelectron model.

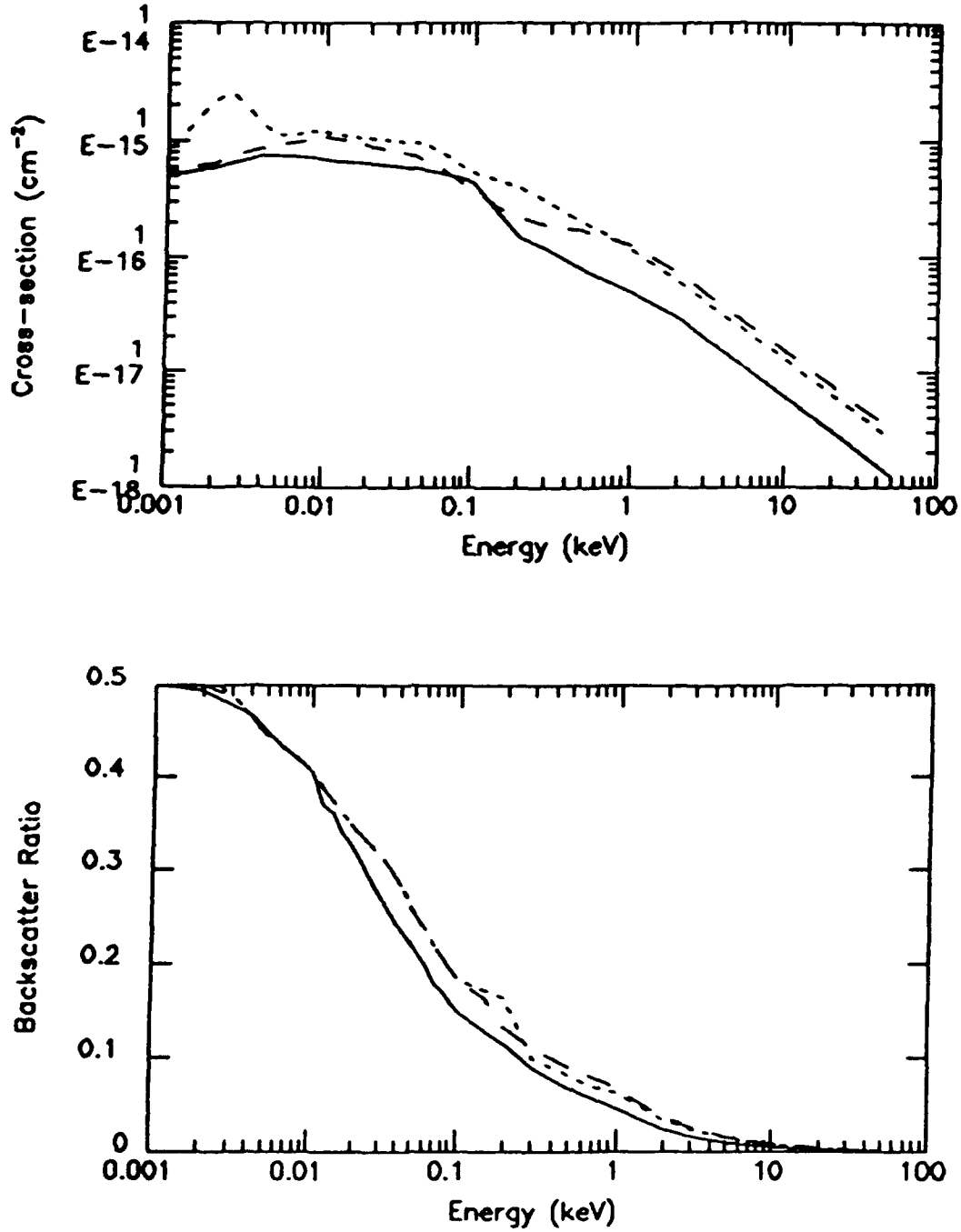

Figure C.1 Elastic Cross sections and Backscatter Ratios used in the Photoelectron model (from Solomon, 1987).

APPENDIX D

INTRODUCTION TO TWILIGHT

Twilight is defined by Chamberlain (1961) as the time when sunlight is shining on an emitting layer of the atmosphere from below. This is distinctive from the daytime when the sun is shining on the emitting layer from above and at night when the emitting layer receives no direct sunlight at all. Ground based twilight observations may be used as a substitute for a series of rocket flights which will give much better continuity of coverage (Hunten, 1967).

The twilight has several different periods all of which are based on the relative position of the sun to the emitting region of the atmosphere. These divisions are based on the instant when the geocentric zenith angles of the central point of the solar disk in increments of about 6 degrees as indicated in Table D.1. The times of these periods are tabulated annually in the Astronomical Almanac (from US Government Printing Office, Washington and HM Stationary Office, London).

The simplest figure for twilight is given in Figure D.1 where the atmosphere is singly scattering. The more realistic picture is given in Figure D.2 where complications arise from multiple scattering, adsorption, and refraction by the atmosphere and by reflections from the

Period	Solar Zenith Angle (degrees)
Sunrise/Sunset	90.83
Civil Twilight	96
Nautical Twilight	102
Astronomical Twilight	108

Table D.1 List of the points for the various twilight periods.

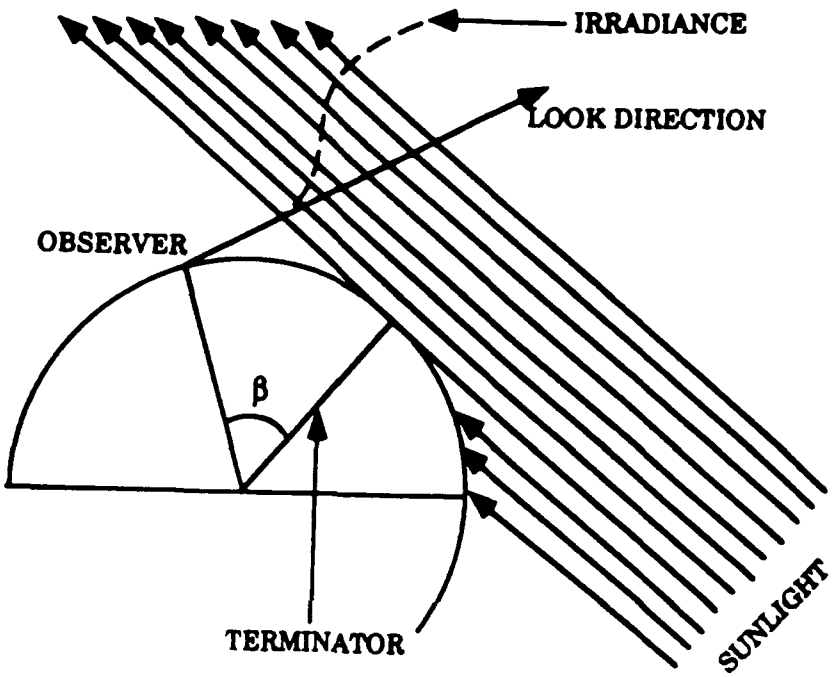

Figure D.1 The simplest interpretation of twilight observations by a singly scattering Rayleigh atmosphere.

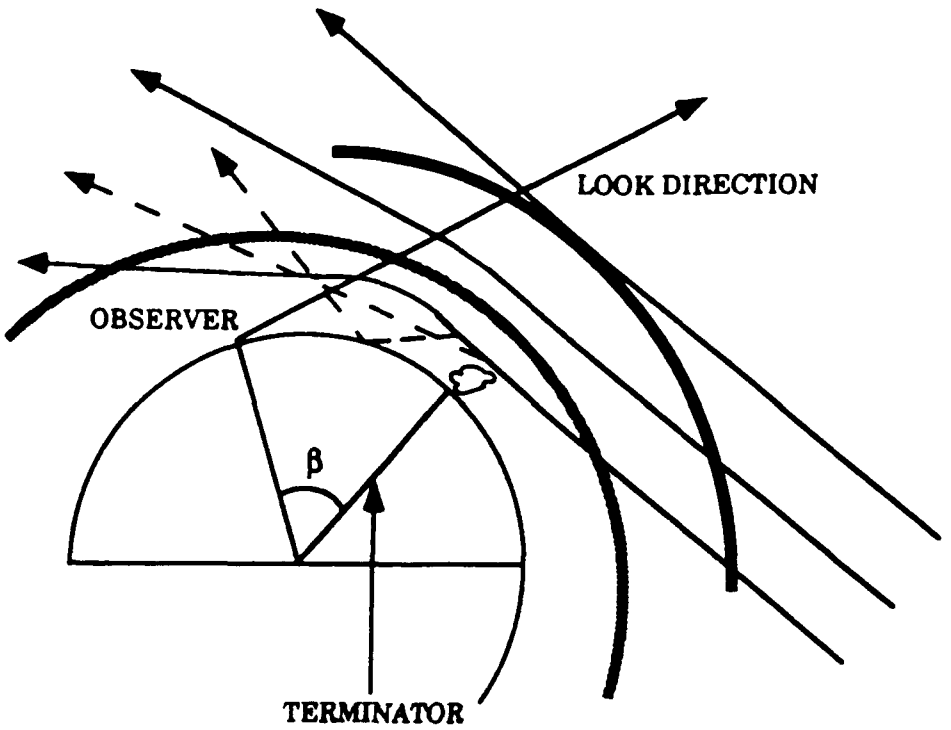

Figure D.2 Schematic indications of the interfering processes that can occur in the twilight including multiple scattering.

surface and clouds. These topics are reviewed by Gadsden (1967) and discussed in detail by Rozenberg (1966).

Observations of the daytime airglow began about 1961, study of the twilight started about 1938 (Kvifte, 1969). The study of the emissions during twilight can provide valuable information about the atmospheric structure, dynamics and chemistry. The period of twilight covers changes from when the daytime airglow which is dominated by solar and photoelectron driven processes into the nighttime where the emissions are provided by various chemiluminescent processes. During this period the total sky brightness diminishes rapidly and the weaker radiation become easier to observe. The change in the atmosphere can be used to study either the dayglow or nightglow by treating it as perturbation of a quasi-steady state (Gadsden, 1967).

The twilight emissions have been subdivided by Hunten (1967) into groups that are separated by altitude. The lowest is from O_2 bands at 30 to 50 km, with some emission of OH in the same region. The alkali metals of Na, K, Li and Ca^+ form the next group. The first three are in a layer at about 90 km with Ca^+ being somewhat higher. The emissions from these metals is due to resonance scattering. The third group is the F-region emissions from forbidden transitions of atomic oxygen and nitrogen, N_2^+ and orthohelium.

The excitation processes for the emission in the twilight is expected to be those in the dayglow only at a much smaller rate. This is especially true for those processes that are directly driven by solar and photoelectron processes. As the solar zenith angles increase, the path of the light through the atmosphere lengthens. This screening by the lower atmosphere to the radiation changes the effective radius of the earth as

shown in Figure D.3. Due to increased attenuation, from adsorption and scattering, the flux will decrease and photoelectron production will drop for a given point in the atmosphere.

The atomic oxygen lines observed in the twilight glow at the F-region altitudes are the red (6300Å) and green (5577Å) forbidden lines for $O(^1D)$ and $O(^1S)$ and a weak 4368Å line from the allowed transition of (4^3P-3^3S). At F-regions, the red line is greater in intensity than the green line emission. Both lines have the same excitation mechanisms as in the dayglow. Photodissociation of O_2 in the Schumann-Runge continuum produces the bulk of the $O(^1D)$. The $O(^1S)$ is mainly produced by the photoelectron excitation but as twilight progresses, dissociative recombination is the responsible mechanism which will continue into the nightglow.

At twilight, the 6300Å OI emission has an enhancement over the nightglow (Chamberlain, 1961; Gadsden, 1967; Hunten, 1967, Kvifte, 1969). The 5577Å greenline has been reported to have an enhancement, much weaker than that for the red line, of a factor of two (Dufay and Dufay, 1948). It was not observed for many years, until Megill (1960) using a birefringent filter substantiated the observations. The expected photon emission from fluorescence of 2972Å radiation is not expected to contribute significantly to the twilight 5577Å emission due to the low screening height for 2972Å radiation at about 50 km due to ozone absorption and the altitude of the peak in atomic oxygen near 100 km (Gadsden, 1967). This excludes resonance fluorescence as a source of the late twilight enhancement. The most likely source is the dissociative recombination of O_2^+, (Reaction [3.3]), which would also provide the enhancement for the red line.

Frederick *et al.* (1976) suggested that Reaction [3.12], the ion-atom interchange between atomic nitrogen and O_2^+, can explain the structure of

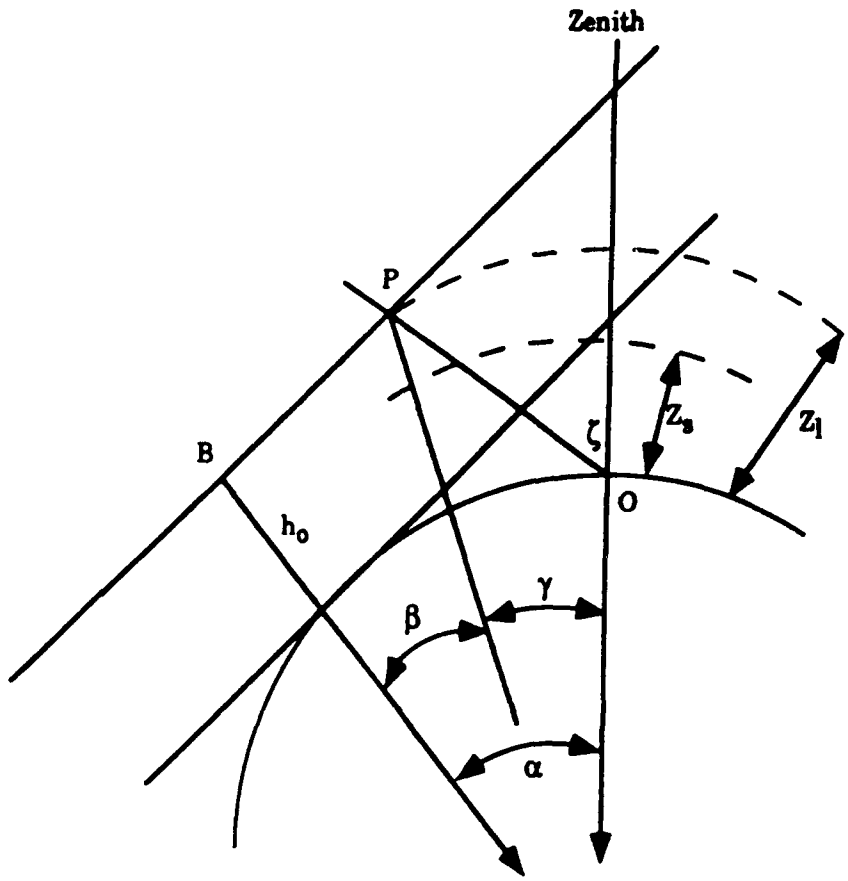

Figure D.3 Geometry of twilight observations from the ground The observer at O measures the emission at P. The geometrical shadow height is Z_s and the true screening height is Z_l.

the 5577Å emission in the twilight. The behavior of the twilight 5577Å emission has been studied by Schaeffer and Feldman (1972), Hays and Sharp (1973), and Kopp *et al.* (1977). Kopp *et al.* (1977) demonstrated that the 5577Å emission is asymmetric in the morning and evening terminators. This is shown in Figure D.4 and they concluded the differences can be explained by using Reaction [3.12] with a rate coefficient of 2.5×10^{-11} cm^3 s^{-1}, which supports the results of Frederick *et al.* (1976).

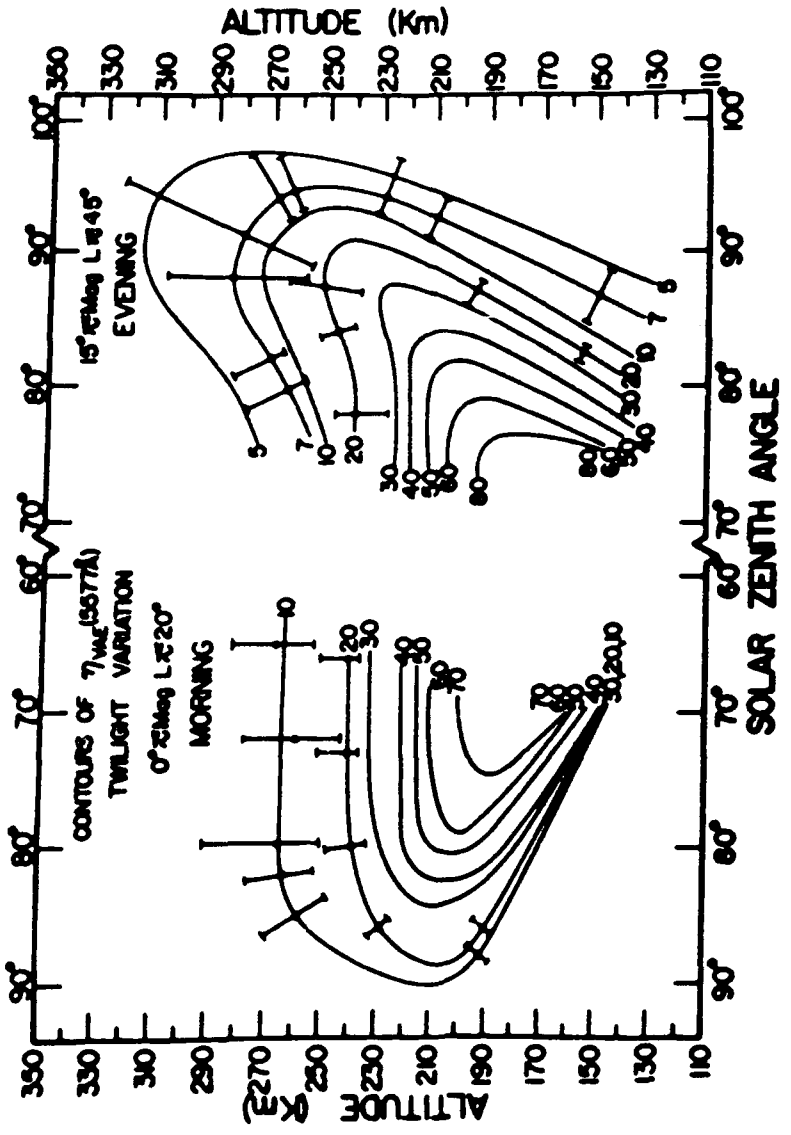

Figure D.4 Contour of the 5577Å emission rate as a function of altitude and SZA. (After Kopp *et al.*, 1977).

BIBLIOGRAPHY

BIBLIOGRAPHY

Abreu, V. J., S. C. Solomon, W. E. Sharp, and P. B. Hays, The Dissociative-Recombination of O_2+: The Quantum Yield of O(1S) and O(1D), *J. Geophys. Res.*, 88, 4140, 1983.

Abreu, V. J., P. B. Hays, and S. C. Solomon, The Tomographic Inversion of Satellite Photometric Data, in *RSRM '87: Advances in Remote Sensing Retrieval Methods* edited by A. Deepak, H. E. Fleming, and J. S. Theon, A. Deepak Publishing, 1989.

Abreu, V. J., D. Wu, J. H. Yee, and S. Solomon, The Inversion of Satellite Photometeric Data Using Sequential Estimation Techniques, *EOS Spring Meeting Supplement*, 205, 1991.

Ahmed, M., N_2 Vegard-Kaplan Band System In Aurora Rotational Temperatures and Vibrational Populations, *J. of Atmos. and Terr. Phys.*, 31, 1259, 1969.

Anger, C. D., A. T. Y. Lui, and S. I. Akasoufu, Observations of the Auroral Oval and a Westward Traveling Surge From the ISIS 2 Satellite and the Alaskan Meridian All-sky Cameras, *J. Geophys. Res.*, 78, 3020, 1973.

Ångstrom, A. J., Recherches sur le Spectre Solair, Spectre Normal du Soleil, W. Shultz, *Imprimeur de l'Universite*, Uppsala, Sweden, 1868.

Armstrong, E. B., The Association of Visible Airglow Features with a Gravity Wave, *J. Atmos. Terr. Phys.*, 44, 325, 1982.

Atkinson, R. and K. H. Welge, Temperature Dependence of O(^{1}S) Deactivation by CO_2, O_2, N_2, and AR, *J. Chem. Phys.*, 57, 3689, 1972.

Babcock, H. D., Note on the Polarization of the Night Sky, *Astrophys. J.*, 50, 228-231, 1919.

Babcock, H. D., A Study of the Green Auroral Line by the Interference Method, *Astrophys. J.*, 57, 209-221, 1923.

Baker, D. J. and R. O. Waddups, Rocket Measurement of Midlatitude Night Airglow Emissions, *J. Geophys. Res.*, 72, 4881, 1967.

Baker, D. J. and R. O. Waddups, Correction to Paper by D. Baker and R. Waddups 'Rocket Measurement of Midlatitude Night Airglow Emissions', *J. Geophys. Res.*, 73, 2456, 1968.

Banks, P. M., C. R. Chappell and A. F. Nagy, A New Model for the Interaction of Auroral Electrons With the Atmosphere: Spectral Degradation, Backscatter, Optical Emission, and Ionization, *J. Geophys. Res.*, 79, 1459, 1974.

Barth, C. A., The 5577-Angstrom Airglow, *Science*, 134, 1426, 1961.

Barth, C. A., in Abstracts of Papers Presented at the First Western National Meeting, American Geophysical Union, Los Angeles, California, December 27-29, 1961, *J. Geophys. Res.*, 67, 1628, 1962.

Barth, C. A., Three-body Reaction, *Ann. Geophys.*, 20, 182, 1964.

Bates, D. R., Collisional Deactivation and the Night Airglow, *J. Atmos. Terr. Phys.*, 6, 171, 1955.

Bates, D. R., Some Problems Concerning the Terrestrial Atmosphere Above the 100 km Level, *Proc. Roy. Soc, Ser. A*, 253, 451, 1959.

Bates, D. R., in *Physics of the Upper Atmosphere* , edited by G. P. Kuiper, University of Chicago Press, Chicago, Il, 1960.

Bates, D. R., Forbidden Oxygen and Nitrogen Lines in the Nightglow, *Planet. Space Sci.*, 26, 897, 1978.

Bates, D. R., On the Proposals of Chapman and of Barth for O(^{1}S) Formation in the Upper Atmosphere, *Planet. Space Sci.*, 27, 717, 1979.

Bates, D. R., The Green Light of the Night Sky, *Planet. Space Sci.*, 29, 1061, 1981.

Bates, D. R., Excitation of 557.7 nm OI Line in Nightglow, *Planet. Space Sci.*, 36, 883, 1988.

Bates, D. R., Oxygen Green and Red Line Emission and O_2+ Dissociative Recombination,, *Planet. Space Sci.*, 38, 889, 1990.

Bates, D. R. and H. S. W. Massey, The Basic Reactions in the Upper Atmosphere II. The Theory of Recombination in the Ionized Layers, *Proc. Royal Soc. of London,* 192, 1, 1947.

Bates, D. R. and A. Dalgarno, Theoretical Considerations Regarding the Dayglow, *J. Atmos. Terr. Phys.*, 5, 329, 1954.

Bates, D. R. and E. C. Zipf, The O(1S) Quantum Yield From O_2+ Dissociative Recombination, *Planet. Space Sci.*, 28, 1081,1980.

Beiting III, E. F. and P. D. Feldman, Ultraviolet Spectrum of the Aurora (2000-2800Å), *J. Geophys. Res.*, 84, 1287, 1979.

Berg, O. E., M. J. Koomen, L. H. Meredith, and R. Scolnik, The Altitude of the [OI] 5577Å Line in the Night Airglow Measured From a Rocket, *J. Geophys. Res.*, 61, 302, 1956.

Berrington, K. A., Private Communication, 1991.

Berry, M. V. and Gibbs, D. F., The Interpretation of Optical Projections, *Proc. Roy. Soc.*, A314, 143, 1970.

Bilitza, D., Improved Analytical Representation of Electron Temperature in the IRI, *Adv. Space Res.*, 4 (1), 93, 1984.

Bilitza, D., International Reference Ionosphere: Recent Developments, *Radio Sci.*, 21,343,1986.

Bilitza, D. and K. Rawer, New Options for IRI Electron Density in the Middle Ionosphere, *Adv. Space Res.*, 10 (11), 7, 1990.

Bilitza, D., *International Reference Ionosphere 1990*, NSSDC/WDC-A-R&S 90-22, Goddard Space Flight Center, Greenbelt, MD, 1990a.

Bilitza, D., Empirical Modeling of Ion Composition in the Middle and Topside Ionosphere, *Adv. Space Res.*, 10 (11), 47, 1990b.

Bilitza, D. and W. R. Hoegy, Solar Activity Variation of Ionospheric Plasma Temperatures, *Adv. Space Res.*, 10 (8), 81, 1990.

Bilitza, D. and K. Rawer, New Options for IRI Electron Density in the Middle Ionosphere, *Adv. Space Res.*, 10 (11), 7, 1990.

Booker, H. G., Fitting of Multi-region Ionospheric Profiles of Electron Density by a Single Analytic Function of Height, *J. Atmos. Terr. Phys.*, 39, 619, 1977.

Bowen, I. S., The Origin of the Nebulium Spectrum, *Nature*, 120, 473, 1927.

Bowen, I. S., The Presence of Neutral Oxygen in the Gaseous Nebulae, *Phys. Rev.*, 36, 600, 1930.

Brace, L. H., R. G. Theis, and A. Dalgarno, The Cylindrical Electrostatic Probes for Atmosphere Explorer-C, -D, and -E, *Radio Sci.*, 8, 341,1973.

Brinton, H. C., L. R. Scott, M. W. Pharo,III, and J. T. C. Coulson, The Bennett Ion-Mass Spectrometer on Atmosphere Explorer -C and -E, *Radio Sci.*, 8, 323, 1973.

Brown, L. D., R. E. Daniell, Jr., M. W. Fox, J. A. Klobuchar, and P. A. Doherty, Evaluation of Six Ionospheric Models as Predictors of Total Electron Content, *Radio Science*, 26, 1007, 1991.

Bucholtz, A., The Retrieval of Aerosol, Molecular, and Surface Parameters From the Stratospheric Measurements of the High Resolution Doppler Imager, *Doctoral Thesis*, Univ. of Michigan, Ann Arbor, 1991.

Buonsanto, M. J., Comparison of Incoherent Scatter Observations of Electron Density, and Electron and Ion Temperature at Millstone Hill with the International Reference Ionosphere, *J. Atmos. Terr. Phys.*, 51, 441, 1989.

Burgess, E. and D. Torr, *Into the Thermosphere, The Atmosphere Explorers*, NASA SP-490, NASA, Washington, DC, 1987.

Cartwright, D. C., S. Trajmar and W. Williams, Vibrational Population of the $A3\Sigma_u+$ and $B3\Pi_g$ States of N_2 in Normal Auroras, *J. Geophys. Res.*, 76, 8368, 1971.

Cartwright, D. C., S. Trajmar and W. Williams, Reply, *J. Geophys. Res.*, 78, 2365, 1973.

Cartwright, D. C., S. Trajmar, A Chutjian, and W. Williams, Electron Impact Excitation of the Electronic States of N_2. II. Integral Cross Sections at Incident Energies From 10 to 50 eV, *Phys. Rev. A*, 3, 1041, 1977.

Cartwright, D. C., Total Cross Sections for the Excitation of the Triplet States in Molecular Nitrogen, *Phys. Rev. A*, 2, 1331, 1970.

Cartwright, D. C., Vibrational Populations of the Excited States of N_2 Under Auroral Conditions, *J. Geophys. Res.*, 83, 517, 1978.

Campbell, W. W., Note of the Spectrum of the Aurora Borealis, *Astrophys. J.*, 2, 162, 1895.

Campbell, I. M. and B. A. Thrush, The Recombination of Nitrogen Atoms and the Nitrogen Afterglow, *Proc. R. Soc. London, Ser. A*, 296, 201,1967.

Camberlain, J. W., *Physics of the Aurora and Airglow*, Academic Press, New York, NY, 1961.

Chapman, S., Some Phenomena of the Upper Atmosphere (Bakerian Lecture), *Proc. Roy. Soc. (London)*, A132, 353, 1931.

Cogger, L. L. and C. D. Anger, The OI 5577Å Airglow Experimenton the ISIS 2 Satellite, *J. Atmos. Terr. Phys.*, 35, 2081, 1973.

Cogger, L. L. and J. S. Murphee, The Latitudinal and Seasonal Variation of Atomic Oxygen Deduced From Observations of the E-Region OI 5577.7 nm Airglow, *Space Research XX*, 115, 1980.

Cogger, L. L., R. D. Elphinstone, and J. S. Murphee, Temporal and Latitudinal 5577Å Airglow Variations, *Can. J. Phys.*, 59, 1296, 1981.

Cogger, L. L., J. S. Murphree, C. A. Tepley, and J. W. Meriwether, Jr, Measurements of the E Region Neutral Wind Field, *Planet. Space Sci.*, 33, 373, 1985.

Cooper, H. W., I. S. Gulledge, M. J. Koomen, and D. M. Packer, in Abstracts of the Papers Presented at the Forty-first Annual Meeting, American Geophysical Union, Washington, D. C., April 27-30, 1960 , *J. Geophys. Res.*, 65, 2484, 1960.

Conway, R. R., Comments on the Interpretation of 3371Å Filter-Photometer Observations and Its Implications for the AE-E Photoelectron Fluxes, *Planet. Space Sci.*, 31, 1223, 1983.

Conway, R. R. and A. B. Christensen, The Ultraviolet Dayglow at Solar Maximum. II. Photometer Observations of N_2 Second Positice (0,0) Band Emission, *J. Geophys. Res.*, 90,___, 1985.

Cormack, A. M., Representation of a Function by its Line Integrals, With Some Radiological Applications, *J. Appl. Phys*, 34, 2722, 1963.

Cormack, A. M., Representation of a Function by its Line Integrals, With Some Radiological Applications,II, *J. Appl. Phys*, 35, 2906, 1964.

Cormack, A. M., Reconstruction of Densities From Their Projections, With Applications in Radiological Physics, *Phys. Med. Biol.*, 18, 195, 1973.

Dalgarno, A., Vibrationally Excited Molecules in Atmospheric Reactions, *Planet. Space Sci.*, 10, 19, 1963.

Dalgarno, A. and S. P. Khare, The λ5577/λ3914 Intensity Ratio in Aurora, *Planet. Space Sci.*, 15, 938, 1967.

Dalgarno, A., W. B. Hanson, N. W. Spencer, and E. R. Schemerling, The Atmosphere Explorer Mission, *Radio Science*, 8, 263, 1973.

Dandekar, B. S., Atomic Oxygen Concentrations from Measurements of (OI) 5577Å Emission of the Airglow, *Planet. Space Sci.*, 20, 1781, 1972.

Dandekar, B. S., Equitorial Measurements of the [OI] 5577Å Emission of the Dayglow with a Photometer, *Planet. Space Sci.*, 17, 1609, 1969.

Dandekar, B. S. and J. P. Turtle, Atomic Oxygen Concentration from the Measurements of the [OI] 5577Å Emission of the Airglow, *Planet. Space Sci.*, 19, 957, 1971.

Deans, A. J. and G. G. Shepherd, Rocket Measurements of Oxygen and Nitrogen Emissions in the Aurora, *Planet. Space Sci.*, 26, 319, 1978.

Deehr, C. S. and A. Egeland, Auroral Morphology, *Ann. Geophys.*, 28, 415, 1972.

De Souza, A. R., G. Gousset, M. Touzeau, and Tu Khiet, Note on the determination of the efficiency of the reaction $N_2(A^3\Sigma) + O(^3P) \rightarrow N_2 + O(^1S)$, *J. Phys. B*, 18, L661, 1985.

Doering, J. P., W. G. Fastie, and P. D. Feldman, Photo Electron Excitation of N_2 in the Day Airglow, *J. Geophys. Res.*, 75, 4787, 1970.

Doering, J. P. and E. E. Gulcicek, Absolute Differential and Integral Electron Excitation Cross-sections for Atomic Oxygen. 7. The 3P-1D and 3P-1S Transitions From 4.0 to 30 eV, *J. Geophys. Res.*, 94, 1541, 1989.

Donahue, T. M., T. Parkinson, E. C. Zipf, J. P. Doering, W. G. Fastie, and R. E. Miller, Excitation of the Auroral Greenline by Dissociative Recombination of the Oxygen Molecular Ion: An Analysis of Two Rocket Experiments, *Planet. Space Sci.*, 16, 737, 1968.

Donahue, T. M., B. Guenther, and R. J. Thomas, Distribution of Atomic Oxygen in the Upper Atmosphere Deduced From OGO 6 Airglow Observations, *J. Geophys. Res.*, 78, 6662, 1973.

Donahue, T. M., B. Guenther, and R. J. Thomas, Spatial and Temporal Behavior of Atomic Oxygen Determined From OGO 6 Airglow Observations, *J. Geophys. Res.*, 79, 1959, 1974.

Donahue, T. M., OGO 6 Observations of OI 5577Å, in *Atmospheres of the Earth and the Plants*, Reidel, Dordrecht, 1975.

Dreyer, J. W. and D. Perner, Deactivation of $N_2(A^3\Sigma_u^+, v=0\text{-}7)$ by Ground State Nitrogen, Ethane, and Ethylene Measured by Kinetic Absorption Spectroscopy, *J. Chem. Phys.*, 58, 1195, 1973.

Dufay, J., Recherches sur la Lumiere du Ciel Nocturne, Published as *Bull. Obs. Lyon*, 10, num 9, 1-188, 1928.

Dufay, J., Spectre, Couleur, et Polarization la Lumiere du Ciel Nocturne, *J. Phys. Radium (6)*, 10, num 9, 219-240, 1929.

Dufay, J. and M. Dufay, Excitation de la raie verte de l'oxygene au crepuscule., *Comp. Rend.*, 232, 426, 1948.

Eather, R. H., *Majestic Lights: The Aurora in Science, History, and the Arts*, American Geophysical Union, 1980.

Elphinstone, R. D., J. S. Murphee, and L. L. Cogger, Dynamics of the Lower Thermosphere Consistent with Satellite Observations of 5577Å Airglow: II. Atomic Oxygen, Local Turbulence, and Global Circulation Results, *Can. J. Phys.*, 62, 382, 1984.

Elvey, C. T., Note on the Spectrum of the Airglow in the Red Region, *Astrophys. J.*, 111, 432-433, 1950.

Fabry, C., The General Illumination of the Sky, *Astrophys. J.*, 50, 308-310, 1919.

Fabry, C., Le Probleme de la Luminosite du Ciel Nocturne, *Scientia*, 30, 271-278, 1921.

Fath, E. A., The Northern Limit of the Zodiacal Light, *Lick Obs. Bull.*, 5, Num. 142, 45-49, 1908.

Felder, W. and N. A. Young, Quenching of $O(^1S)$ by $O(^3P)$, *J. Chem. Phys.*, 56, 6028, 1972.

Feldman, P. D., J. P. Doering, and E. C. Zipf, Excitation of $O(^1S)$ Atoms in the Day Airglow, *J. Geophys. Res.*, 76, 3087, 1971.

Fesen, C. G., The Mg^+ Airglow in the Low Latitude Ionosphere, Observations and Theoretical Modelling, *Doctoral Thesis*, Univ. of Michigan, Ann Arbor, 1981.

Fesen, C. G. and P. B. Hays, Mg^+ Morphology From Visual Airglow Experiment Observations, *J. Geophys. Res.*, 87, 9217, 1982.

Frederick, J. E., D. W. Rusch, G. A. Victor, W. E. Sharp, P. B. Hays, and H. C. Brinton, The OI(5577Å) Airglow: Observations and Excitation Mechanism, *J. Geophys. Res.*,81,3923,1976.

Frerichs, R., The Singlet System of the Oxygen Arc Spectrum and the Origin of the Green Auroral Line, *Phys. Rev.*, 36, 398, 1930.

Frerichs, R. and J. S. Campbell, , *Phys. Rev.*, 36, 1460, 1930.

Freund, J. T. and F. Jacka, Structure in the λ557.7 nm [OI] Airglow, *J. Atmos. Terr. Phys.*, 41, 25, 1979.

Fukuyama, K., Airglow Variations and Dynamics in the Lower Thermosphere and Upper Mesosphere-I. Diurnal Variations and Its Seasonal Dependency., *J. Atmos. Terr. Phys.*, 38, 1279, 1976.

Fukuyama, K., Airglow Variations and Dynamics in the Lower Thermosphere and Upper Mesosphere-II. Seasonal and Longterm Variations, *J. Atmos. Terr. Phys.*, 39, 1, 1977.

Fukuyama, K., Airglow Variations and Dynamics in the Lower Thermosphere and Upper Mesosphere-I. Variations during Stratospheric Warming Events, J. *Atmos. Terr. Phys.*, 39, 317, 1977.

Gadsen, M., Twilight Observations in *Aurora and Airglow* edited by B. M. McCormac, Reinhold Publishing Corp., NY, 1967.

Gadsen, M., Interpretation of Twilight Emissions in *Aurora and Airglow* edited by B. M. McCormac, Reinhold Publishing Corp., NY, 1967.

Gattinger, R. L., F. R. Harris, and A. Vallance Jones, The Height Spectrum and Mechanism of Type-B Aurora and its Bearing on the Excitation of $O(^1S)$ in Aurora, *Planet. Space Sci.*, 33, 207, 1985.

Gerdikova, M. G. and G. G. Shepherd, Evaluation of Auroral 5577Å Excitation Processes Using Intercosmos Bulgaria 1300 Satellite Measurements, *J. Geophys. Res.*, 92 , 3367 , 1987.

Gilmore, F. R., Comment, Proceedings of the Symposium on Laboratory Measurements of Aeronomic Emission Rates and Heating Effects, *Can. J. Chem.*, 47, 1779, 1969.

Green, A. E. S. and R. S. Stolarski, Analytical Models of Electron Impact Excitation Cross Sections, *Jou. Atmos. Terr. Phys.*, 34, 1703, 1972.

Green, B. D., Atomic Recombination into Excited Molecular - a Possible Mechanism for Shuttle Glow, *Geophys. Res. Lett.*, 11, 576, 1984.

Green, B. D., W. T. Rawlins, and W. J. Marinelli,_____, *Planet. Space Sci.*, 34, 879, 1986.

Greer, R. G. H. and G. T. Best, A Rocket-Borne Photometric Investigation of the Oxygen Lines at 5577Å and 6300Å, The Sodium D-Lines and the Continuum at 5300Å in the Night Airglow, *Planet. Space Sci.*, 15, 1857, 1967.

Greer, R. G. H., D. P. Murtagh, I. C. McDade, P. H. G. Dickenson, L. Thomas, D. B. Jenkins, J. Stegman, E. J. Llewellyn, G. Whitt, J. MacKinnon, and E. R. Williams, ETON1: A Database Pertinent to the Study of Energy Transfer in the Oxygen Nightglow, *Planet. Space Sci.*, 34, 771, 1986.

Guberman, S. L., The Production of O(1S) From Dissociative Recombination of O_2+, *Nature*, 327, 408, 1987.

Guberman, S. L., *Ab initio* Studies of Dissociative Recombination, in *Dissociative Recombination: Theory, Experiment and Applications* edited by J. B. A. Mitchell and S. L. Guberman, World Scientific Publishing Co. PTE, LTD, Singapore, 1989.

Gulledge, I. S., D. M. Packer, S. G. Tilford, and J. T. Vanderslice, Intensity Profiles of the 6300Å and 5577Å OI Lines in the Night Airglow, *J. Geophys. Res.*, 73, 5535, 1968.

Hanson, W. B., D. R. Zuccaro, C. R. Lippincott, and S. Sanatani, The Retarding-Potential Analyzer on Atmosphere Explorer, *Radio Sci*, 4, 333, 1973.

Hays, G. N. and H. J. Oskam, Population of the $N_2(B^3\Pi_g)$ by $N_2(A^3\Sigma_u^+)$ During the Nitrogen Afterglow, *J. Chem. Phys.*, 59, 1507, 1973.

Hays, P. B. and W. E. Sharp, Twilight Airglow 1 Photo-electrons and [OI] 5577 Angstrom Radiation, *J. Geophys. Res.*, 78, 1153, 1973.

Hays, P. B., G. Carignan, B. C. Kennedy, G. G. Shepherd, and J. G. C. Walker, The Visible Airglow Experiment on Atmosphere Explorer, *Radio Sci*, 8, 369,1973.

Hays, P. B., T. L. Killeen, and B. C. Kennedy, The Fabry-Perot Interferometer on Dynamics Explorer, *Space Sci. Inst.*, 5, 395, 1981.

Hays, P. B., V. J. Abreu, S. C. Solomon, and J. H. Yee , The Visible Airglow Experiment - A Review, *Planet. Space Sci.*, 36, 21, 1988.

Hedin, A. E., A Revised Thermospheric Model Based on Mass Spectrometer and Incoherent Scatter Data: MSIS-83, *J. Geophys. Res.*, 88, 188, 1983.

Hedin, A. E., MSIS-86 Thermospheric Model, *J. Geophys. Res.*, 92, 4649, 1987.

Hedin, A. E., H. G. Mayr, C. A. Reber, N. W. Spencer, G. R. Carignan, Empirical Model of Global Thermospheric Temperature and Composition Based on Data From the OGO-6 Quadrupole Mass Spectrometer, *J. Geophys. Res.*, 79, 215, 1974.

Henriksen, K. and A. Egeland, The Interpretation of the Auroral Green Line, A Historic Preamble and the Present State of Knowledge, *EOS*, 721, 1988.

Henry, R. J. W., P. G. Burke, and A-L. Sinfailam, Scattering of Electrons By C,N,O,N+,O+, and O++, *Phys. Rev.*, 178, 218, 1969.

Heppner, J. P. and L. H. Meredith, Nightglow Emission Altitudes From Rocket Measurements , *J. Geophys. Res.*, 63, 51, 1958.

Hernandez, G., The Signature Profile of O(1S) in the Airglow, *Planet. Space Sci.*, 19, 468, 1971.

Hernandez, S. P., J. P. Doering, V. J. Abreu, and G. A. Victor, Comparison of Absolute Photoelectron Fluxes Measured on AE-C and AE-E with Theoretical Fluxes and Predicted and Measured N_2 2PG 3371Å Volume Emission Rates, *Planet. Space Sci.*, 31, 221, 1983.

Hinteregger, H. E., K. Fukui, and B. R. Gilson, Observational, Reference, and Model Data On Solar EUV, From Measurements on AE-E, *Geophys. Res. Lett.*, 8, 1147,1981.

Hoffman, J. H., W. B. Hanson, C. R. Lippincott, and E. E. Ferguson, The Magnetic Ion-Mass Spectrometer on Atmosphere Explorer, *Radio Sci.*, 8, 315, 1973.

Hoffman, R. A. and E. R. Schmerling, Dynamics Explorer Program: An Overview, *Space Science Inst.*, 5, 345,1981.

Hoffman, R. A., G. D. Hogan, and R. C. Maehl, Dynamics Explorer Spacecraft and Ground Operations Systems, *Space Science Inst.*, 5, 349,1981.

Horan, D. M. and R. W. Kreplin, Simultaneous Measurements of EUV and Soft X-ray Solar Flare Emission, *Solar Physics*, 74, 265, 1981.

Houghton, J. T., F. W. Taylor, and C. D. Rodgers, *Remote Sounding of Atmospheres*, Cambridge University Press, New York, 1984.

Howorka, F., I. Dotan, F. C. Fehsenfeld, and D. L. Albritton, Kinetic Energy Dependance of the Branching Ratios of the Reaction of N+ with O_2, *J. Chem. Phys.*, 73, 758, 1980.

Hunten, D. M., Spectroscopic Studies of the Twilight Airglow, *Space Science Rev.*, 6, 493, 1967.

Hunten, D. M., F. E. Roach, and J. W. Chamberlain, A Photometric Unit for the Airglow and Aurora, *J. Atmos. Terr. Phys.*, 8, 345, 1956.

Hunten, D. M. and M. B. McElroy, Quenching of Metastable States of Atomic and Molecular Oxygen and Nitrogen, *Rev. Geophys. Space Phys.*, 4, 303, 1966.

Huruhata, M., T. Nakamura, J. Nakamura, and M. Nakamura, in *Proceedings of the 4th International Symposium on Space Science and Technology*, Japan, p. 459, 1962.

Itikawa, Y. and A. Ichimura, Cross-sections For Collisions of Electrons and Photons With Atomic Oxygen, ISAS Research Note, 406, 1989.

Jackman, C. H., R. H. Garvey, A. E. S. Green, Electron Impact on Atmospheric Gases, I, Updated Cross Sections, *J. Geophys. Res.*, 82, 5081, 1977.

Kaplan, J., The Light of the Night Sky, *Phys. Rev.*, 38, 1048, 1931.

Kernahan, J. A. and P. H-L. Pang, Experimental Determination of Absolute A Coefficients For 'Forbidden' Atomic Oxygen Lines, *Can. J. Phys.*, 53, 455, 1975.

Killeen, T. L. and P. B. Hays, O(^{1}S) From Dissociative Recombination Of O_2^+: Nonthermal Line Profile Measurements From Dynamics Explorer, *J. Geophys. Res.*, 88, 10163,1983.

Kirby, K., E. R. Constantinides, S. Babeu, M. Oppenheimer, and G. A. Victor, Photoionizaation and Photoabsorption Cross Sections of He, O N_2, and O_2 for Areonomical Calculations, *At. Data and Nucl. Data Tables*, 23, 63, 1979.

Kita, K., N. Iwagami, T. Ogawa, A. Miyashita, and H. Tanabe, Height Distributions of the Night Airglow Emissions in the O_2 Hertzberg I System and Oxygen Greenline from a Simultaneous Rocket Observation, *J. Geomag. Geoelectr.*, 40, 1067, 1988.

Konishi, A., K. Wakiya, M. Yamamoto, and H. Suzuki, Cross-Sections for Excitation of the $a^1\Delta_g$, $b^1\Sigma_g^+$, and $A^3\Sigma_u^+ + C^3\Delta_u$ States in O_2 by Electron Impact, *J. Phys. Soc. Jpn.*, 29, 526, 1970.

Koomen, M. J., R. Scolnik, and R. Tousey, Distribution of the Night Airglow [OI]5577Å and Na D Layers Measured From a Rocket, *J. Geophys. Res.*, 61, 304, 1956.

Kopp, J. P., D. W. Rusch, R. G. Robel, G. A. Victor, and P. B. Hays, Photoemission in the Second Positive System of Molecular Nitrogen in the Earth's Dayglow, *J. Geophys. Res.*, 82, 555, 1977.

Kopp, J. P., J. E. Frederick, D. W. Rusch, and G. A. Victor, Morning and Evening Behavior of the F-Region Green Line Emission: Evidence Concerning the Source of O(1S), *J. Geophys. Res.*, 82, 4715, 1977.

Krauss, M. and D. Neumann, On The Interaction Of O(1S) With O(3P), *Chem. Phys. Lett.*, 36, 372, 1975.

Krasnopolsky, V. A., Oxygen Emissions in the Night Airglow of the Earth, Venus, and Mars, *Planet. Space Sci.*, 34, 511,1986.

Krassovsky, V. I., The Nature of Emissions of the Upper Atmosphere, *Ann. Geophys.*, 14, 395, 1958.

Kulkarni, P. V., Rocket Study of 5577Å OI Emission at Night Over the Magnetic Equator, *J. Geophys. Res.*, 81, 3740, 1976.

Kvifte, G., Twilight Observations, in *Atmospheric Emissions*, edited by B. M. McCormac and A. Omholt, Van Nostrand Reinhold co., 1969.

Kvifte, G. and L. Vegard, On the Emission of the Forbidden Lines From Metastable Ground States $^1S_0$ and $^1D_2$ of the Neutral Oxygen Atoms, *Geofys. Publik.*, 17, 1, 1947.

Lawerence, G. M. and M. J. McEwan, Production of O(^{1}S) from Photodissociation of O_2, *J. Geophys. Res.*, 78, 8314, 1973.

Langford, A. O., V. M. Bierbaum, and S. R. Leone, Branching Ratios for Electronically Excited Oxygen Atoms Formed in the Reaction of N+ with O_2, at 300 K, *J. Chem. Phys.*, 84, 2158, 1986.

Lloyd, J. W. F., L. Nardone, B. L. Cochrun, and S. M. Silverman, in *Space Research VIII*, p 185, North-Holland, Amsterdam, 1968.

Lloyd, N. D., A. H. Manson, D. J. McEwan, and C. E. Meek, A Comparison of Middle Atmosphere Dynamics at Saskatoon (52°N, 107°W) as Measured by a Medium-Frequency Radar and a Fabry-Perot Interferometer, *J. Geophys. Res.*, 95, 7653, 1990.

Lopez-Moreno, J. J., S. Vidal, R. Rodrigo, and E. J. Llewellyn, Rocket Borne Photometric Measurements of $O_2(^1\Delta_g)$, Greenline, and OH Meinal Bands in the Nightglow, *10th Annual Meeting on Upper Atmospheric Studies by Optical Methods*, Grasse, France, 1982.

Lorents, D. C. and D. L. Huestis, in *Laser Spectroscopy*, eds. S. Haroche, J. C. Pebay-Peyoula, W. Hansch, and S. E. Harris, Springer, Berlin, 1975.

McClennan, J. C., The Aurora and Its Spectrum (Bakerian Lecture), *Proc. R. Soc. London*, A120, 327, 1928.

McClennan, J. C., _____, *Proc. R. Soc. London*, A129, 31, 1930.

McClennan, J. C. and G. M. Shrum, On the Luminescence of Nitrogen, Argon, and Other Condensed Gases at Very Low Temperatures, *Proc. R. Soc. London*, A106, 138, 1924.

McClennan, J. C. and G. M. Shrum, On the Origin of the Auroral Green Line 5577Å and Otner Spectra Associated With the Aurora Borealis, *Proc. R. Soc. London*, A106, 138, 1924.

McClennan, J. C. and J. H. McLeod, On the Wavelength of the Green Auroral Line in the Oxygen Spectrum, *Proc. R. Soc. London*, A115, 515, 1927.

McClennan, J. C., J. H. McLeod, and W. C. McQuarrie, An Investigation into the Nature and Occurrence of the Auroral Green Line λ5577Å, *Proc. R. Soc. London*, A114, 1, 1927.

McClennan, J. C., J. H. McLeod, and R. Ruedy, On the Zeeman Resolution of the Oxygen Spectral Line at λ5577Å. The Auroral Green Line, *Phil. Mag.*, 6, 558, 1928.

McDade, I. C. and E. J. Llewellyn, A Comment On Proposed Mechanisms For The Excitation Of O(1S) in The Aurora, *Planet. Space Sci.*, 32, 1195, 1984.

McDade, I. C. and E. J. Llewellyn, The Excitation of O(1S) by O_2 Bands in the Nightglow: A Brief Review and Preview, *Can. J. Phys.*, 64, 1626, 1986.

McNamara, L. F., Prediction of Total Electron Content Using the IRI, *Adv. Space Res.*, 4 (1), 25, 1984.

Megill, L. R., Photometric Observations of the Twilight Glow [OI] 5577 and [OI] 6300, *J. Atmos. Terr. Phys.*, 17, 276, 1960.

Mehr, F. J. and M. A. Biondi, Electron Temperature Dependence of Recombination of O_2+ and N_2+ Ions With Electrons, *Phys. Rev.*, 181, 264, 1969.

Menke, W., *Geophysical Data Analysis: Discrete Inverse Theory*, Academic Press, New York, 1989.

Metzger, P. H. and G. R. Cook, A Reinvestigation of the Absorption Cross Sections of Molecular Oxygen in the 1050-1800Å Region, *J. Quant. Spectrosc. Radiat. Transfer*, 4, 107, 1964.

Meyer, J. A., D. W. Setser. and D. H. Stedman, Excitation of the Auroral Green Line of Atomic Oxygen (1S-1D) by $N_2(A3\Sigma_u+)$, *Astrophys. J.*, 157, 1023, 1969.

Meyer, J. A., D. W. Setser. and D. H. Stedman, Energy Transfer Reactions of $N_2(A3\Sigma_u+)$, 2, Quenching and Emission by Oxygen and Nitrogen Atoms, *J. Phys. Chem.*, 74, 2238, 1970.

Meyerott, R. E. and G. R. Swenson, A Surface Chemistry Model for the Production of N_2 LBH Spacecraft Glow, *Planet. Space Sci.*, 38, 555, 1990.

Miller, K. J. and M. Krauss, Born Inelastic Differential Cross Sections in H_2, *J. Chem. Phys.*, 47, 3754, 1967.

Millman, P. M., The Canadian Visual Auroral Program, *Ann. Geophys.*, 24, 513, 1968.

Misaua, K. and I. Takeuchi, Correlation among O_2(0-1) Band, OH(8-3_ Band and [OI] 5577Å Line and Among $P_1(2)$, $P_1(3)$ and $P_1(4)$ Lines of OH(8-3) Band, *J. Atmos. Terr. Phys.*, 40, 421, 1978.

Moreels, G. and M. Hearse, Photographic Evidence of Waves Around the 85 km Level, *Planet. Space Sci.*, 35, 413, 1987.

Mount, G. H. and G. J. Rottman, The Solar Spectral Irradiance 1200-3184 Å Near Solar Maximum, July 15, 1980, *J. Geophys. Res.*, 86, 6697, 1981.

Mount, G. H. and G. J. Rottman, The Solar Absolute Spectral Irradiance 1150-3173 Å: 17 May 1982, *J. Geophys. Res.*, 88, 5403, 1983.

Mount, G. H. and G. J. Rottman, The Solar Absolute Spectral Irradiance 118-300 nm: July 25, 1983, *J. Geophys. Res.*, 90, 13031, 1985.

Mul, P. M. and J. W. McGowan, Merged Electron-Ion Beam Experiments III. Temperature Dependence of Dissociative Recombination for Atmospheric Ions NO+, O_2+ and N_2+, *J. Phys. B: Atomic. Molec. Phys.*, 12, 1591, 1979.

Nagy, A. F. and P. M. Banks, Photoelectron Fluxes In The Ionosphere, *J. Geophys. Res.*, 75, 6260, 1970.

Nardi, B., An Inversion Technique to Recover Lower Thermospheric Winds From Space-Borne Remote Measurements of [OI] 5577Å, *Doctoral Thesis,* Univ. of Michigan, Ann Arbor, 1991.

Nicolet, M., Origin of the Emission of the Oxygen Green Line in the Airglow, *Phys. Rev.*, 93, 633, 1954.

Nicolet, M., La Thermosphere, *Ann. Geophys.*, 15, 1, 1959.

Nicolet, M., _____, *Discuss. Farad. Soc.*, 37, 7, 1964.

Nicolet, M., in *Mesospheric Models and Related Experiments*, ed. J. Fiocco, Reidel, Dordrecth, 1, 1971.

Nier, A. O., W. E. Potter, D. R. Hickman, and K. Mauersberger, The Open-Source Neutral-Mass Spectrometer On Atmosphere Explorer-C, -D, and -E, *Radio Sci.*, 8, 271,1973.

O'Brien, B. J., F. R. Allum, and H. C. Goldwire, Rocket Measurements of the Midlatitude Airglow and Particle Precipitation, *J. Geophys. Res.*, 70, 161, 1965.

O'Brien, B. J., Satellite Observations of Particle Fluxes and Atmospheric Emissions, in *Aurora and Airglow*, ed. B. McCormac, Reinhold Publishing Co., New York, 623, 1967.

Offermann, D. and A. Drescher, Atomic Oxygen Densities in the Lower Thermosphere as Derived from In Situ 5577Å Night Airglow and Mass Spectrometer Measurements, *J. Geophys. Res.*, 78, 6690, 1973.

Olholt, A., *The Optical Aurora*, Springer, New York, 1971.

Olsen, R. E., _____, *Chem. Phys. Lett.*, 19, 137, 1973.

O'Neil, R. R., E. T. P. Lee and E. R. Huppi, Auroral O(1S) Production and Loss Processes: Ground-Based Measurements of the Artificial Auroral Experiment Precede, *J. Geophys. Res.*, 84,823, 1979.

Opal, C. B., W. K/ Peterson, and E. C. Beaty, Measurements of Secondary-electron Spectra Produced by Electron Impact Ionization of a Number of Simple Gasses, *J. Chem. Phys.*, 55, 4100, 1971.

Packer, D. M., Altitude of the Night Airglow Radiations, *Ann. Geophysicae*, 17, 67, 1961.

Park, H., P. D. Feldman, and W. G. Fastie, The Extreme Ultraviolet (750-1230 Å) Spectrum of an Aurora, *Geophys. Res. Lett.*, 4, 41, 1977.

Parkinson, T. P., A Phase and Amplitude Study of Auroral Pulsations, *Planet. Space Sci.*, 19, 251, 1971.

Parkinson, T. P., E. C. Zipf, and T. M. Donahue, Rocket Investigation of Auroral Green Light, *Planet. Space Sci.*, 18, 187, 1970.

Paxton, L. J., Atomic Carbon in the Venus Thermosphere: Observations and Theory, *Doctoral Thesis,* Univ. of Colorado, Boulder, 1983.

Pelz, D. T. , C. A. Reber, A. E. Hedin, and G. R. Carignan, A Neutral-Atmosphere Composition Experiment For The Atmosphere Explorer-C, -D, and -E, *Radio Sci.*, 8, 277, 1973.

Phillips, J. G., The Determination of the Widths of the Airglow And Twilight Flash, in *The Airglow and Aurorae*, ed. E. B. Armstrong and A. Dalgarno, Pergamon Press, London, 1956.

Piper, L. G., and G. E. Caledonia, Rate Constants For Deactivation of $N_2(A3\Sigma_u+,n'=0,1)$ by O, *J. Chem. Phys.*, 75, 2847, 1981.

Piper, L. G., The Excitation Of O(1S) In The Reaction Between $N_2(A3\Sigma_u+)$ and O(3P), *J. Chem. Phys.*, 77, 2373, 1982.

Queffelec, J. L., B. R. Rowe, F. Vallee, J. C. Gomet, and M. Moralis, The Yield of Metastable Atoms Through Dissociative Recombination of O_2+ Ions With Electrons, J. Chem. Phys., 91, 5335, 1989.

Radon, J., Uber die Bestimmung von Funktionen durch ihre Intergralwerte langs gewisser Mannigfultigkeiten, *Ber. Verb. Saechs. Acad. Wiss., Leipzig, Math. Phys. Kl.*, 69, 262, 1917.

Ramsay, W., *The Gases in the Atmosphere*, 4th ed, McMillan, London, 1915.

Ratcliffe, J. A., *An Introduction to the Ionosphere and Magnetosphere*, Cambridge University Press, London, 1972.

Rawer, K.(chairman), J. V. Lincln (ed.), and R. O. Conkright (ed.), International Reference Ionosphere-IRI-79, World Data Center A for Solar Terrestrial Physics, *Report UAG-82*, Boulder, 1981.

Rawer, K., Joint Analytical Profiles of Electron Density Profiles Through the Whole Ionosphere, *Adv. Space Res.*, 7(6), 25, 1987.

Rawer, K., Synthesis of Ionospheric Electron Density Profiles with Epstein Functions, *Adv. Space Res.*, 8(4), 191, 1988.

Rayleigh, Lord(Strutt, R. J.), Polarization of the Night Sky, *Astrophys. J.*, 50, 227-228, 1919.

Rayleigh, Lord(Strutt, R. J.), The Auroral Line in the Spectrum of the Night Sky, *Proc. Roy. Soc. (London)*, A100, 367-378, 1922a.

Rayleigh, Lord(Strutt, R. J.), A Study of the Presence or Absence of Nitrogen Bands in the Auroral Spectrum, *Proc. Roy. Soc. (London)*, A101, 312-315, 1922b.

Rayleigh, Lord(Strutt, R. J.), Further Observations on the Spectrum of the Night Sky, *Proc. Roy. Soc. (London)*, A103, 45-52, 1923.

Rayleigh, Lord(Strutt, R. J.), The Light of the Night Sky: Its Intensity Variations When Analysed by Colour Filters, *Proc. Roy. Soc. (London)*, A106, 117-137, 1924.

Rayleigh, Lord(Strutt, R. J.), The Light of the Night Sky: Its Intensity Variations When Analysed by Colour Filters III, *Proc. Roy. Soc. (London)*, A119, 11-33, 1928.

Rayleigh, Lord(Strutt, R. J.), Absolute Intensity of the Auroral Line in the Night Sky and The Number of Atomic Transitions,, *Proc. Roy. Soc. (London)*, A129, 458-467, 1930.

Rayleigh, Lord(Strutt, R. J.), On a Night Sky of Exceptional Brightness, and on the Distinction Between the Polar Aurora and the Night Sky, *Proc. Roy. Soc. (London)*, A131, 376-381, 1931.

Reed, E. I. and S. Chandra, The Global Characteristics of Atmospheric Emissions in the Lower Thermosphere and Their Aeronomic Implications, *J. Geophys. Res.*, 80, 533, 1975.

Rees, M. H., A. I. Stewart, W. E. Sharp, P. B. Hays, R. A. Hoffman, L. H. Brace, J. P. Doering, and W. K. Peterson, Coordinated Rocket and Satellite Measurements of an Auroral Event 1. Satellite Observations and Analysis, *J. Geophys. Res.*, 82, 2250, 1977.

Rees, M. H., Excitation of O(1S) and Emission Of 5577Å Radiation In Aurora, *Planet. Space Sci.*, 22, 373, 1984.

Richards, P. G. and D. G. Torr, An Investigation of the Consistency of the Ionospheric Measurements of the Photoelectron Flux and Solar EUV Flux, *J. Geophys. Res.*, 89, 5625, 1984.

Roach, F. E., and H. B. Pettit, On the Diurnal Variation of [OI] 5577 in the Nightglow, *J. Geophys. Res.*, 56, 325-353, 1951.

Roble, R. G. and P. B. Hays, A Technique for Recovering the Vertical Number Density Profile of Atmospheric Gases From Planetary Occultation Data, *Planet. Space Sci.*, 20, 1727, 1972.

Rodgers, C. D., Retrieval of Atmospheric Temperature and Composition From Remote Measurements of Thermal Radiation, *Rev. Geophys. Space Phys.*, 14, 609, 1976.

Rodgers, C. D., Characterization and Error Analysis of Profiles Retrieved from Remote Sounding Measurements, *J. Geophys. Res..*, 95, 5587, 1990.

Rottman, G. J., Rocket measurements of the Solar Spectral Irradiance During Solar Minimum, 1972 to 1977, *J. Geophys. Res.*, 86, 6697, 1981.

Rottman, G. J., Observations of Solar UV and EUV Variability, *Adv. Space Res.*, 8, (7)53, 1988.

Rowe, B. R. and J. L. Quffelec, Experimental Studies of Dissociative Recombination Branching Ratios, in *Dissociative Recombination: Theory, Experiment and Applications* edited by J. B. A. Mitchell and S. L. Guberman, World Scientific Publishing Co. PTE, LTD, Singapore, 1989.

Rozenberg, G. V., *Twilight, A Study in Atmospheric Optics*, Plenum Press, New York, 1966.

Rundle, H. W., _____, in *The Radiating Atmosphere*, edited by B. M. McCormac, D. Reidel Publishing Co., Dordrecht, Holland, 1971.

Saito, B. and Y. Kiyama, Variation of Night Airglow OI 5577Å Intensity-I. Long Term Variations, *Bulletin of the Nigata Airglow Observatory*, No. 15, Nigata University Publication, 1988.

Samson, J. A. R. and P. N. Pareek, Absolute Photoionization Cross sections of Atomic Oxygen, *Phys, Rev. A*, 31, 1470, 1985.

Schaffer, R. C., P. D. Feldman, and E. C. Zipf, Dayglow [OI] λ6300 and 5577Å Lines in the Early Morning Ionosphere, *J. Geophys. Res.*, 77, 6828, 1972.

Setser, D. W., D. H. Stedman, and J. A. Coxon, Chemical Applications of Metastable Argon Atoms. IV. Excitation and Relaxation of Triplet States of N_2, *J. Chem. Phys.*, 53, 1004, 1970.

Sharp, W. E., M. H. Rees, and A. I. Stewart, Coordinated Rocket and Satellite Measurements Of An Auroral Event 2. The Rocket Observations and Analysis, *J. Geophys. Res.*, 84, 1977, 1979.

Sharp, W. E. and D. G. Torr, Determination Of The Auroral O(^{1}S) Production Sources From Coordinated Rocket and Satellite Measurements, *J. Geophys. Res.*, 84, 5345, 1979.

Shemansky, D. E., and N. P. Carleton, Lifetime of the N_2 Vegard-Kaplan System, *J. Chem. Phys.*, 51, 682, 1969.

Shemansky, D. E., The N_2 Vegard-Kaplan System in Absorption, *J. Chem. Phys.*, 51, 689, 1969.

Shepherd, G. G., C. D. Anger, L. H. Brace, J. R. Burrow, W. J. Heikkila, J. Hoffman, E. J. Maier, and J. H. Whitteker, An Observation of Polar Aurora and Airglow From the ISIS-2 Spacecraft, *Planet. Space Sci.*, 21, 819, 1973.

Shyn, T. W., S. Y. Cho and W. E. Sharp, Differential Excitation Cross-section of Atomic Oxygen by Electron Impact (3P-1S) Transition, *J. Geophys. Res.*, 91, 13571, 1986.

Silverman, S. M., J. W. F. Lloyd, B. L. Cochrun, and L. Nardone,__-, *Nature*, 204, 461, 1964.

Slanger, T. G., B. J. Wood, and G. Black, The Temperature Dependence of O(^{1}S) Quenching by O_2, *Chem. Phys. Lett.*, 17, 401, 1972.

Slanger, T. G. and K. H. Welge, Rate Constants for Reactions of O(^{1}S), in *Chemical Kinetics Data Survey V. Sixty-six Contributed Rate and Photo-chemical Data Evaluation on Ninety-four Reactions, NBSIR 73-206,* edited by D. Garvin, National Bureau of Standards, Washington, D. C., pages 22-32, 1973.

Slanger, T. G. and G. Black, O(^{1}S) Quenching by O(^{3}P), *J. Chem. Phys.*, 64, 3763, 1976a.

Slanger, T. G. and G. Black, O(^{1}S) Production from Oxygen Atom Production, *J. Chem. Phys.*, 64, 3767, 1976b.

Slanger, T. G. and G. Black, O(^{1}S) in the Lower Thermosphere: Chapman vs Barth, *Planet. Space Sci.*, 25, 79, 1977.

Slanger, T. G. and G. Black, Quenching of O(^{1}S) by $O_2(a^1\Delta_g)$, *Geophys. Res. Lett.*, 8, 535, 1981.

Slipher, V. M., On the General Auroral Illumination of the Sky and the Wavelength of the Chief Auroral Line, *Astrophys. J.*, 49, 266-275, 1919.

Smith, D., N. G. Adams, and T. M. Miller, A Laboratory Study of the Reactions of N^+, N_2^+, N_3^+, N_4^+, O^+, O_2^+, and NO^+ Ions with Several Molecules at 300 K, *J. Chem. Phys.*, 69, 308, 1978.

Smith, E. V. P. and D. M. Gottleib, Solar Flux and Its Variations, *Space Sci. Rev.*, 16, 771, 1974.

Smith, K., R. J. W. Henry and P. G. Burke, Calculations on the Scattering of Electrons by Atomic Systems with Configurations 2pq, *Physical Review*, 157, 51, 1967.

Smith, L. L. and W. R. Steiger, Night Airglow Intensity in the [OI] 5577Å, [OI] 6300Å and NaI 5890-90Å Emission Lines, *J. Geophys. Res.*, 73, 2531, 1968.

Solheim, B. H. and E. J. Llewellyn, An Indirect Mechanism for the Production of O(^{1}S) in the Aurora, *Planet. Space Sci.*, 27, 423, 1979.

Solomon, S. C., Tomographic Inversion of Auroral Emissions, *Doctoral Thesis*, Univ. of Michigan, Ann Arbor, 1987.

Solomon, S. C., P. B. Hays, and V. J. Abreu, Tomographic Inversion of Satellite Photometry, *App. Optics*, 23, 3409, 1984.

Solomon, S. C., P. B. Hays, and V. J. Abreu, Tomographic Inversion of Satellite Photometry. Part 2, *App. Optics*, 24, 4134, 1985.

Solomon, S. C., P. B. Hays, and V. J. Abreu, The Auroral 6300Å Emission: Observations and Modeling, *J. Geophys. Res.*, 93, 9867, 1988.

Solomon, S. C., and V. J. Abreu, The 630 nm Dayglow, *J. Geophys. Res.*, 94, 6817, 1989.

Sommer, L. A., Di Quantentheoretische Deutung der Grunen Nordlight Linie auf Grund Interferometrischer Zeemaneffektmessung, *Z. Phys.*, 51, 451, 1928.

Spencer, N. W., H. B. Niemann, and G. R. Carignan, The Neutral-Atmosphere Temperature Instrument, *Radio Sci.*, 8, 284, 1973.

Strobel, D. F., E. Hyman, P. D. Feldman, W. G. Fastie, P. S. Julienne, and D. J. Strickland, Auroral O(1S) and 5577Å Emission (Abstract), *EOS Trans, AGU*, 56, 1032, 1975.

Swartz, W. E., Optimization of Energetic Electron Energy Degradation Calculations, *J. Geophys. Res.*, 90, 6587, 1985.

Takahashi, H., Y. Sahai, B. R. Clemesha, P. P. Batista, and N. R. Teixeria, Diurnal and Seasonal Variations of the OH(8,3) Airglow Band and its Correlation with OI 5577Å, *Planet. Space Sci.*, 25, 541, 1977.

Takahashi, H., Y. Sahai, and P. P. Batista, Tidal and Solar Effects on the OI 5577Å, NaD, and OH(8,3) Airglow Emissions Observed at 23°S, *Planet. Space Sci.*, 32, 897, 1984.

Takahashi, H., P. P. Batista, Y. Sahai, and B. R. Clemesha, Atmospheric Wave Propagations in the Mesopause Region Observed by the OH(8,3), NaD, O_2A(8645Å) Band and OI 5577Å Nightglow Emissions, *Planet. Space Sci.*, 33, 897, 1985.

Takahashi, H., B. R. Clemesha, P. P. Batista, Y. Sahai, M. A. Abdu, and P. Muralikrisna, Equitorial F-region OI 6300 Å and OI 5577 Å Emission Profiles Observed By Rocket-Borne Airglow Photometers, *Planet. Space Sci.*, 38, 547, 1990.

Tarasova, T. M., in *Space Research III*, ed W. Priester, North-Holland, Amsterdam, 162, 1963.

Taylor, M. J., M. A. Hapgood, and P. Rothwell, Observations of Gravity Wave Propagation in the OI (557.7 nm), Na (589.2 nm) and the Near Infrared OH Nightglow Emissions, *Planet. Space Sci.*, 35, 413, 1987.

Thomas, J. M. And F. Kaufman, Rate Constants of the Reaction of Metastable $N_2(A3\Sigma_u+)$ in v=0,1,2,3 With Ground State O_2 and O, *J. Chem. Phy.*, 83, 2900, 1985.

Thomas, L. and M. R. Bowman, The Diurnal Variations of Hydrogen and Oxygen Constituents in the Mesosphere and Lower Thermosphere, *J. Atmos. Terr. Phys.*, 34, 1843, 1972.

Thomas, L. D., and R. K. Nesbet, Low Energy Electron Scattering By Atomic Oxygen, *Phys. Rev. A4*, 1482, 1975.

Thomas, L., R. G. H. Greer, and P. H. G. Dickinson, The Excitation of the 557.7 nm Line and Hertzberg Bands in the Nightglow, *Planet. Space Sci.*, 27, 925, 1979.

Thomas, R. J., Analysis of Atomic Oxygen, the Greenline, and Hertzberg Bands in the Lower Thermosphere, *J. Geophys. Res.*, 86, 206, 1981.

Thomas, R. J. and T. M. Donahue, Analysis of OGO 6 Observations of the OI 5577Å Tropical Nightglow, *J. Geophys. Res.*, 77, 3557, 1972.

Thrush, B. A. and I. P. Stott, Discussion, *Phil. Trans. R. Soc. (London)*, A323, 594, 1987.

Tobiska, W. K. and C. A. Barth, A Solar EUV Flux Model, *J. Geophys. Res.*, 95, 8243, 1990.

Torr, D. G., M. R. Torr, J. G. C. Walker, A. O. Neir, L. H. Brace, and H. C. Brinton, Recombination of O_2^+ In The Ionosphere, *J. Geophys. Res.*, 81, 5578, 1976.

Torr, M. R., D. G. Torr, and H. E. Hinteregger, Solar Flux Variability in the Schumann-Runge Continuum as a Function of Solar Cycle 21, *J. Geophys. Res.*, 85, 6063, 1980.

Torr, M. R. and D. G. Torr, The Role of Meta-stable Species in the Thermosphere, *Rev. Geophys. Space Phys.*, 20, 91, 1982.

Torr, M. R. and D. G. Torr, Ionization Frequencies for Solar Cycle 21, Revised, *J. Geophys. Res.*, 90, 6675, 1985.

Tousey, R., Rocket Measurements of the Night Airglow, *Ann. Geophysicae*, 14, 186, 1958.

Tully, J. C., Z. Herman, and R.Wolfgang, Crossed-beam Study of the Reaction $N^+ + O_2 \longrightarrow NO^+ + O(^1S)$, *J. Chem. Phys.*, 54, 1730, 1971.

Twomey, S., *Introduction to the Mathematics of Inversion in Remote Sensing and Indirect Measurements*, Elsiver Scientific Publishing, Co., Amsterdam, 1977.

Vallance Jones, A., *Aurora*, D. Reidel, Hingham, Mass., 1974.

Van Rhijn, P. J., On the Brightness of the Sky at Night and The Total Amount of Starlight, *Publ. Ast. Lab. Groningen*, 31, 1, 1921.

Vegard, L., Photographischen Afnahmen des Nordlichtspectrums mit Einen Spectrographen von Grosser Dispersion, *Phys. Z.*, 14, 677, 1913.

Vegard, L., The Aurora Spectrum and the Upper Strata of the Atmosphere: Preliminary Communications, *Philos. Mag.*, 46, 193, 1923a.

Vegard, L., The Constitution of the Upper Strata of the Atmosphere, *Philos. Mag.*, 46, 557, 1923b.

Vegard, L., Light Emitted From Solid Nitrogen When Bombarded With Cathode Rays, and Its Bearing on the Auroral Spectrum, *Proc. R. Acad. Amsterdam*, 27, 113, 1924.

Vegard, L., Results of Investigations of the Auroral Spectrum During the Years 1921-1926, *Geofys. Publ.*, 9, 11, 1932.

Vegard, L., Investigations of the Auroral Spectrum Based on Observations From The Auroral Observatory, Tromso, *Geofys. Publ.*, 10, 41, 1933.

Vegard, L., The Aurora Polaris aand the Upper Upper Atmosphere, in *Terrestrial Magnetism and Electricity*, ed. J. A. Fleming, McGraw-Hill, New York, 1939.

Vegard, L. and E. Tonsberg, Variations of the Intensity Distribution Within the Auroral Spectrum, *Geofys. Publ.*, 11, 16,1937.

Viereck, R. A., E. Murad, B. D. Green, P. Joshi, C. P. Pike, R. Heib, and G. Harbough, Origin of the Shuttle Glow, *Nature*, 354, 48, 1991.

Vogel, H., Uber das Spectrum des Zodiacallichtes, *Ast. Nachr.*, 79, 327-330, 1872.

Vo Ky Lan, N. Feautrier, M. LeDournefu, and H. VanAegemorter, Cross-section Calculations For Electron Oxygen Scattering Using Polarized Orbital Close Coupling Theory, *J. Phys. B5*, 1506, 1972.

Wagner, W. J., Observations of 1-8Å Solar X-ray Variability During Solar Cycle 21, *Adv. Space Res.*, 8, (7)67, 1988.

Walker, J. G. C., The Greenline of Atomic Oxygen in the Day Airglow, *J. Atmos. Sci.*, 22, 361, 1965.

Wallace, J. M. and P. V. Hobbs, *Atmospheric Science, An Introductory Survey*, Academic Press, Harcourt Brace Jovanovich, Publishers, New York, 1977.

Wallace, L. and R. A. Nidey, Measurements of the Daytime Airglow in the Visual Region, *J. Geophys. Res.*, 69, 471, 1964.

Wallace, L. and M. B. McElroy, The Visual Dayglow, *Planet. Space Sci.*, 14, 677, 1966.

Walls, F. L., and G. H. Dunn, Measurement of Total Cross Sections for Electron Recombination With NO+ and O_2+ Using Ion Storage Techniques, *J. Geophys. Res.*, 79, 1911, 1974.

Warnecke, G., E. I. Reed, W. B. Fowler, E. R. Krems, L. J. Allison, and J. E. Blamont, Meteorological Results from Multispectral Photometry in Airglow Bands by the OGO-4 Satellite, *J. Atmos. Terr. Phys.*, 26, 1329, 1969.

Wasser, B. and T. M. Donahue, Atomic Oxygen Between 80 and 120 km: Evidence for a Latitudinal Variation in Vertical Transport Near the Mesopause, *J. Geophys. Res.*, 84, 1297, 1979.

Watson, C. E., V. A. Dulock,Jr., R. S. Stolarski, and A. E. S. Green, Electron Impact Cross Sections for Atmospheric Species, 3, Molecular Oxygen, *J. Geophys. Res.*, 72, 3961, 1967.

Wegener, A., *Thermodynamik der Atmosphare*, J. A. Barth, Leipzig, Austria, 1911.

Wiechert, E., Polarlichtbeobachtungen in Gottingen, *Z. Phys.*, 3, 365-366, 1902.

Weins, R. H. and G. Weill, Diurnal, Annual and Solar Cycle Variations of Hydroxyl and Sodium Nightglow Intensities in the Europe-Africa Sector, *Planet. Space Sci.*, 21, 1011, 1973.

Weins, R. H., G. G. Shepherd, W. A. Gault, and P. R. Kosteniuk, Optical Measurements of Winds in the Lower Thermosphere, *J. Geophys. Res.*, 93, 5973, 1988.

Wraight, P. C., Association of Atomic Oxygen and Airglow Excitation, *Planet. Space Sci.*, 30, 251, 1982.

Yau, A. W. and G. G. Shepherd, Energy Transfer From Excited N_2 and O_2 as a Source of O(^{1}S) in the Aurora, Planet. Space Sci., 27, 481, 1979.

Yee, J. H. and V.J. Abreu, Visible Airglow Induced By Spacecraft-Environment Interaction, *Geophys. Res. Lett.*, 10,126, 1983.

Yee, J. H., V.J. Abreu, and A. Dalgarno, Characteristics of the Spacecraft Optical Glow, *Geophys. Res. Lett.*, 11, 1192, 1984.

Yee, J. H. and T. L. Killeen, Thermospheric Production of O(^{1}S) by Dissociative Recombination of Vibrationallly Excited O_2^+, *Planet. Space Sci.*, 34, 1101, 1986.

Yee, J. H. and V. J. Abreu, Mesospheric 5577Å Green Line and Atmospheric Motions-Atmosphere Explorer Satellite Observations, *Planet. Space Sci.*, 35, 1389, 1987.

Yee, J. H., V. J. Abreu and W. B. Colwell, Aeronomical Determinations of The Quantum Yield of $O(^1S)$ and $O(^1D)$ From Dissociative Recombination of O_2^+ , in *Dissociative Recombination: Theory, Experiment and Applications* edited by J. B. A. Mitchell and S. L. Guberman, World Scientific Publishing Co. PTE, LTD, Singapore, 1989.

Yntema, L., On the Brightness of the Sky and the Total Amount of Starlight, *Publ. Ast. Groningen*, num 22, 1-55, 1909.

Young, R. A. and K. C. Clark, Vibrational Distribution in Late Nitrogen Afterglow, *J. Chem. Phys.*, 32, 607, 1960.

Young, R. A., G. Black, and T. G. Slanger, Vacuum Ultraviolet Photolysis of N_2O Reaction Rates of $O(^1S)$, *J. Chem. Phys.*, 50, 309, 1969.

Zipf, E. C., _____, *Bull. Amer. Phys. Soc.*, 12, 225, 1967.

Zipf, E. C., Photodissociation of O_2: A Major Source of the Auroral Greenline (Abstract), *EOS Trans. AGU*, 54, 403, 1973.

Zipf, E. C., The $OI(^1S)$ State: Its Quenching and Formation By Dissociative Recombination of Vibrationally Excited O_2^+ Ions, *Geophys. Res. Lett.*, 6, 881, 1979.

Zipf, E. C., A Laboratory Study On The Dissociative Recombination Of Vibrationally Excited O_2+ Ions, *J. Geophys. Res.*, 85, 4232,1980.

Zipf, E. C., The Excitation of the $O(^1S)$ State by the Dissociative Recombination of O_2^+ Ions: Electron Temperature Dependence, *Planet. Space Sci.*, 36, 621, 1988.

Zipf, E. C. and R. W. McLaughlin, On the Dissociation of Nitrogen by Electron Impact and by EUV Photoabsprption, *Planet. Space Sci.*, 26, 449, 1978.